# Dissecting molecular mechanisms of disease in the wheat pathogen, *Parastagonospora nodorum*

Oliver L. Mead, March 2019

A thesis submitted for the degree of Doctor of Philosophy of The Australian National University

I, Oliver L. Mead, declare that the following work is entirely the product of my own efforts, except as where otherwise indicated.

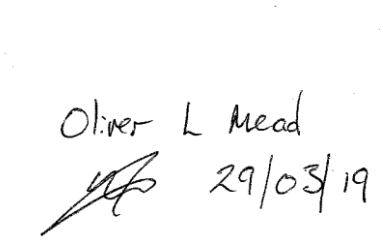


……

## Acknowledgements

Peter, thank you for your support, direction and mateship over the last seven years. Within and outside of your you have provided an environment that combines a drive for excellent science and the thrill of enquiry with a casual and supportive gregariousness. I appreciate the time you made for me- especially for my habit of leaning in your door way to ask “Hey uh… quick question”, often chaotic home life and wandering attention. I have enjoyed my time in your lab very much and couldn’t have asked for more. Thank you for taking on that idealistic undergraduate.

Megan, Simon, Susan, Eli, Erin and Jordi, thank you for being my second family. Your companionship (and couches) made some of my hardest moments a pleasure.

Mum and Dad, thank you for listening to my abundant outbursts (both angry and overly enthusiastic) about primers, fungi and the scientific accuracy of TV programs. Please forgive my absence, both physically and mentally, I’ve been preoccupied having fun.

This project was supported by an Australian Government Research Training Program (RTP) Scholarship and a Grain Research and Development Corporation (GRDC) scholarship top-up.

# “Don’t Panic”

-Douglas Adams

# “Panic!”

-Every single neuron in my possession

Dashing scientists:

“Stago! Give up your secrets!”

Spores drift on the breeze

## Abstract

The wheat pathogen *Parastagonospora nodorum* (Syn. *Phaeosphaeria nodorum*) belongs to the pathogen-enriched class of fungi known as the Dothideomycetes. *P. nodorum* is a host specific pathogen that causes annual losses to the Australian wheat industry in excess of $100 million AUD. These losses are due to the pathogens' mechanism of infection and reproduction. *P. nodorum*, like other Dothideomycetes, is a polycyclic necrotroph. Typical infection begins with either wind-dispersed ascospores or splash-dispersed pycnidiospores landing on a leaf, followed by invasive hyphal growth. The fungus uses effector proteins in a gene-for-gene manner with the host to kill the plant tissue, generating lesions of necrotic tissue surrounding the infection site. The decaying plant tissue is then assimilated and over the course of several days pycnidia develop, continuing the disease cycle. By decreasing the photosynthetic area of the Flag and Flag-1 leaves, the fungus inhibits grain-filling leading to yield losses. Sporulation and virulence are the two crucial aspects for disease development in the *P. nodorum*-wheat pathosystem and form the basis of this project.

A forward genetics approach was employed to discover novel mechanisms by which *P. nodorum* facilitates infection on wheat. A library of random insertion mutants of *P. nodorum* was generated utilising *Agrobacterium*-mediated transformation. Subsequently, the library was screened for loss of virulence phenotypes on a susceptible cultivar of wheat. This was complemented by a second screen identifying gain of virulence phenotypes on a non-susceptible cultivar. From a library of 950 transformants seven displayed a consistent avirulent phenotype on the susceptible wheat cultivar, and one displayed a partial gain of virulence on the non-susceptible cultivar. The genomes of the seven strains of avirulent *P. nodorum* were then sequenced via the Illumina

MiSeq short-read platform. *De novo* genome assembly identified two disrupted loci in a single avirulent strain. These loci were identified through BLAST homology as a putative *Copper-dependent amine oxidase*, and a *Catechol-1,2-dioxygenase*. A previous study identified a *Catechol-1,2-dioxygenase* as a key virulence factor in *Fusarium oxysporum*. However, an independent gene disruption concluded that this gene is not required for virulence in *P. nodorum*.

Complementary to the forward genetics approach to identifying novel mechanisms of virulence, a combined transcriptomics and metabolomics approach was employed to decipher sporulation in this pathogen. This is of particular interest as the canonical sporulation pathways in *Aspergillus* or *Neurospora* have been previously shown to be not applicable in *P. nodorum*. This aspect of my project involved a differential gene analysis of fungal material collected at three key developmental time points. Sporulation was initiated *in vitro* by the non-proteinaceous amino acid, *gamma-aminobutyric acid* (GABA). I have previously published a reported describing sporulation induction in *P. nodorum* and related species by application of exogenous GABA. By comparing gene expression in the fungus just prior to pycnidia formation, sporulation and subsequent to sporulation, I was able to identify several key genes which are involved in initiating a sporulation cascade. Further, I was able to elucidate a polyamine pathway intrinsically linked to *P. nodorum* sporulation. This study garners genetic and biochemical insight into the two aspects of the *P. nodorum* life cycle that are crucial for disease development.

## Table of Contents

## List of Figures

| | |
|---|---|
| **Supplementary Figure 3.05** | *InterProScan prediction of protein domains in the SNOG_02686 amino acid sequence* |
| **Supplementary Figure 3.06** | *InterProScan prediction of protein domains in the SNOG_07954 amino acid sequence* |
| **Supplementary Figure 3.07** | *Catechol-1,2-dioxygenase detached leaf pathogenicity assay, repetition* |
| **Figure 4.01** | *Schematic representation of the GABA shunt. Image adapted from Mead et al (2013)* |
| **Figure 4.02** | *Diagram of experimental design, indicating the key developmental time points and treatments of* P. nodorum *from which RNA and metabolite samples were taken* |
| **Figure 4.03a** | *Pycnidiation at key developmental time points of P. nodorum during in vitro growth* |
| **Figure 4.03b** | *Sporulation at key developmental time points of* P. nodorum *during* in vitro *growth* |
| **Figure 4.04** | *Multivariate analysis of RNAseq samples taken from key developmental time points of* P. nodorum *growth in the presence and absence of GABA* |
| **Figure 4.05** | *Cellular function of the top 50 differentially expressed genes in* P. nodorum *between undifferentiated cells and cells undergoing various stages of asexual reproduction* |
| **Figure 4.06** | *Expression of the non-ribosomal peptide synthase biosynthetic gene cluster, Pn.03620, during* P. nodorum *asexual development* |
| **Figure 4.07** | *Expression of the polyketide synthase biosynthetic gene cluster, Pn.08274, during* P. nodorum *development* |
| **Figure 4.08** | *Expression of the polyketide synthase biosynthetic gene cluster, Pn.11076, during P. nodorum asexual development* |
| **Figure 4.09** | *Expression of the polyketide synthase biosynthetic gene cluster, Pn.15829, in the during* P. nodorum *asexual development* |
| **Figure 4.10** | *Principal component analysis, depicting dimensions 1 and 2, of P nodorum samples chemically analysed by gas chromatography-mass spectrometry* |
| **Figure 4.11** | *Abundance of trehalose in* P. nodorum *at key developmental time points* |
| **Figure 4.12** | *Gene expression of known Trehalose-6-phosphate synthase at developmental stages of* P. nodorum *asexual development in the presence and absence of GABA* |
| **Figure 4.13** | *Abundance of ornithine in P. nodorum at key developmental time points* |
| **Figure 4.14** | *Radial growth of* P. nodorum *colonies grown on solid minimal medium supplemented with 5mM of intermediates of the ornithine biosynthetic pathway* |

## List of Tables

## List of Abbreviations

| Abbreviation | Description |
|---|---|
| AA | Amino acid |
| ALMT | Aluminium activated malate transporter |
| BAM | Binary alignment map |
| BLAST | Basic local alignment sequence tool |
| BLASTp | Basic local alignment sequence tool for proteins |
| bp | Base pairs |
| BRF | Biomolecular resource facility |
| Bs | *Bipolaris sorokiniana* |
| ca. | Circa |
| CAP | Cysteine-rich secreted protein |
| CAPE | CAP-derived peptide |
| cm | Centimeters |
| CPM | Counts per million |
| diam. | Diameter |
| DNA | Deoxynucleic acid |
| dpi | Days post inoculation |
| ETI | Effector triggered immunity |
| ETS | Effector triggered susceptibility |
| eV | Electron volt |
| *f. sp.* | *Forma specialis* |
| GABA | γ-aminobutyric acid |
| GABOB | γ-amino-ß-hydroxybutyric acid |
| GC-MS | Gas chromatography-Mass spectrometry |
| GCqTOF-MS | Gas Chromatography quantitative Time of Flight-Mass Spectrometer |
| gDNA | Genomic DNA |
| GFF | Gene feature format |
| GFP | Green fluorescent protein |
| GLM | General linear model |
| GTF | Gene transfer format |
| GUI | Graphical user interface |
| HGT | Horizontal gene transfer |
| Hph | Hygromycin B phosphotransferase |
| HR | Homologous recombination |
| Hz | Hertz |
| InDel | Insertion deletion |
| kb | Kilo base pairs |
| KEGG | Kyoto encyclopaedia of genes and genomes |
| log2CPM | Counts per million measured on a log2 scale |
| M | Molar |
| *m/z* | Mass to charge ratio |
| Mb | Mega base pairs |
| mil | Million |

| | |
|---|---|
| ml | Millilitres |
| mm | Millimetres |
| mM | Millimolar |
| NBLRR | Nuclear-binding leucine rich repeats |
| NCBI | National centre for biotechnology information |
| NEB | New England Biolabs |
| ng | Nanogram |
| NHEJ | Non-homologous end joining |
| nm | Nanometres |
| nr | Non-redundant |
| $OD_{600}$ | Optical density at 600nanometers |
| Pat | *Phaesophaeria avenaria-tritici* |
| PC | Principal component |
| PCR | Polymerase chain reaction |
| PE | Paired-End |
| PEG | Polyethylene glycol |
| Pfam | Protein family |
| PKS | Polyketide synthase |
| *pl.* | Plural |
| PPO | Polyphenol Oxidases |
| PR1 | Pathogenesis related protein 1 |
| PTI | Pathogen triggered immunity |
| Ptr | *Pyrenophora tritici-repentis* |
| RNA | Ribonucleic acid |
| RNAi | Interference RNA |
| rpm | Revolutions per minute |
| SAM | Sequence alignment map |
| SDS | Sodium dodecyl sulphate |
| Sn | *Stagonospora nodorum* |
| SNB | Stagonospora nodorum blotch |
| SNOG | Stagonospora nodorum gene |
| SNP | Single nucleotide polymorphism |
| *sp.* | *Species* |
| TAIL PCR | Thermo asymmetrical interlaced polymerase chain reaction |
| TCA | Tricarboxylic acid |
| TMS | Trimethylsilyl |
| U.V. | Ultraviolet |
| UAS | Upstream activation sequence |
| UTR | Upstream untranslated region |
| WAK | Wall associated kinase |
| WGS | Whole genome sequencing |
| wt | Wild type |
| µg | Microgram |
| *µl* | Microliters |
| *µm* | Micrometres |
| µM | Micromolar |

# Chapter 1: General introduction to *Parastagonospora nodorum* and forward genetics

## *1.1 Parastagonospora nodorum*

### *1.1.1 Parastagonospora nodorum* is a threat to food production

Many economically important crop diseases are caused by fungi in the class, Dothideomycetes. This pathogen-enriched class of fungi includes *Parastagonospora nodorum* (syn. *Phaesophaeria nodorum*) the causal agent of the wheat disease, Septoria nodorum blotch (SNB) (Hane et al., 2007; Oliver et al., 2012). In 2009, SNB was the third most economically destructive disease to the Australian wheat industry estimated to cost over $108mil AUD annually in losses alone (Table 1.01) (Murray and Brennan, 2009). These losses are due to the polycyclic life strategy of the fungus (Oliver et al., 2012).

*(Table 1.01 The five most economically significant wheat pathogens in Australia, adapted from Murray and Brennan (2009))*

| DISEASE | $/ha | $ million |
|---|---|---|
| Yellow spot | 17.82 | 212 |
| Stripe rust | 10.62 | 127 |
| Septoria nodorum blotch | 9.07 | 108 |
| Crown rot | 6.63 | 79 |
| *Pratylenchus neglectus* | 6.13 | 73 |
| Total losses from others | 26.37 | 314 |
| TOTAL PRESENT LOSS | 76.64 | 913 |

### 1.1.2 A polycyclic infection cycle is key to disease development

Like many other Dothideomycetes, *P. nodorum* exhibits a polycyclic lifestyle whereby the pathogen infects the host, asexually reproduces, and reinfects the host multiple times throughout a growing season (Solomon et al., 2006; Rudd et al., 2015). Field infection by

*P. nodorum* begins with the use of infected grain or when a wheat leaf comes in contact with a spore. Sexual spores from infected stubble of the previous year are wind dispersed over long distances. While, asexual spores are splash dispersed by water droplets within or between plants (Figure 1.01) (Oliver et al., 2012). After landing on the plant surface, the spore germinates and invades the plant tissue through natural openings or by directly penetrating the host (Solomon et al., 2006). Germinating spores and penetration of host tissue can be seen in Figure 1.02.

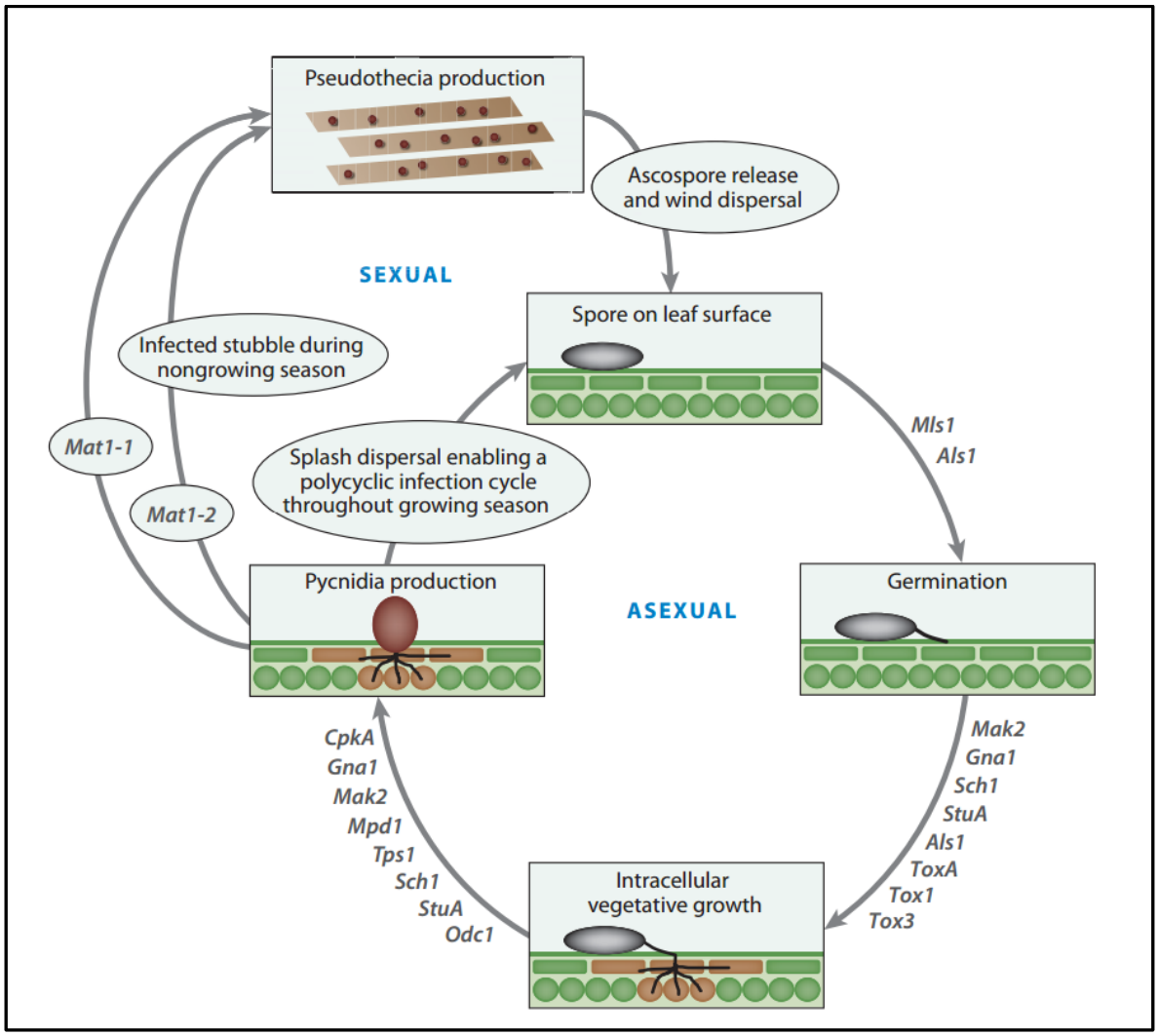


*(Figure 1.01: The polycyclic nature of* P. nodorum *relies upon several genetic and primary metabolic components. Image adapted from (Oliver et al., 2012))*

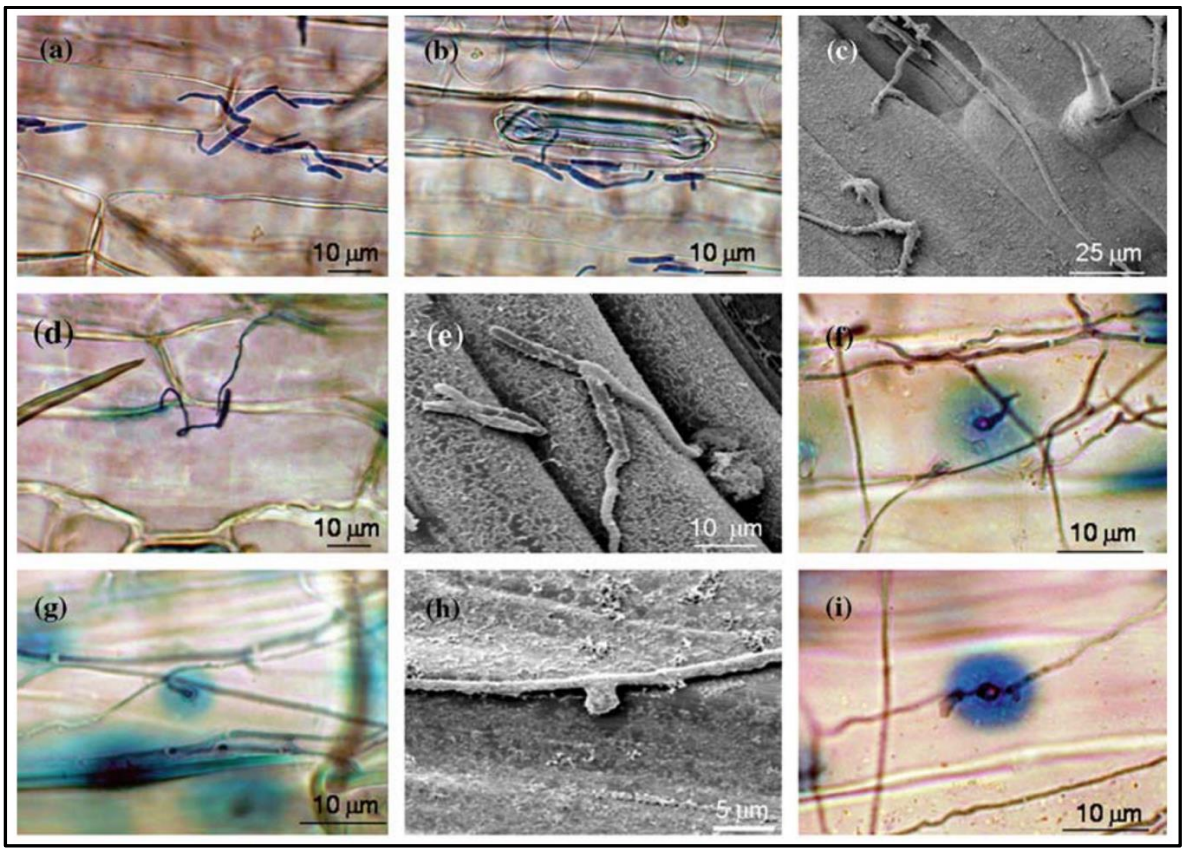


*(Figure 1.02: Germination and penetration of host tissue by* P. nodorum *spores. Panels a, b, d, f, g and i show aniline blue stained fungal spores germinating* ***(a)*** *and penetrating the host via a stomate* ***(b)*** *or by direct penetration* ***(d)***, ***(f)*** *and* ***(g)***. ***(i)*** *depicts the callose deposition underneath a penetrating hypha in blue. Panels c, e and h, show electron microscopy images of hyphae extending across the leaf surface and penetrating the host- via a stomate* ***(c)*** *or direct penetration* ***(e)(h)***. *Adapted from Solomon et al (2006))*

### 1.1.3 Proteinaceous effectors are the driving cause of SNB

Upon invasion of the host, the fungus secretes small, cysteine-rich proteins known as effectors (Oliver et al., 2012). These effector proteins interact in a gene-for-gene manner with dominant susceptibility genes in the host to induce cell death. Figure 1.03 demonstrates the requirement for both of these components to be present with the SnToxA-*Tsn1* interaction.

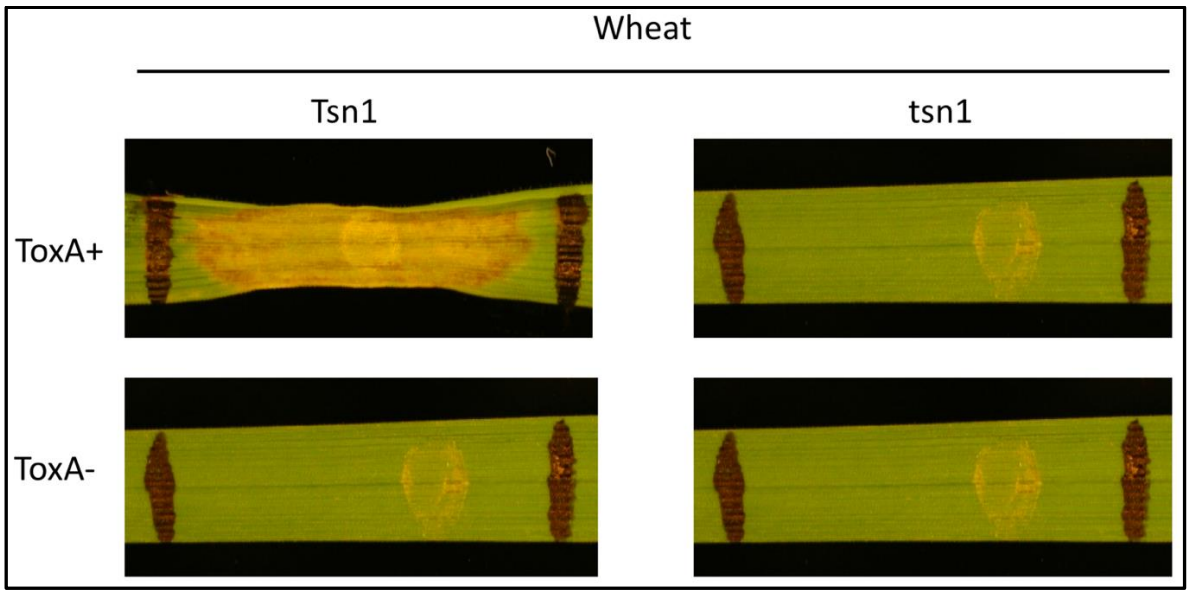


*(Figure 1.03: Interaction of the* P. nodorum *effector, ToxA, with susceptible* Tsn1 *and non-susceptible* tsn1 *wheat cultivars. The Sn.ToxA protein has been infiltrated into the wheat leaf in the upper two panels, while buffer has been infiltrated in the lower two. The left two panels show a wheat cultivar harbouring the ToxA susceptibility gene, Tsn1, while the right two panels show a wheat cultivar lacking this particular susceptibility gene. The smaller brown patches in the right two panels and bottom panels is due to damage by the syringe during infiltration. Adapted from in house data.)*

This interaction is known as effector triggered susceptibility (ETS) and acts in an inverse manner to the traditional, gene-for-gene, effector trigger immunity (ETI) observed in biotrophs (Jones and Dangl, 2006; McDonald and Solomon, 2018). Lesions of necrotic plant tissue surround infections sites when both a susceptibility gene and corresponding effector are present (Friesen et al., 2008). The effectors are expressed by the pathogen within 72 hours of contact with the host before necrosis develops (Faris et al., 2011; Liu et al., 2016, 2009). The decaying plant tissue then provides nutrients for the fungus to proliferate in the host and reproduce, leading to field epidemics. The ability to kill host

tissue, conferred by the effectors, has allowed *P. nodorum* to become a destructive pathogen.

The molecular mechanisms leading to plant cell death, during ETS interactions, are currently unknown. However, the *P. nodorum*-wheat pathosystem provides a model for dissecting ETS interactions and advancing our understanding of effector proteins (Breen et al., 2016; Lin et al., 2018). *P. nodorum* harbors three effector genes (*Sn.ToxA, Sn.Tox1* and *Sn.Tox3)* known to interact with the wheat susceptibility genes *Tsn1, Snn1* and *Snn3* and result in necrotic lesions (Friesen et al., 2008). The complex role these genes play in disease is beginning to be revealed through a concerted effort of localization, structural elucidation, protein-protein interaction, population genetics and bioinformatic studies (Breen et al., 2016; Liu et al., 2016; McDonald et al., 2018; Sperschneider et al., 2017; Zhang et al., 2017). Figure 1.04 summarises the current understanding of *P. nodorum* effector interactions with the wheat host.

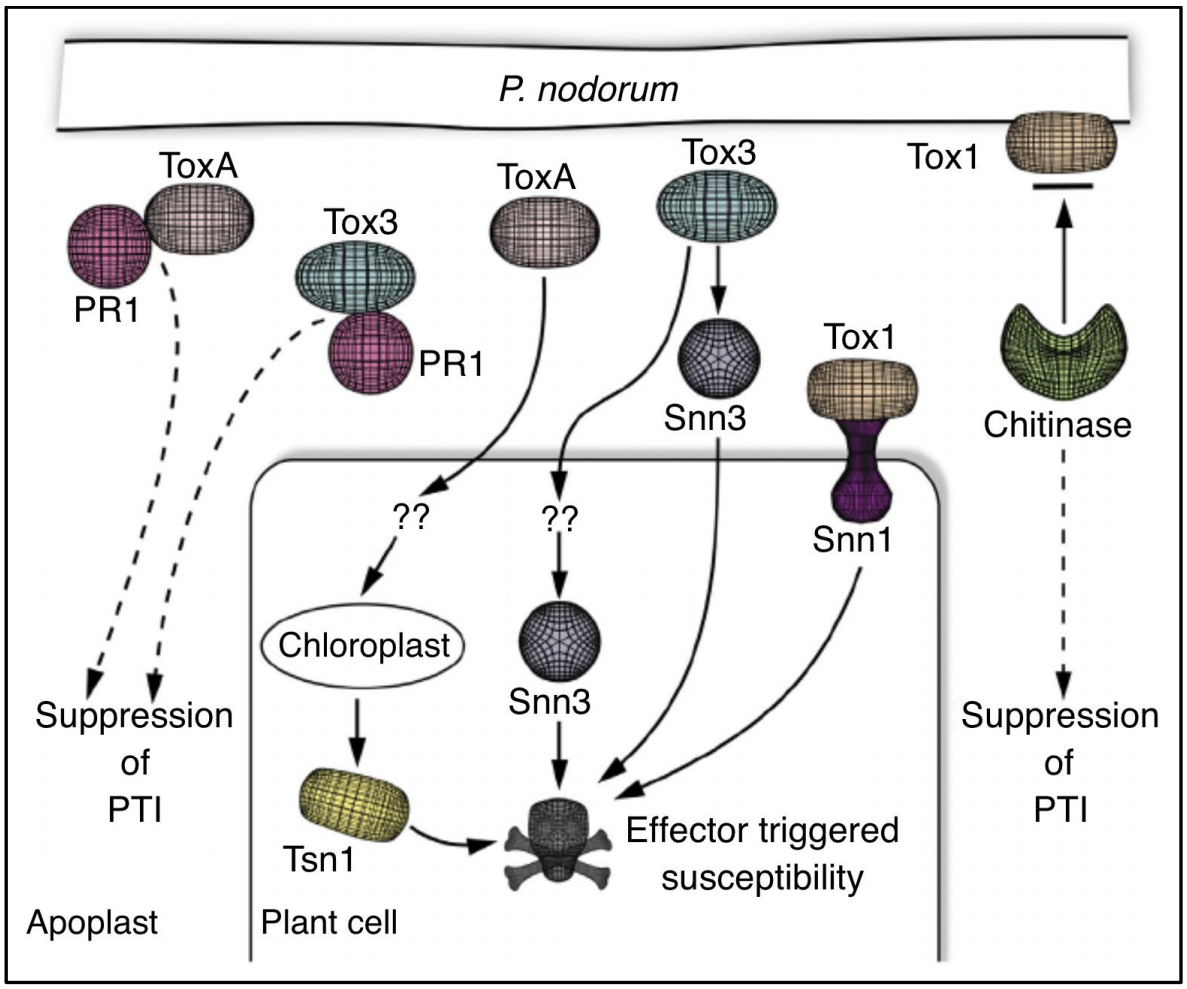


*(Figure 1.04: Model of proposed interactions between* P. nodorum *effectors, Sn.ToxA, Sn.Tox1 and Sn.Tox3, with the host. PR1, Pathogenesis related protein 1. PTI, Pathogen triggered immunity. Source:* (McDonald and Solomon, 2018)*)*

### 1.1.3.1 Sn.ToxA

The proteinaceous effector, Sn.ToxA, is secreted by *P. nodorum* during infection on wheat cultivars carrying the susceptibility gene, *Tsn1* (Liu et al., 2006). *ToxA* has no known function other than to induce necrosis in a gene-for-gene manner with *Tsn1* - contrary to the classical biotrophic model of effectors and R-genes (Jones and Dangl, 2006; McDonald and Solomon, 2018). This compatible interaction results in plant cell death and the formation of necrotic lesions. The molecular basis for the Sn.ToxA-*Tsn1* interaction and subsequent progression to lesion development is currently unknown, however, significant progress has

been made in the last 15 years. The susceptibility gene, *Tsn1*, has been cloned and determined to encode the serine/threonine protein kinase, nucleotide binding-leucine rich repeat (NB-LRR) and a wall associated kinase (WAK) domains normally associated with resistance genes (Faris et al., 2010). The plant Pathogen Response 1 (PR-1-5) protein was recently discovered to directly interact with the Sn.ToxA protein (Breen et al., 2016; Lu et al., 2014). Further, GFP fusion and localisation experiments have revealed that Ptr.ToxA is internalised by the plant cell and localised to the chloroplast (Manning and Ciuffetti, 2005; Manning et al., 2007).

Intriguingly, *P. nodorum* is not the only fungal necrotroph to harbour the *ToxA* gene. *ToxA* has also been identified in the wheat pathogen *Pyrenophora tritici-repentis* (*Ptr.ToxA*) the wheat and barley pathogen *Bipolaris sorokiniana* (*Bs.ToxA*) and the oat pathogen *Phaesophaeria avenaria tritici* (*Pat.ToxA*) (Friesen et al., 2006; McDonald et al., 2018, 2012). *P. nodorum* is thought to have donated *ToxA* to *P. tritici-repentis* through horizontal gene transfer (HGT) c.a. 1941. This subsequently led to the emergence of *P. tritici-repentis* as a new and devastating pathogen (Friesen et al., 2006). The *ToxA* locus in these pathogens is *nearly* identical leading to a range of *ToxA* haplotypes in the global pathogen population. The global population of *P. nodorum* contains the highest variation in *ToxA* haplotypes, suggesting that it has harboured this genetic region the longest. Conversely, the recent discovery of *ToxA* in *B. sorokiniana* casts doubt over the progenitor of *ToxA*. The *B. sorokiniana ToxA* haplotype has not been found in any isolate of *P. nodorum*, suggesting independent acquisition of this virulence factor (Friesen et al., 2006; McDonald et al., 2018).

#### 1.1.3.2 Sn.Tox1

*P. nodorum* expresses the proteinaceous effector, Sn.Tox1, during a compatible interaction with wheat cultivars containing the dominant susceptibility gene, *Snn1*. This inverse gene-for-gene interaction results in plant cell death and necrotic lesions (Liu et al., 2012). Similar to the Sn.ToxA-*Tsn1* interaction, little is known about the molecular mechanism linking the virulence factor to the susceptibility genes. However, *Snn1* has been cloned and found to encode serine/threonine protein kinase, nucleotide binding-leucine rich repeat (NB-LRR) and a wall associated kinase (WAK) domains (Shi et al., 2016)). Further, significant advances have been made to determine the role of Sn.Tox1 during infection. Liu et al (2016) determined Sn.Tox1 chitin binding activity and used a GFP:Tox1 fusion protein to visualise Sn.Tox1 localisation to the hyphal tips of *P. nodorum* and penetration points on the leaf surface. They go on to show that the Sn.Tox1 protein confers protection from wheat chitinases to *P. nodorum* and three other fungi. These results suggest that Sn.Tox1 protects the fungus from cell wall degrading chitinases and masks chitin fragments from triggering the plant immune system (Liu et al., 2016). Despite benefits from harbouring this virulence factor, implied by these observations, *Sn.Tox1* has not been driven to allelic fixation and exists as a presence/absence polymorphism in the global *P. nodorum* population. This, interestingly, indicates that *Sn.Tox1* may be dispensable during disease formation in the field or interacts in a more dynamic way on a population level (McDonald and Solomon, 2018).

#### 1.1.3.3 Sn.Tox3

The *P. nodorum* effector, *Sn.Tox3,* induces necrosis in an inverse gene-for-gene interaction on wheat cultivars harbouring the dominant host susceptibility gene, *Snn3.* Although *Sn.Tox3* has been cloned and characterised, *Snn3* is yet to be identified (Friesen et al., 2008;

Liu et al., 2004). Recently, Sn.Tox3 was found to directly interact with the plant Pathogen Response 1 protein, PR-1-1 and six other members of this family (Breen et al., 2016). PR-1-1 contains a peptide domain known as CAPE1. Wheat plants pre-treated with a synthesised CAPE1 peptide showed enhanced susceptibility to *P. nodorum* infection. Enhanced susceptibility was only observed during Tox3-*Snn3* interactions and did not extend to the other PR-1 interacting effector, *Sn.ToxA*. This indicates that CAPE1 is integral to the Sn.Tox3-*Snn3* molecular cascade, resulting in cell death, but doesn't play a role during the Sn.ToxA-*Tsn1* interaction (Breen et al., 2017, 2016; Lu et al., 2014).

### 1.1.4 Effector driven virulence is only one component of SNB

Despite the substantial role of *Sn.ToxA, Sn.Tox1* and *Sn.Tox3* during infection, they are not the only virulence factors involved and there is evidence for their redundancy. Through a presently unknown mechanism, the disruption of one effector can increase expression of another during infection (Phan et al., 2016). Further, culture extract from a triple effector knock-out in the SN15 strain is able to induce necrosis (Tan et al., 2015). These two pieces of evidence indicate the presence of additional, undiscovered virulence factors. Aside from the secreted effector proteins, a plethora of primary metabolic pathways are proven requirements for *P. nodorum* to cause disease. For example, a *Short-chain dehydrogenase* was found by Tan et al (2008) to play an integral role in formation of the pathogens reproductive structure, the pycnidium. Without this metabolic gene the fungus is unable to reproduce, this disrupting the disease cycle. As such, there are potentially many virulence factors yet to be discovered.

#### 1.1.4.1 A short-chain dehydrogenase is required for differentiation of the pycnidium sub-parietal layer, leading to sporulation

G-protein signalling is a highly conserved eukaryotic signalling pathway that relies upon a heterotrimeric protein complex bound to the cytoplasmic side of a membrane bound receptor (Li et al., 2007; Urano et al., 2013). Inhibiting this pathway in *P. nodorum*, by disrupting the Gα subunit of the protein complex, lead to a pleiotropic phenotype. The *Pn.gna1* mutant was unable to colonise the host, sporulate or melanise (Solomon et al., 2004).

To deconvolute the *Pn.gna1* phenotype, protein gel analysis combined with protein mass-spectrometry identified differentially abundant proteins between the wild-type and *Pn.gna1* strains (Tan et al., 2008). This revealed a Short-chain dehydrogenase (Shc1) to be 18-fold less abundant in the *Pn.gna1* mutant, indicating its regulation by G-protein signalling. Subsequent disruption of the identified *P. nodorum* short-chain dehydrogenase (*Pn.Sch1*) did not affect virulence. However the *Pn.sch1*strains displayed reduced growth on minimal medium as well as both *in vitro* and *in planta* sporulation (Tan et al., 2008). Pycnidia produced by the mutant strains were smaller than the wildtype counterparts and, *in planta*, failed to produce the spore exudate known as cirrus. GFP tagging Pn.Sch1 in the wildtype strain indicated high expression of the protein in the inner layer of the pycnidium, known as the sub-parietal layer, but not in the melanised outer layer or vegetative hyphae. On a finer scale, electron microscopy revealed that the sub-parietal layer was malformed in the mutant strains and the conidiogenic cells failed to differentiate into pycnidiospores (Tan et al., 2008).

Tan et al (2008) showed that a *Short-chain dehydrogenase* was regulated by the G-protein signalling cascade and played a key role in pycnidial cell differentiation during sporulation in *P. nodorum* (Solomon et al., 2004; Tan et al., 2008). The signalling cascade from G-protein to sporulation exemplifies the complex nature of asexual development in fungal pathogens and that there are more facets to SNB than the effectors. To resolve more of these pathways a forward genetics approach was employed- an approach not previously reported to have been applied to *P. nodorum*.

### 1.1.5 Sporulation is a vital component for *P. nodorum* to cause disease

Sexual reproduction in Ascomycetes is initiated by pheromone communication between hyphae of compatible mating types (Jones, S. K. Jr. and Bennett R. J., 2011). Upon recognition of a compatible mating type, hyphal cells differentiate into sexual structures known as gamatangia. The female gamatangium is composed of a large polynucleated cell, known as the ascogonium. The ascogonium is attached to a trichogyne, a multicellular attachment that grows towards and entangle male cells (Debuchy et al, 2010). These male cells may be specialised hyphae known as antheridium, but also include asexual spores and broken hyphae These various male cells donate a nucleus to the trichogyne, introducing new DNA and initiating sexual fruiting body development (Bouhouche et al, 2004; Debuchy et al, 2010).

This process leading to sexual fruiting body development is finely orchestrated by a genetic cascade controlled by genetic loci known as mating type loci. The single mating type locus in Ascomycetes, known as MAT1, is bi-allelic leading to a bipolar method of reproduction. Conversely, ancestral Basidiomycetes were tetrapole, containing two multi-allelic MAT

loci (Metzenberg, R. L. and Glass, L. N., 1990; Bakkeren, G. and Kronstad, J.W., 1994). The sequence variants leading to polarity are known as idiomorphs. Idiomorphs contain a diverse set of genes in the Ascomycetes. This variation leads to species that are able to mate with individuals of the same mating type, homothallism, and species that require individuals to harbour differing mating types, heterothallism (Metzenberg, R. L. and Glass, L. N., 1990; Bennett et al, 2003). Despite high variation in idiomorph content Ascomycete mating types invariably contain either of two transcription factors. These transcription factors are similar to either the MATα1 or the High-Mobility Group (HMG) proteins found in *Saccharomyces cerevisiae*, and are the identifying features of the two Ascomycete mating types MAT1-1 and MAT1-2 (Bennett et al, 2003).

Despite the content variation of Ascomycete MAT1 loci they are highly conserved within the class Dothideomycete, including *P. nodorum*. *P. nodorum* is heterothallic, or self-incompatible, requiring two strains of opposing mating types for sexual reproduction (Bennett et al, 2003). These mating types have been isolated from field infections and epidemiological studies have identified genetic recombination patterns that indicate *P. nodorum* undergoes sexual reproduction in the field (Sommerhalder et al, 2010; Bennett et al, 2003). Unfortunately, there have been no reports of *P. nodorum* consistently reproducing sexually under laboratory conditions.

Asexual reproduction in *P. nodorum* begins with the melanisation of vegetative mycelia, which differentiate and fuse into the asexual fruiting body known as a pycnidium (*pl.* pycnidia). Spores developing within a pycnidium are shown in Figure 1.05 (Douaiher et al., 2004; Solomon et al., 2006). Asexual spores develop within pycnidia, eventually releasing in a pink fluid known as cirrus before splash dispersing across infected leaf tissue or onto

nearby plants, repeating the infection cycle. Infection and re-infection of the host occurs multiple times throughout the growing season leading to large losses of leaf tissue in the field. This reduced leaf tissue lowers the photosynthetic capability of the plant, ultimately diminishing the plants productivity and grain yield (Douaiher et al., 2004; Solomon et al., 2006).

Disrupting sporulation in *P. nodorum* breaks the infection cycle, effectively disarming the pathogen. Although able to infect the host plant, the fungus is unable to cause yield-reducing field epidemics. Several core genetic elements and primary metabolic pathways, essential for *P. nodorum* sporulation, have been elucidated over the last few decades and are summarised in Figure 1.01 (Oliver et al., 2012). Despite these advances, many of the key genes and pathways required for lesion formation and asexual sporulation in *P. nodorum* remain undiscovered.

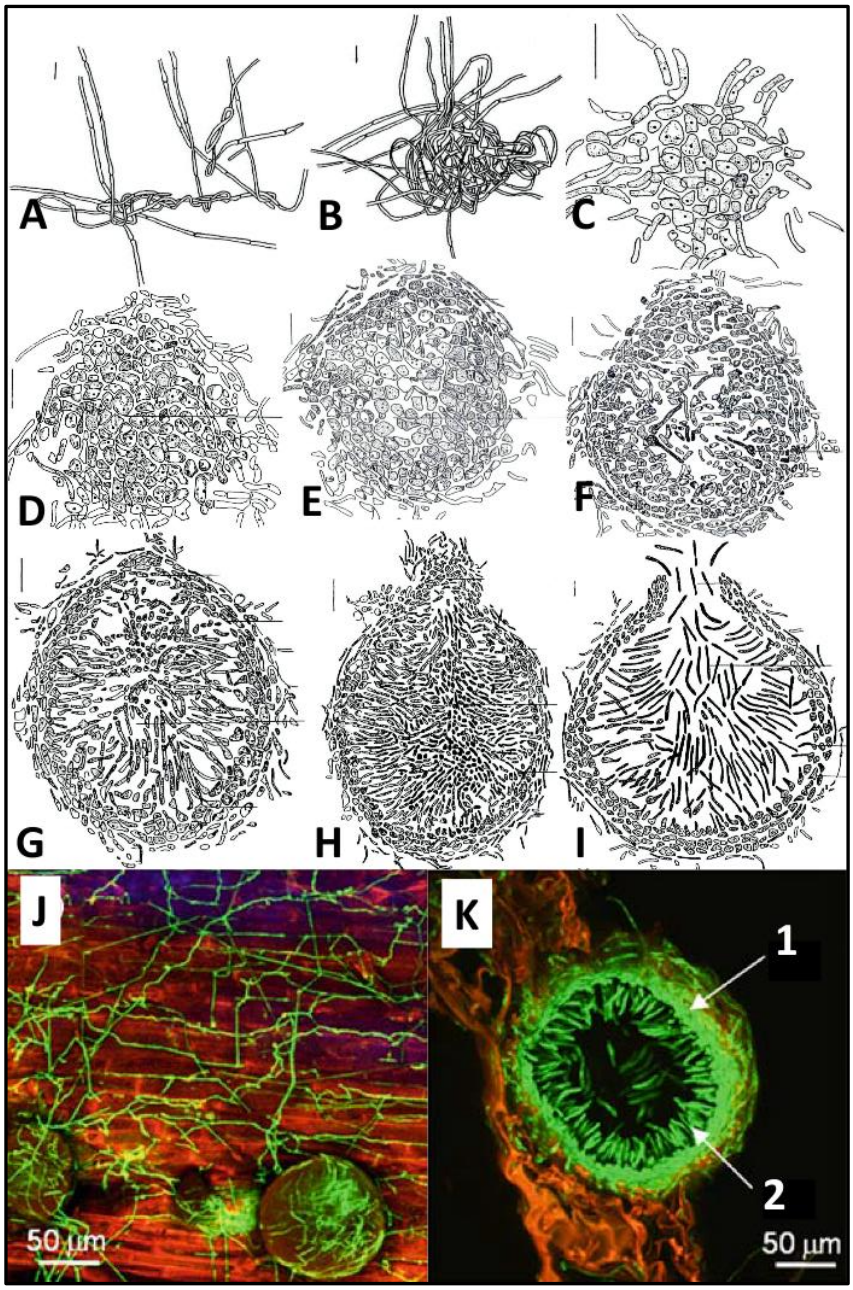


*(Figure 1.05:* P. nodorum *asexual reproductive cycle.* ***A-I****) Cartoon sketch depicting* P. nodorum *cell differentiation leading to pycnidium formation. Mycelia aggregate into a knot in box A, and develop into a ruptured pycnidium releasing spores in box I. Scale bar represents 10µm. Images adapted from* (Douaiher et al., 2004)*.* ***J and K****) Electron microscopy image of* P. nodorum *infecting a wheat leaf, and the developing spores within a pycnidium. Scale bar represents 50µm. Arrow 1 indicates the sub-parietal layer and arrow 2 indicates developing spores. Images adapted from* (Solomon et al., 2006)*)*

## 1.2 Forward genetics

### 1.2.1 Definition, types and history

Many of the greatest breakthroughs in our understanding of biological systems have come from randomly inactivating individual genes within an organism followed by targeted phenotypic screens (Bleecker et al., 1988; Clutterbuck, 1969; Epstein et al., 1963; Hartwell et al., 1973; MacGurn and Cox, 2007; Weitz et al., 2005). This process is known as forward genetics. Although the effects of mutagenesis were known decades earlier (Muller, 1927), the first active forward genetics studies weren't reported until the early 1940's focussing on the common mould *Neurospora crassa* and the bacterium *Escherichia coli* (Beadle and Tatum, 1941; Gray and Tatum, 1944). Ionising radiation was used to create libraries of randomly generated mutants, which were subsequently screened for the absence of growth on specific nutrient sources (Beadle and Tatum, 1941; Gray and Tatum, 1944). At this time, before the structure of DNA was known, interesting phenotypes could not be linked to a specific nucleotide sequence. Modern forward genetic screens have overcome this limitation using advanced molecular techniques, such as inverse PCR, plasmid rescue and Thermo Asymetic InterLaced PCR (TAIL-PCR) (Kemppainen et al., 2008; Schumacher et al., 2014; Villalba et al., 2001). These contemporary studies cover many model and non-model organisms and not only screen for observable loss of function mutants but also gain of function mutants and encompass multigenerational screens (Brown et al., 2014; Minty et al., 2011; Scalliet et al., 2012; Urban et al., 2015).

A plethora of mutagenesis methods have been developed for generating a mutant library, allowing screens to be tailored to a specific organism. The crucial advantage of forward genetics lies in its ability to "blindly" elucidate the role of distinct genomic loci whose functions were previously unknown. On numerous occasions, novel lines of investigation

have been opened through forward genetic screens applied to non-model organisms of industrial, medical or agricultural value (Brown et al., 2014; Minty et al., 2011; Urban et al., 2015).

Historically, forward genetics screens have faced a trade-off between the difficulty of generating and screening mutants, and the potential biological insight gained. There are three prominent complications when considering a forward genetics screen: **(1) Comprehensive mutant libraries are difficult to generate, (2) Screening mutant libraries is laborious and (3) Causal mutation sites are difficult to determine.** Until now, the most formidable hindrance to a forward genetics screen has been linking the desired phenotypes with the responsible mutations. These mutations were filtered from other mutations in the strains of interest using sexual back-crossing. Crossing provides a controlled genetic background for the desired mutation to be introduced during sexual recombination (Balhadere et al., 1999; Gout et al., 2006). The progeny from this recombination were then screened again for the desired phenotype. Mutations in strains exhibiting the phenotype of interest were then identified. Commonly identified mutations between strains of the same phenotype were then confirmed to be the causal mutation by reverse genetics (Gout et al., 2006). The secondary value of sexual crossing comes from its ability to filter untagged mutations from tagged. For example, Balhadere et al. (1999) identified five avirulent strains of *Fusarium graminearum* generated by random insertion mutagenesis with a Hygromycin B resistance marker. However, the resistance marker segregated with the avirulence phenotype after sexual crossing in only two of the five avirulent strains (Balhadere et al., 1999). This indicated that the mutagenesis technique, Restriction Enzyme Mediated Integration, or background mutation rates were responsible

for the phenotype, but not the insertion sequence. This inhibits using the insertion sequence to find the disrupted genomic loci responsible for these phenotypes.

Identifying these sites using molecular techniques, and the sexual crossing itself, requires months of laboratory work and is often unsuccessful if the mutation lies in a repetitive genome area. However, this complication is now largely resolved by Whole Genome Sequencing (WGS). Current sequencing technology can assemble full microbial genomes from several mutants of interest with minimal resources. Bioinformatic software is available for quality control, genome assembly and determination of mutation sites. These range from simple Graphical User Interfaces (GUIs) with basic predetermined pipelines and parameters, to intensive command line and scripting based packages (Bankevich et al., 2012; Kearse et al., 2012; Zerbino and Birney, 2008). The relative ease with which these data are now obtained not only allows for rapid identification of mutations but also enables the use of older mutagenesis methods that induce single nucleotide polymorphisms.

### 1.2.2 Random Insertional Mutagenesis

There are two main forms of mutation used in forward genetic screens. The first, historically, induced single nucleotide polymorphisms and insertion-deletions (SNP/InDels) by ionizing radiation and DNA alkylating reagents. The second form of mutagenesis, random insertional mutagenesis, has been used to introduce large, exogenous, genetic sequences into target genomes in an unbiased fashion. Random insertional mutagenesis, disrupting loci with a selectable marker, allows mutant strains to be filtered from wild type, as well as providing a known tagging sequence for loci identification. Design and synthesis of disruption constructs for random insertional mutagenesis is more time consuming than methods used SNP-based mutagenesis. Disruption constructs vary in their complexity, but

at the minimum must contain a suitable selectable marker and regulatory elements for the target organism. Current synthetic biology enables a combination of complex insertion sequences and molecular methods to retrieve disrupted loci. However, the declining cost of Whole Genome Sequencing (WGS) makes these loci retrieval systems obsolete.

Insertional mutagenesis has traditionally been favoured as it was generally considered to induce few mutations and allowed the disrupted loci to be identified via molecular methods. Popular molecular methods include plasmid rescue, TAIL-PCR and inverse PCR (Kemppainen et al., 2008; Schumacher et al., 2014; Villalba et al., 2001). However, the benefits of insertional mutagenesis are inconsistent. Several studies have shown that insertional mutagenesis often yields multiple insertion events, fragmented or unstable insertions, or causes severe chromosomal rearrangements and deletions. Further, these chromosomal rearrangements can be found in transformants that have indicated a single insertion via Southern blot analysis resulting in masked or hidden mutations, irretrievable by molecular methods (Balhadere et al., 1999; Urban et al., 2015). Through WGS, disrupted loci can be identified in multiple strains more rapidly and accurately than through traditional molecular methods. Further, by combining *de novo* genome assembly and reference-guided assembly, accurate locus identification can be accomplished in strains containing multiple insertions, chromosomal rearrangements and insertion fragmentations (Urban et al., 2015). Even when chromosomal rearrangements can be identified, these large-scale mutations remove or inactive great swathes of genes which nullify attempts to link genes with phenotypes. Insertional mutagenesis is further limited to vary degrees by logistics of scalability and insertion site bias. Regardless, insertional mutagenesis remains a popular form of creating a mutant library for forward genetics screens and has proven fruitful for many investigations (Schumacher et al., 2014; Yu et al., 2015). One of the most

popular forms of insertional mutagenesis has been via *Agrobacterium*-mediated transformation.

### 1.2.3 Random gene disruption via *Agrobacterium*-mediated transformation

Agrobacter have been a powerful tool to molecular biologists and continue to prove their worth after several decades of use (Marton L., Wullems G. J., Molendijk L., 1979; Rho et al., 2001). The Agrobacterium transformation system originated from a plant pathogen that inserted foreign DNA elements into a plant host to induce tumours and polyamine growth for its nutrients. This pathogen has since been modified for biotechnological application across Kingdoms (Kunik et al., 2001) (de Groot et al., 1998; Frandsen, 2011; Gelvin, 2009, 2003). In the laboratory, the working elements of the Agrobacterium DNA transfer system are separated into two separate plasmids that work in concert. The primary plasmid contains a prokaryotic selectable marker, origin of replication, multiple cloning site and T-DNA sequences which border the insertion sequence (de Framond et al., 1983; Hoekema et al., 1984). A second plasmid, known as the helper plasmid, contains a prokaryotic selectable marker and virulence (vir) genes (de Framond et al., 1983; Hoekema et al., 1984). Activation of the vir genes, by the plant hormone acetosyringone, initiates the transfer of DNA from within the T-DNA borders into the host cell genome (Lee et al., 1992; Wang et al., 1987).

The crucial advantage of the Agrobacterium transformation system is the known insertion sequence between the T-DNA borders, and delegation of transformation to a bacterium, producing readily identifiable mutations (Kemppainen et al., 2008). Selection bias towards certain integration sites, as well as the insertion rate has been the subject of thorough investigation (Alonso et al., 2003; Choi et al., 2007; Meng et al., 2007; Qin et al., 2003).

Agrobacterium generally introduces a single insertion into the host genome, with low frequency of insert fragmentation (Alonso et al., 2003; Meng et al., 2007). This is advantageous when determining the causal loci for observed phenotypes but may be disadvantageous in organisms with large or highly redundant genomes. The Agrobacterium disruption vector is developed either through cloning or direct vector synthesis, and a range of designs may be employed to optimise a forward genetics screen. Initial strain development is time consuming, however, once a strain of bacterium is established the subsequent genetic transformations are quick, inexpensive and easily scalable (Meng et al., 2007; Idnurm et al., 2009).

## 1.3 Aims of this project

In order to cause SNB, *P. nodorum* must infect and kill the host, as well as sporulate and reinfect the host. Without either of these elements, the fungus is unable to cause the yield losses that make this pathogen a threat to food security. I employed a forward genetics approach to discover novel genetic elements required by *P. nodorum* to infect the host. I then combined transcriptomics and metabolomics to investigate the genetic and biochemical mechanisms orchestrating asexual development.

**Aims:**

**1) Elucidation of novel virulence factors in *P. nodorum***

a) To generate a library of phenotypically characterised random *P. nodorum* mutants, with few mutations per strain, that can be stored long-term and repeatedly screened.

b) To develop a high throughput pathogenicity assay then screen the random mutant library for strains unable to cause disease symptoms on a susceptible host, and those that can cause disease symptoms on a non-susceptible host.

c) To identify mutations in strains displaying phenotypes of interest, then independently verify the mutation and mechanism producing the observed phenotype.

**2) Genetic and biochemical investigation of asexual development in *P. nodorum***

a) To determine key developmental time-points during asexual reproduction

b) To identify key gene expression changes leading to cell differentiation and the development of pycnidia and pycnidospores.

c) To identify metabolites, differentially abundant between stages of asexual development, and characterise their role in vegetative growth, pycnidiation and sporulation.

## 1.4 References for Chapter 1


Alonso, M., Stepanova, A.N., Leisse, T.J., Kim, C.J., Chen, H., Shinn, P., Stevenson, D.K., Zimmerman, J., Barajas, P., Cheuk, R., Gadrinab, C., Heller, C., Jeske, A., Koesema, E., Meyers, C.C., Parker, H., Prednis, L., Ansari, Y., Choy, N., Deen, H., Geralt, M., Hazari, N., Hom, E., Karnes, M., Mulholland, C., Ndubaku, R., Schmidt, I., Guzman, P., Aguilar-henonin, L., Schmid, M., Weigel, D., Carter, D.E., Marchand, T., Risseeuw, E., Brogden, D., Zeko, A., Crosby, W.L., Berry, C.C., Ecker, J.R., 2003. Genome-Wide Insertional Mutagenesis of *Arabidopsis thaliana*. Science (80) 301, 653–657.

Atsumi, S., Wu, T.-Y., Machado, I.M.P., Huang, W.-C., Chen, P.-Y., Pellegrini, M., Liao, J.C., 2010. Evolution, genomic analysis, and reconstruction of isobutanol tolerance in *Escherichia coli*. Molecular Systems Biology 6, 449. https://doi.org/10.1038/msb.2010.98

Bakkeren, G. and Kronstad, J.W., 1994. Linkage of mating-type loci distinguishes bipolar from tetrapolar mating in basidiomyceteous smut fungi. Proceedings of the National Academy of Sciences USA 91, 7085-7089

Balhadere, P. V, Foster, A.J., Talbot, N.J., 1999. Identification of pathogenicity mutants of the rice blast fungus *Magnaporthe grisea* by insertional mutagenesis. Molecular Plant Microbe Interactactions 12, 129–142.

Bankevich, A., Nurk, S., Antipov, D., Gurevich, A.A., Dvorkin, M., Kulikov, A.S., Lesin, V.M., Nikolenko, S.I., Pham, S., Prjibelski, A.D., Pyshkin, A. V., Sirotkin, A. V., Vyahhi, N., Tesler, G., Alekseyev, M. a., Pevzner, P. a., 2012. SPAdes: A New Genome Assembly Algorithm and Its Applications to Single-Cell Sequencing. Journal of Computational Biology 19, 455–477. https://doi.org/10.1089/cmb.2012.0021

Beadle, G.W., Tatum, E.L., 1941. Genetic Control of Biochemical Reactions in *Neurospora*. Proceedings of the National Acadamy of Science U. S. A. 27, 499–506. https://doi.org/10.1086/281267

Bennett, R. S., Hun, S. H., Lee, T. Y., Turgeon, B. G., Arseniuk, E., Cunfer, B. m., Bergstrom, G. C., 2003. Identity and conservation of mating type genes in geographically diverse isolates of *Phaeosphaeria nodorum*. Fungal Genetics and Biology 40, 25-37

Betts, M.F., Tucker, S.L., Galadima, N., Meng, Y., Patel, G., Li, L., Donofrio, N., Floyd, A., Nolin, S., Brown, D., Mandel, M.A., Mitchell, T.K., Xu, J., Dean, R.A.,

Farman, M.L., Orbach, M.J., 2007. Development of a high throughput transformation system for insertional mutagenesis in *Magnaporthe oryzae.* Fungal Genetics and Biology 44, 1035–1049. https://doi.org/10.1016/j.fgb.2007.05.001

Bleecker, A.B., Estelle, M.A., Somerville, C., Kende, H., 1988. Insensitivity to Ethylene Conferred by a Dominant Mutation in *Arabidopsis thaliana*. Science (80). 241, 1086–1089. https://doi.org/10.1126/science.241.4869.1086

Bouhouche, K., Zickler, D., Debuchy, R., Arnaise, S., 2004. Altering a Gene Involved in Nuclear Distribution Increases the Repeat-Induced Point Mutation Process in the Fungus *Podospora anserine*. Genetics 167, 151-159.

Breen, S., Williams, S.J., Outram, M., Kobe, B., Solomon, P.S., 2017. Emerging Insights into the Functions of Pathogenesis-Related Protein 1. Trends in Plant Science 22, 871–879. https://doi.org/10.1016/j.tplants.2017.06.013

Breen, S., Williams, S.J., Winterberg, B., Kobe, B., Solomon, P.S., 2016. Wheat PR-1 proteins are targeted by necrotrophic pathogen effector proteins. Plant Journal 88, 13–25. https://doi.org/10.1111/tpj.13228

Brown, K.M., Suvorova, E., Farrell, A., McLain, A., Dittmar, A., Wiley, G.B., Marth, G., Gaffney, P.M., Gubbels, M.J., White, M., Blader, I.J., 2014. Forward Genetic Screening Identifies a Small Molecule That Blocks *Toxoplasma gondii* Growth by Inhibiting Both Host- and Parasite-Encoded Kinases. PLoS Pathogens 10, https://doi.org/10.1371/journal.ppat.1004180

Bundock, P., Hooykaas, P.J.J., 1996. Integration of *Agrobacterium tumefaciens* T-DNA in the *Saccharomyces cerevisiae* genome by illegitimate recombination. Proceedings of the National Acadamy of Science U. S. A. 93, 15272–15275. https://doi.org/10.1073/pnas.93.26.15272

Chambers, K., Lowe, R., Howlett, B., Zander, M., Batley, J., Van de Wouw, A., Elliott, C., 2014. Next-generation genome sequencing can be used to rapidly characterise sequences flanking T-DNA insertions in random insertional mutants of *Leptosphaeria maculans*. Fungal Biology and Biotechnology 1, 10. https://doi.org/10.1186/s40694-014-0010-y

Choi, J., Park, J., Jeon, J., Chi, M.H., Goh, J., Yoo, S.Y., Park, J., Jung, K., Kim, H., Park, S.Y., Rho, H.S., Kim, S., Kim, B.R., Han, S.S., Kang, S., Lee, Y.H., 2007. Genome-wide analysis of T-DNA integration into the chromosomes of *Magnaporthe oryzae*. Molecular Microbiology 66, 371–382. https://doi.org/10.1111/j.1365-2958.2007.05918.x

Clutterbuck, A.J., 1969. A mutational analysis of conidial development in *Aspergillus*

*nidulans*. Genetics 63, 317–327.

de Framond, A.J., Barton, K.A., Chilton, M.-D., 1983. MINI-Ti: A NEW VECTOR STRATEGY FOR PLANT GENETIC ENGINEERING. Nature Biotechnology 1, 262–269.

de Groot, M.J., Bundock, P., Hooykaas, P.J., Beijersbergen, a G., 1998. *Agrobacterium tumefaciens*-mediated transformation of filamentous fungi. Nature Biotechnology 16, 839–842. https://doi.org/10.1038/nbt0998-839

Debuchy, R., Berteaux-Lecellier, V., and Silar, P., 2010.Cellular and Molecular Biology of Filamentous Fungi: Chapter 34 Mating Systems and Sexual Morphogenesis in Ascomycetes, 501-535

Douaiher, M.N., Halama, P., Janex-Favre, M.C., 2004. The ontogeny of *Stagonospora nodorum* pycnidia in culture. SYDOWIA-HORN- 56, 39–50.

Epstein, R.H., Bolle, A., Steinberg, C.M., Kellenberger, E., Boy de la Tour, E., Chevalley, R., 1963. Physiological Studies of Conditional Lethal Mutants of Bacteriophage T4D. Cold Spring Harbour Symposium on Quantitative Biology 28, 375–394. https://doi.org/10.1101/SQB.1963.028.01.053

Faris, J.D., Zhang, Z., Lu, H., Lu, S., Reddy, L., Cloutier, S., Fellers, J.P., Meinhardt, S.W., Rasmussen, J.B., Xu, S.S., Oliver, R.P., Simons, K.J., Friesen, T.L., 2010. A unique wheat disease resistance-like gene governs effector-triggered susceptibility to necrotrophic pathogens. Proceedings of the National Acadamy of Science U. S. A. 107, 13544–13549. https://doi.org/10.1073/pnas.1004090107

Faris, J.D., Zhang, Z., Rasmussen, J.B., Friesen, T.L., 2011. Variable Expression of the *Stagonospora nodorum* Effector SnToxA Among Isolates Is Correlated with Levels of Disease in Wheat. Molecular Plant-Microbe Interactions. 24, 1419–1426. https://doi.org/10.1094/MPMI-04-11-0094

Frandsen, R.J.N., 2011. A guide to binary vectors and strategies for targeted genome modification in fungi using *Agrobacterium* tumefaciens-mediated transformation. Journal of Microbiology Methods 87, 247–262. https://doi.org/10.1016/j.mimet.2011.09.004

Friesen, T.L., Stukenbrock, E.H., Liu, Z., Meinhardt, S., Ling, H., Faris, J.D., Rasmussen, J.B., Solomon, P.S., McDonald, B.A., Oliver, R.P., 2006. Emergence of a new disease as a result of interspecific virulence gene transfer. Nature Genetics. 38, 953–956.

Friesen, T.L., Zhang, Z.C., Solomon, P.S., Oliver, R.P., Faris, J.D., 2008. Characterization of the interaction of a novel *Stagonospora nodorum* host-selective

toxin with a wheat susceptibility gene. Plant Physiology 146, 682–693. https://doi.org/10.1104/pp.107.108761

Garnjobst, L., Tatum, E.L., 1967. A survey of new morphological mutants in *Neurospora crassa*. Genetics 57, 579–604.

Gelvin, S.B., 2009. *Agrobacterium* in the genomics age. Plant Physiology 150, 1665–76. https://doi.org/10.1104/pp.109.139873

Gelvin, S.B., 2003. *Agrobacterium*-Mediated Plant Transformation: the Biology behind the "Gene-Jockeying" Tool. Microbiology and Molecular Biology Reviews. 67, 16–37. https://doi.org/10.1128/MMBR.67.1.16

Gheysen, G., Montagu, M. V, Zambryski, P., 1987. Integration of *Agrobacterium tumefaciens* transfer DNA (T-DNA) involves rearrangements of target plant DNA sequences. Proceedings of the National Acadamy of Science U. S. A. 84, 6169–6173. https://doi.org/10.1073/pnas.84.17.6169

Gout, L., Fudal, I., Kuhn, M-L., Blaise, F., Eckert, M., Cattolico, L., Balesdent, M-H., Rouxel, T., 2006. Lost in the middle of nowhere: the *AvrLm1* avirulence gene of the Dothideomycete *Leptosphaeria maculans*. Molecular Microbiology. 60, 67-80

Gray, C.H., Tatum, E.L., 1944. X-ray induced Growth factor requirements in Bacteria. Proceedings of the National Acadamy of Science U. S. A. 30, 404–410.

Hane, J.K., Lowe, R.G.T., Solomon, P.S., Tan, K.-C., Schoch, C.L., Spatafora, J.W., Crous, P.W., Kodira, C., Birren, B.W., Galagan, J.E., Torriani, S.F.F., McDonald, B.A., Oliver, R.P., 2007. Dothideomycete Plant Interactions Illuminated by Genome Sequencing and EST Analysis of the Wheat Pathogen *Stagonospora nodorum*. Plant Cell Online 19, 3347–3368. https://doi.org/10.1105/tpc.107.052829

Hartwell, L.H., Mortimer, R.K., Culotti, J., Culotti, M., 1973. Genetic control of the cell division cycle in yeast: Genetic analysis of cdc mutants. Genetics 74, 267–286. https://doi.org/74(2): 267–286.

Hoekema, A., Roelvink, P.W., Hooykaas, P.J.J., 1984. Delivery of T-DNA from the *Agrobacterium tumefaciens* chromosome into plant cells 3, 2485–2490.

Idnurm, A., Reedy, J.L., Nussbaum, J.C., Heitman, J., 2004. *Cryptococcus neoformans* Virulence Gene Discovery through Insertional Mutagenesis. Eukaryotic Cell 3, 420–429. https://doi.org/10.1128/EC.3.2.420-429.2004

Idnurm, A., Walton, F.J., Floyd, A., Reedy, J.L., Heitman, J., 2009. Identification of ENA1 as a virulence gene of the human pathogenic fungus *Cryptococcus neoformans* through signature-tagged insertional mutagenesis. Eukaryotic Cell 8,

315–326. https://doi.org/10.1128/EC.00375-08

Jones, J.D.G., Dangl, J.L., 2006. The plant immune system. Nature 444, 323–329. https://doi.org/10.1038/nature05286

Jones, S. K. Jr. and Bennett R. J., 2011. Fungal mating pheromones: Choreographing the dating game. Fungal Genetics and Biology 48, 668-676

Kearse, M., Moir, R., Wilson, A., Stones-Havas, S., Cheung, M., Sturrock, S., Buxton, S., Cooper, A., Markowitz, S., Duran, C., Thierer, T., Ashton, B., Meintjes, P., Drummond, A., 2012. Geneious Basic: An integrated and extendable desktop software platform for the organization and analysis of sequence data. Bioinformatics 28, 1647–1649. https://doi.org/10.1093/bioinformatics/bts199

Kemppainen, M., Duplessis, S., Martin, F., Pardo, A.G., 2008. T-DNA insertion, plasmid rescue and integration analysis in the model mycorrhizal fungus *Laccaria bicolor*. Microbial Biotechnology 1, 258–269. https://doi.org/10.1111/j.1751-7915.2008.00029.x

Kunik, T., Tzfira, T., Kapulnik, Y., Gafni, Y., Dingwall, C., Citovsky, V., 2001. Genetic transformation of HeLa cells by *Agrobacterium*. Proceedings of the National Acadamy of Sciemce U. S. A. 98, 1871–1876. https://doi.org/10.1073/pnas.98.4.1871

Laufs, P., Autran, D., Traas, J., 1999. A chromosomal paracentric inversion associated with T-DNA integration in *Arabidopsis*. Plant Journal 18, 131–139. https://doi.org/10.1046/j.1365-313X.1999.00436.x

Lee, K., Dudley, M.W., Hess, K.M., Lynn, D.G., Joerger, R.D., Binns, a N., 1992. Mechanism of activation of *Agrobacterium* virulence genes: identification of phenol-binding proteins. Proceedings of the National Acadamy of Science U. S. A. 89, 8666–70. https://doi.org/10.1073/pnas.89.18.8666

Li, L., Wright, S.J., Krystofova, S., Park, G., Borkovich, K.A., 2007. Heterotrimeric G Protein Signaling in Filamentous Fungi. Annuals Reviews in Microbiology. 61, 423–452. https://doi.org/10.1146/annurev.micro.61.080706.093432

Lim, J.K., Simmons, M.J., 1994. Gross chromosome rearrangements mediated by transposable elements in *Drosophila melanogaster*. Bioessays 16, 269–275. https://doi.org/10.1002/bies.950160410

Lin, S.Y., Chooi, Y.H., Solomon, P.S., 2018. The global regulator of pathogenesis PnCon7 positively regulates Tox3 effector gene expression through direct interaction in the wheat pathogen *Parastagonospora nodorum*. Molecular Microbiology. 109, 78–90. https://doi.org/10.1111/mmi.13968

Liu, Z., Friesen, T.L., Ling, H., Meinhardt, S.W., Oliver, R.P., Rasmussen, J.B., Faris, J.D., 2006. The Tsn1 – ToxA interaction in the wheat – *Stagonospora nodorum* pathosystem parallels that of the wheat – tan spot system. Genome 49, 1265–1273. https://doi.org/10.1139/G06-088

Liu, Z., Gao, Y., Kim, Y.M., Faris, J.D., Shelver, W.L., de Wit, P.J.G.M., Xu, S.S., Friesen, T.L., 2016. SnTox1, a *Parastagonospora nodorum* necrotrophic effector, is a dual-function protein that facilitates infection while protecting from wheat-produced chitinases. New Phytologist 211, 1052–1064. https://doi.org/10.1111/nph.13959

Liu, Z., Zhang, Z., Faris, J.D., Oliver, R.P., Syme, R., McDonald, M.C., McDonald, B.A., Solomon, P.S., Lu, S., Shelver, W.L., Xu, S., Friesen, T.L., 2012. The cysteine rich necrotrophic effector SnTox1 produced by *Stagonospora nodorum* triggers susceptibility of wheat lines harboring *Snn1*. PLoS Pathogens 8. https://doi.org/10.1371/journal.ppat.1002467

Liu, Z.H., Faris, J.D., Meinhardt, S.W., Ali, S., Rasmussen, J.B., Friesen, T.L., 2004. Genetic and Physical Mapping of a Gene Conditioning Sensitivity in Wheat to a Partially Purified Host-Selective Toxin Produced by *Stagonospora nodorum*. Phytopathology 94, 1056–1060. https://doi.org/10.1094/PHYTO.2004.94.10.1056

Liu, Z.H., Faris, J.D., Oliver, R.P., Tan, K.C., Solomon, P.S., McDonald, M.C., McDonald, B.A., Nunez, A., Lu, S., Rasmussen, J.B., 2009. SnTox3 acts in effector triggered susceptibility to induce disease on wheat carrying the Snn3 gene. Plos Pathogens 5. https://doi.org/ 10.1371/journal.ppat.1000581

Lu, S., Faris, J.D., Sherwood, R., Friesen, T.L., Edwards, M.C., 2014. A dimeric PR-1-type pathogenesis-related protein interacts with ToxA and potentially mediates ToxA-induced necrosis in sensitive wheat. Molecular Plant Pathology 15, 650–663. https://doi.org/10.1111/mpp.12122

MacGurn, J.A., Cox, J.S., 2007. A genetic screen for *Mycobacterium tuberculosis* mutants defective for phagosome maturation arrest identifies components of the ESX-1 secretion system. Infection and Immuninty 75, 2668–2678. https://doi.org/10.1128/IAI.01872-06

Mandal, A., Lång, V., Orczyk, W., Palva, E.T., 1993. Improved efficiency for T-DNA-mediated transformation and plasmid rescue in *Arabidopsis thaliana*. Theoretical and Applied Genetics 86, 621–628. https://doi.org/10.1007/BF00838718

Manning, V. a, Ciuffetti, L.M., 2005. Localization of Ptr ToxA Produced by *Pyrenophora tritici-repentis* Reveals Protein Import into Wheat Mesophyll Cells.

Plant Cell 17, 3203–3212. https://doi.org/10.1105/tpc.105.035063

Manning, V.A., Hardison, L.K., Ciuffetti, L.M., 2007. Ptr ToxA Interacts with a Chloroplast-Localized Protein. Molecular Plant-Microbe Interactions 20, 168–177. https://doi.org/10.1094/MPMI-20-2-0168

Marton L., Wullems G. J., Molendijk L., S.R.A., 1979. In vitro transformation of cultured cells from *Nicotiana tabacum* by *Agrobacterium tumefaciens*. Nature 277, 129–131.

McDonald, M.C., Ahren, D., Simpfendorfer, S., Milgate, A., Solomon, P.S., 2018. The discovery of the virulence gene ToxA in the wheat and barley pathogen *Bipolaris sorokiniana*. Molecular Plant Pathology 19, 432–439. https://doi.org/10.1111/mpp.12535

McDonald, M.C., Razavi, M., Friesen, T.L., Brunner, P.C., McDonald, B.A., 2012. Phylogenetic and population genetic analyses of *Phaeosphaeria nodorum* and its close relatives indicate cryptic species and an origin in the Fertile Crescent. Fungal Genetics and Biology 49, 882–895. https://doi.org/10.1016/j.fgb.2012.08.001

McDonald, M.C., Solomon, P.S., 2018. Just the surface: advances in the discovery and characterization of necrotrophic wheat effectors. Current Opinions in Microbiology 46, 14–18. https://doi.org/10.1016/j.mib.2018.01.019

Meng, Y., Patel, G., Heist, M., Betts, M.F., Tucker, S.L., Galadima, N., Donofrio, N.M., Brown, D., Mitchell, T.K., Li, L., Xu, J.-R., Orbach, M., Thon, M., Dean, R.A., Farman, M.L., 2007. A systematic analysis of T-DNA insertion events in *Magnaporthe oryzae*. Fungal Genetics and Biology 44, 1050–64. https://doi.org/10.1016/j.fgb.2007.04.002

Metzenberg, R. L. and Glass, L. N., 1990. Mating Type and Mating Strategies in *Neurospora*. BioEssays 12, 53-59

Minty, J.J., Lesnefsky, A. a, Lin, F., Chen, Y., Zaroff, T. a, Veloso, A.B., Xie, B., McConnell, C. a, Ward, R.J., Schwartz, D.R., Rouillard, J.-M., Gao, Y., Gulari, E., Lin, X.N., 2011. Evolution combined with genomic study elucidates genetic bases of isobutanol tolerance in *Escherichia coli*. Microbial Cell Factories 10, 18. https://doi.org/10.1186/1475-2859-10-18

Muller, H.J., 1927. Artificial Transmutation of the Gene. Science (80) https://doi.org/10.1126/science.66.1699.84

Murray, G.M., Brennan, J.P., 2009. Estimating disease losses to the Australian wheat industry. Australasian Plant Pathology. 38, 558–570.

Nacry, P., Camilleri, C., Courtial, B., Caboche, M., Bouchez, D., 1998. Major

chromosomal rearrangements induced by T-DNA transformation in *Arabidopsis*. Genetics 149, 641–50.

Nüsslein-Volhard, C., Wieschaus, E., 1980. Mutations affecting segment number and polarity in *Drosophila*. Nature 287, 795–801. https://doi.org/10.1038/287795a0

Oliver, R.P., Friesen, T.L., Faris, J.D., Solomon, P.S., 2012. *Stagonospora nodorum* : From Pathology to Genomics and Host Resistance. Annual Reviews in Phytopathology. 50, 23–43. https://doi.org/10.1146/annurev-phyto-081211-173019

Phan, H.T.T., Rybak, K., Furuki, E., Breen, S., Solomon, P.S., Oliver, R.P., Tan, K.C., 2016. Differential effector gene expression underpins epistasis in a plant fungal disease. Plant Journal 87, 343–354. https://doi.org/10.1111/tpj.13203

Qin, G., Kang, D., Dong, Y., Shen, Y., Zhang, L., Deng, X., Zhang, Y., Li, S., Chen, N., Niu, W., Chen, C., Liu, P., Chen, H., Li, J., Ren, Y., Gu, H., Deng, X., Qu, L.J., Chen, Z., 2003. Obtaining and analysis of flanking sequences from T-DNA transformants of *Arabidopsis*. Plant Science 165, 941–949. https://doi.org/10.1016/S0168-9452(03)00218-8

Rho, H., Kang, S., Lee, Y., 2001. *Agrobacterium tumefaciens*-mediated transformation of the plant pathogenic fungus, *Magnaporthe grisea*. Molecules and Cells 12, 407-411

Roe, J.L., Rivin, C.J., Sessions, R.A., Feldmann, K.A., Zambryski, P.C., 1993. The Tousled gene in *A. thaliana* encodes a protein kinase homolog that is required for leaf and flower development. Cell 75, 939–950. https://doi.org/10.1016/0092-8674(93)90537-Z

Rudd, J.J., Kanyuka, K., Hassani-Pak, K., Derbyshire, M., Andongabo, A., Devonshire, J., Lysenko, A., Saqi, M., Desai, N.M., Powers, S.J., Hooper, J., Ambroso, L., Bharti, A., Farmer, A., Hammond-Kosack, K.E., Dietrich, R.A., Courbot, M., 2015. Transcriptome and Metabolite Profiling of the Infection Cycle of *Zymoseptoria tritici* on Wheat Reveals a Biphasic Interaction with Plant Immunity Involving Differential Pathogen Chromosomal Contributions and a Variation on the Hemibiotrophic Lifest. Plant Physiology 167, 1158–1185. https://doi.org/10.1104/pp.114.255927

Scalliet, G., Bowler, J., Luksch, T., Kirchhofer-Allan, L., Steinhauer, D., Ward, K., Niklaus, M., Verras, A., Csukai, M., Daina, A., Fonné-Pfister, R., 2012. Mutagenesis and functional studies with succinate dehydrogenase inhibitors in the wheat pathogen *Mycosphaerella graminicola*. PLoS One 7. https://doi.org/10.1371/journal.pone.0035429

Schumacher, J., Simon, A., Cohrs, K.C., Viaud, M., Tudzynski, P., 2014. The Transcription Factor BcLTF1 Regulates Virulence and Light Responses in the Necrotrophic Plant Pathogen *Botrytis cinerea*. PLoS Genetics 10. https://doi.org/10.1371/journal.pgen.1004040

Shalem, O., Sanjana, E.N., Hartenian, E., Zhang, F., 2014. Genome-Scale CRISPR-Cas9 Knockout. Science (80). 343, 84–88. https://doi.org/10.1038/nbt.2647

Shi, G., Zhang, Z., Friesen, T.L., Raats, D., Fahima, T., Brueggeman, R.S., Lu, S., Trick, H.N., Liu, Z., Chao, W., Frenkel, Z., Faris, J.D., 2016. The hijacking of a receptor kinase – driven pathway by a wheat fungal pathogen leads to disease. Science Advances. 2, 10, e1600822 https://doi.org/10.1126/sciadv.1600822

Solomon, P.S., Lowe, R.G.T., Tan, K.-C., Waters, O.D.C., Oliver, R.P., 2006. *Stagonospora nodorum*: cause of stagonospora nodorum blotch of wheat. Molecular Plant Pathology. 7, 147–156. https://doi.org/10.1111/j.1364-3703.2006.00326.x

Solomon, P.S., Tan, K.-C., Sanchez, P., Cooper, R.M., Oliver, R.P., 2004. The Disruption of a Gα Subunit Sheds New Light on the Pathogenicity of *Stagonospora nodorum* on Wheat. Molecular Plant-Microbe Interactions. 17, 456–466. https://doi.org/10.1094/MPMI.2004.17.5.456

Solomon, P.S., Wilson, T.J.G., Rybak, K., Parker, K., Lowe, R.G.T., Oliver, R.P., 2006. Structural characterisation of the interaction between *Triticum aestivum* and the dothideomycete pathogen *Stagonospora nodorum*. European Journal of Plant Pathology. 114, 275–282.

Sommerhalder, R. K., McDonald, B. A., Mascher, F., Zhan, J. 2010. Sexual Recombinants Make a Significant Contribution to Epidemics Caused by the Wheat Pathogen *Phaeosphaeria nodorum.* The American Phytopathology Society 100, 850-862

Song, X., Guo, J., Ma, W. xiu, Ji, Z. yuan, Zou, L. fang, Chen, G. you, Zou, H. song, 2015. Identification of seven novel virulence genes from *Xanthomonas citri* subsp. *citri* by Tn5-based random mutagenesis. Journal of Microbiolgy. 53, 330–336. https://doi.org/10.1007/s12275-015-4589-3

Sperschneider, J., Catanzariti, A.M., Deboer, K., Petre, B., Gardiner, D.M., Singh, K.B., Dodds, P.N., Taylor, J.M., 2017. LOCALIZER: Subcellular localization prediction of both plant and effector proteins in the plant cell. Scientific Reports 7, 1–14. https://doi.org/10.1038/srep44598

Sugui, J.A., Chang, Y.C., Kwon-Chung, K.J., 2005. *Agrobacterium tumefaciens* -

Mediated Transformation of *Aspergillus fumigatus*: an Efficient Tool for Insertional Mutagenesis and Targeted Gene Disruption. Applied and Environmental Microbiology. 71, 1798–1802. https://doi.org/10.1128/AEM.71.4.1798

Tan, K.-C., Phan, H.T.T., Rybak, K., John, E., Chooi, Y.H., Solomon, P.S., Oliver, R.P., 2015. Functional redundancy of necrotrophic effectors – consequences for exploitation for breeding. Frontiers in Plant Science. 6, 1–9. https://doi.org/10.3389/fpls.2015.00501

Tan, K.C., Heazlewood, J.L., Millar, A.H., Thomson, G., Oliver, R.P., Solomon, P.S., 2008. A signaling-regulated, short-chain dehydrogenase of *Stagonospora nodorum* regulates asexual development. Eukaryotic Cell 7, 1916–1929. https://doi.org/10.1128/EC.00237-08

Tatum, E.L., 1945. X-Ray induced mutant strains of *Escherichia coli*. Proceedings of the National Acadamy of Science U.S.A. 31, 215–219. https://doi.org/10.1126/science.132.3438.1488

Tatum, E.L., Beadle, G.W., 1942. Genetic Control of Biochemical Reactions in *Neurospora*: An "Aminobenzoicless" Mutant. Proceedings of the National Acadamy of Science U. S. A. 28, 234–43.

Urano, D., Chen, J.-G., Botella, J.R., Jones, A.M., 2013. Heterotrimeric G protein signalling in the plant kingdom. Open Biology 3, 120186–120186. https://doi.org/10.1098/rsob.120186

Urban, M., King, R., Hassani-Pak, K., Hammond-Kosack, K.E., 2015. Whole-genome analysis of *Fusarium graminearum* insertional mutants identifies virulence associated genes and unmasks untagged chromosomal deletions. BMC Genomics 16, 261. https://doi.org/10.1186/s12864-015-1412-9

Valvekens, D., Montagu, M. V, Van Lijsebettens, M., 1988. *Agrobacterium tumefaciens*-mediated transformation of *Arabidopsis thaliana* root explants by using kanamycin selection. Proceedings of the National Acadamy of Science U.S.A. 85, 5536–5540. https://doi.org/10.1073/pnas.85.15.5536

Villalba, F., Lebrun, M.H., Hua-Van, A., Daboussi, M.J., Grosjean-Cournoyer, M.C., 2001. Transposon impala, a novel tool for gene tagging in the rice blast fungus *Magnaporthe grisea*. Molecular Plant Microbe Interactactions 14, 308–315. https://doi.org/10.1094/MPMI.2001.14.3.308

Wang, K.A.N., Statchel, S.E., Timmerman, B., Van Montagu, M., Zambryscki, P.C., 1987. Site-Specific Nick in the T-DNA Border Sequence as a Result of

*Agrobacterium* vir Gene Expression. Science (80). 235, 587–591. https://doi.org/10.1126/science.235.4788.587

Weitz, J., Koch, M., Debus, J., Hohler, T., Galle, P.R., Buchler, M.W., 2005. Colorectal cancer. Lancet (London, England) 365, 153–165. https://doi.org/10.1016/S0140-6736(05)17706-X

Yu, M., Yu, J., Hu, J., Huang, L., Wang, Y., Yin, X., Nie, Y., Meng, X., Wang, W., Liu, Y., 2015. Identification of pathogenicity-related genes in the rice pathogen *Ustilaginoidea virens* through random insertional mutagenesis. Fungal Genetics and Biology 76, 10–19. https://doi.org/10.1016/j.fgb.2015.01.004

Zerbino, D.R., Birney, E., 2008. Velvet: Algorithms for de novo short read assembly using de Bruijn graphs. Genome Research 18, 821–829. https://doi.org/10.1101/gr.074492.107

Zhang, X., Nguyen, N., Breen, S., Outram, M.A., Dodds, P.N., Kobe, B., Solomon, P.S., Williams, S.J., 2017. Production of small cysteine-rich effector proteins in *Escherichia coli* for structural and functional studies. Molecular Plant Pathology 18, 141–151. https://doi.org/10.1111/mpp.12385

# Chapter 2: Construction and characterisation of a *Parastagonospora nodorum* random mutation library

## 2.1 Introduction

Sequencing the *Parastagonospora nodorum* genome in 2005 (Birren et al., 2005) has identified genes that are required for normal pathogen growth, reproduction and infection of the host via reverse genetics (Lowe et al., 2009; Solomon et al., 2005; Tan et al., 2008). Reverse genetics is a hypothesis driven method that relies on reliable gene annotations and predicted functions. For example, Lowe et al (2009) utilised mass-spectrometry to show the disaccharide, trehalose, accumulates in *P. nodorum* during sporulation. Disrupting the *P. nodorum* gene with the closest homology to known trehalose-6-phosphate synthases (*Tps1*), resulted in sporulation-deficient mutants that did not accumulate trehalose. Thereby reverse genetics, directed by functional mass-spectrometry data, demonstrated that trehalose accumulation plays a critical role in sporulation (Lowe et al., 2009). While productive, this method relies on previous studies such as metabolomics or transcriptomics to direct hypothesis testing. This reliance can bias research towards biochemical pathways shared with model organisms and limit the discovery of novel genes involved in sporulation, virulence or other pathogen traits.

Forward genetics offers an alternative approach to elucidating the role of genetic loci. This approach involves the random disruption of genes in an organism and screening the subsequent mutants for a phenotype of interest. The impaired genes within mutants displaying a phenotype of interest are identified and independently verified as being causal to the observed phenotype. Such an approach has led to the identification of novel mechanisms of fungal development and virulence over the last several decades (Akamatsu et al., 1997; Bölker et al., 1995; Urban et al., 2015). For example, Xu et al (2013) utilised *Agrobacterium*-mediated transformation to randomly mutate the pathogenic fungus *Sclerotinium sclerotiorum* and screen the subsequent mutants for a

loss of virulence on pea leaves. The disrupted genetic locus in the single avirulent isolate obtained was then identified, via inverse PCR, and confirmed by enzymatic analysis as Super Oxide Dismutase (*Ss.SOD1*) (Xu and Chen, 2013). Here-by a forward genetics approach has revealed a biochemical mechanism in *S. sclerotiorum* which maybe be exploited to limit disease.

This chapter describes the generation, statistical analysis and screening of a random mutation library of *P. nodorum*. This library was generated using *Agrobacterium*-mediated transformation to insert a known disruption sequence, harbouring the Hygromycin resistance:Green fluorescence protein fusion gene (*Hph:GFP*), into the *P. nodorum* genome. This method was chosen as current literature suggests that *Agrobacterium* generally introduces few mutations per transformant, is readily scalable and produces easily identified mutations (Betts et al., 2007; Choi et al., 2007; Idnurm et al., 2009). Further, *P. nodorum* is amenable to genetic modification by *Agrobacterium* and a well-established protocol exists within the Solomon lab that I modified for high throughput generation of mutants. Insertional mutagenesis is preferable to SNP based mutagenesis for identification of mutation sites as well as screening for mutants. Furthermore, a method introducing fewer mutations per transformant facilitates the identification of the mutation causing the observed phenotype. However, there is evidence that this transformation method displays bias towards introducing mutations in promoter regions of fungal genomes (Choi et al., 2007). By generating a library of 21,070 mutants of the pathogenic fungus, *Magnaporthe oryzae,* Choi et al (2007) showed that insertions by *Agrobacterium* were 2.3-fold over represented in the 5' untranslated region (5'UTR) of genes, and two-fold underrepresented in coding regions of the genome. The bias observed in *M. oryzae* does not outweigh the advantages of the *Agrobacterium* system, as a disruption to the promoter region is likely to impair gene

function. For these reasons, *Agrobacterium*-mediated transformation was the chosen method for generating random mutations in the *P. nodorum* genome to screen for genes involved in pathogenicity.

***Aim:*** ***1)*** *To generate a library of randomly mutated strains of* P. nodorum *via* Agrobacterium-*mediated transformation and determine the rate and stochasticity of mutation via Southern blot analysis.* ***2)*** *To isolate avirulent strains of the fungus, Parastagonospora nodorum, from a library of random mutation strains which display an avirulence phenotype on the wheat cultivar Grandin.* ***3)*** *To microscopically observe the* P. nodorum- *wheat interaction and determine whether avirulent strains of the fungus were able to penetrate the host tissue.* ***4)*** *To isolate strains of* P. nodorum *from the random mutation library which display virulence towards a non-susceptible wheat cultivar.*

## 2.2 Materials and Methods

2.2.1 *(Table 2.01: Primers used in Chapter 2 to amplify the Southern blot probe for the pPK2-Hph:GFP insertion)*

| Name | Oligonucleotide (5'--3') |
|---|---|
| **Southern_probe_F** | GTGGTGTAAACAAATTGACGC |
| **Southern_Probe_R** | TTGTTTGTCTGCCATGATGT |

2.2.2 *(Table 2.02 Media used in chapter 2 to culture fungi and bacteria. The following table lists the recipes for media named in the following methods sections used for culturing fungi and bacteria. The concentrations of each reagent and their origins are also listed)*

| Abbreviation | Name | Constituent | /L |
|---|---|---|---|
| **V8PDB/V8PDA** | V8 Potato Dextrose Broth | Centrifuged Campbell's V8 Juice™ | 150ml |
| | V8 Potato Dextrose Agar | Bacto™ Potato Dextrose | 10g |
| | | Astral Scientific™ Agar (optional) | 15g |
| | | up to 1L with MilliQ water | |
| | | pH 6.0 | |
| **CzV8PDB** | CzaPek Dox V8 agar | Bacto™ CzaPek Dox | 33g |
| | pH 6.0 | Potato Dextrose Broth | 10g |
| | | Centrifuged Campbell's V8 Juice™ | 200ml |
| | | Astral Scientific™ Agar | 15g |
| | | up to 1L with MilliQ water | |
| | | | |
| **Soft Overlay** | CzaPek Dox V8 soft agar | Bacto™ CzaPek Dox | 33g |
| | pH 6.0 | Centrifuged Campbell's V8 Juice™ | 200ml |
| | | Astral Scientific™ Agar | 7.5g |
| | | up to 1L with MilliQ water | |

| | | | |
|---|---|---|---|
| **TWB Agar** | Tap Water Benzimidazol Agar | Sigma Scientific™ Benzimidazol | 0.3g |
| | | Astral Scientific™ Agar | 15g |
| | | up to 1L with MilliQ water | |
| | | | |
| **LB** | Lysogeny Broth | Bacto™ Tryptone | 10g |
| | | Astral Scientific™ Yeast Extract | 10g |
| | | Astral Scientific™ Sodium Chloride | 5g |
| | | Astral Scientific™ Agar (optional) | 15g |
| | | up to 1L with MilliQ water | |
| | | | |
| **IM+** | Induction Medium | Bacto™ Tryptone | 10g |
| | pH 5.5 | Astral Scientific™ Yeast Extract | 10g |
| | | Astral Scientific™ Sodium Chloride | 5g |
| | | Astral Scientific™ Magnesium Sulphate | 240mg |
| | | Astral Scientific™ Na2HPO4 | 13.4g |
| | | Astral Scientific™ NaH2PO4 | 1.3g |
| | | Astral Scientific™ Agar (optional) | 15g |
| | | 10% Astral Scientific™ Glucose (Autoclave separately) | 100ml |
| | | 10% Sigma Aldrich™ Glycerol (Autoclave separately) | 100ml |
| | | up to 1L with MilliQ water | |

2.2.3 *(Table 2.03: Buffers and solutions in Chapter 2 used for storing, visualising and manipulating nucleic acids, as well as DNA extractions. The following table lists recipes of the buffers and solutions named in the following methods section, along with the company from which they were bought. These were used for storing, visualising and manipulating nucleic acids, as well as DNA extractions)*

| Buffer or Solution | Constituent | Proportion |
|---|---|---|
| **TAE Buffer** | Tris-HCl (Astral Scientific™) | 40mM |
| | EDTA (Astral Scientific™) | 1mM |
| | Acetic Acid (Sigma-Aldrich™) | 20mM |
| | pH 8.6 | |
| | | |
| **TE Buffer** | EDTA 1mM (Astral Scientific™) | 1mM |
| | Tris-HCl 10mM pH 8.0 (Astral Scientific™) | 10mM |
| | | |
| **Sodium Dodecyl Sulphate (SDS) 20%** | SDS (Astral Scientific™) | 20g |
| | MilliQ water | 80ml |
| | | |
| **Lysis buffer** | 10mg/ml RNAseA (Astral Scientific™) | 100µl |
| | TE Buffer | 94.9ml |
| | 20% SDS | 5ml |
| | | |
| **Potassium Acetate 2.8M (Astral Scientific™)** | 274.4g/l | |
| | | |
| **Sodium Acetate 3M (Astral Scientific™)** | 256g/l | |
| | | |

2.2.4 *(Table 2.04: Fungal and bacterial strains, and their selective markers and mutations, used in Chapter 2. This table lists the fungi and bacteria mentioned in the following methods, as well as the results and discussion. Specific mutations, selection markers and harboured plasmids are also listed, while their origin and growth conditions are mentioned in the methods.)*

| **Genus** | **Species** | **Strain** | **Mutant** | **Mutation** | **Gene/Plasmid ID** | **Marker** |
|---|---|---|---|---|---|---|
| *Parastagonospora* | *nodorum* | SN15 | wild-type | nil | NA | nil |
| *Parastagonospora* | *nodorum* | SN15 | t112 | TBD | TBD | HYG |
| *Agrobacterium* | *tumefaciens* | LBA1126$^{rif}$ | Deactivated *vir* | Helper plasmid pAL1100$^{spec}$ | pPK2$^{kan}$ | HYG/KAN/SPEC |

### 2.2.5 Protocols

#### 2.2.5.1 Culturing of *Agrobacterium tumefaciens*

*Agrobacterium tumefaciens* was cultivated in 50ml culture tubes containing 10ml of either LB broth, or liquid induction medium with additional antibiotics. 50µg/ml spectinomycin hydrochloride was used to maintain the helper plasmid, pAL1100. 50µg/ml kanamycin sulphate was used to maintain the T-DNA plasmid. Cultures were grown over night at 28°C while shaking at 280 rpm.

#### 2.2.5.2 Culturing of *Parastagonospora nodorum*

*Parastagonospora nodorum* was grown on V8 Potato Dextrose Agar (V8PDA) medium at 22°C with a 12 hour day/night cycle under near U.V. fluorescence and white light. Asexual spore production was achieved by spot inoculating solid agar V8PDA plates with 10µl of an asexual spore suspension at $1x10^6$ spores/ml, followed by incubation for 12 days.

#### 2.2.5.3 Collecting and counting *P. nodorum* asexual spores

Asexual spores of *P. nodorum* were collected from 12-day-old V8PDA plates by gently washing the plate twice with 4 ml of sterile water under sterile conditions. The water was then passed through sterile, hydrophobic, cotton wool in a syringe before centrifugation at 4,000g for 10 minutes. The supernatant was then discarded and the spore pellet washed again in 8 ml of sterile water. The resulting pellet was then resuspended in 2 ml of sterile water. An aliquot was then diluted 40 fold for spore counting with a haemocytometer.

#### 2.2.5.4 Agrobacterium mediated transformation of *P. nodorum*

A starter culture of *A. tumefaciens LBA1126,* harbouring pPK2 (Covert et al. 2001) (Figure 2.01), was grown over night in 10ml of LB broth containing 50µg/ml

spectinomycin hydrochloride (Astral Scientific™, Australia) and 50µg/ml kanamycin sulphate (Astral Scientific™, Australia) at 28°C with 280 RPM shaking. 100µl of this starter culture was used to inoculate 10ml of induction medium containing 50µg/ml spectinomycin hydrochloride, 50µg/ml kanamycin sulphate and 200µM acetosyringone (Astral Scientific™, Australia) which was then incubated at 28°C, 280 RPM shaking until the culture reached an optical density at 600nm ($OD_{600}$) of 0.6 (ca. 6 hours).

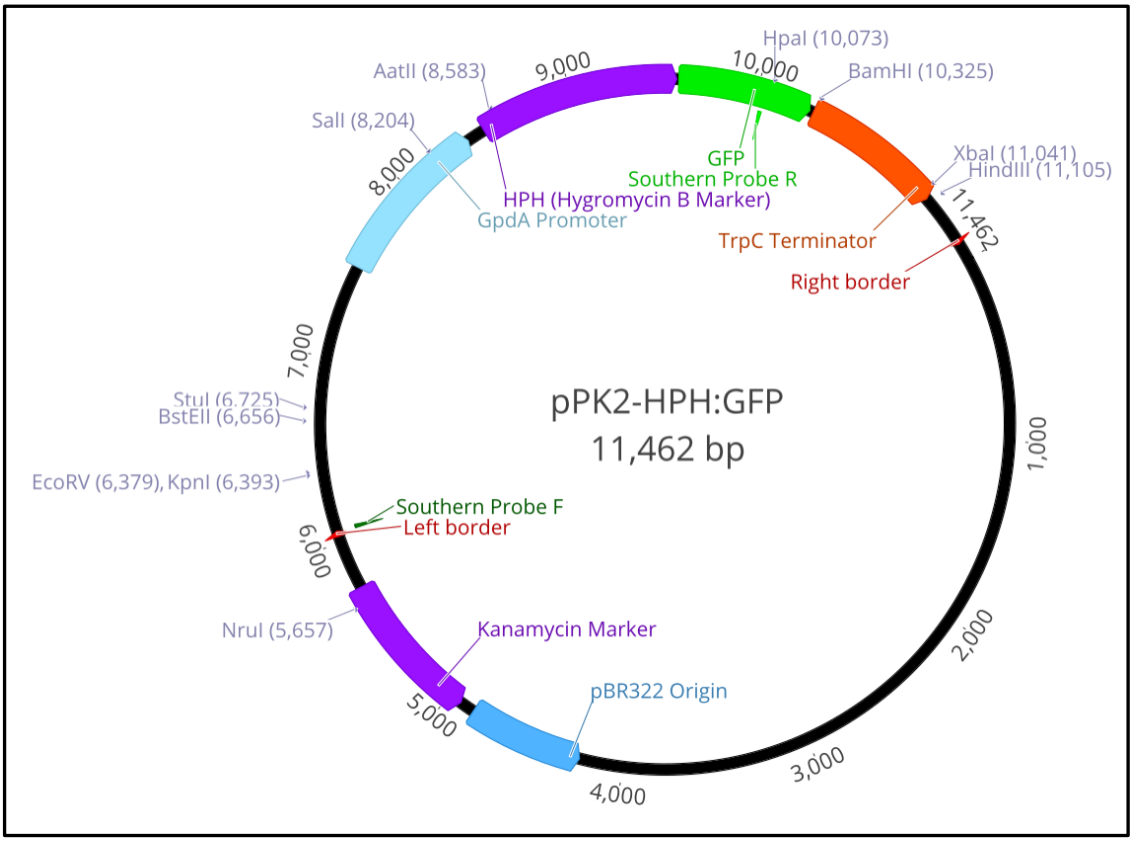


*(Figure 2.01: Plasmid map of pPK2-Hph:GFP. This plasmid contained the bacterial origin of replication, BR322 labelled in dark blue, and kanamycin resistance marker adjacent, labelled in purple. The* Agrobacterium *left and right border sequences for T-DNA strand transfer are labelled in red. Between the borders reside the eukaryotic elements involved in fungal transformation. These elements included the Hygromycin B phosphotransferase gene labelled in purple as HPH (Hygromycin B Marker) and Green fluorescent protein gene labelled in green as* GFP*. HPH and GFP were fused and regulated by the glucose-6-phosphate dehydrogenase promoter (*GpdA*) and indole-3-glycerol phosphate synthase (*TrpC*) terminator. The* Bam*HI restriction site utilised in Southern blot analysis was located between GFP and the* TrpC *terminator. The primer binding sites generating the Southern blot probe are labelled in green)*

While the *A. tumefaciens* induction culture was growing, wild-type asexual *P. nodorum* spores were collected from 12day old cultures grown on V8PDA plates under a 12-hour day night cycle with near U.V. and white light. The spores were collected under sterile conditions, counted, a control aliquot reserved and then the spore suspension was centrifuged at 4,000g for 10 minutes. The spore pellet was then resuspended in the *A. tumefaciens LBA1126* $OD_{600}$ induction culture at $1x10^7$ spores/ml. This co-culture was then spread inoculated onto 20ml solid induction medium plates lacking antibiotics but containing 200µM acetosyringone at 100µl per plate ($1x10^6$ spores per plate). The reserved control aliquot of spores was spread onto 20ml solid induction medium plates lacking antibiotics but containing 200µM acetosyringone at $1x10^6$ spores per plate. The plates were then incubated in the dark at 22°C for 72 hours.

After 72 hours 10ml of V8PDA containing 600µg/ml of Hygromycin B (Astral Scientific™, Australia) and 600µg/ml of sodium cefotaxime (Astral Scientific™, Australia) was poured over each plate, to reach a final concentration of 200µg/ml of each antibiotic. One plate containing both *P. nodorum* spores and *A. tumefaciens* was left with V8PDA and no antibiotics as a positive control, while the plate with *P. nodorum* and no *A. tumefaciens* received antibiotics as a negative control. These plates were incubated in the dark at 22°C. Emerging colonies were sub-cultured onto V8PDA plates containing 200µg/ml of Hygromycin B and 200µg/ml sodium cefotaxime (colonies emerged between 6 – 14 days). For generation of a random *P. nodorum* mutant library this protocol was used to inoculate 60 transformation plates. Each transformation plate produced between 10 and 30 colonies. Due to the logistics of generating large numbers of mutants for a forward genetic screen these mutants were not re-isolated from single spores to ensure a homogeneous culture. In lieu of single spore isolation these colonies were sub-cultured under selection for the *Hph* insertion

for three generations. Each generation was sub-cultured by transferring a 1mm cube of the leading edge of each colony to fresh V8PDA plates containing 200µg/ml Hygromycin B. Additionally to Hygromycin B resistance, fluorescence microscopy visualised GFP expression, using the Leica DFC7000t microscope and camera, in of a random selection of mutants. In total this protocol was used to generate 950 Hygromycin B resistant random mutation strains of *P. nodorum.*

#### 2.2.5.5 SDS potassium acetate-based gDNA extraction

Fungal material for genomic DNA extraction was either collected by scraping fungal growth from agar plates or growing fungal cultures in liquid medium in the extraction tube. Alternatively, high output extractions for Southern blots *P. nodorum* was cultured in 20 ml of stationary liquid V8PD in 45mm sterile Petri dishes. This method of cultivation produced a thick mycelial mat that was dried with paper towel, rolled up and pressed into a 2ml microfuge tube.

Fungal material was snap frozen with liquid nitrogen a 2ml microfuge tube then freeze dried overnight. A tungsten carbide ball bearing then pulverised the dried material in a tissue lyser for 30 seconds at 60 hertz, producing a fine power. 500µl of lysis buffer was added to the powdered fungus and the microfuge tube shaken at 900rpm for 20 minutes at room temperature. 500µl of potassium acetate 2.8M was then added to the tube and mixed by inverting the tube 20x. The precipitate was then collected at the bottom of the tube by centrifugation at 21,000g for 5 minutes and the supernatant added to another tube containing 900µl of ice-cold isopropanol and 50µl of sodium acetate 3M, inverted 20x and incubated on ice for 10 minutes. The cold isopropanol solution was then centrifuged at 21,000g for 20 minutes. After the DNA pelleted in the bottom of the 2ml microtube the isopropanol was discarded and the pellet washed twice each with 100µl of 70% ethanol and 100% ethanol. The DNA was then air dried and dissolved in 50µl of

MilliQ water. This protocol was provided by personal communication with Dr. Yit-Heng Chooi, The University of Western Australia.

#### 2.2.5.6 Restriction endonuclease digestion of DNA

To fragment 30µg of fungal genomic DNA at the *Bam*HI restriction site (GGATTC) 20µl of CutSmart 10x Buffer NEB™ was added to 170µl of MilliQ water. This buffered solution was used to elute 30µg of genomic DNA. 10µl of *Bam*HI-HF NEB™ was added to the reaction to make a total volume of 200µl. The reaction was incubated at 37°C overnight, then an aliquot was visualised on a 0.8% agarose gel in TAE buffer (30 minutes at 110v) to ensure a smear formed, indicative of digestion. The digested genomic DNA was then purified and concentrated using isopropanol precipitation and re-elution.

#### 2.2.5.7 Generation of Southern blot probe

The template used to generate the Southern blot probe was PCR amplified from pPK2 plasmid DNA. This PCR product was then DIG labelled with the DIG-High Prime DNA labelling kit (Sigma-Aldrich™, Germany) according to the manufacturers' instructions. The template was generated using the forward and reverse primers indicated in Table 2.01 and the following reaction on ice:10ng of plasmid DNA in 1 µl was diluted in 5.16 µl. 1 µl of Takara™ 10x Buffer was added to this dilution along with 0.8 µl of a 10µM dNTP solution containing 2. 5µM each of ATP, GTP, CTP and TTP. 1µl of each forward and reverse primer were added to a final concentration of 0.5µM. Finally, 0.04µl ExTaq Takara™ polymerase was added to the reaction. This reaction was set up in parallel to two other reactions, one lacking genomic DNA and the other lacking primers. These additional reactions form negative controls.

Thermocycler conditions: The reactions were then denatured at 98°C for 5.5 minutes then the primers were annealed at 57°C for 30 seconds. The primary PCR product was

then extended at 72°C for one minute per kilobase before the reaction was denatured again at 98°C for 30 seconds. Denaturation, annealing and extension was repeated 34 times before the reaction was terminated at 72°C for 10 minutes.

#### 2.2.5.8 Southern blot of digested fungal gDNA

20µg of *Bam*HI digested P. nodorum genomic DNA from each mutant and wild-type strain was loaded into a 0.8% agarose gel measuring 10cm in length, containing 0.1% (v/v) SYBR™ Safe DNA Gel Stain (ThermoFisher Scientific™). This gel was subjected to 30v electrophoresis in TAE buffer at 4°C for 10 hours. The gel was then visualised and blotted onto a Hybond® ECL™ nitrocellulose membrane (Sigma-Aldrich™, Germany). Blotting and blot visualisation with the Roche CDP-Star® Southern blot kit (Sigma-Aldrich™, Germany) was carried out according to the manufactures' instructions.

#### 2.2.5.9 Growth of wheat for pathogenicity assays

40cm high, 30cm diameter round seed raising pots were 1/3 filled with Vermiculite™. 1g of seed raising slow release fertiliser granules were then even dispersed across the surface of the soil, and the pots filled 2/3 with vermiculite™. 15 seeds were then even dispersed across the surface of the soil in each pot and the remainder of the pot filled with vermiculite™. The pots were then watered until water ran freely from the drainage holes in the pots, and then placed into sealed trays in the green house. The plants were then maintained in the green house at 26°C under natural lighting cycles and bottom watered daily. After 14 days the second emerging leaf of each plant was removed with a scalpel for pathogenicity assays.

#### 2.2.5.10 Detached leaf pathogenicity assay

The Solomon lab traditionally used a detached leaf assay to determine the virulence of fungal strains. This method used many replicates and was not high through-put. Here I

will describe the low through-put and statistically robust protocol, followed by a high through-put protocol with low statistical robustness that I developed for this and future projects. The low through-put, highly statistically robust protocol is as follows:

The second emergent leaves from 14-day-old wheat seedlings were removed from the seedlings with a scalpel. The leaves were then trimmed of their top and bottom 2cm, cut into 4cm section and incubated at room temperature in beakers of tap water to regain turgidity.

The 4cm section of leaves were embedded in TapWaterBenzimidazol agar plates by slitting the agar with a scalpel 1/3 from the edge of the agar plat, sloped at 45° towards the middle of the plate. Then the leaves were pushed into the slit with tweezers, top of the leaf facing upwards and 5-10mm separated each leaf. Once a row of leaves protruded from the agar, the raised end of the leaf was gentle inserted into the agar of the other side of the plate using a scalpel. This creates a row of leaf arches that were curved away from the agar but wouldn't touch the Petri dish lid.

Each leaf apex was then inoculated with a 5µl droplet of a *P. nodorum* spore suspension with a concentration of $1x10^5$ spores/ml in 0.02% Tween 80 (polyoxyethylene 80 sorbitan laurate) (Sigma-Aldrich™, Germany). The plates were then sealed with plastic and incubated at 22°C with a 12-hour day-night cycle under near U.V. and white light. The leaves were then checked daily for symptoms of infection.

The optimized method involved growing the mutant library in stationary liquid culture in Greiner™ 96 well plates resulting in the fungus forming a rubbery mat of mycelia at the surface. This was used as the inoculum for the pathogenicity assay. To inoculate

leaves, 200ul pipette tips were cut at a 45-degree angle, 15mm from the tip, creating a sharp tube with a standard diameter. 1000 of these pipette tips were cut, and a toothpick inserted inside every second tip (Figure 2.02). The pipette tips were used to puncture the mycelial mat of the stationary liquid culture and then the mycelial plug, lodged inside the tip, was gently ejected onto the leaf surface using the toothpick. Only 500 toothpicks were required as both ends can be used. Depending upon the natural variation in leaf thickness and turgidity, ca. 15 wheat leaves were embedded in each 90mm Petri dish. This allowed 13 mutant strains to be screened in each Petri dish as two leaves were left as either un-inoculated or wild type controls. In the interest of time only single replicates were produced.

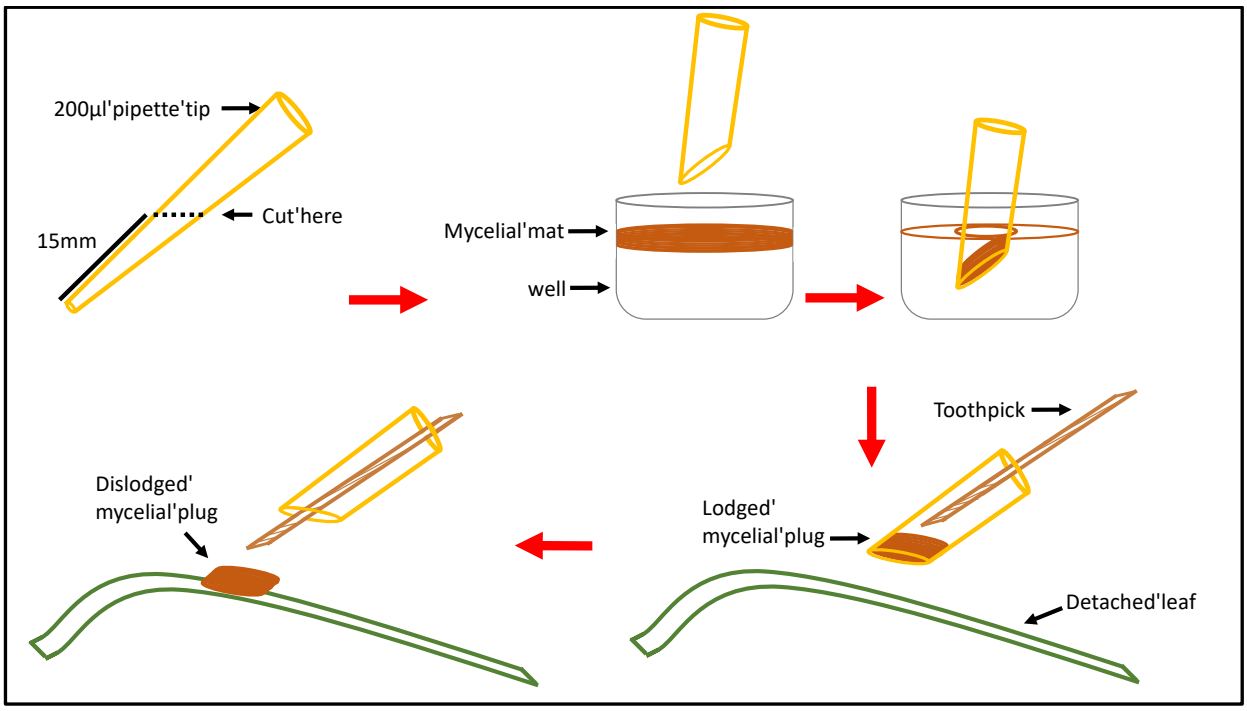


*(Figure 2.02: Schematic of the high throughput method of inoculating detached wheat leaves with* P. nodorum *strains grown in 96 well liquid cultures. This diagram is not to scale. A new cut pipette tip was used for each transformant however one toothpick was used between two transformants as each end of the toothpick was used)*

## 2.3 Results

### 2.3.1 A *Parastagonospora nodorum* random mutation library was generated by *Agrobacterium*-mediated transformation

*Agrobacterium tumefaciens* strain LBA1126, harbouring a helper plasmid and the pPK2 plasmid described in Figure 2.01, was used for a series of transformations of *Parastagonospora nodorum*. The transformation method is described in section 2.2.5.4. The pPK2 plasmid contained the Hygromycin B phosphotransferase (*Hph*) and green fluorescent protein (*GFP)* fusion gene under regulatory control of the *Aspergillus gpdA* promoter and *trpC* terminator. *Hph* confers resistance to Hygromycin B in *P. nodorum,* and the protein produced by *GFP* fluoresces when excited by wavelengths of light at 395 nm or 475 nm (Chalfie et al., 1994). These genes were flanked by the left and right T-DNA borders which signalled the transfer of the encompassed sequence as single stranded DNA, into the eukaryotic nucleus for genomic integration. Integration was intended to be as stochastic as possible, therefore no homologous sequences to the *P. nodorum* genome were included in the pPK2 plasmid. Fungal colonies were sub-cultured from transformation plates containing 200ug/ml Hygromycin B until the negative controls, containing untransformed spores, showed fungal growth. In total 950 Hygromycin B resistant colonies were sub-cultured onto CzV8Agar medium containing 200ug/ml Hygromycin B prior to being sub-cultured into single wells of a 96 well plate containing liquid CzV8 medium. This library was used for the following forward genetic screens. Due to time and logistical constraints the mutants generated were not isolated from single spores prior to generating the mutant library, nor to subsequent screens.

### 2.3.2 Southern blot analysis determined *A. tumefaciens* introduced few and random mutations to the *P. nodorum* genome

Mutation rate is important in a forward genetics screen as it determines the number of mutants that require screening to find the desired phenotype, as well as the difficulty in identifying the responsible locus. Increasing the number of disrupted genes per transformant (genome saturation) increases the likelihood of finding a desired phenotype as well the difficulty in determining which disruption lead to that phenotype. To quantify the T-DNA random insertion rate in *P. nodorum* I randomly selected 30 of the first 150 transformants then probed these strains genomic DNA for the known T-DNA insertion using Southern blot analysis. These Southern blots are shown in Figure 2.03. The Southern blot analysis also indicated the degree of insertion site bias at a genome level. Mutation bias dictates the quality of a forward genetics screen using these mutants. Common band patterns indicate that particular genetic loci are more susceptible to integration, and the level of bias introduced to the screen.

A 4kb amplicon encompassing the *Hph* gene, and adjacent to a *Bam*HI restriction site, was used as a probe in the DIG-CDP:STAR immuno-Southern blot system (described in section 2.2.5.8). This amplicon was generated using the primers Southern_Probe_F and Southern_Probe_R. Extracted genomic DNA (gDNA) samples were digested with the restriction endonuclease, NEB™ *Bam*HI-HF, hybridized with the DNA probe and then visualised. The pPK2-HPH:GFP plasmid was spotted onto the top of the membrane as a positive control. Genomic DNA from the wild type strain was used as a negative control. Single bands were observed in 22 of the 32 (69%) transformants analysed, and no more than two bands were ever observed in a single strain indicating a low rate of T-DNA insertion. No band was observed in t1, t17 or t18 and a faint band was seen in t123 at the same height as the neighbouring sample. This band could be contamination between wells during loading.

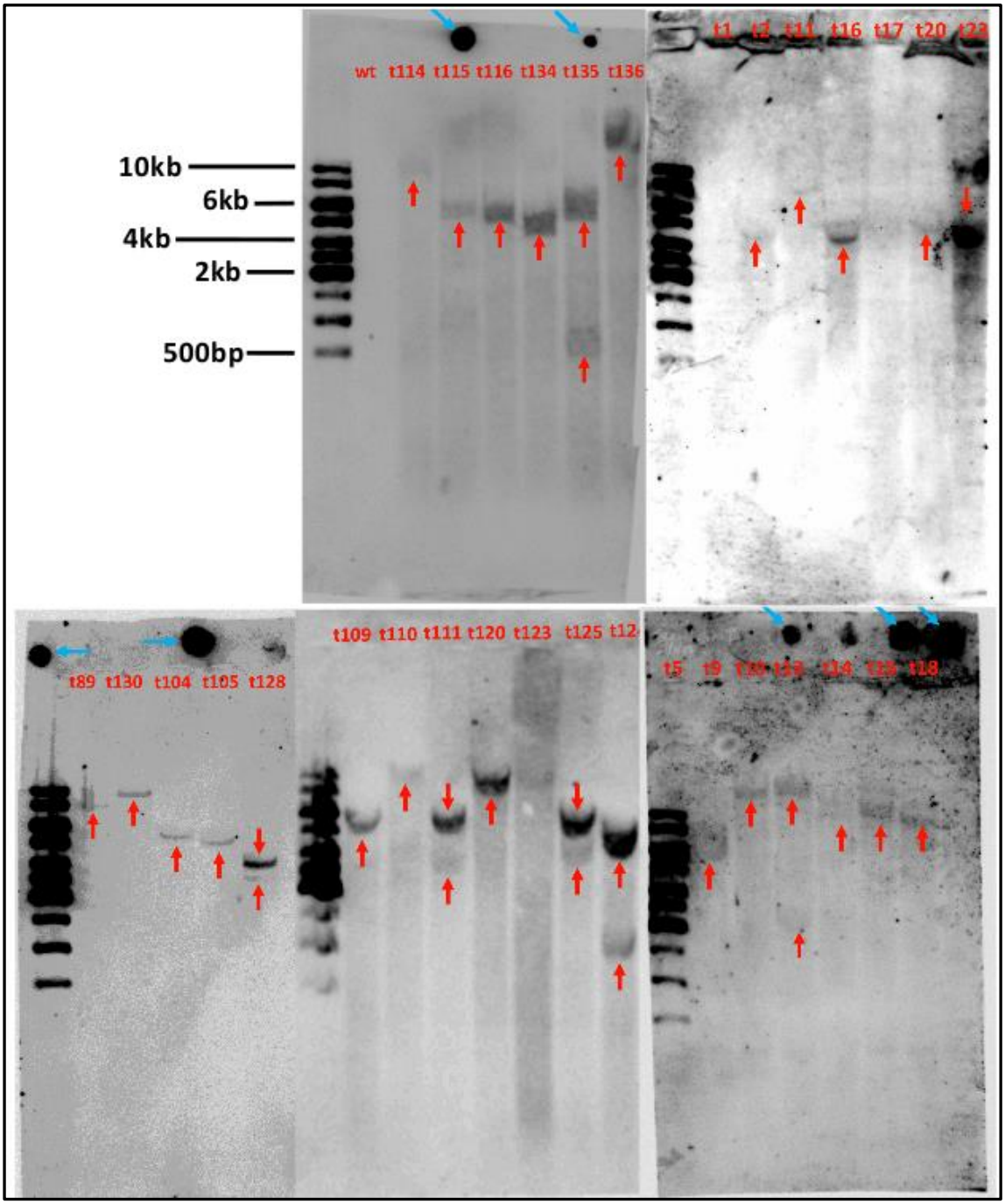


*(Figure 2.03: Southern blot analysis of* Bam*HI digested gDNA from randomly generated* P. nodorum *transformants. Red arrows indicate hybridization bands. Blue arrows indicate where the pPK2 plasmid was spotted onto the membrane as a positive control)*

### 2.3.3 A descriptive database of *P. nodorum* strains in the random mutant library

The *P. nodorum* mutant library was stored in 96 well plates containing CzV8 liquid medium, providing an accessible platform to rescreen the library for multiple phenotypes. So that mutants could be re-used easily in the future six observable growth characteristics of each mutant were recorded and stored in an excel database. These traits are shown in Table 2.05, alongside their relative frequency, to illustrate the library's range and recurrence of phenotypic traits. These traits included mycelial growth rate, texture and pigmentation, as well as the strains' ability to produce pycnidia and cirrus (the spore containing fluid exuded by pycnidia), virulence and any other abnormal characteristics. Figure 2.04 exemplifies the strong pigmentation differences between some mutants whereby t675 produces a bright pink metabolite while the wild type does not.

*(Table 2.05: Frequency of common phenotypic traits observed in a* P. nodorum *random mutation library grown on rich medium, two minimal media and* in planta*. The frequency of traits is non-redundant, shown once for each strain irrespective of that trait appearing on multiple media. GABA induces a strong morphological change in the fungus through an unknown mechanism, as such the frequency of phenotypes is shown inclusive and exclusive of those traits observed on GABA minimal medium.)*

| | Medium | | | | | Proportion (%) | |
|---|---|---|---|---|---|---|---|
| **Trait** | **V8PDA** | **Minimal Medium (γ-)** | **Minimal Medium (γ+)** | ***In Planta*** | **Total** | **Including GABA** | **Excluding GABA** |
| **Abnormal Pycnidia** | **178** | **147** | **279** | | **604** | **63.6%** | **34.2%** |
| *Increase* | 26 | 9 | 6 | | 41 | 4.3% | 3.7% |
| *Decrease* | 152 | 130 | 273 | | 555 | 58.4% | 29.7% |
| **Excess Cirrus** | **18** | **0** | **0** | | **18** | **1.9%** | **1.9%** |
| **Pigmentation** | **46** | **17** | **70** | | **133** | **14.0%** | **6.6%** |
| *Pink* | 14 | 1 | 3 | | 18 | 1.9% | 1.6% |
| *Yellow* | 9 | 12 | 58 | | 79 | 8.3% | 2.2% |
| *Orange* | 4 | 0 | 3 | | 7 | 0.7% | 0.4% |
| *Green* | 6 | 0 | 0 | | 6 | 0.6% | 0.6% |
| *Black* | 12 | 1 | 1 | | 14 | 1.5% | 1.4% |
| *Grey* | 1 | 3 | 5 | | 9 | 0.9% | 0.4% |
| *Secreted* | 2 | 0 | 0 | | 2 | 0.2% | 0.2% |
| **Growth defect** | **37** | **9** | **14** | | **60** | **6.3%** | **4.8%** |
| **Miscellaneous** | **11** | **0** | **0** | | **11** | **1.2%** | **1.2%** |
| *Hydrophilic* | 6 | 0 | 0 | | 6 | 0.6% | 0.6% |
| *Aggressive growth* | 3 | 0 | 0 | | 3 | 0.3% | 0.3% |
| *Thick/Tough Mycelia* | 2 | 0 | 0 | | 2 | 0.2% | 0.2% |
| **Virulence** | | | | **8** | **8** | **0.8%** | **0.8%** |
| *Increase* | | | | 7 | 7 | 0.7% | 0.7% |
| *Decrease* | | | | 1 | 1 | 0.1% | 0.1% |

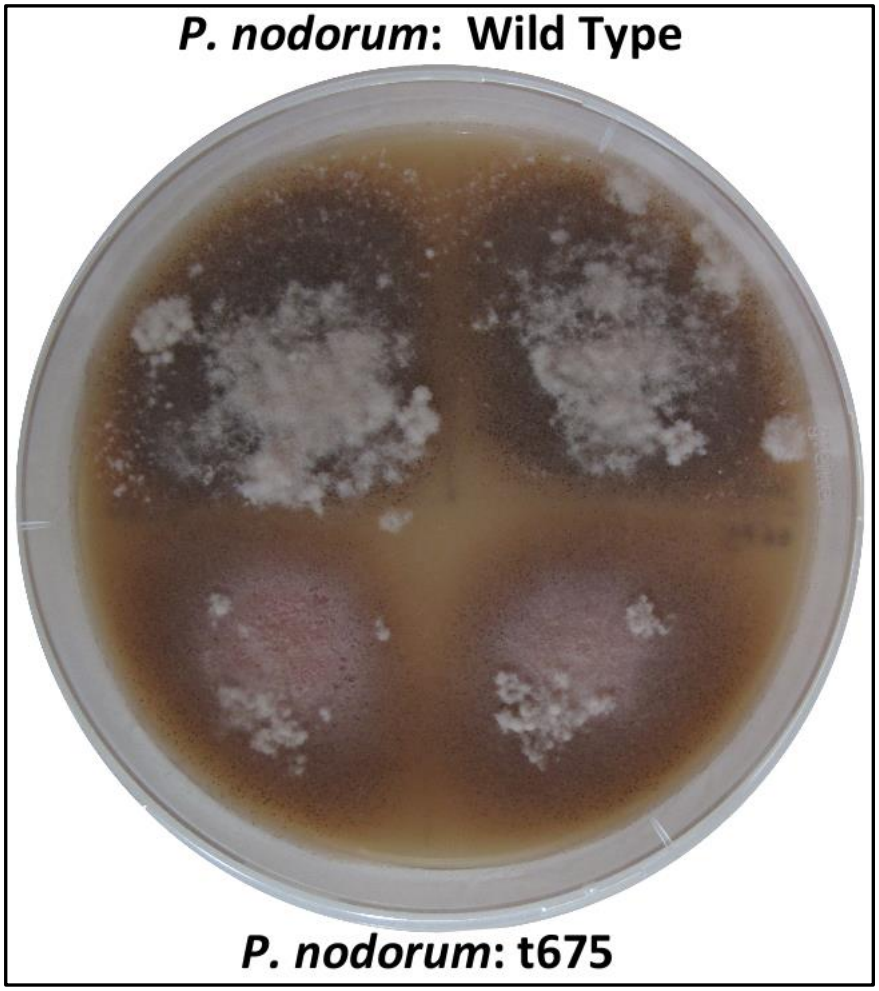


*(Figure 2.04: Comparison of the* P. nodorum *wild type strain (top) and the highly pigmented pink t675 strain (bottom). The two strains were grown side by side on V8PDA medium to illustrate the strong colour differences between mutants in the* P. nodorum *random mutant library. t675 showed comparable growth, pycnidiation and virulence to the wild type.)*

To elucidate phenotypic differences as efficiently as possible the strains were grown on both a rich medium (V8PDA) and two minimal media. Basic minimal medium is not conducive to pycnidiation and sporulation. However, a state of *hyper-sporulation* is induced on minimal medium containing the non-proteinaceous amino acid, γ-aminobutyric acid (GABA) (Mead et al., 2013). The presence and absence of GABA further differentiated mutants defective in reproduction. Table 2.05 illustrates the frequency of

disruptions to genes required for mycelial growth (4.8%-6.3%) and reproduction (34.2%-63.6%). Pycnidiation defects were the most commonly observed trait, followed by pigmentation. Interestingly, mutants with tough, hydrophilic mycelia were also periodically encountered, as well as mutants able to traverse the plastic wall and lid of the Petri-dish.

### 2.3.4 A pathogenicity assay was optimized for high throughput screening of *P. nodorum* mutants

Traditionally, the Solomon lab has assayed the pathogenicity of *P. nodorum* mutants using either whole seedling spray assays or by spot inoculating agar-embedded leaf segments with a standardised spore suspension. Neither of these assays were practical to screen the virulence of 950 strains of *P. nodorum*. Therefore, I altered the detached leaf assay method for the purpose of high throughput screening. Both the low and high through-put protocols are described in section 2.2.5.10. The optimized method involved growing the mutant library in stationary liquid culture in Greiner™ 96 well plates resulting in the fungus forming a rubbery mat of mycelia at the surface. Plugs of mycelia were cut using pipette tips and used as inoculum for detached leaf assays. Depending upon the natural variation in leaf thickness and turgidity, ca. 15 wheat leaves were embedded in each 90mm Petri dish. This allowed 13 mutant strains to be screened in each Petri dish as two leaves were left as either un-inoculated or wild type controls. In the interest of time only single replicates were produced. Figure 2.05 exemplifies the product of this method, with fewer leaves for clarity.

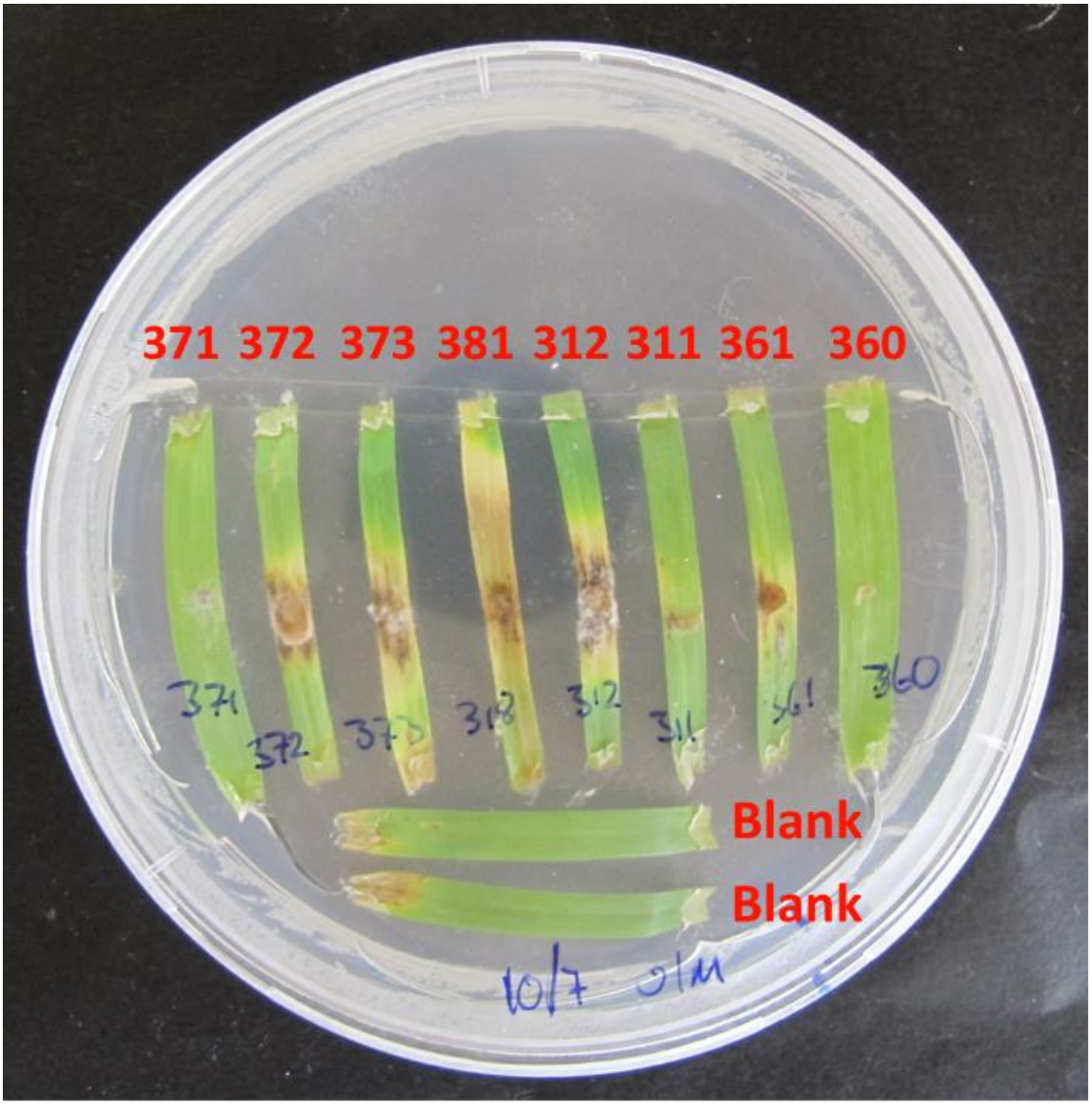


*(Figure 2.05: Example of the high throughput detached leaf assay for the* P. nodorum *mutant library on the susceptible cultivar, Grandin, after 7 days post inoculation. Transformants t371, t372, t373, t381, t312, t311, t361, t360 are shown in the top vertical leaves, whilst blank water controls are shown on the bottom horizontal leaves. These leaves were inoculated using the high through put, mycelial plug method described in Section 2.2.5.10. Note the variation in size of mycelial plug due to dehydration of the plug or lack of* in vitro *growth of that strain)*

### 2.3.5 A forward genetic screen identified seven strains of *P. nodorum* that do not elicit disease symptoms on the susceptible wheat cultivar Grandin

The mutant library of *P. nodorum* was screened to identify strains exhibiting reduced disease symptoms on the susceptible wheat cultivar Grandin using the method described above. Candidate strains, from the initial screen, were then re-assessed with four biological replicates (section 2.2.3). Of the 950 strains screened, seven consistently showed reduced disease symptoms. These were labelled t112, t177, t255, t388, t697, t784, t799 and are shown in Figure 2.06a and Figure 2.06b. The wild type infection showed white, fluffy, mycelia extending aerially from the agar plug used to inoculate the leaf. Brown necrotic tissue surrounded the inoculation site. Necrosis, chlorosis (yellowing of the leaf tissue), and pycnidia formation were the predominant symptoms associated with disease. In comparison, the mutant strains showed little to no necrosis or chlorosis and varying degrees of hyphal growth. Strain t112 induced limited necrosis at the inoculation site in two of four replicates and failed to do so in the other two. In all four inoculations, this strain failed to induce strong disease symptoms, nor did it produce pycnidia. t177 did not appear to recognise the host. Exploratory mycelia did not extend from the agar plugs, used as inoculum, across the leaves or aerially. Further, the leaves showed no signs of necrosis or chlorosis. t255 was able to initiate minor disease symptoms in a single replicate, but they did not eventuate into tissue collapse or pycnidia formation. In symptomless replicates the inoculation plugs showed faint signs of hyphal growth, but these appeared to be aerial and not interacting with the host.

Similar to t112, strain t388 induced limited necrosis at the inoculation site, but no hyphae could be seen extending across the leaves. t697 hyphae grew abundantly from the agar plug inoculum, however no disease symptoms and no obvious interaction between host and

pathogen occurred. Strain t784 hyphal growth extended across the leaf surface and was the most abundant of any mutant. This strain failed to induce any disease symptoms, despite comparatively more interaction with the host. t799 displayed similar host-pathogen interaction patterns to t255 characterised by modest hyphal growth from the inoculum, and a small to nil halo of necrosis surrounding the agar, but no ensuing disease symptoms. These strains were designated as asymptomatic as they did not induce typical disease symptoms. However, it was unknown if they were able to penetrate the leaf tissue and infect the host. These strains were chosen for subsequent characterisation.

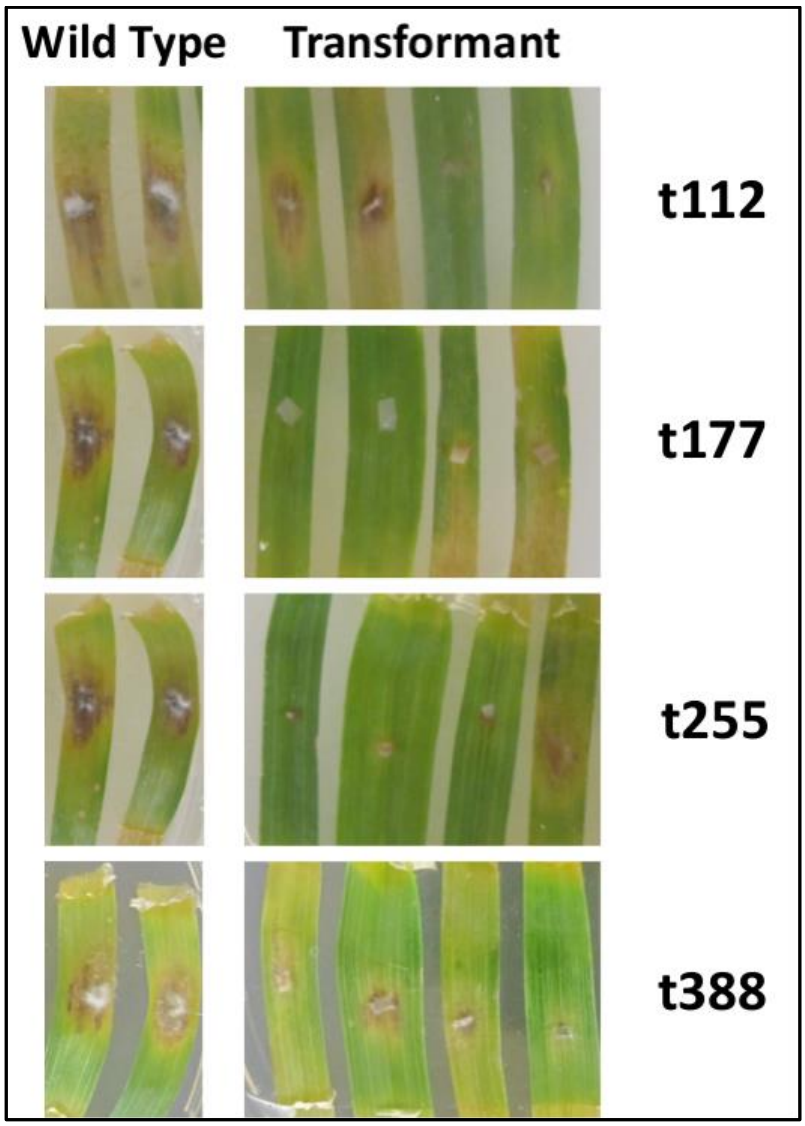


*(Figure 2.06a: Confirmation of asymptomatic strains, t112, t177, t255, t388 via detached leaf assay on the susceptible wheat cultivar, Grandin. These interactions were allowed to progress over 14 days from the time of inoculation. The images shown, taken at 7-days post inoculation, are representative of the overall interaction between each strain and the host. Leaves were inoculated with 5mm agar cubes cut from V8-PDA plates. The wild-type strain, in the left-hand panel, induced consistent patterns of necrosis across all assay plates and between replicates within assay plates. Several mutants were screened on each plate utilising a common wild type control.)*

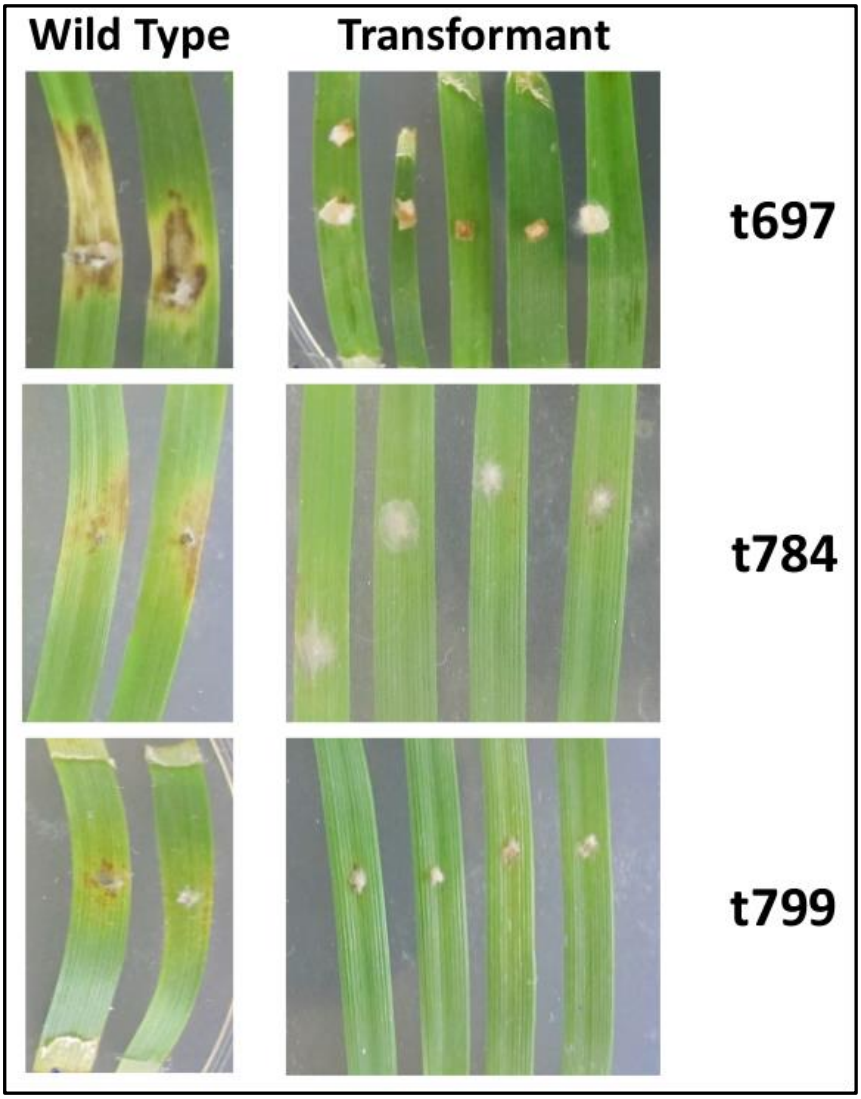


*(Figure 2.06b: Confirmation of asymptomatic strains, t697, t784, t799, using detached leaf assays on the susceptible wheat cultivar, Grandin. These interactions were allowed to progress over 14 days from the time of inoculation. The images shown, taken at 7-days post inoculation, are representative of the over-all interaction between each strain and the host. Leaves were inoculated with 5mm agar cubes cut from V8-PDA plates. The wild-type strain, shown in the left-hand panel, induced somewhat inconsistent patterns of necrosis in the leaf between assay plates but was consistent between replicates within assay plates and induced strong disease symptoms relative to the mutant strains. Several mutants were screened on each DLA plate utilising a common wild type control on each plate. Therefore, the wild type control may be seen repeatedly)*

To gain a better insight into the physical mechanisms by which the asymptomatic strains of *P. nodorum* were unable to initiate disease, I observed the pathogen-host interaction at a microscopic level. The Leica DFC7000t microscope and camera were used to take the images in Figure 2.07. Figure 2.07 shows the inoculation site of the wheat cultivar, Grandin, with the wild type, t255, t388, t784, and t799 strains. Not all strains could be observed interacting with the host microscopically as the microscope was damaged and considerable time was taken for repairs. As such, the study was advanced having only microscopically examined several strains interacting with the host. Microscopically, t255 hyphae appeared not to invade the leaf tissue. The leaf tissue surrounding the inoculation site was necrotic and brown, but with no apparent hyphae. t388 showed a similar lesion at the inoculation site, with hyphae extending from the lesion. However, the necrosis was confined to the inoculation site and did not extend with the hyphae. t784 produced a mass of hyphae progressing from the inoculation site across the leaf without inducing necrosis. Little necrosis formed around the t799 inoculation site and explorative hyphae failed to extend. It is interesting to note that hyphae growth of t784, t388 and t799 appear unresponsive to stomatal openings in the leaf. During infection with the wild type strain, the plant cells appear brown and mycelia were seen extending throughout the tissue, shown by red arrows in Figure 2.07. In contrast, the mutant strains showed very little to no necrotic tissue at the inoculation site and varying hyphal growth. As seen in Figure 2.06b, strain t784 showed a large degree of growth, seemingly across the surface of the leaf, with no indication of disease formation, while strain t112 showed some mycelial growth surrounded by limited necrosis. This suggests pathogenesis had been disrupted in different ways for each of these mutants. The characteristics of each mutant during interaction with the host are summarised in Table 2.06

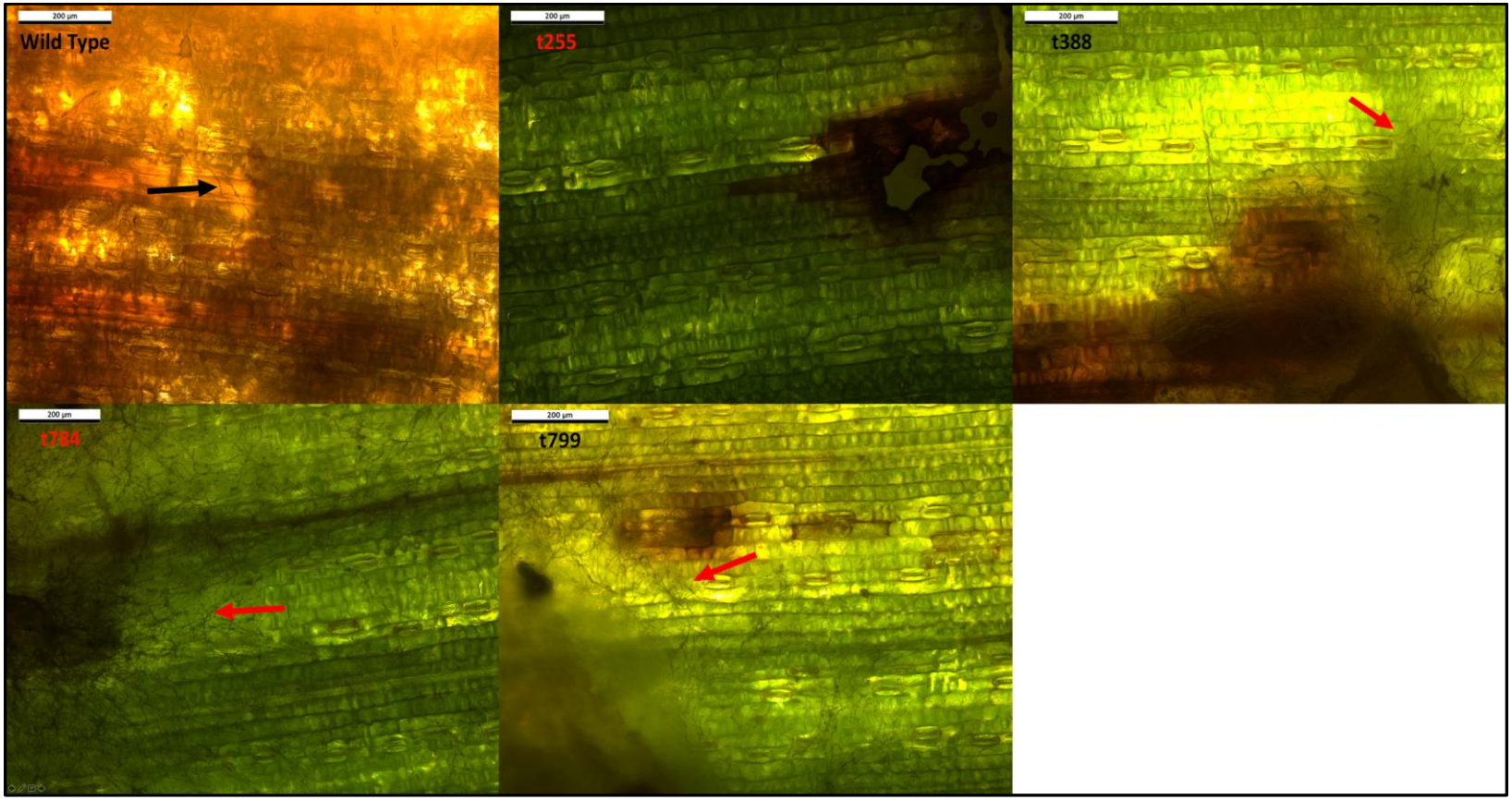


*(Figure 2.07: Microscopic image of the detached leaf assay inoculation sites of* P. nodorum *wild-type and asymptomatic mutants selected from the random mutation library. The arrows indicate hyphal growth. Scale bar represents 200µm at 100x magnification. The inoculation site is shown the left-hand side of the wild-type, t784 and t799 panels. Whilst the inoculation site is seen to the right-hand side of panel t255 and the bottom of t388)*

*(Table 2.06: Inoculation characteristics of avirulent* P. nodorum *mutants)*

| ***P. nodorum* mutant** | **Inoculation characteristics** |
|---|---|
| t112 | This strain caused limited necrosis at the inoculation site. No pycnidia were produced. |
| t177 | Extensive hyphal growth that failed to produce penetration structures or recognise natural openings in the host. No necrosis, chlorosis or pycnidia were observed. |
| t255 | Limited necrosis in a single replicate, but no pycnidia. The other replicates produced limited aerial hyphae and did not interact with the host. |
| t388 | Induced limited necrosis at the inoculation site, but hyphae failed to invade host tissue or produce pycnidia. |
| t697 | Hyphae grew extensively from the inoculation plug, however failed to penetrate the host, induce disease symptoms or produce pycnidia. |
| t784 | Hyphal growth covered far greater areas of the leaf but failed to induce any disease symptoms or produce pycnidia. |
| t799 | limited necrosis surrounded the inoculation site, however the fungus failed to proliferate through host tissue or produce pycnidia. |

### 2.3.6 *P. nodorum* strain, t26, partially induces disease symptoms in the non-susceptible wheat cultivar, Br34

Complementary to the loss of virulence screen, I performed a gain of virulence screen of the mutant library against the non-susceptible wheat cultivar, Br34. Septoria nodorum blotch (SNB) is currently controlled by breeding wheat cultivars that lack susceptibility genes to *P. nodorum* effectors rather than resistance (Vleeshouwers and Oliver, 2015). Mutations leading to gain of virulence are informative for two reasons. First, they indicate pathway adaptations available to the pathogen to overcome current disease control methods. Second, these mutations begin to elucidate elements of immunity and pathogen recognition in the host. This screen mimicked the method of the previous screen, however looking for a gain of disease symptoms rather than loss. An example of these assays is shown in Figure 2.08.

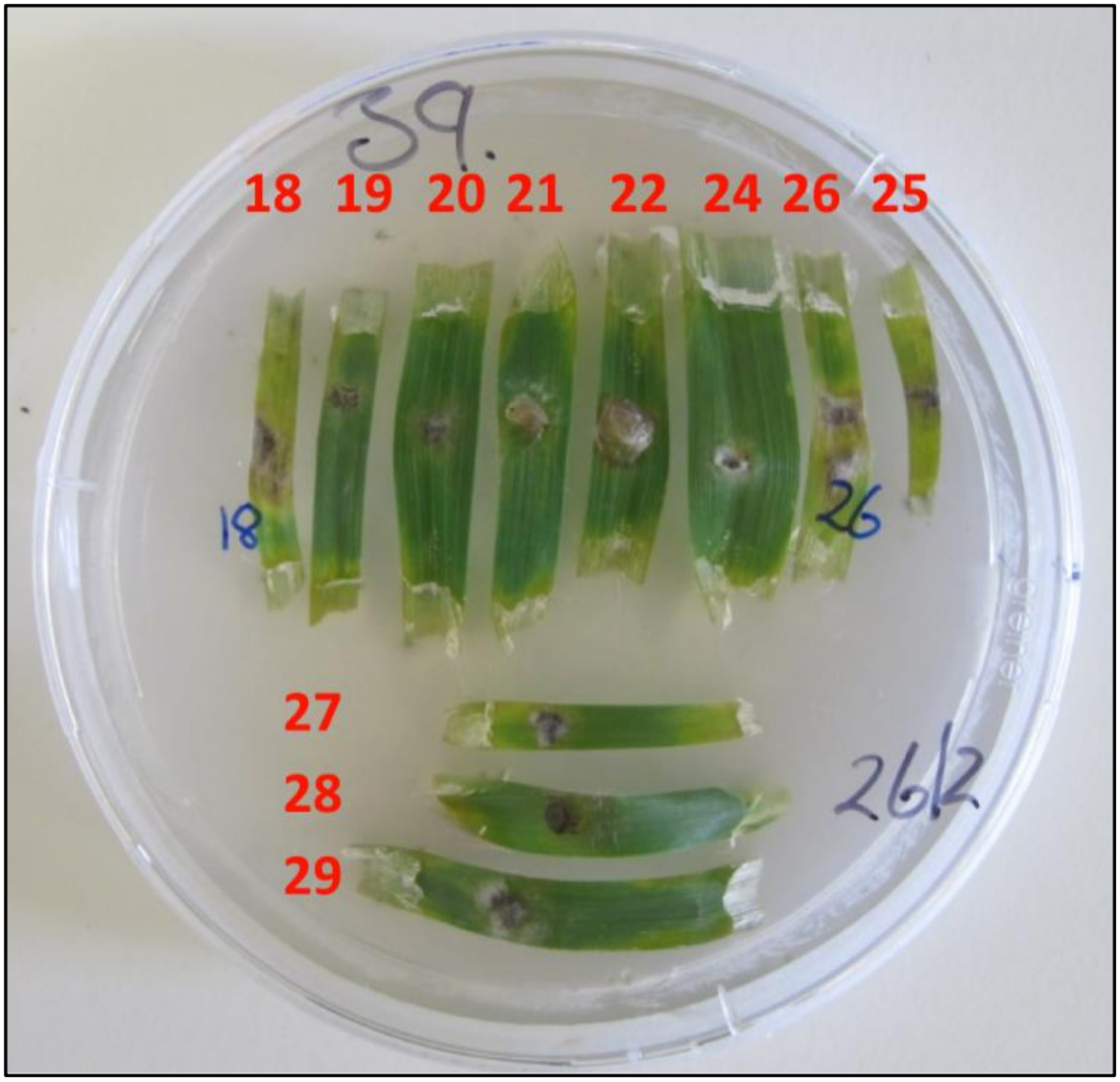


*(Figure 2.08: Example of the high throughput detached leaf assay for the* P. nodorum *mutant library on the non-susceptible wheat cultivar, Br34. Leaves were inoculated with plugs of fungal hyphae after being imbedded in agar. The interactions were allowed to progress for 14 days)*

Br34 did not contain any of the known susceptibility genes rendering the wild type strain of *P. nodorum* Sn15 avirulent on this cultivar. Of the 950 mutant strains of *P. nodorum* screened, a single isolate, t26, was observed to produce disease symptoms greater than those of the wild type strain on Br34. One such interaction is shown in Figure 2.09 where by disease symptoms are clear on both the non-susceptible (Br34) and susceptible (Grandin) wheat cultivars. Although the necrosis induced on Br34 by t26 was not as extensive as that seen during the interaction with Grandin, there was more necrotic tissue when compared to the wild-type interaction. However, this compatible interaction between t26 and Br34 could not be repeated consistently. Due to this inconsistent result t26 was not investigated further.

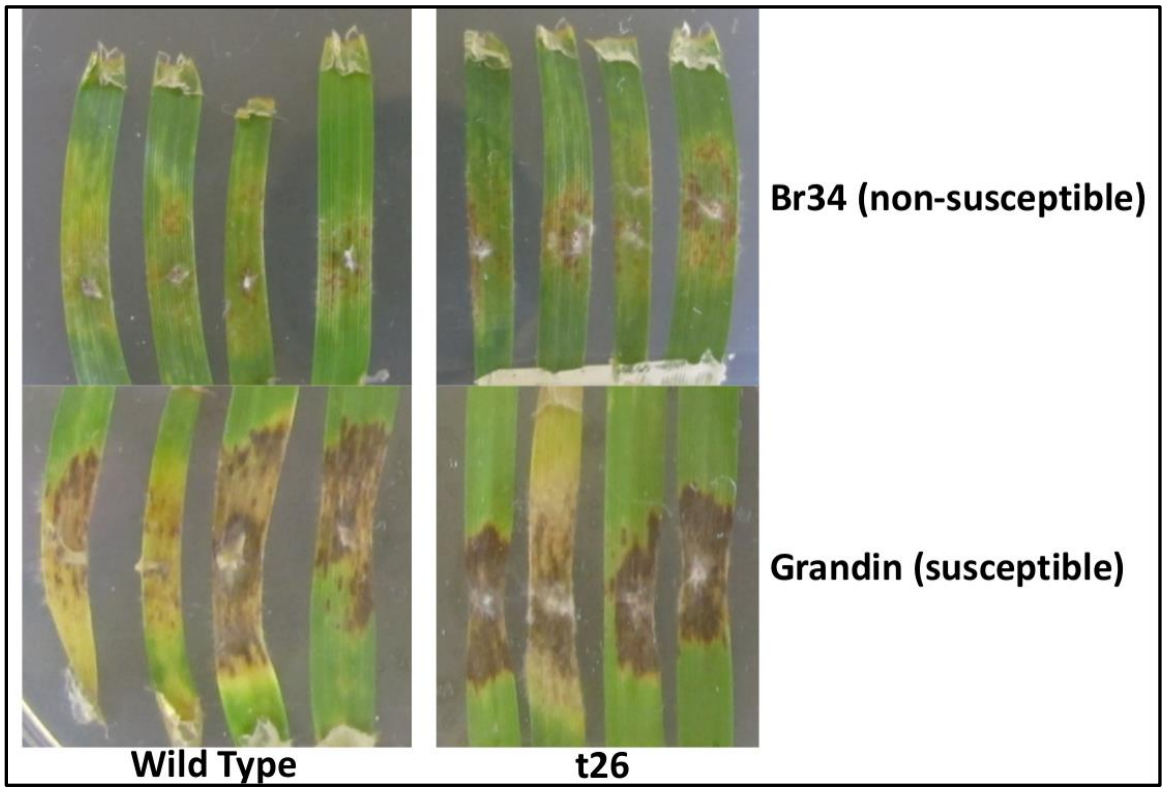


*(Figure 2.09: Comparison of disease symptoms between the susceptible and non-susceptible wheat cultivars Br34 and Grandin during interaction with the wild type and t26 strains of* P. nodorum. *These interactions were allowed to progress for 14. The interactions were photographed at 7dpi. The host was inoculated with 5mm agar cubes cut from inoculated V8-PDA plates. Symptoms were comparable between the two fungal strains on the susceptible cultivar, showing equivalent amounts of brown necrotic tissue. In contrast, strains t26 was able to induce a moderate amount of necrosis extending from the inoculation site on the non-susceptible host, as compared with the wild type strain.)*

## 2.4 Discussion

### 2.4.1 Generation and statistical analysis of a *P. nodorum* random mutation library

*Agrobacterium* mediated random mutagenesis has proven to be a useful tool for generating a random mutation library in *Parastagonospora nodorum*. This method facilitated the rapid production of 950 stochastic, low T-DNA copy number transformants, with accompanying morphological descriptions. This is ideal for a forward genetics screen focusing on an organism with a small genome as it allows the phenotype of interest to be quickly identified and linked to a genotype.

The rate T-DNA insertion was measured by Southern blot analysis of 32 randomly chosen transformants. No sample in this analysis displayed more than two hybridization bands, suggesting a relatively low rate of T-DNA insertion per mutant. Betts et al (2007) also used a Southern blot analysis to determine a low (1-3) integration rate of T-DNA in the rice pathogen, *Magnaportha oryzae*. This study generated over 55,000 transformants, from a combination of *Agrobacterium* and PEG/$CaCl_2$ mediated transformation methods, which were screened for growth defects, pigmentation and virulence, similarly to the analyses conducted in this chapter (Betts et al., 2007). Betts et all showed an average insertion rate of 1.4 integrations per *M. oryzae* genome, compared to 1.2 integrations per *P. nodorum* genome observed in this study.

There are other sources of mutation in a T-DNA screen, fragmentated T-DNA inserting into multiple loci. Fragmentation was reported by Choi et al (2007), in their comprehensive, genome wide, analysis of T-DNA insertions in the *M. oryzae* genome (Choi et al., 2007). Fragmentation of the T-DNA insertion cassette used in this study would not be readily identified by Southern blot I used. The Southern blot probe used in

my experiments only included 4,000 bp encompassing mainly the PgpdA promoter, *Hph:GFP* gene and 5'UTR. The *trpC* terminator and 3' prime portion of *GFP* of a fragmented T-DNA insert would not be visualised on a Southern. Disruptions caused by fragments outside of the probe would not be observed. Several blots visualised a fragment smaller than the 4,000 bp probe. All blots displaying bands smaller than 4,000 bp displayed two bands suggesting the probe binding sequence may have fragmented and disrupted multiple loci. Additional, mutations to the genome that are not associated with the T-DNA insert, such as chromosomal breakage or single nucleotide polymorphisms, will not be apparent. Using whole genome sequencing, Chambers et al (2014) showed *Agrobacterium* mutagenesis induced chromosomal rearrangement in the canola pathogen, *Leptosphaeria maculans*. Whole genome sequencing would be a powerful tool to distinguish chromosomal rearrangements and fragmentation events in the *P. nodorum* library generated in this study.

Southern Blot analysis also demonstrated that the T-DNA integration events were randomly distributed throughout the genome. In comparison to the ladder, no bands were observed at exactly the same height indicating there was no site bias for integration on the genomic level. Choi et al (2007) sequenced the surrounding regions of T-DNA random insertion in *M. oryzae* and report a bias for T-DNA to preferentially integrate into the 5' UTR of a gene, over the coding region (Choi et al., 2007). A chromosome level bias was not reported in this study. However, integration hotspots in a genome may influence a forward genetics screens' stochasticity as much as a bias towards promoters or AT rich regions. For example, a tendency to integrate into gene poor regions would require production of more transformants to find one of interest.

### 2.4.2 A morphological database of *P. nodorum* mutants is an informative tool for future investigations

Traits in the morphological database were chosen for their potential to prompt future investigations and to circumvent the need to re-screen the entire library (Table 2.05). Pycnidiation and cirrus production are easily observable *in vitro* and directly linked to the fungus' ability to cause disease. Without the ability to sporulate *P. nodorum* forgoes it's polycyclic infection cycle, and field epidemics cannot ensue (Solomon et al., 2006). Novel mechanisms of sporulation are readily investigated by selecting pycnidia deficient mutants from the library. On this basis, Thermo Asymmetric InterLaced PCR (TAIL-PCR) identified the T-DNA disrupted locus in the pycnidia deficient strain, t116. This strain and identification of its' disrupted loci is described in Chapter 4. As sporulation is crucial to *P. nodorum* field epidemics this database and mutant library provide a useful tool for future investigations.

Pigmentation is most likely indicative of metabolic disruptions, either directly or via mis-regulation. For example, adenine auxotrophy in *Saccharomyces cerevisiae* lead to pink colonies (Sharma et al., 2003) and disruptions to the sterigmatocystin pathway in *Aspergillus nidulans* resulted in accumulation of a coloured precursor (Pfannenstiel et al., 2017). Pigmented mutants are potentially interesting with regards to secondary metabolism. Pfannenstiel et al (2017) investigated the sterigmatocystin pathway in *A. nidulans* as this pathway has been closely linked to sporulation and toxin production. Similarly, disruptions to secondary metabolite production in *Alternaria alternata* negatively affect virulence (Chen et al., 2013; Johnson et al., 2000). Conversely, disruptions to the *Ace1* hybrid secondary metabolite cluster in *Magnaporthe grisea* abolished avirulence on resistance rice cultivars (Böhnert et al., 2004). In this way,

pigmented *P. nodorum* mutants provide prospects for discovering novel metabolites and mechanisms of virulence.

Pigmented mutants displaying otherwise normal growth and infection characteristics may also serve as useful *'soft landing'* sites for site directed mutagenesis. Soft landing sites provide genomic loci to insert exogenous sequences, such as reporter, overexpression, RNAi, CRISPR/cas9, and Transcriptional Activator-Like EndoNuclease (TALEN) constructs. Disruptions to these loci will not affect the normal functioning of the organism, but produce a selectable phenotype. For example, the *P. nodorum Malate synthase* mutant (*mls1*) exhibits wild-type traits except that its spores fail to germinate in the absence of a carbon source (Solomon et al., 2004). Utilising the *Mls1* locus as a soft-landing site, mutants need to be screened twice. Once for the selectable marker denoting insertion fragment (*Hph*) integration. Those colonies are then screened for failure to germinate in the absence of a carbon source, indicating disruption of the *Mls1* locus by the insertion cassette. Rather than screening for a loss of function, it would be easier to screen for a visual phenotype such as pigmentation. There are pigmented mutants in the descriptive database which displayed otherwise usual growth, sporulation and virulence. These mutants may warrant future investigation for expediting mutant screening, and limiting off target and positional effects by ectopic integration of constructs.

Growth and miscellaneous traits also direct future investigation. For example, hydrophobins are a family of proteins playing roles in cell structure, immuno-recognition and are known virulence known factors in plant and insect fungal pathogens (Aimanianda et al., 2009; Ebbole, 1997). In the entomopathogenic fungus, *Metarhizium brunneum*, disruptions to various hydrophobin proteins lead to reduced virulence in all

mutants, but not all mutants produced hydrophilic hyphae (Sevim et al., 2012). While in the phytopathogen, *Ophiostoma quercus*, over expression of a hydrophobin lead to increased hydrophobicity and gain of virulence (Del Sorbo et al., 2000; Temple et al., 1997). Further, Aimanianda et al (2009) propose the hydrophobicity of hydrophobins hide *Aspergillus fumigatus* spores from the mammalian immune system (Aimanianda et al., 2009). The *P. nodorum* mutant library identified several hydrophilic mutants, indicating mis-regulation or loss of one or multiple cell surface proteins. These mutants retained their virulence suggesting hydrophobicity of the hyphal cell wall is not essential for *P. nodorum* mycelium to infect wheat. However, the role of spore surface hydrophobins remains unknown and may, like *A. fumigatus*, play a role in spore dispersal and pathogenicity. The growth and miscellaneous traits described in the mutant database provide convenient avenues for future investigations.

The miscellaneous growth characteristics described are interesting beyond the scope of plant-microbe interaction, in an industrial context. Several of the mutants grew slower but with toughened hyphae that were difficult to cut with a scalpel. Further, several strains grew aggressively, climbing the plastic wall and lids of Petri dishes. Such mutants may find utility in materials, tissue or chemical engineering as well as bioremediation (Gamerith et al., 2016; Li et al., 2005; Lutolf and Hubbell, 2005). These traits are unusual for *P. nodorum* but showcase the potential of the descriptive database for fungal biotechnology. Further, linking traits together such as virulence and pigmentation opens avenues for rapid and novel, future investigation.

### 2.4.3 Forward genetics identifies seven avirulent strains of *P. nodorum*

The wheat cultivar Grandin was chosen as the host in the loss of virulence screen for two reasons. Primarily, Grandin contains multiple susceptibility genes to *P. nodorum*

(Tsn1, *Snn1, Snn2* and *Snn3*), which act in a gene for gene manner with the effector genes *ToxA Tox1 and Tox3* (Friesen et al., 2008; Liu et al., 2004). Previous work shows that on this cultivar any of these known effectors cause strong necrotic symptoms. (Friesen et al., 2008; Liu et al., 2004). If the T-DNA insertion disrupts one of the effector genes, remaining effectors compensate for this loss and the resulting strain will display a virulent phenotype on Grandin. Thereby selecting against mutations to these known virulence genes.

I was able to isolate seven strains of *P. nodorum* that display an avirulent phenotype on a susceptible wheat cultivar. Figures 2.06a, 2.06b and 2.07 illustrate these strains during interaction with the host and their different growth patterns. These differences indicate that each strain has been disrupted in a different part of the infection process and represent a unique avenue for investigation. For instance, t112 in Figure 2.07 initiates disease symptoms but fails to progress beyond the initial interaction with the host. This strain may be unable to respond to host defences, or to utilise the nutrients released by the decaying plant tissue. Strain t784, on the other hand, grows extensively with the host without initiating disease and, for a period, the two organisms appear to mutually coexist. It is possible that strain t784 lacks the ability to correctly recognise the host, or some aspect of the host such as the stomata, and so extends its hyphae, searching for an opening, until it depletes its nutrient reserves. Microscopic images of the leaf surface fail to determine whether the hyphae are extending across the surface or through the tissue interior. It is unclear whether the fungus is unable to recognise or penetrate the host, or if host defences remain un-triggered and the fungus is growing sapro-, endo- or epiphytically. The molecular basis for these strains' behaviour will elucidate some of the mechanisms behind plant-microbe interactions. In particular,

strain t784 may begin to reveal more basal aspect of mutualistic fungal-plant interactions.

This screen was successful in comparison to other forward genetic screens of fungal pathogens for three reasons. First, of 950 random mutants, seven were identified displaying the phenotype of interest. Second, the high throughput assay I designed for screening was efficient and cheap. Third, transformants contained few and readily identifiable mutations. In comparison, Idnurm et al (2009) screened 450 haploid *Cryptococcus neoformans* transformants, produced by *Agrobacterium* mediated transformation, to find a single avirulent transformant in a mouse inhalation assay (Idnurm et al., 2009). An animal model, which is notoriously difficult and prohibitively expensive, was required to screen this pathogen. Further *C. neoformans* is able to infect humans, and displays both haploidy and diploidy, making this organism difficult to work with (Fu et al., 2014). A monumental effort was required by Idnurm et al (2009) to find this single avirulent mutant. In contrast, *P. nodorum* is a host specific plant pathogen displaying only haploidy under laboratory conditions. The high throughput pathogenicity assay I developed permits a forward genetics approach to be utilised without a prohibitively difficult or expensive screen. Through this screen, I was able to isolate seven strains displaying the desired phenotype. On the other hand, *C. neoformans* harbours approximately half the genes of *P. nodorum* (Birren et al., 2005; Loftus, 2005; Syme et al., 2016) and using a similar mutagenesis technique Idnurm et al (2009) isolated fewer avirulent mutants were obtained per volume screened. The success of this screen was contingent upon the development of the labour and cost efficient, high throughput pathogenicity screen.

Utilizing other methods of mutagenesis have led to the disruption of multiple loci, and chromosomal rearrangement, such as the PEG/$CaCl_2$ mediated integration of linear DNA by Urban et al (2015) in the wheat pathogen, *Fusarium graminearum*. Urban et al (2005) generated 650 random transformants identifying eight avirulent strains, a higher rate than the *P. nodorum* screen in a similar sized genome (King et al., 2015). However, whole genome sequencing revealed chromosomal rearrangement and multiple insertions in three of the eight transformants, confounding identification of the disrupted loci (Urban et al., 2015). Other phenotypes are more prevalent or more easily identified, which influences the number of transformants needed to find the phenotype of interest. Although not pathogenic, a secondary metabolic screen in *Aspergillus nidulans* using chemical mutagenesis exemplifies a less laborious screen and mutagenesis method, resulting in a higher yield of interesting mutants. Butchko et al (1999) generated random mutants of *Aspergillus nidulans* through chemical mutagenesis. These mutants were screened by Butchko et al (1999), and re-screened by Pfannenstiel et al (2017), for mutants deficient in the ability to produce the secondary metabolite, sterigmatocystin. The phenotype of interest in these cases was visible during *in vitro* growth, as the mutants would accumulate a coloured precursor to the final product, leading to 23 strains being isolated. These 23 strains lead to the elucidation of four genes that were previously unknown to play a role in the production of the toxic secondary metabolite (Butchko et al., 1999; Pfannenstiel et al., 2017). This *A. nidulans* screen obtained more transformants than the *P. nodorum* screen as both the mutagenesis technique and screen were less laborious. Further, saturation of the 25 Mb *A. nidulans* genome (Galagan et al., 2005) is reached with fewer mutations than the 36 Mb *P. nodorum* genome (Birren et al., 2005; Syme et al., 2016). However, the SNP based mutagenesis employed by Butchko et al (1999) lead to difficulties in linking the genotype with the phenotype of interest. Pfannenstiel et al (2017) required whole genome sequencing to resolve these

mutations nearly two decades later. *Agrobacterium*-mediated mutagenesis of *P. nodorum*, although less high through-put than SNPs based methods provides a readily identifiable marker at the mutated loci (Betts et al., 2007; Idnurm et al., 2009).

### 2.4.4 A gain of virulence screen identifies a single strain of *P. nodorum* able to grow on a non-susceptible cultivar

The strain t26 induced greater areas of necrosis than its wild-type progenitor on the non-susceptible host Br34. Although these results indicate that *P. nodorum* may be able to adapt to infect a non-susceptible host, the strain isolated in this screen produced inconsistent infection patterns. Subsequently this line of investigation was discontinued.

Three reasons could explain these inconsistent results. **One**, detached leaf assays are ideal for high throughput screening, however, lack the consistency of whole seedling spray assays. **Two**, due to the logistical constraints of generating a mutant library in a short period of time no strains were re-isolated via single spore. Isolated colonies were sub-cultured for three generations on plates containing Hygromycin B, but not confirmed to be genetically homogeneous. However, from experience in reverse genetics with *P. nodorum*, the Solomon lab has found that colonies from transformant plates are generally homogeneous prior to single-spore isolation. Further, if colonies isolated from random mutagenesis were genetically heterogeneous then I would not have identified avirulent strains. Avirulent cells would be masked by virulent cells harbouring a different mutation. **Three**, a mutation that is only circumstantially evident may lead to an inconsistent phenotype. For example, in *Saccharomyces cerevisiae* GAL80 inhibits transcription of genes under the control of promoters containing gal4 upstream activation sequences (UAS). This inhibition is redundant under growth on glucose, as glucose inhibits transcription of these genes via the MIG1 protein

(Weinhandl et al., 2014). Disruption to Gal80 only elicits its pleotropic phenotype when glucose is not present in the growth medium (Xie et al., 2014). Similarly, miss-regulation of an environmental sensing cascade combined with small experimental variations may explain the inconsistent phenotype of t26.

Current breeding programs aim to remove susceptibility genes from wheat cultivars to limit SNB disease (Vleeshouwers and Oliver, 2015), however this places selective pressure on *P. nodorum*. This screen shows that *P. nodorum* can mutate to partially overcome this disease management strategy. Field epidemics of Nodorum blotch disease require the fungus to sporulate and re-infect the host. t26 was not observed to produce pycnidia while interacting with the non-susceptible host, despite an apparent increase in virulence. This partial gain of virulence may represent the first of many incremental steps in pathogen evolution where by multiple mechanisms are required to initiate disease. Steele et al (2001) and Jiménez-Gasco, Milgroom and Jiménez-Díaz (2003) begin to experimentally explore the concept of emerging pathotypes or races, in *Puccinia striiformis* and *Fusarium oxysporum* respectively, via incremental adaptation (Jiménez-Gasco et al., 2004; Steele et al., 2001). Parker and Gilbert (2004) and particularly Pariaud et al (2009) provide interesting reviews of plant pathogen evolution and host adaptation (Pariaud et al., 2009; Parker and Gilbert, 2004).

The virulence of t26 on a non-susceptible cultivar could arise from two different mechanisms. First, mutations resulting in overexpression of virulence factors, such as cell wall degrading enzymes could lead to plant tissue damage. This explains the necrosis caused by t26 but does not explain why the fungus is unable to proliferate. Second, disrupting a protein recognised by the host may allow the pathogen to avoid triggering host defences before it penetrates the leaf tissue. The inverse gene-for-gene

interaction between pathogen effectors and host susceptibility genes dominates the *P. nodorum*- wheat interaction on the susceptible cultivar, Grandin. However, on Br34, the absence of susceptibility genes may reveal a subtler interaction involving very early pathogen recognition. Disruption to t26 resulting in a loss of recognition by the host may explain the necrotic lesions but lack of disease development. In this scenario, the fungus avoids triggering early plant defences and penetrates the host causing tissue damage. However, in the absence of the dominant effector-susceptibility gene interaction, *P. nodorum* is unable to initiate mass cell death and proliferate. Stotz et al (2014) propose the idea of Effector Triggered Defence (ETD) in their review of plant immunity to fungal pathogens (Stotz et al., 2014). ETD juxtaposes PAMP Triggered Immunity (PTI) by recognition of an effector rather than an essential pathogen molecule, and Effector Triggered Immunity (ETI) by a milder response to the pathogen lacking cell death (Jones and Dangl, 2006; Stotz et al., 2014). Stotz et al (2014) propose that a subdued innate defence responds to the effectors of a pathogen in which cell death is not initiated but hinders disease progression. The host-pathogen interactions in Figure 2.09 is more readily explained by the hypothesis that t26 harbours a mutation rendering it unrecognisable by the plant at early stages of infection, but the absence of susceptibility genes inhibits disease progression. Focusing on plant recognition of *P. nodorum* provides insight into the basal immunity of the host, which opens avenues to exploring disease resistance against other pathogens.

The search for virulence on Br34 could be improved by using a mutagenesis method more ideal to generating and screening gain of function phenotypes. UV mutagenesis would allow large batches of spores to be randomly mutagenized and inoculated, without single genotype isolation, onto non-susceptible cultivars or related non-host species. Mutants able to initiate disease could then be re-isolated from infected host

tissue. Using the host as selection the desired phenotype could be rapidly screened for. This circumvents screening for mutations with a selectable marker and sub-culturing before performing an infection assay. Further, SNP/InDel mutagenesis approaches would utilise subtler changes in protein sequence and gene regulation than insertional mutagenesis. This gain of function screen may provide insight into the future development of field epidemics of *P. nodorum* and other pathogens.

### 2.4.5 Conclusions

The successful loss of function screen in this study has proven fruitful, yielding seven avirulent strains. These strains display different microscopic interactions with the host implying that different mechanism have been disrupted. This provides avenues for elucidating multiple mechanisms of virulence in the *P. nodorum*- wheat interaction which were previously undiscovered. The genetic basis for the observed phenotypes of these strains will subsequently be investigated utilising a whole genome sequencing approach to discern the disrupted loci, and reverse genetics to verify the bioinformatics analysis.

## 2.5 References for Chapter 2


Aimanianda, V., Bayry, J., Bozza, S., Kniemeyer, O., Perruccio, K., Elluru, S.R., Clavaud, C., Paris, S., Brakhage, A.A., Kaveri, S. V., Romani, L., Latgé, J.-P., 2009. Surface hydrophobin prevents immune recognition of airborne fungal spores. Nature 460, 1117–1121. doi:10.1038/nature08264

Akamatsu, H., Itoh, Y., Kodama, M., Otani, H., Kohmoto, K., 1997. AAL-Toxin-Deficient Mutants of *Alternaria alternata* Tomato Pathotype by Restriction Enzyme-Mediated Integration. Phytopathology 87, 967–972. doi:10.1094/PHYTO.1997.87.9.967

Betts, M.F., Tucker, S.L., Galadima, N., Meng, Y., Patel, G., Li, L., Donofrio, N., Floyd, A., Nolin, S., Brown, D., Mandel, M.A., Mitchell, T.K., Xu, J., Dean, R.A., Farman, M.L., Orbach, M.J., 2007. Development of a high throughput transformation system for insertional mutagenesis in *Magnaporthe oryzae.* Fungal Genetics and Biology 44, 1035–1049. doi:10.1016/j.fgb.2007.05.001

Birren, B., Lander, E., Galagan, J., Devon, K., Nusbaum, C., Jaffe, D., Butler, J., Alvarez, P., Gnerre, S., Grabherr, M., Kleber, M., Mauceli, E., Brockman, W., Rounsley, S., Young, S., LaButti, K., Pushparaj, V., DeCaprio, D., Crawford, M., Koehrsen, M., Engels, R., Montgomery, P., Pearson, M., Howarth, C., Kodira, C., Zeng, Q., Yandava, C., Alvarado, L., Oleary, S., Oliver, R.O., Solomon, P., 2005. Genome Sequence of *Stagonospora nodorum* [WWW Document]. URL https://www.ncbi.nlm.nih.gov/protein/EAT90417.2 (accessed 3.1.17).

Böhnert, H.U., Fudal, I., Dioh, W., Tharreau, D., Notteghem, J.-L., Lebrun, M.-H., 2004. A putative polyketide synthase/peptide synthetase from *Magnaporthe grisea* signals pathogen attack to resistant rice. Plant Cell 16, 2499–513. doi:10.1105/tpc.104.022715

Bölker, M., Böhnert, H.U., Braun, K.H., Görl, J., Kahmann, R., 1995. Tagging pathogenicity genes in *Ustilago maydis* by restriction enzyme-mediated integration (REMI). MGG Molecular and General Genetics 248, 547–552. doi:10.1007/BF02423450

Butchko, R.A.E., Adams, T.H., Keller, N.P., 1999. *Aspergillus nidulans* mutants defective in stc gene cluster regulation. Genetics 153, 715–720.

Chalfie, M., Tu, Y., Euskirchen, G., Ward, W.W., Prashert, D.C., 1994. Green Fluorescent Protein as a Marker for Gene Expression. Science (80). 263, 802–805.

Chambers, K., Lowe, R., Howlett, B., Zander, M., Batley, J., Van de Wouw, A., Elliott,

C., 2014. Next-generation genome sequencing can be used to rapidly characterise sequences flanking T-DNA insertions in random insertional mutants of *Leptosphaeria maculans*. Fungal Biology and Biotechnology 1, 10. doi:10.1186/s40694-014-0010-y

Chen, L.H., Lin, C.H., Chung, K.R., 2013. A nonribosomal peptide synthetase mediates siderophore production and virulence in the citrus fungal pathogen *Alternaria alternata*. Molecular Plant Pathology 14, 497–505. doi:10.1111/mpp.12021

Choi, J., Park, J., Jeon, J., Chi, M.H., Goh, J., Yoo, S.Y., Park, J., Jung, K., Kim, H., Park, S.Y., Rho, H.S., Kim, S., Kim, B.R., Han, S.S., Kang, S., Lee, Y.H., 2007. Genome-wide analysis of T-DNA integration into the chromosomes of *Magnaporthe oryzae*. Molecular Microbiology. 66, 371–382. doi:10.1111/j.1365-2958.2007.05918.x

Collemare, J., Billard, A., Böhnert, H.U., Lebrun, M.H., 2008. Biosynthesis of secondary metabolites in the rice blast fungus *Magnaporthe grisea*: the role of hybrid PKS-NRPS in pathogenicity. Mycological Research 112, 207–215. doi:10.1016/j.mycres.2007.08.003

Covert, S., Kapoor, P., Lee, M. H., Briley, A., Nairn, C. J., 2001. *Agrobacterium tumefaciens*-mediated transformation of *Fusarium circinatum*. Mycological Research 105, 259-264. doi: 10.1017/S0953756201003872

Del Sorbo, G., Scala, F., Parrella, G., Lorito, M., Comparini, C., Ruocco, M., Scala, a, 2000. Functional expression of the gene cu, encoding the phytotoxic hydrophobin cerato-ulmin, enables *Ophiostoma quercus*, a nonpathogen on elm, to cause symptoms of Dutch elm disease. Molecular Plant Microbe Interactions 13, 43–53. doi:10.1016/S1369-5266(00)80030-8

Ebbole, D.J., 1997. Hydrophobins and fungal infection of plants and animals. Trends in Microbiology 5, 405–408. doi:10.1016/S0966-842X(97)01130-X

Friesen, T.L., Zhang, Z.C., Solomon, P.S., Oliver, R.P., Faris, J.D., 2008. Characterization of the interaction of a novel *Stagonospora nodorum* host-selective toxin with a wheat susceptibility gene. Plant Physiology 146, 682–693. doi:10.1104/pp.107.108761

Fu, C., Sun, S., Billmyre, R.B., Roach, K.C., Heitman, J., 2014. Unisexual versus bisexual mating in *Cryptococcus neoformans*: Consequences and biological impacts. Fungal Genetics and Biology. 78, 65–75. doi:10.1016/j.fgb.2014.08.008

Galagan, J.E., Calvo, S.E., Cuomo, C., Ma, L.-J., Wortman, J.R., Batzoglou, S., Lee, S.-I., Başẗurkmen, M., Spevak, C.C., Clutterbuck, J., Kapitonov, V., Jurka, J.,

Scazzocchio, C., Farman, M., Butler, J., Purcell, S., Harris, S., Braus, G.H., Draht, O., Busch, S., D'Enfert, C., Bouchier, C., Goldman, G.H., Bell-Pedersen, D., Griffiths-Jones, S., Doonan, J.H., Yu, J., Vienken, K., Pain, A., Freitag, M., Selker, E.U., Archer, D.B., Peñalva, M.Á., Oakley, B.R., Momany, M., Tanaka, T., Kumagai, T., Asai, K., Machida, M., Nierman, W.C., Denning, D.W., Caddick, M., Hynes, M., Paoletti, M., Fischer, R., Miller, B., Dyer, P., Sachs, M.S., Osmani, S.A., Birren, B.W., 2005. Sequencing of *Aspergillus nidulans* and comparative analysis with A. fumigatus and A. oryzae. Nature 438, 1105–1115. doi:10.1038/nature04341

Gamerith, C., Herrero Acero, E., Pellis, A., Ortner, A., Vielnascher, R., Luschnig, D., Zartl, B., Haernvall, K., Zitzenbacher, S., Strohmeier, G., Hoff, O., Steinkellner, G., Gruber, K., Ribitsch, D., Guebitz, G.M., 2016. Improving enzymatic polyurethane hydrolysis by tuning enzyme sorption. Polymer Degradation and Stability. 132, 69–77. doi:10.1016/j.polymdegradstab.2016.02.025

Idnurm, A., Walton, F.J., Floyd, A., Reedy, J.L., Heitman, J., 2009. Identification of ENA1 as a virulence gene of the human pathogenic fungus *Cryptococcus neoformans* through signature-tagged insertional mutagenesis. Eukaryotic Cell 8, 315–26. doi:10.1128/EC.00375-08

Jiménez-Gasco, M. del M., Milgroom, M.G., Jiménez-Díaz, R.M., 2004. Stepwise Evolution of Races in *Fusarium oxysporum* f. sp. *ciceris* Inferred from Fingerprinting with Repetitive DNA Sequences. Phytopathology 94, 228–235. doi:10.1094/PHYTO.2004.94.3.228

Johnson, R.D., Johnson, L., Itoh, Y., Kodama, M., Otani, H., Kohmoto, K., 2000. Cloning and characterization of a cyclic peptide synthetase gene from *Alternaria alternata* apple pathotype whose product is involved in AM-toxin synthesis and pathogenicity. Molecular Plant Microbe Interactactions 13, 742–753. doi:10.1094/MPMI.2000.13.7.742

Jones, J.D.G., Dangl, J.L., 2006. The plant immune system. Nature 444, 323–329. doi:10.1038/nature05286

King, R., Urban, M., Hammond-Kosack, M.C.U., Hassani-Pak, K., Hammond-Kosack, K.E., 2015. The completed genome sequence of the pathogenic ascomycete fungus *Fusarium graminearum*. BMC Genomics 16, 544. doi:10.1186/s12864-015-1756-1

Li, M., Mondrinos, M.J., Gandhi, M.R., Ko, F.K., Weiss, A.S., Lelkes, P.I., 2005. Electrospun protein fibers as matrices for tissue engineering. Biomaterials 26, 5999–6008. doi:10.1016/j.biomaterials.2005.03.030

Liu, Z.H., Faris, J.D., Meinhardt, S.W., Ali, S., Rasmussen, J.B., Friesen, T.L., 2004. Genetic and Physical Mapping of a Gene Conditioning Sensitivity in Wheat to a Partially Purified Host-Selective Toxin Produced by Stagonospora nodorum. Phytopathology 94, 1056–1060. doi:10.1094/PHYTO.2004.94.10.1056

Loftus, B.J., 2005. The Genome of the Basidiomycetous Yeast and Human Pathogen *Cryptococcus neoformans*. Science (80). 307, 1321–1324. doi:10.1126/science.1103773

Lowe, R.G.T., Lord, M., Rybak, K., Trengove, R.D., Oliver, R.P., Solomon, P.S., 2009. Trehalose biosynthesis is involved in sporulation of *Stagonospora nodorum*. Fungal Genetics Biology 46, 381–389. doi:10.1016/j.fgb.2009.02.002

Lutolf, M.P., Hubbell, J.A., 2005. Synthetic biomaterials as instructive extracellular microenvironments for morphogenesis in tissue engineering. Nature Biotechnology 23, 47–55. doi:10.1038/nbt1055

Mead, O., Thynne, E., Winterberg, B., Solomon, P.S., 2013. Characterising the Role of GABA and Its Metabolism in the Wheat Pathogen *Stagonospora nodorum*. PLoS One 8, e78368. doi:10.1371/journal.pone.0078368

Pariaud, B., Ravigné, V., Halkett, F., Goyeau, H., Carlier, J., Lannou, C., 2009. Aggressiveness and its role in the adaptation of plant pathogens. Plant Pathology 58, 409–424. doi:10.1111/j.1365-3059.2009.02039.x

Parker, I.M., Gilbert, G.S., 2004. The Evolutionary Ecology of Novel Plant-Pathogen Interactions. Annual Reviews in Ecology, Evolution and Systematics. 35, 675–700. doi:10.1146/annurev.ecolsys.34.011802.132339

Pfannenstiel, B.T., Zhao, X., Wortman, J., Wiemann, P., Throckmorton, K., Spraker, J.E., Soukup, A.A., Luo, X., Lindner, D.L., Lim, Y., Knox, B.P., Haas, B., Fischer, G.J., Choera, T., Butchko, R.A.E., Bok, J., Affeldt, K.J., Keller, N.P., Palmer, J.M., 2017. Revitalization of a Forward Genetic Screen Identifies Three New Regulators of Fungal Secondary Metabolism in Genus Aspergillus. American Society of Microbiology 8, 1–15. doi:https://doi.org/10.1128/ mBio.01246-17

Sevim, A., Donzelli, B.G.G., Wu, D., Demirbag, Z., Gibson, D.M., Turgeon, B.G., 2012. Hydrophobin genes of the entomopathogenic fungus, *Metarhizium brunneum*, are differentially expressed and corresponding mutants are decreased in virulence. Current Genetics 58, 79–92. doi:10.1007/s00294-012-0366-6

Sharma, K.G., Kaur, R., Bachhawat, A.K., 2003. The glutathione-mediated detoxification pathway in yeast: An analysis using the red pigment that accumulates in certain adenine biosynthetic mutants of yeasts reveals the

involvement of novel genes. Archives of Microbiology. 180, 108–117. doi:10.1007/s00203-003-0566-z

Solomon, P.S., Lee, R.C., Wilson, T.J.G., Oliver, R.P., 2004. Pathogenicity of *Stagonospora nodorum* requires malate synthase. Molecular Microbiology 53, 1065–1073. doi:10.1111/j.1365-2958.2004.04178.x

Solomon, P.S., Lowe, R.G.T., Tan, K.C., Waters, O.D.C., Oliver, R.P., 2006. *Stagonospora nodorum*: cause of stagonospora nodorum blotch of wheat. Molecular Plant Pathology 7, 147–156. doi:10.1111/j.1364-3703.2006.00326.x

Solomon, P.S., Waters, O.D.C., Simmonds, J., Cooper, R.M., Oliver, R.P., 2005. The Mak2 MAP kinase signal transduction pathway is required for pathogenicity in *Stagonospora nodorum*. Current Genetics. 48, 60–68. doi:10.1007/s00294-005-0588-y

Solomon, P.S., Wilson, T.J.G., Rybak, K., Parker, K., Lowe, R.G.T., Oliver, R.P., 2006. Structural characterisation of the interaction between *Triticum aestivum* and the dothideomycete pathogen *Stagonospora nodorum*. European Journal of Plant Pathology 114, 275–282.

Steele, K.A., Humphreys, E., Wellings, C.R., Dickinson, M.J., 2001. Support for a stepwise mutation model for pathogen evolution in australasian *Puccinia striiformis* f.sp. *tritici* by use of molecular markers. Plant Pathology 50, 174–180. doi:10.1046/j.1365-3059.2001.00558.x

Stotz, H.U., Mitrousia, G.K., de Wit, P.J.G.M., Fitt, B.D.L., 2014. Effector-triggered defence against apoplastic fungal pathogens. Trends in Plant Science 19, 491–500. doi:10.1016/j.tplants.2014.04.009

Syme, R.A., Tan, K.C., Hane, J.K., Dodhia, K., Stoll, T., Hastie, M., Furuki, E., Ellwood, S.R., Williams, A.H., Tan, Y.F., Testa, A.C., Gorman, J.J., Oliver, R.P., 2016. Comprehensive Annotation of the *Parastagonospora nodorum* Reference Genome Using Next-Generation Genomics, Transcriptomics and Proteogenomics. PLoS One 11, 1–20. doi:10.1371/journal.pone.0147221

Tan, K.C., Heazlewood, J.L., Millar, A.H., Thomson, G., Oliver, R.P., Solomon, P.S., 2008. A signaling-regulated, short-chain dehydrogenase of *Stagonospora nodorum* regulates asexual development. Eukaryotic Cell 7, 1916–1929. doi:10.1128/EC.00237-08

Temple, B., Horgen, P. a, Bernier, L., Hintz, W.E., 1997. Cerato-ulmin, a hydrophobin secreted by the causal agents of Dutch elm disease, is a parasitic fitness factor. Fungal Genetics and Biology. 22, 39–53. doi:10.1006/fgbi.1997.0991

Urban, M., King, R., Hassani-Pak, K., Hammond-Kosack, K.E., 2015. Whole-genome analysis of *Fusarium graminearum* insertional mutants identifies virulence associated genes and unmasks untagged chromosomal deletions. BMC Genomics 16, 261. doi:10.1186/s12864-015-1412-9

Vleeshouwers, V.G.A.A., Oliver, R.P., 2015. Effectors as Tools in Disease Resistance Breeding Against Biotrophic, Hemibiotrophic, and Necrotrophic Plant Pathogens. Molecular Plant-Microbe Interactactions. 2015, 40–50. doi:10.1094/MPMI-10-13-0313-TA.testissue

Weinhandl, K., Winkler, M., Glieder, A., Camattari, A., 2014. Carbon source dependent promoters in yeasts. Microbial Cell Factories 13, 1–17. doi:10.1186/1475-2859-13-5

Xie, W., Liu, M., Lv, X., Lu, W., Gu, J., Yu, H., 2014. Construction of a controllable β-carotene biosynthetic pathway by decentralized assembly strategy in *Saccharomyces cerevisiae*. Biotechnology and Bioengineering. 111, 125–133. doi:10.1002/bit.25002

Xu, L., Chen, W., 2013. Random T-DNA Mutagenesis Identifies a Cu/Zn Superoxide Dismutase Gene as a Virulence Factor of *Sclerotinia sclerotiorum*. Molecular Plant-Microbe Interactactions 26, 431–441. doi:10.1094/MPMI-07-12-0177-R

# Chapter 3: The identification of disrupted loci in avirulent mutants of *Parastagonospora nodorum* generated by random insertional mutagenesis

## 3.1 Introduction

### 3.1.1 There are multiple techniques for identifying T-DNA insertion sites

After isolating a strain of interest, the next critical step in a forward genetics screen is to link the phenotype with a genotype. Phenotype is causally linked to genotype by identifying the altered genomic locus. The loci disrupted by insertional mutagenesis can be identified through whole genome sequencing (WGS) (Chambers et al., 2014), as well as established molecular techniques, such as inverse PCR, plasmid rescue and Thermo Asymmetric InterLaced PCR (TAIL-PCR) (Idnurm et al., 2004). Once the disrupted loci are identified, independent mutants can be then generated in the wild-type or background strain to verify the locus-phenotype link.

### 3.1.2 Inverse PCR, Plasmid rescue and TAIL-PCR

For inverse PCR, a restriction endonuclease is used to digest the transformants' genome. The digested fragments are then diluted and self-ligated generating circular fragments of gDNA. Fragments harbouring the disruption cassette will bind primers designed to amplify outward from the disruption cassette (Figure 3.01). Subsequent PCR products can be sequenced to identify the genomic locus harbouring the disruption cassette (Ochman et al., 1988). Idnurm et al (2004) and Maruthachalam et al (2011) successfully identified T-DNA insertion loci in the human pathogenic fungus *Cryptococcus neoformans* and plant pathogenic fungus *Verticillium dahliae*, using this technique (Idnurm et al., 2004; Maruthachalam et al., 2011).

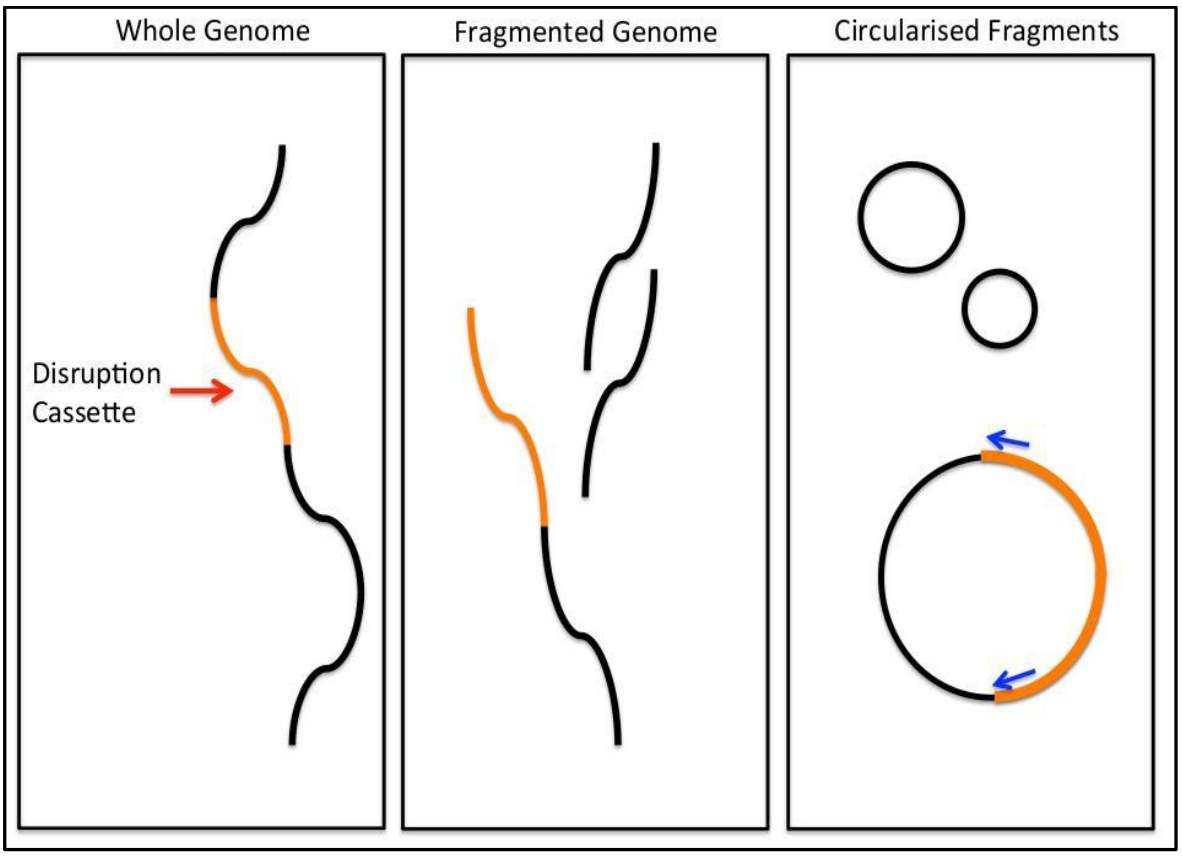


*(Figure 3.01: Generation of circularised genomic DNA fragments for inverse PCR or plasmid rescue. The first panel shows the intact genome, highlighting the disruption cassette in orange. The disruption cassette requires an origin of replication and selection marker for traditional plasmid rescue. The middle panel shows the fragmented genome, digested by a restriction endonuclease. The third panel shows the circularized fragments. Insert-specific primers, shown in blue, are used to amplify the unknown genomic sequence during inverse PCR. Plasmid rescue purifies circularized fragments from a mixture by transformation and selection for the marker gene.)*

The plasmid rescue approach retrieves the disruption cassette and flanking genomic sequences using a prokaryotic origin of replication and selectable marker embedded in the cassette (Figure 3.01). The disruption cassette is separated from the host genome by digestion with a restriction endonuclease. The fragmented genome is then self-ligated, generating a circularized DNA library. DNA fragments containing the disruption cassette

are then isolated by transforming the library of circularised fragments into *Escherichia coli*. Bacterial cells harbouring the insert and disrupted locus are then selected for by the selectable marker. Mandel et al (1992) successfully identified T-DNA disrupted loci in *Arabidopsis thaliana* using this technique. In this study, genomic DNA from *A. thaliana* T-DNA mutants was digested with *Hind*III and then self-ligated. The circularized genome fragments were then cloned into *E. coli.* Fragments that contained the T-DNA insert also contained a prokaryotic origin of replication and selectable marker needed for growth and purification (Mandal et al., 1993). Similarly, Idnurm et al (2004) successfully used plasmid rescue and inverse PCR to identify T-DNA mutation sites in the pathogenic fungus, *C. neoformans* (Idnurm et al., 2004).

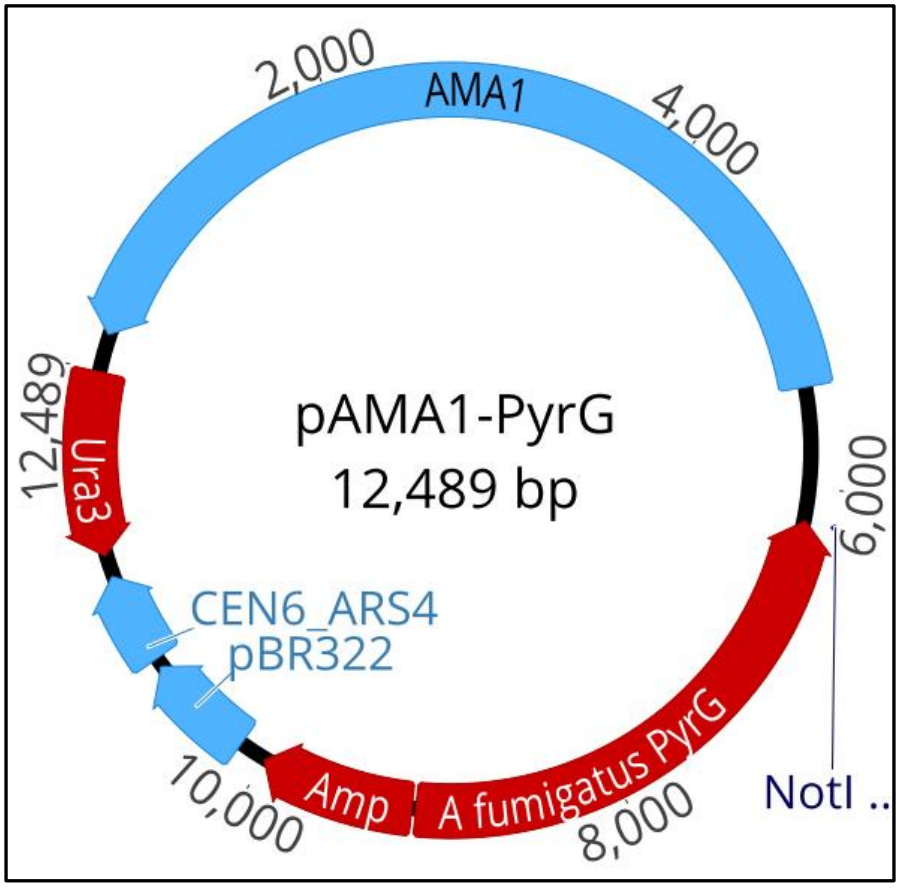


*(Figure 3.02: Plasmid map of* Aspergillus *pAMA1-PyrG vector used for plasmid rescue of T-DNA insertion loci in* P. nodorum *mutants. This plasmid contains the pBR322 bacterial origin of replication, pMB1, yeast origin of replication, CEN6_ARS4, the* Aspergillus *origin of replication* AMA1*. It also contains the Ampicillin resistance gene for bacterial selection, as well as orotidine 5'-phosphate decarboxylase genes from yeast (Ura3) and* Aspergillus fumigatus *(PyrG), for yeasts and filamentous fungi selection.)*

Plasmid rescue approaches traditionally utilise prokaryotic elements in the insertion cassette. These elements facilitate re-generation of replicating, selectable DNA fragments. However, the pPK2-HPH:GFP insertion sequence used to mutagenize *P. nodorum* lacks any prokaryotic elements. In order to isolate the pPK2-HPH:GFP insertion sequence from *P. nodorum* mutants I used the shuttle plasmid pAMA1-PyrG. This plasmid can be transferred between bacteria, yeast and *Aspergillus* sp. because it contains all of the respective origins

of replication and selectable markers (Figure 3.02). Selection for *Aspergillus* cells harbouring the pAMA1-PyrG plasmid uses the *PyrG* gene, a homolog of the yeast *Ura3* gene, and an auxotrophic strain of *Aspergillus nidulans* (*An.ΔpyrG*). This strain is unable to produce uracil or uridine for polynucleotide synthesis due to a defective *orotidine 5'-phosphate decarboxylase (PyrG)*. Subsequently, this *A. nidulans* strain fails to grow in the absence of uridine or uracil. However, the wild-type phenotype is restored by the pAMA1-PyrG plasmid as it contains the *Aspergillus fumigatus orotidine 5'phosphate decarboxylase* (*PyrG*) homolog. *An.ΔpyrG* mutants harbouring pAMA1-PyrG are selected on minimal medium lacking uracil and uridine. This system does not require antibiotics and allows for additional fungal selective markers to be used such as the Hygromycin B resistance gene on the pPK2-HPH:GFP plasmid, *Hph*.

TAIL PCR identifies genomic loci harbouring known insertion fragments by amplifying one genomic flank of the insert. The flank is amplified by a series of insert-specific primers, nested within the known sequence, and a degenerate primer that binds randomly. These are used in three sequential PCR; each alternating between high and low stringency cycles (Figure 3.03) (Liu et al., 1995). The initial PCR uses the outermost specific primer (TR1, innermost primer, Figure 3.03) and a primer containing a random combination of nucleotides. These primers are annealed in high- and low-stringency amplification stages with a long extension time, to produce a range of PCR products. The mix of PCR products is then diluted and used as template for a subsequent PCR, using the nested primer TR2 (between TR1 and TR3, Figure 3.03) and high- and low-stringency annealing cycles. This second PCR selectively amplifies the DNA fragments containing the insertion fragment. A

third PCR using the nested primer TR3 further selects for the DNA fragment of interest from the diluted previous PCR. Sequencing the resulting amplicons then identifies the disruption cassettes genomic flank (Liu et al., 1995). Li et al (2007) and Tsuji et al (2003) identified the T-DNA insertion loci in *Magnaporthe oryzae* and *Colletotrichum lagenarium*, respectively, using a TAIL-PCR technique (Li et al., 2007; Tsuji et al., 2003). A review of forward genetics studies over the last several decades reveals TAIL-PCR has successfully elucidated more loci than either inverse PCR or plasmid rescue. However, these techniques for identifying disrupted loci are notoriously difficult, laborious and are unable to identify SNP and InDels type mutations. The use of these techniques has been due to a lack of cheap alternatives rather than their efficacy. Consequently, the diminishing costs of whole genome sequencing (WGS) as well as increased accessibility and reliability has led to a trend towards sequencing interesting mutants.

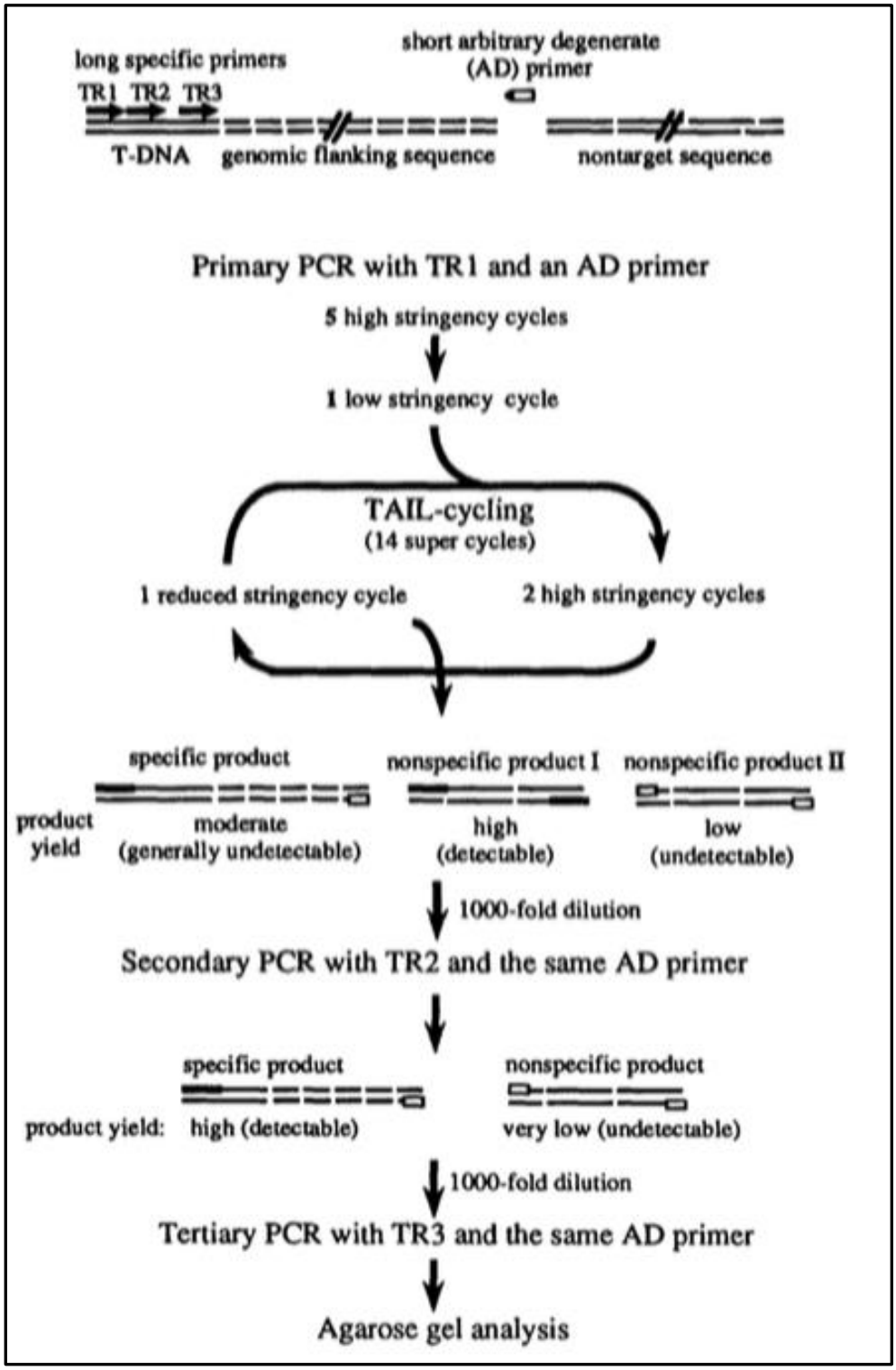


*(Figure 3.03: Schematic of TAIL-PCR by Liu et al (1995). TR1, TR2, TR3 are nested primers within the known insertion sequence. AD is the degenerate primer outside of the insertion sequence.)*

### 3.1.3 Whole Genome Sequencing

Whole genome sequencing (WGS) offers a viable alternative to the above molecular methods for identifying disrupted loci. The prohibitive expense and bioinformatic infrastructure required for WGS has diminished rapidly over the last decade and has led to an increase in forward genetic screens using this method to locate disruption cassettes. In addition, whole genome sequencing identifies other mutations in the genome such as SNPs, InDels and chromosomal rearrangements (Chambers et al., 2014; Pfannenstiel et al., 2017; Urban et al., 2015). These secondary mutations are important as they may cause the phenotype of interest rather than the primary mutagenesis. Large exogenous genome insertions can be readily identified through short-read whole genome re-sequencing on a platform such as the Illumina Mi-Seq followed by *de novo* genome assembly. The relatively low expense of WGS allows multiple isolates to be sequenced in parallel. For example, Urban et al (2015) sequenced three avirulent *Fusarium graminearum* isolates with an average of 22-fold coverage of each genome. This allowed them to identify the insertion fragment in all isolates, as well as discover chromosomal rearrangements and deletions that prohibited identification of virulence genes (Urban et al., 2015). Based on the success of these studies, a whole genome sequencing approach was employed to determine the disrupted loci in the avirulent *P. nodorum* mutants generated in Chapter 2.

This chapter describes the elucidation of T-DNA disrupted loci in the seven, avirulent, *P. nodorum* random mutants generated in Chapter 2. Once identified, the disrupted loci were independently disrupted in the *Pn.Δlig4* background strain of *P. nodorum*. *DNA ligase IV* (*lig4*) is required for non-homology-based DNA repair. Without ligase IV DNA

repair is limited to homologous recombination resulting in improved efficiency of homologous recombination-based gene disruption. Previous studies have shown disruptions to *DNA ligase IV* reduce ectopic integrations leading to transformation efficiencies from 5% in *Aspergillus fumigatus* to 100% in *Neurospora crassa* and *C. neoformans* (Krappmann, 2007). The *Pn.Δlig4* strain was used to generate knock-out mutants of candidate virulence genes identified from the forward genetics screen. The virulence of these mutants determined the role these genes play during the *P. nodorum*-wheat interaction.

***Aim:*** ***1)*** *To identify the disrupted loci in the seven avirulent strains of* Parastagonospora nodorum *generated in Chapter 2.* ***2)*** *To describe the disrupted genes and speculate their function from predicted protein domains* ***3)*** *To verify the mutations leading to the avirulent phenotypes by independently disrupting the identified loci in the Δlig4 background strain of* P. nodorum.

## 3.2 Materials and Methods

3.2.1 *(Table 3.01: Primers used in Chapter 3 to identify loci of genomic insertions, confirm mutations and generate knock-out constructs. Bolden sequences indicates a homologous overhang used for cloning.)*

| Name | Oligonucleotide (5'--3') |
|---|---|
| **Inverse_F** | AGCTGGCGTAATAGCGAA |
| **Inverse_R** | TATCTTTGCGAACCCAGG |
| **Degen_BamHI** | CAGGCTCGACGTATTTCAGTGT |
| **TAIL-1** | TTATCCGCTCACAATTCCACA |
| **TAIL-2** | TTAATTGCGTTGCGCTCA |
| **TAIL-3** | NNNNNNNNNNGGATC |
| **Scaffold_#4_F** | GATCTCTCGCTCTTCCAAC |
| **Scaffold_#4_R** | AAGAAGGGTTGTGGGAAC |
| **Scaffold_#12_F** | AATCTACCCGCGCAACAAC |
| **Scaffold_#12_R** | TGGTGGTGTTGGTGCTGTAG |
| **trpC_HYG_F** | CTTGGCTGGAGCTAGTGGAG |
| **trpC_HYG_R** | GAGCGGATTCCTCAGTCTCG |
| **02686_5'_F** | **TTCGGCCGGCGTATTGGGTGTTACGGACCTGCA**CAGTCATAGATTTACGGGTGG |
| **02686_5'_R** | **GTCAAGAGACCTACGAGACTGAGGAATCCGCTC**AGAGGCAAAGAGGTATCCTGTA |
| **02686_3'_F** | **ATTCATTGTTGACCTCCACTAGCTCCAGCCAAG**TAGTTACCTAATGTGGATTCGAGG |
| **02686_3'_R** | **GTAAAACGACGGCCAGTGCCAAGCTTGCATGCC**AACGCAACCAGGAGCTTATAT |
| **02686_pCon_F** | CTCGTGGTCATTCAGGTTG |
| **02686_pCon_R** | TGCTGGTGACATAATGCG |
| **07954_5'_F** | **GAAACAGCTATGACATGATTACGAATTCTTAAT**GTGGCAAACCCGTACTACCT |
| **07954_5'_R** | **GTCAAGAGACCTACGAGACTGAGGAATCCGCTC**AGCCCTCTCCCATCTTAGAAG |
| **07954_3'_F** | **ATTCATTGTTGACCTCCACTAGCTCCAGCCAAG**TGCAGATGCGAAGTGAGT |
| **07954_3'_R** | **GTCTCTCCGCATGCCAGAAAGAGTCACCGGTTA**AGCTTAATGCTGCGTAGGTC |
| **07954_pCon_F** | CTGAGCTTGCTCGCTTTTC |
| **07954_pCon_R** | GACTCACTTCGCATCTGCA |
| **HY_F** | AAGCATCAGCTCATCGAGA |
| **YG_R** | GGTCAATACACTACATGGCGT |
| **07954_ConI_F** | CTCGGCATACTTGTAGACCTACTG |
| **HYG_Con_R** | TAGCAGACAGGAACGAGGA |
| **ITS_1** | TCCGTAGGTGAACCTGCGG |
| **ITS_4** | TCCTCCGCTTATTGATATGC |
| **07954_ConII_F** | CTGAGCTTGCTCGCTTTTC |
| **07954_ConII_R** | GACTCACTTCGCATCTGCA |
| **02686_ConI_F** | CGACAGCAGTGGTCTTCATATT |
| **02686_ConII_F** | CTCGTGGTCATTCAGGTTG |
| **02686_ConII_R** | TGCTGGTGACATAATGCG |

3.2.2 *(Table 3.02: Media used in chapter 3 to culture fungi and bacteria. The following table lists the recipes for media named in the following methods sections used for culturing fungi and bacteria. The concentrations of each reagent and their origins are also listed)*

| Media Abbreviation | **Name** | **Constituent** | **/L** |
|---|---|---|---|
| **V8PDB/V8PDA** | V8 Potato Dextrose Broth | Centrifuged Campbells V8 Juice™ | 150ml |
| | V8 Potato Dextrose Agar | Bacto™ Potato Dextrose | 10g |
| | | Astral Scientific™ Agar (optional for V8PDA) | 15g |
| | | up to 1L with MilliQ water | |
| | | pH 6.0 | |
| | | | |
| **TWB Agar** | Tap Water Benzimidazole Agar | Sigma Scientific™ Benzimidazole | 0.3g |
| | | Astral Scientific™ Agar | 15g |
| | | up to 1L with MilliQ water | |
| | | | |
| **LB** | Lysogeny Broth | Bacto™ Tryptone | 10g |
| | | Astral Scientific™ Yeast Extract | 10g |
| | | Astral Scientific™ Sodium Chloride | 5g |
| | | Astral Scientific™ Agar (optional) | 15g |
| | | up to 1L with MilliQ water | |
| | | | |
| **LB+** | Optimal Lysogeny Broth | Bacto™ Tryptone | 10g |
| | | Astral Scientific™ Yeast Extract | 10g |
| | | Astral Scientific™ Sodium Chloride | 5g |
| | | Astral Scientific™ Magnesium Sulphate | 240mg |
| | | Astral Scientific™ $Na_2HPO_4$ | 13.4g |
| | | Astral Scientific™ $NaH_2PO_4$ | 2.4g |
| | | Astral Scientific™ Agar (optional) | 15g |

| | | | |
|---|---|---|---|
| | | 10% Astral Scientific™ Glucose (Autoclave separately) | 100ml |
| | | up to 1L with MilliQ water | |
| | | pH 7.5 | |
| | | | |
| **S.O.C.** | NEB™ Super Optimal Broth with Catabolite repression | NEB™ S.O.C outgrowth medium | |
| | | | |
| **IM+** | Induction Medium | Bacto™ Tryptone | 10g |
| | | Astral Scientific™ Yeast Extract | 10g |
| | | Astral Scientific™ Sodium Chloride | 5g |
| | | Astral Scientific™ Magnesium Sulphate | 240mg |
| | | Astral Scientific™ $Na_2HPO_4$ | 13.4g |
| | | Astral Scientific™ $NaH_2PO_4$ | 1.3g |
| | | Astral Scientific™ Agar (optional) | 15g |
| | | 10% Astral Scientific™ Glucose (Autoclave separately) | 100ml |
| | | 10% Sigma Aldrich™ Glycerol (Autoclave separately) | 100ml |
| | | up to 1L with MilliQ water | |
| | | pH 5.5 | |
| | | | |
| **Soft Overlay** | CzaPek Dox V8 soft agar | Bacto™ CzaPek Dox | 33g |
| | | Centrifuged Campbells V8 Juice™ | 200ml |
| | | Astral Scientific™ Agar | 7.5g |
| | | up to 1L with MilliQ water | |
| | | pH 6.0 | |
| | | | |
| **YPG** | Yeast Peptone Glucose | Bacto™ Peptone | 10g |
| | | Astral Scientific™ Yeast Extract | 5g |
| | | Astral Scientific™ Glucose | 10g |

| | | | |
|---|---|---|---|
| | | Astral Scientific™ Agar (optional) | 20g |
| | | up to 1L with MilliQ water | |
| | | | |
| **Ura DO** | Uracil Uradine Drop-out | Astral Scientific™ Yeast synthetic nitrogen base | 3.6g |
| | | Astral Scientific™ Yeast Amino acid supplements -Ura | 1.2g |
| | | Astral Scientific™ Glucose | 10g |
| | | | |
| | *Aspergillus* min. medium | 10% Astral Scientific™ Glucose (Autoclave separately) | 10g |
| | | 20x nitrate salts | 50ml |
| | | trace elements | 1ml |
| | | Astral Scientific™ Agar (optional) | 16g |
| | | pH 6.5 | |
| | | | |
| | *Aspergillus* osmotic medium | 10% Astral Scientific™ Glucose (Autoclave seperately) | 10g |
| | | 20x nitrate salts | 50ml |
| | | trace elements | 1ml |
| | | Astral Scientific™ Sorbitol | 218.6g |
| | | Astral Scientific™ Agar | 16g |
| | | pH 6.5 | |
| | | | |
| | Trace elements | Astral Scientific™ $ZnSO_4$ | 2.2g |
| | | Astral Scientific™ $H_3BO_3$ | 1.1g |
| | | Astral Scientific™ $MnCl_2.4H_2O$ | 500mg |
| | | Astral Scientific™ $FeSO_4.tH_2O$ | 160mg |
| | | Astral Scientific™ $CoCl_2.5H_2O$ | 160mg |
| | | Astral Scientific™ $CuSO_4.5H_20$ | 160mg |
| | | Astral Scientific™ $(NH_4)_6Mo_7O_{24}.4H_20$ | 110mg |
| | | Astral Scientific™ Na4EDTA | 5g |

| | | |
|---|---|---|
| | upto 100ml of MilliQ water<br>(may need KOH to dissolve fully) | |
| | | |
| 20x nitrate salts | Astral Scientific™ $NaNO_3$ | 120g |
| | Astral Scientific™ KCl | 10.4g |
| | Astral Scientific™ $MgSO_4.7H_2O$ | 10.4g |
| | Astral Scientific™ $KH_2PO_4$ | 30.4g |
| | Up to 1 litre of MilliQ water | |

3.2.3 *(Table 3.03: List of fungi and bacteria used in Chapter 3. This table lists the fungi and bacteria mentioned in the following methods, as well as the results and discussion. Specific mutations, selection markers and harboured plasmids are also listed, while their origin and growth conditions are mentioned in the methods.)*

| Genus | Species | Strain | Mutant | Mutation | Gene/Plasmid ID | Marker |
|---|---|---|---|---|---|---|
| ***Parastagonospora*** | *nodorum* | SN15 | wild-type | Nil | NA | nil |
| ***Parastagonospora*** | *nodorum* | SN15 | Δlig4 | ligase IV | SNOG_10525 | BAR |
| ***Parastagonospora*** | *nodorum* | SN15 | t112 | TBD | TBD | HYG |
| ***Parastagonospora*** | *nodorum* | SN15 | Δlig4/Δcatd1-3 | ΔCatechol-1,2-Dioxygenease | SNOG_07954 | BAR/HYG |
| ***Parastagonospora*** | *nodorum* | SN15 | Δlig4/Δcatd1-4 | ΔCatechol-1,2-Dioxygenease | SNOG_07954 | BAR/HYG |
| ***Parastagonospora*** | *nodorum* | SN15 | Δlig4/Δcatd1-21 | ΔCatechol-1,2-Dioxygenease | SNOG_07954 | BAR/HYG |
| ***Aspergillus*** | *nidulans* | LO7891 | ΔpyrG | ΔOrotidine 5'-Phosphate Decarboxylase | nil | nil |
| ***Saccharomyces*** | *cerevisiae* | BJ5464 | Δura3 | ΔOrotidine 5'-Phosphate Decarboxylase | nil | nil |
| ***Saccharomyces*** | *cerevisiae* | BJ5464 | Δura3 | ΔOrotidine 5'-Phosphate Decarboxylase | pYAE:SNOG_02686$^{ura}$ | URA3/HYG/KAN |
| ***Saccharomyces*** | *cerevisiae* | BJ5464 | Δura3 | ΔOrotidine 5'-Phosphate Decarboxylase | pYAE:SNOG_07954$^{ura}$ | URA3/HYG/KAN |
| ***Escherichia*** | *coli* | DH5-α | wild-type | Nil | NA | nil |
| ***Escherichia*** | *coli* | DH5-α | wild-type | Nil | pYAE:SNOG_02686$^{kan}$ | URA3/HYG/KAN |
| ***Escherichia*** | *coli* | DH5-α | wild-type | Nil | pYAE:SNOG_07954$^{kan}$ | URA3/HYG/KAN |

| | | | | | | |
|---|---|---|---|---|---|---|
| ***Agrobacterium*** | *tumefaciens* | LBA1126$^{rif}$ | Deactivated *vir* | Helper plasmid pAL1100$^{spec}$ | pAL1100$^{spec}$ | SPEC |
| ***Agrobacterium*** | *tumefaciens* | LBA1126$^{rif}$ | Deactivated *vir* | Helper plasmid pAL1100$^{spec}$ | pYAE:SNOG_02686$^{kan}$ | URA3/HYG/KAN/SPEC |
| ***Agrobacterium*** | *tumefaciens* | LBA1126$^{rif}$ | Deactivated *vir* | Helper plasmid pAL1100$^{spec}$ | pYAE:SNOG_07954$^{kan}$ | URA3/HYG/KAN/SPEC |

### 3.2.4 Protocols

#### 3.2.4.1 Culturing of an auxotrophic *Aspergillus nidulans* strain

Solid *Aspergillus* minimal medium, containing uracil and uridine, was streak inoculated with an *A. nidulans* LO7891 ΔpyrG asexual spore suspension taken from the -80°C glycerol stock. Inoculated plates were incubated at 37ºC, in the dark, for three days. This strain and growth conditions were supplied by Dr. Yit-Heng Chooi, The School of Molecular Sciences, The University of Western Australia.

#### 3.2.4.2 Collection and quantification of *A. nidulans* asexual spores

Asexual spores were collected by gently washing the plates with 4ml of sterile water containing 0.1% Tween-80. The spore suspension was collected in a sterile 15ml centrifuge tube and centrifuged at 3,000g for 10 minutes. The supernatant was decanted, and the resulting spore pellet was resuspended in 1ml of sterile MilliQ water. A 1/100 dilution aliquot was then prepared for spore counting using a haemocytometer.

#### 3.2.4.3 Extraction of *A. nidulans* protoplasts

500ml of liquid *Aspergillus* minimal medium, containing uracil and uridine, was inoculated with $10^9$ freshly collected asexual spores then shaken at 280rpm, 28ºC for 10 hours. Every 30 minutes after 10 hours post inoculation, samples of the culture were observed microscopically for spore germination. Once germlings had formed the culture was divided into pre-weighed 50ml sterile centrifuge tubes and centrifuged at 3,000g for 10 minutes at 4ºC. The supernatant was discarded and the fresh-weight of the fungal biomass recorded.

The germlings were resuspended in 10ml of osmotic suspension buffer containing 40mg of Glucanex® Sigma-Aldrich™ per gram of germlings. The germling suspension was

incubated without shaking at 28ºC for 4 hours. Every 30 minutes, samples of the suspension were observed microscopically for the release of protoplasts.

Once the majority of germlings were digested, the suspension was filtered through sterile, hydrophobic, cotton wool in a 20ml syringe. The cotton wool and cell debris were discarded, and the protoplasts were centrifuged at 1,000g, 4 ºC for 10 minutes. The resulting cell pellet was washed twice with 1ml of STC, and finally resuspending in 1ml of STC. The cell density of a 1/40 dilution of this suspension was measured using a haemocytometer. The protoplasts were then diluted in STC buffer to a concentration of $10^8$ cells/ml. This protocol was provided through personal communication with Dr. Yit-Heng Chooi, The School of Molecular Sciences, The University of Western Australia.

#### 3.2.4.4 PEG/CaCl2 mediated transformation of *A. nidulans* protoplasts

3µg of DNA dissolved in 100µl of STC buffer was combined with 100µl of the $10^8$ cells/ml protoplast suspension in a sterile 2ml microfuge tube. 100µl of DNA free STC buffer was added to a second 100µl aliquot of $10^8$cells/ml suspension as a negative control. The suspensions were gently mixed by inverting the microfuge tubes 5x and then incubated on ice for 30 minutes. After the incubation, 1600µl of 60% PEG/$CaCl_2$ was added to each tube and gently mixed at room temperature for 5 minutes by rolling and inverting the tubes. The protoplasts were then incubated on ice again for 30 minutes. During this 30minute incubation six plates containing *Aspergillus* osmotic medium and one containing uracil (1.2mg/l) and uridine (600mg/l) were pre-warmed to 37°C. After the incubation, 300µl of the protoplast + DNA suspension was spread inoculated onto the *Aspergillus* osmotic medium containing uracil and uridine, as well as five plates lacking uracil and uridine. The remaining plate lacking uracil and uridine was inoculated with 300µl of the DNA free protoplast/PEG/$CaCl_2$ suspension. The

plates were air dried at room temperature, under sterile conditions for an hour, then incubated in a sealed plastic bag at 37°C in the dark. The plates were checked for growth each day for 10 days. Transformants were subcultured from hyphal tips onto minimal *Aspergillus* medium lacking uracil and uridine as they developed. This protocol was provided by Dr. Yit-Heng Chooi, The School of Molecular Sciences, The University of Western Australia.

#### 3.2.4.5 Plasmid rescue library

Genomic DNA (~10ug) extracted from each of the seven avirulent mutants described in Chapter 3 was digested with the restriction endonuclease, NEB™ *Not*I-HF. The pAMA1-PyrG plasmid (~1ug) was also linearized with *Not*I-HF. *Not*I does not cut the pPK2-HPH:GFP disruption cassette, so *Not*I digestion of *P. nodorum* mutant genomes produces gDNA fragments of which some will contain a functional *Hph* gene. The digested genome DNA was then ligated with NEB™ T4 DNA Ligase using the exposed *Not*I restriction site overhangs into the linearized pAMA1-PyrG plasmid, according to the manufacturer's instructions (NEB™, M0202). The pAMA1-PyrG+gDNA ligation mix, along with plasmid only and unligated controls, were then transformed into NEB™ electro-competent *E. coli* DH5-α cells with selection for ampicillin resistance. The linearized pAMA1-PyrG without gDNA transformation produced no *E. coli* colonies, while each pAMA1-PyrG+ gDNA ligation mix produced a bacterial lawn. These bacterial lawns were then harvested with sterile MilliQ water and a made into two aliquots for each transformation. One aliquot of each transformation was prepared with 20% glycerol for cryogenic storage. The other was grown overnight in lysogeny broth$^{Amp}$ (LB$^{Amp}$) cultures. This protocol was developed in conjunction with Dr. Yit-Heng Chooi, The University of Western Australia.

### 3.2.4.6 Inverse PCR template

1µg of gDNA from each sample was digested overnight by the restriction endonuclease, NEB™ *Bam*HI-HF, in 10µl of NEB CutSmart 10x Buffer ™ buffered MilliQ water (NEB, R3136S). The digests were then purified using Sephadex™ g25 (Sigma Aldrich, U.S.A.). Concentrations of each sample were measured via Nanodrop™ spectrophotometry and then dehydrated under vacuum centrifugation. Once dry the digested gDNA samples were redissolved in MilliQ water to a concentration of 10ng/µl. 10µl aliquots of each sample were then buffered in NEB™ 10x ligase buffer and ligated overnight at 16°C with NEB™ T4 DNA ligase (NEB, M0202). The ligation reactions were purified using Sephadex™ g25 and the concentrations measured via Nanodrop™ spectrophotometry. Inverse PCR was then employed, using primers Inverse_F and Inverse_R, to amplify the flanking sequences of the pPK2-HPH:GFP insertion fragment. This protocol was developed in conjunction with Dr. Britta Winterberg.

### 3.2.4.7 Inverse PCR

Inverse PCR amplified DNA from the template generated in section 3.2.4.6 using the forward and reverse primers indicated in Table 2.01 in the following reaction. This reaction was set up on ice:10ng of plasmid DNA in 1 µl was diluted in 5.16 µl. 1 µl of Takara™ 10x Buffer was added to this dilution along with 0.8 µl of a 10µM dNTP solution containing 2. 5µM each of ATP, GTP, CTP and TTP. 1µl of each forward and reverse primer were added to a final concentration of 0.5µM. Finally, 0.04µl ExTaq Takara™ polymerase was added to the reaction. This reaction was set up in parallel to two other reactions, one lacking plasmid DNA and the other lacking primers. These additional reactions form negative controls.

Thermocycler conditions: The reactions were then denatured at 98°C for two minutes then the primers were annealed at 57°C for 30 seconds. The primary PCR product was then extended at 72°C for one minute per kilobase before the reaction was denatured again at 98°C for 30 seconds. Denaturation, annealing and extension was repeated 34 times before the reaction was terminated at 72°C for 10 minutes.

#### 3.2.4.8 Thermo Asymmetric InterLaced PCR

TAIL-PCR series were set up on ice using the primers indicated in Table 2.01 in the following reaction:10ng of fungal genomic DNA in 1 µl was diluted in 5.16 µl. 1 µl of Takara™ 10x Buffer was added to this dilution along with 0.8 µl of a 10µM dNTP solution containing 2. 5µM each of ATP, GTP, CTP and TTP. 1µl of each forward and reverse primer were added to a final concentration of 0.5µM. Finally, 0.04µl ExTaq Takara™ polymerase was added to the reaction. This reaction was set up in parallel to two other reactions, one lacking genomic DNA and the other lacking primers. These additional reactions form negative controls. Thermal cycling was as described by *Liu et al (1995)* with variations in annealing temperatures, deviating incrementally till +-5°C from the published protocol.

#### 3.2.4.9 Bacterial colony PCR

Single colonies were picked with sterile 10µl pipette tips and each deposited into 20ul of sterile MilliQ water. The bacterial suspensions were then spot inoculated (3µl) onto LB agar medium containing the corresponding selection antibiotic. Plates were incubated at 28°C for two days for *A. tumefaciens* and *E. coli* at 37°C for 16 hours. 1µl of bacterial suspension was then used for PCR confirmation and the corresponding colonies from the spot inoculation were grown in suspension for storage in 20% glycerol at -80°C.

On ice 1µ1 of bacterial suspension was diluted in 5µl GoTaq Green™. To this suspension 1µl of each forward and reverse primer was added, to reach a final concentration of 0.5µM of each primer. Then 2µl of sterile water was added. These reaction were set up in sets of six for each construct along with two other reactions, one lacking DNA and the other lacking primers. These additional reactions form negative controls.

Thermocycler conditions: The reactions were then denatured at 98°C for 5 minutes then the primers were annealed at 57°C for 30 seconds. The primary PCR product was then extended at 72°C for one minute per kilobase before the reaction was denatured again at 98°C for 30 seconds. Denaturation, annealing and extension was repeated 34 times before the reaction was terminated at 72°C for 10 minutes.

#### 3.2.4.10 Yeast colony PCR

Single colonies were picked with sterile 10µl pipette tips and each deposited into 10ul of sterile water. The yeast suspensions were then spot inoculated (3µl) onto solid URA drop out medium. Plates were incubated at 28°C for three days. 10µl of 20mM NaOH was then added to the yeast suspension which was then incubated at 98°C for 10 minutes. 1µl of yeast suspension was then used for PCR confirmation and the corresponding colonies from the spot inoculation were grown in suspension for plasmid extraction and storage in 20% glycerol at -80°C.

On ice 1µ1 of yeast lysate was diluted in 5µl GoTaq Green™. To this solution 1µl of each forward and reverse primer was added, to reach a final concentration of 0.5µM of each primer. Then 2µl of sterile water was added. These reaction were set up in sets of six for each construct along with two other reactions, one lacking DNA and the other lacking primers. These additional reactions form negative controls.

Thermocycler conditions: The reactions were then denatured at 98°C for 5 minutes then the primers were annealed at 57°C for 30 seconds. The primary PCR product was then extended at 72°C for one minute per kilobase before the reaction was denatured again at 98°C for 30 seconds. Denaturation, annealing and extension was repeated 34 times before the reaction was terminated at 72°C for 10 minutes.

#### 3.2.4.11 Filamentous fungi colony PCR

The Thermoscientific™ Phire Plant Direct PCR Kit was used as per the manufacturer's instructions for PCR amplification of amplicons directly from fungal material. A sterile pipette tip was dragged gently across 2cm of the leading edge of a fungal colony grown on solid medium. The soft, unpigmented mycelial collected on the point of the pipette tip and was deposited into 50µl the storage buffer supplied with the kit. Fungal samples were incubated overnight in storage buffer at 4°C. 1µl of the storage buffer-fungus mixture was then used as the template in subsequent PCR reactions using the supplied polymerase and buffer.

#### 3.2.4.12 Gel excision and purification of PCR products

PCR products were isolated by agarose (Astral Scientific™) gel electrophoresis separation followed by visualisation under a blue light. The agarose gel contained 0.01% SybrSafe (ThermoFisher Scientific™) DNA stain. Bands corresponding to the correct size relative to the DNA ladder were excised using a scalpel blade, placed into a separate 2ml microfuge per product then purified using the QIAquick™ PCR gel extraction kit (Qiagen™, Netherlands), as recommended by the manufacturer's instructions.

#### 3.2.4.13 Sanger Sequencing

PCR products were purified from the PCR reaction, or extracted subsequent to gel electrophoresis using the QIAquick™ PCR gel extraction kit (Qiagen™, Netherlands), as recommended by the manufacturer's instructions. The PCR products were quantified by Nanodrop™ spectrophotometry and diluted to a concentration of 30ng/µl. The diluted samples were then submitted to the Biomolecular Resource Facility (BRF) at the John Curtin School of Medical Research (JCSMR) along with 2.3µM aliquots of forward and reverse primers.

#### 3.2.4.14 Large-scale genomic DNA extraction

The avirulent transformants, t112, t177, t255, t388, t697, t784, t799, identified through a forward genetics screen were grown in liquid, stationary cultures of V8PDB. The biomass from these cultures was then freeze-dried and the gDNA extracted via the SDS-potassium acetate method (section 2.2.5.5) and purified using a Qiagen™ genomic DNA extraction column.

### 3.2.4.15 FastQC

The bioinformatics program FastQC assessed the quality of short-read sequencing data generated by Illumina platforms. This included adapter contamination from the sequencing run as well as the likelihood of each basepair being correctly identified. An Example script is shown below:

**Example:**

cd ~/Desktop/FastQC

./fastqc -t 10 -f fastq -o ~/Desktop/stago_genome_assembly/02_FastQC
/home/oliver/Desktop/stago_genome_assembly/01_RAW_DATA/t255_R1_001.fastq.gz

### 3.2.4.16 Trimm-o-matic

The bioinformatics program Trimm-o-matic was used to remove poor quality bases and adapters from the short read sequencing data generated by the Illumina platform. A moderate stringency was used to trim poor quality bases from the heads and tails of reads, as well as using a “sliding window” to detect and remove sections of poor overall quality.

**Example:**

java -jar /usr/local/bin/trimmomatic-0.32.jar PE -threads 10 -phred33 -1
/home/oliver/Desktop/stago_genome_assembly/01_RAW_DATA/t255_R1_001.fastq.gz -2
/home/oliver/Desktop/stago_genome_assembly/01_RAW_DATA/t255_R2_001.fastq.gz t255_R1_001_paired.fastq.gz t255_R1_001_unpaired.fastq.gz
t255_R2_001_paired.fastq.gz t255_R2_001_unpaired.fastq.gz ILLUMINACLIP:/usr/local/bin/Trimmomatic-0.32/adapters/NexteraPE-PE.fa:2:30:10
LEADING:20 TRAILING:20 SLIDINGWINDOW:4:24 MINLEN:50

#### 3.2.4.17 SPAdes

The bioinformatics program SPAdes was used to assemble the trimmed and raw reads generated by short read sequencing. The program used progressively larger Kmers to attempt better assemblies, ranging from 21bp Kmers to 63bp Kmers.

**Example:**

/usr/local/bioinfo/SPAdes-3.7.1/bin/spades.py -t 30 -m 300 -k 21,25,33,55,63 -1 /home/oliver/03_trimmed_reads/255_R1_paired.fastq.gz -2 /home/oliver/03_trimmed_reads/255_R2_paired.fastq.gz -o /home/oliver/04_Assemblies/SPAdes/255_SPAdes.fa

#### 3.2.4.18 Velvet

The velvet plugin of the bioinformatic suite Geneious™ was used to generate genome assemblies from short, trimmed, paired end, reads.

#### 3.2.4.19 CEGMA

The bioinformatics program Core Eukaryotic Genes Mapping Approach (CEGMA) provided and estimate of genome completeness and assembly quality by searching the genome for eukaryotic genes predicted to be found singularly in all eukaryotes. The proportion of genes not found, or found in duplicate provides an estimate of genome quality. An example script is shown below:

**Example:**

cd ~/Desktop/Ollie_Cegma/t112

cegma --genome Scaffold_t112

### 3.2.4.20 Yeast assembly of gene knock-out constructs

PCR amplification and gel purification generated ca. 1.5kb amplicons, homologous to the upstream 5' and downstream 3' flanking regions of the gene of interest. Primers generating the 5' homologous flank contained a 5' 30bp overhang homologous to the SmaI target in the pYAE vector in the forward primer, and a 5' 30bp overhang homologous to the 3' tail of the Hygromycin B resistance marker in the reverse primer. Primers generating the 3' homologous flank contained a 5' 30bp overhang homologous to the SmaI target in the pYAE vector in the reverse primer, and a 5' 30bp overhang homologous to the 5' tail of the Hygromycin B resistance marker (*Hph*) on the forward primer. The primers incorporated the pYAE and *Hph* homologous regions, used for cloning, into the amplicons during amplification. 100ng of each homologous flank, 100ng of *Hph* and 200ng of SmaI linearized pYAE vector were combined and freeze dried. The pellet was then dissolved in 50 µl of competent *S. cerevisiae* URA- cells and the transformation performed as per instructions of the Zymo Frozen-EZ Yeast Transformation™ kit.

Colonies growing on URA- yeast medium arose after 3 days and then colony PCR confirmed the correct assembly of the vector by amplification of the joining regions. Colonies harbouring a correctly assembled vector were then grown over night in liquid URA- medium and the plasmid extracted. The plasmid was then transformed into *E. coli* and *A. tumefaciens*.

### 3.2.4.21 Culturing an auxotrophic strain of *Saccharomyces cerevisiae*

The Δura3 BJ5464 auxotrophic strain of *S. cerevisiae* used in this study was cultured in URA drop out yeast medium at 28°C. Cultures on solid medium were incubated for 3 days and liquid cultures were incubated overnight shaking at 180rpm. This strain was

supplied by Dr. Yit-Heng Chooi, The School of Molecular Sciences, The University of Western Australia.

#### 3.2.4.22 Generation and transformation of *S. cerevisiae* competent cells

The Zymo Frozen-EZ Yeast Transformation™ kit was used for the generation of *S. cerevisiae* cells and their subsequent transformation.

#### 3.2.4.23 Plasmid extraction

Plasmids from *S. cerevisiae* and *E. coli* were extracted and purified using the Zymo yeast plasmid miniprep II™ and QIAprep Spin Miniprep™ kits respectively.

## 3.3 Results

### 3.3.1 Sequencing and genome assembly of *P. nodorum* avirulent transformants

A plasmid rescue method was adapted for retrieving fragments of *P. nodorum* genomic DNA containing the Hygromycin B resistance marker (*Hph*) in an auxotrophic strain of *Aspergillus nidulans*. However, this method failed to identify the insertion loci in the avirulent transformants in Chapter 2. Subsequently, inverse PCR method was trialled but also failed to identify the affected locus in the avirulent strains of *P. nodorum*. The final molecular approach for identifying insertion sites involved Thermo Asymetric InterLaced (TAIL) PCR. This approach identified the insertion locus in a trial experiment but failed to identify any of the disrupted loci in the avirulent mutants generated in Chapter 2. Subsequently, whole genome sequencing was employed to determine the loci harbouring T-DNA insertions in the avirulent strains of *P. nodorum*.

Genomic DNA from the avirulent transformants, t112, t177, t255, t388, t697, t784, t799 was extracted and analysed by gel electrophoresis to determine the level of degradation (Figure 3.04). The quality of the gDNA was deemed suitable for subsequent analysis and 250ng of gDNA from each transformant, with 260nm/280nm and 260nm/230nm spectral ratios above 1.8, were submitted to the Biomolecular Resource Facility at the John Curtin School of Medical Research. They were then paired-end, short read (150bp), sequenced on a single lane of the MiSeq Illumina platform. Reserve aliquots of each sample were stored at -80°C.

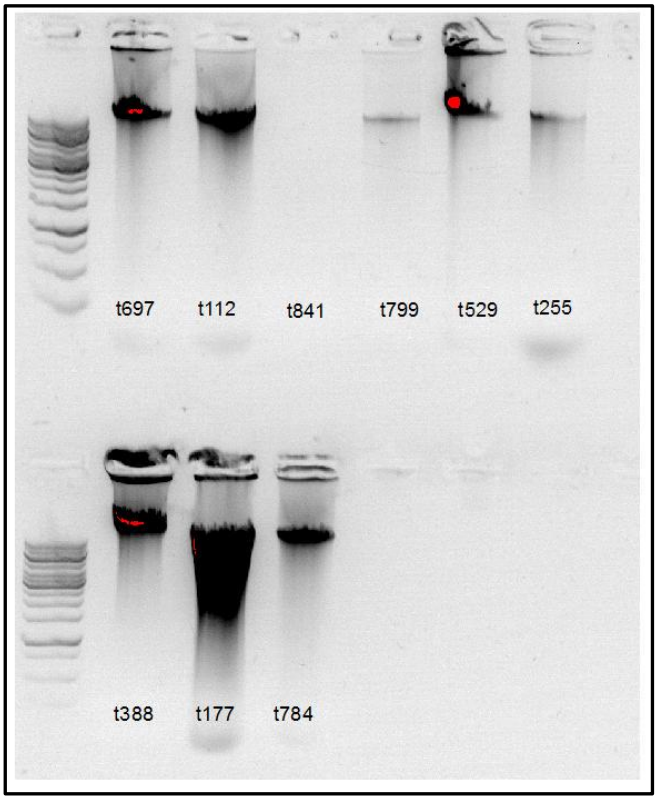


*(Figure 3.04: Electrophoretic gel image showing 5µl of genomic DNA sent for sequencing from avirulent* P. nodorum *transformants. The NEB™ 1kb ruler is juxtaposed in the most left-hand lane for comparison. Transformants t841and t529 are also shown, however these were a part of a separate experiment.)*

The resulting paired-end 150bp reads were quality checked by FastQC (Andrews, n.d.). FastQC indicated all samples were of high quality, containing predominantly ~150bp reads and limited adapters or contaminant from the sequencing preparation. Over represented sequences, such as adapter used during sequencing, poor quality sequences and bases were stringently trimmed and filtered by Trimm-o-matic (Bolger et al., 2014). Re-assessing the Trimm-o-matic output by FastQC indicated that few sequences and bases were removed, specified by read and base counts. This signifies the high quality of the Illumina short read data. The number of raw and trimmed reads for each strain are tabularised in Supplementary Table 3.01.

High quality trimmed reads were then assembled *de novo* using two different software packages; SPAdes (Bankevich et al., 2012) and Velvet (Zerbino, 2011; Zerbino and Birney, 2008). In addition to *de novo* assembly the trimmed reads were also mapped to the available reference genome with SPAdes. Mapping reads to the reference genome gave an indication of genome coverage as well as identifying coverage gaps. Some of these coverage gaps signified insertion sites for the T-DNA, where the assembly program discarded reads mapping to the insertion sequence. Between different transformants the assemblies differed most by contig number (3100-8200) and maximum contig size (85-204kb). However, SPAdes indicated the proportion of the reference genome covered varied much less ranging from 92%-95% coverage. Genome completeness was determined by the Core Eukaryotic Genome Mapping Approach (CEGMA), which identified 80-95% of conserved genes in the *de novo* assembled scaffolds (Parra et al., 2007). These metrics, summarised in Table 3.04, indicate that the assembled genomes were reasonably complete, and of good quality. Velvet consistently produced higher quality genome assemblies. This was assessed by lowest contig number and largest contig size, highest N50 (minimum contig length at which combining all longer contigs encompasses half the genome ie larger = more complete), assembly size compared to the reference and completeness by CEGMA score.

*(Table 3.04: Quality of* P. nodorum *transformant genomes assembled by Velvet from trimmed short reads. BLAST hit indicates the alignment with the pPK2 insertion sequence. Reference covered is by size percentage of the reference genome. t112, in red, showed the best alignment.)*

| | | | | | | | Best BLAST hit | |
|---|---|---|---|---|---|---|---|---|
| **Transformant** | **No. of contigs** | **Largest contig (kb)** | **N50 (bp)** | **Genome size (Mb)** | **Reference covered (%)** | **Genome completeness (%)** | **% identity** | **Length aligned (bp)** |
| t177 | 3351 | 185.3 | 39919 | 35.3 | 95.0 | 95.0 | 35.8 | 255 |
| t799 | 3394 | 203.8 | 38098 | 35.2 | 94.8 | 94.0 | 35.8 | 255 |
| t255 | 3107 | 170.3 | 32636 | 35.0 | 94.2 | 94.4 | 35.8 | 255 |
| t112 | 4096 | 128.7 | 23527 | 34.9 | 94.0 | 91.5 | 93.6 | 4941 |
| t784 | 5339 | 135.7 | 14764 | 34.6 | 93.1 | 84.3 | 35.8 | 255 |
| t697 | 5900 | 135.6 | 12006 | 34.4 | 92.6 | 83.1 | 35.8 | 255 |
| t388 | 8200 | 84.8 | 7917 | 34.1 | 91.9 | 80.1 | 35.8 | 255 |

The BLAST function of Geneious (Kearse et al., 2012) aligned the insertion sequence aligned with genome t112 with ca. 94% identity. However, there was no significant match to the other mutant or wildtype genomes. This indicated that the insertion sequence was not in the *de novo* assembled genomes, except for t112. To determine if the T-DNA insertion has been sequenced raw reads from each sample were then mapped to the T-DNA pPK2-HPH:GFP insertion sequence using Geneious (Kearse et al., 2012). The insertion sequence was identified in genome t112, generating a scaffold containing ca. 4.9kb of the insertion cassette. The reads from all other genomes failed to assemble using the insertion sequence as a reference genome confirming that only the t112 genome harboured the T-DNA insertion.

To determine if *Hph* was indeed present in the avirulent mutants identified in the previous chapter, gDNA from several of the mutants was probed via Southern blot for the T-DNA insert (Figure 3.05). This Southern blot analysis confirmed that t112 contained a T-DNA insert while the other mutants did not, despite being passaged on Hygromycin B [200µg/ml] after the initial transformation. Further, this Southern blot indicated that t112 contained a double insertion.

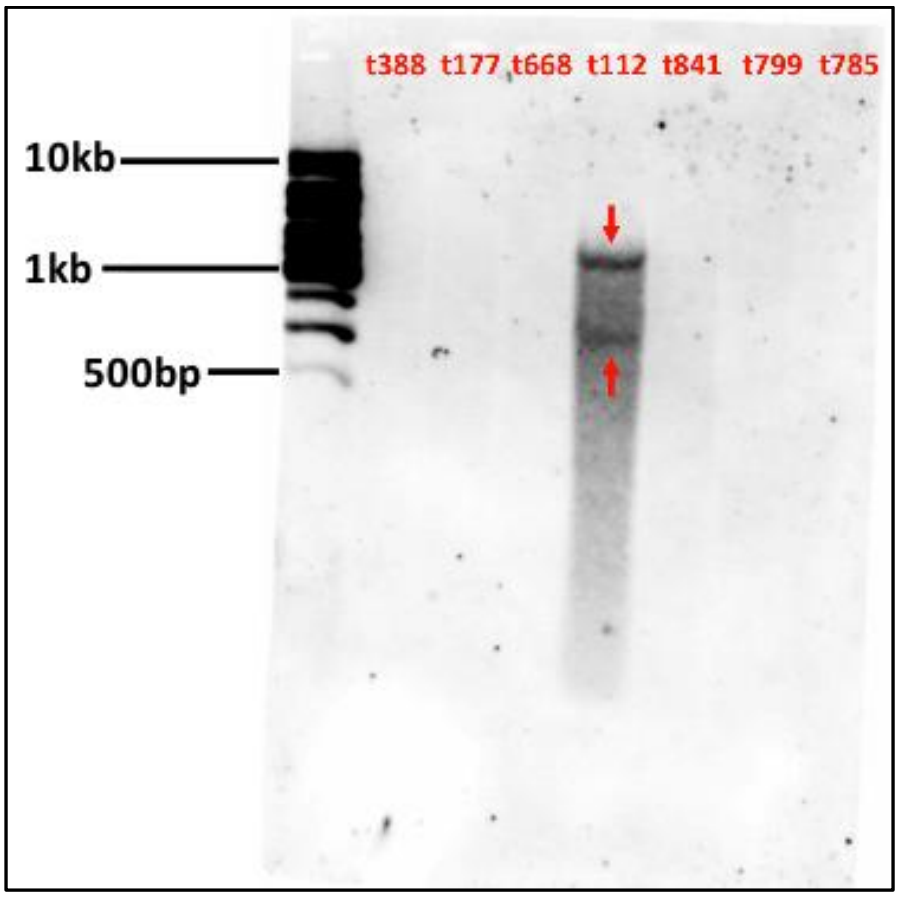


*(Figure 3.05: Southern blot probing for the T-DNA insertion sequence in the mutants, t388, t177, t112, t799, t785 that had been sequenced. t688 was included as part of another experiment. The genomic DNA of each strain was digested with the restriction enzyme* Bam*HI.)*

### 3.3.2 Identification of loci containing the pPK2 disruption cassette in the avirulent strain of *P. nodorum*, t112

The *de novo* assembled t112 genome indicated that there was a single T-DNA insertion flanked by sequences aligning to scaffold #4 and #12 of the reference genome (Figure 3.06). The conjunction of two separate scaffolds suggested the insertion induced chromosomal rearrangement, or genome miss-assembly. Miss-assembly is more likely as the Southern blot analysis in Figure 3.05 indicated a double insertion event had taken place. A double insertion may lead to miss-assembly due to identical reads mapping to two locations overlapping.

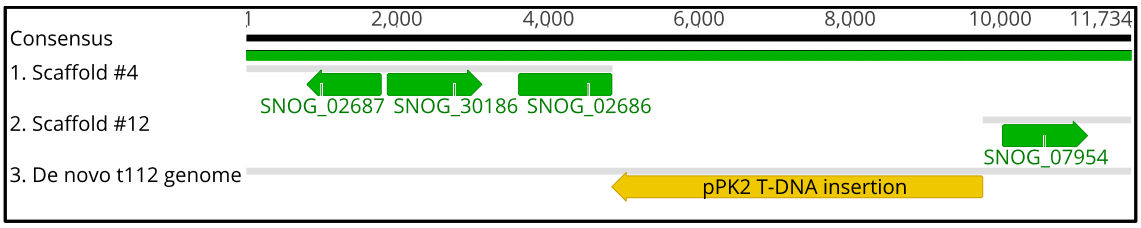


*(Figure 3.06: The pPK2 disruption cassette in the* de novo *assembled t112 genome. The 5' flanking region of the insert aligns with scaffold #4 of the reference genome, while the 3' flanking region aligns with scaffold #12 of the reference genome.)*

Mapping the t112 reads to the reference genome revealed coverage gaps in scaffold #4 and #12, specified by red arrows in Figure 3.07. These coverage gaps coincided with the regions flanking the pPK2 insertion sequence, shown in gold boxes, in the *de novo* t112 genome. The coverage gaps were likely due to the assembly program discarding reads that mapped to the insertion sequence.

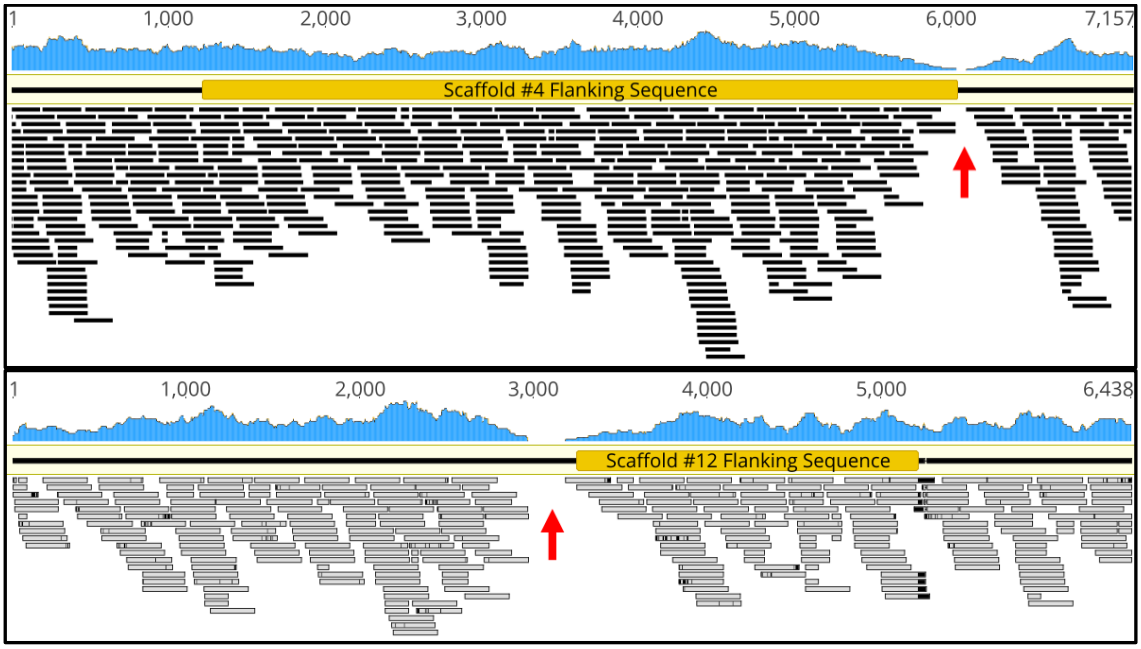


*(Figure 3.07: Scaffold #4 (top) and scaffold #12 (bottom) of the reference genome, with t112 reads mapped underneath each scaffold. Gold boxes indicate flanking sequences of the insertion sequences from the* de novo *assembled t112 genome. Red arrows indicate gaps in the read coverage. The blue graph above the alignment indicates assembly coverage measured in fold change, scaled from 0 to 30x)*

To determine if these coverage gaps were due to reads mapping to the T-DNA sequence being discarded I inserted the T-DNA sequence into the reference genome at the coverage gaps. Re-mapping the t112 reads to this hypothetical reference genome retrieved reads that spanned the junction between T-DNA and *P. nodorum* genome, confirming the exact integrations sites. The reads spanning the junction sites are indicated by red arrows in an alignment between the insertion sequence and the hypothetical genome with mapped reads, shown in Figure 3.08. Aligning the insertion sequence with the hypothetical genome revealed mismatches between the plasmid map for pPK2-HPH:GFP and the sequencing reads at the T-DNA borders. Aligning the insertion sequence also revealed the direction of the T-DNA insertion relative to the surrounding genome. This allowed me to use a specific, differential PCR to confirm the loci harbouring T-DNA.

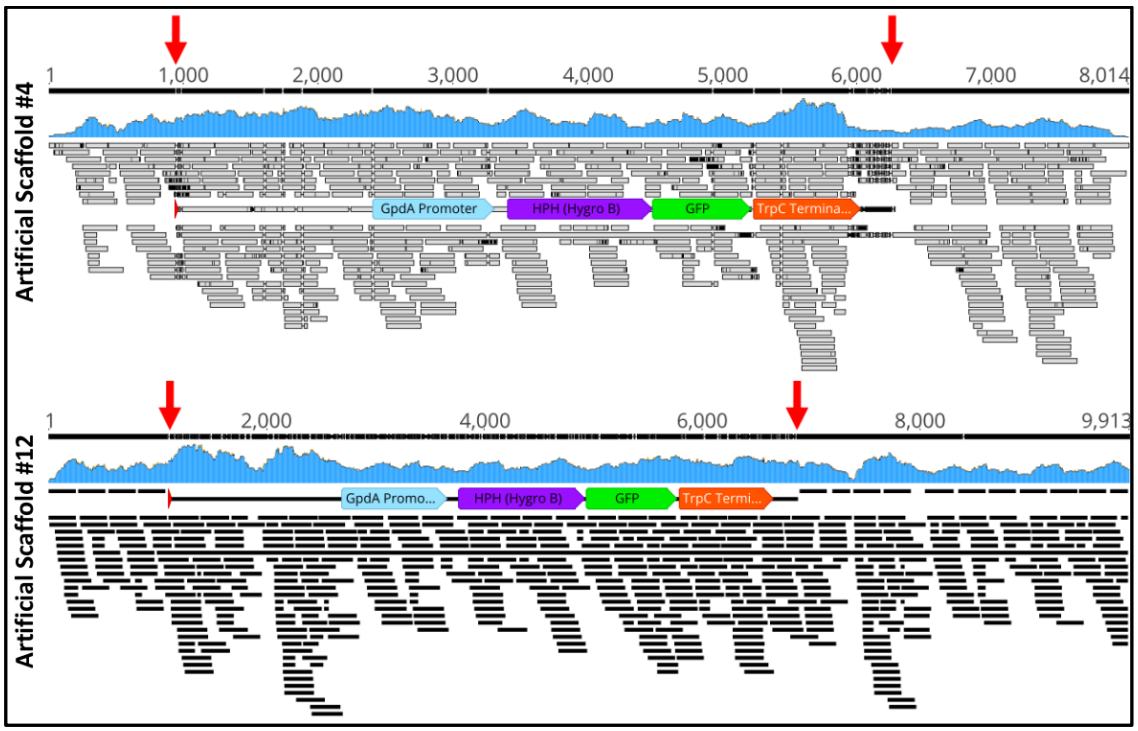


*(Figure 3.08: Reads from t112 mapping to the wild-type genome modified to contain the pPK2-HPH:GFP disruption cassette at the candidate insertion sites. Arrows indicate reads bridging the disruption cassette and the fungal genome. The long sequence in each artificial scaffold is the aligned pPK2-HPH:GFP insertion sequence. The blue graph above the alignment indicates the coverage for that particular region of the assembly, on a scale of 0 to 30x)*

Differential PCR then confirmed the loci containing T-DNA insertions in t112, disrupting SNOG_02686 and the promoter region of SNOG_07954. The amplicons from this PCR are shown in the gel electrophoretic image in Figure 3.09. The primers, HYG_Con_F and Scaffold_#4_R bind inside the *Hph* gene and outside of the T-DNA cassette in scaffold #4, respectively and would generate an 800bp fragment if the T-DNA insertion is present at that locus, but no band in the wild type. Similarly, the primers HYG_Con_F and Scaffold_#12_R are expected to amplify a 1kb fragment if the T-DNA insert has inserted at this locus, and no fragment if the insert is absent. These PCR products confirmed the locations and directions of the T-DNA insertions in the aviruent strain of *P. nodorum*, t112, and are summarised in Figure 3.10

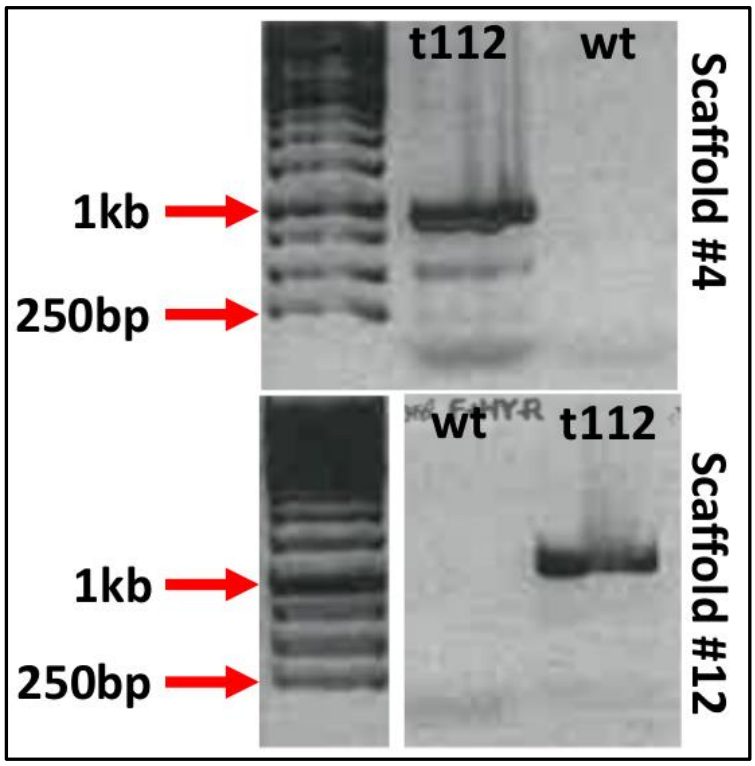


*(Figure 3.09: Gel electrophoresis image showing the PCR products from amplification of the candidate insertion sites in* t112 *and wild type strains of* P. nodorum*)*

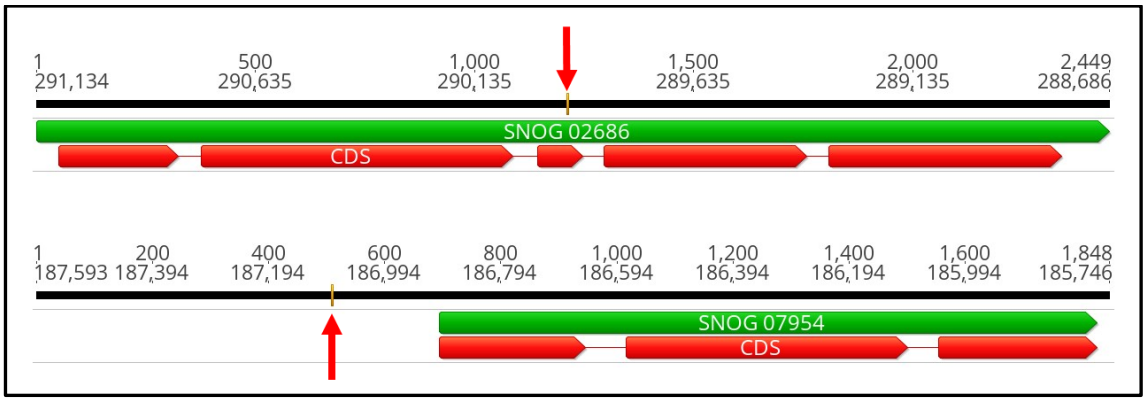


*(Figure 3.10: T-DNA insertion sites relative to Coding Domain Sequences of SNOG_02686 and SNOG_07954. Red arrows indicate the insertion sites of the pPK2-Hph:GFP T-DNA sequence. The solid green sequence labelled SNOG_02686 and SNOG_07954 indicates the gene sequence, while the red segmented sequence labelled CDS represents the Coding Domain Sequence. A T-DNA insertion disrupted the middle of the third SNOG_02686 intron, and another insertion disrupted 182bp upstream of the SNOG_07954 coding sequence)*

A Single Nucleotide Polymorphism/ Insertion-Deletetion (SNP/InDel) analysis of the genomes revealed further mutations. These mutations were identified using the variant analysis pipeline in the bioinformatics suit, Geneious™. Mutations were based on a minimum concensus of five reads confirming the variation from the wild-type genome, and were then filtered for those mutations only found in the Coding Domain Sequences (CDS) regions of the genome. The subsequent genes predicted to harbour mutations are listed in Table 3.05. The gene identifier of genes harbouring at least one mutation are listed alongside the best BLAST hit against the NCBI nr database for the genes predicted amino acid sequence. Table 3.05 only shows BLAST hits for matches with greater than 50% pairwise identity and an E-value less than 0.01. Due to time constraints mutations in regulatory regions were not analysed, nor were the CDS mutations filtered for non-synonymous mutations, stop codon insertions or shifts in reading frame.

*(Table 3.05: Genes, and their estimated function, predicted to harbour SNP and InDel mutations in seven avirulent strains of* P. nodorum. *Variations in coding regions between the mutants and the wild-type are supported by at least five reads and their estimated function is based upon the closest BLAST hit in the NCBI nr database)*

| **t112** | **Best BLAST hit** |
|---|---|
| SNOG_01327 | Unknown |
| SNOG_02219 | short chain type dehydrogenase [Aedes aegypti] |
| SNOG_02375 | tRNA-dihydrouridine synthase 1 [Aspergillus terreus NIH2624] |
| SNOG_02518 | TF3B_MOUSE Transcription factor IIIB 90 kDa subunit (TFIIIB90) (hTFIIIB90) (B-related factor 1) (BRF-1) |
| SNOG_05326 | Unknown |
| SNOG_06173 | related to hsp70 protein [MIPS] [Neurospora crassa OR74A] |
| SNOG_13299 | small G-protein GPA3 [Paracoccidioides brasiliensis] |
| SNOG_30093 | Unknown |
| **Total 8** | |
| | |
| **t177** | |
| SNOG_00062 | peroxisomal biogenesis factor 2 [Aspergillus terreus NIH2624] |
| SNOG_01098 | Unknown |
| SNOG_01885 | Unknown |

| | |
|---|---|
| SNOG_01918 | Unknown |
| **Total 4** | |
| | |
| **t255** | |
| SNOG_01165 | probable Cytokinesis protein sepA [Neurospora crassa] |
| SNOG_01307 | plasma membrane ATPase 2 [Aspergillus terreus NIH2624] |
| SNOG_01493 | CAMP-DEPENDENT PROTEIN KINASE REGULATORY CHAIN [Neurospora crassa OR74A] |
| SNOG_02018 | Aspergillopepsin A precursor (Aspergillopepsin I) |
| SNOG_02219 | short chain type dehydrogenase [Aedes aegypti] |
| SNOG_30093 | Unknown |
| **Total 6** | |

| | |
|---|---|
| **t388** | |
| SNOG_01307 | plasma membrane ATPase 2 [Aspergillus terreus NIH2624] |
| SNOG_01688 | related to MID1 protein [Neurospora crassa] |
| SNOG_01792 | ATP-binding cassette |
| SNOG_04397 | splicing factor 3b |
| SNOG_30093 | Unknown |
| **Total 5** | |
| | |
| **t697** | |
| SNOG_00861 | SCR1 protein [Debaryomyces occidentalis] |
| SNOG_01793 | Unknown |
| SNOG_02018 | Aspergillopepsin A precursor (Aspergillopepsin I) |
| SNOG_30093 | Unknown |
| **Total 4** | |
| | |
| **t784** | |
| SNOG_02018 | Aspergillopepsin A precursor (Aspergillopepsin I) |
| SNOG_02219 | short chain type dehydrogenase [Aedes aegypti] |
| SNOG_02448 | integral membrane protein [Aspergillus fumigatus Af293] |
| SNOG_02734 | Unknown |
| SNOG_04397 | splicing factor 3b |
| SNOG_05326 | Unknown |
| SNOG_06421 | exocyst complex component sec3 [Aspergillus fumigatus Af293] |
| SNOG_07070 | SPAC1327.01c [Schizosaccharomyces pombe] |
| SNOG_07080 | Possible surface protein |
| SNOG_07125 | Unknown |
| SNOG_09038 | Trimeric heat shock transcription factor |
| SNOG_09235 | Unknown |
| SNOG_09293 | protein kinase [Leishmania major strain Friedlin] |
| SNOG_30065 | Unknown |
| SNOG_30093 | Unknown |
| **Total 15** | |

| t799 | |
|---|---|
| SNOG_00273 | sugar transporter [Aspergillus fumigatus Af293] |
| SNOG_00553 | 40S ribosomal protein S19 [Coccidioides immitis RS] |
| SNOG_01666 | Unknown |
| SNOG_02194 | Unknown |
| SNOG_02195 | Unknown |
| SNOG_02518 | TF3B_MOUSE Transcription factor IIIB 90 kDa subunit (TFIIIB90) (hTFIIIB90) (B-related factor 1) (BRF-1) |
| SNOG_02832 | longevity assurance factor [Schizosaccharomyces pombe] |
| SNOG_02918 | annexin ANXC3.2 [Aspergillus fumigatus Af293] |
| SNOG_04397 | splicing factor 3b |
| SNOG_04743 | Unknown |
| SNOG_05309 | Aspergillopepsin II precursor (Acid protease A) (Proctase A) |
| SNOG_05326 | Unknown |
| SNOG_30093 | Unknown |
| SNOG_30237 | Unknown |
| **Total 14** | |

### 3.3.3 The avirulent *P. nodorum* strain, t112, harbours disruptions to putative *Copper-dependent amine oxidase* and *Catechol-1,2-dioxygenase* genes

A BLASTp search of the NCBI nr database revealed the closest homologs to the protein encoded by SNOG_02686 were putative *Copper-dependent amine oxidases* with 99% query coverage and 86% identity to the closest annotated match. While those closest to the protein encoded by SNOG_07954 were putative *Catechol-1,2-dioxygenases* with 97% query coverage, 89% identity to the nearest annotated match (Supplementary Figures 3.01 and 3.02). Further, the NCBI database identified conserved functional domains in these predicted proteins, supporting their expected functions (Supplementary Figures 3.03 and 3.04) (Marchler-Bauer et al., 2017). The Solomon lab has an in-house list of predicted functions for each *P. nodorum* gene based on homology of the predicted amino acid sequence to other sequences in the NCBI nr database. This list revealed at least 19 other genes with homology to amine oxidases, and two other genes with homology to the family containing catechol dioxygenases, the aromatic dioxygenases.

Gene expression analysis failed to produce further evidence for which gene maybe involved in virulence. *In planta* expression of the putative *Pn.Copper-dependent amine oxidase* and *Pn.Catechole-1,2-dioxygenase*, as well as the alpha subunit of the house keeping gene *Pn.Elongation factor1* were graphed from in house microarray data, shown in Figure 3.11 (Ipcho et al, 2012). Both genes of interest showed almost identical consistently low levels of expression during infection, compared to the house keeping gene control.

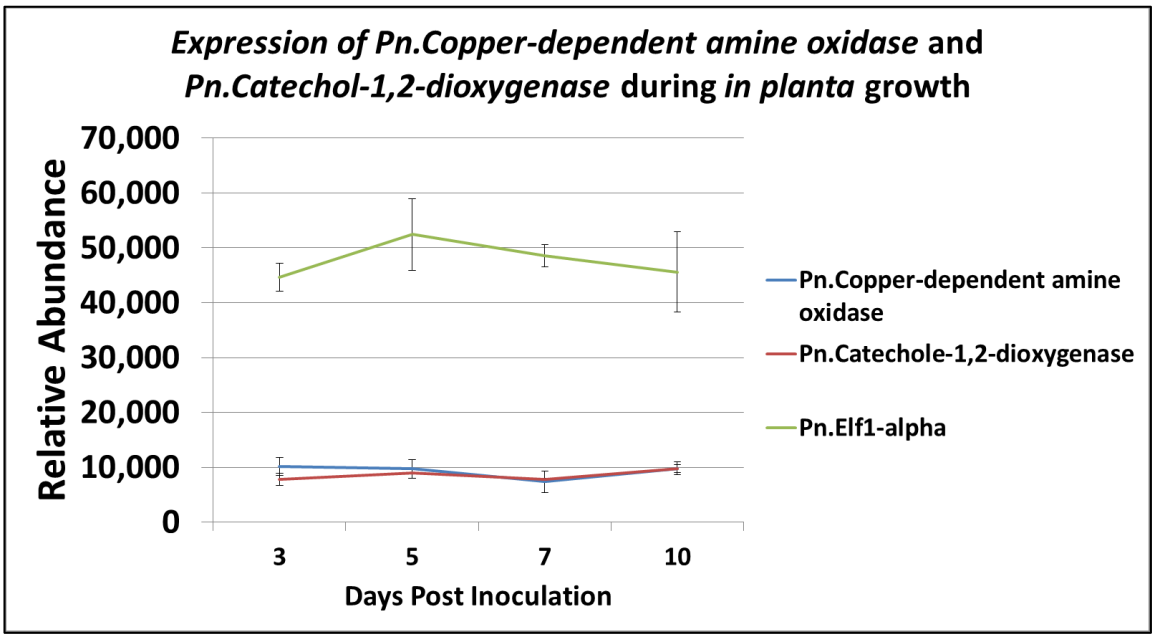


*(Figure 3.11: Gene expression of the two genes of interest from avirulent* P. nodorum *strain, t112,* Pn.Copper-dependent amine oxidase *and* Pn.Catechole-1,2-dioxygenase. *The alpha subunit of the house keeping gene,* Pn.Elongation factor 1 *(*Pn.Elf1-alpha*) is shown for comparison. The microarray expression data is unitless and was generated by Ipcho et al (2012). Error bars indicate 95%CI)*

### 3.3.4 Characterising the role of the predicted *Catechol-1,2-dioxygenase* (SNOG_07954) in the *P. nodorum*- wheat interaction

The mutation leading to t112 avirulence required verification by independently disrupting SNOG_02686 and SNOG_07954. Disruption cassettes were assembled using yeast homologous recombination in the pYAE vector (Figures 3.12 and 3.17). These disruption cassettes were used to independently disrupt SNOG_02686 and SNOG_07954 in the modified Δ*lig4 P. nodorum* strain (Δ*Pn.lig4*).

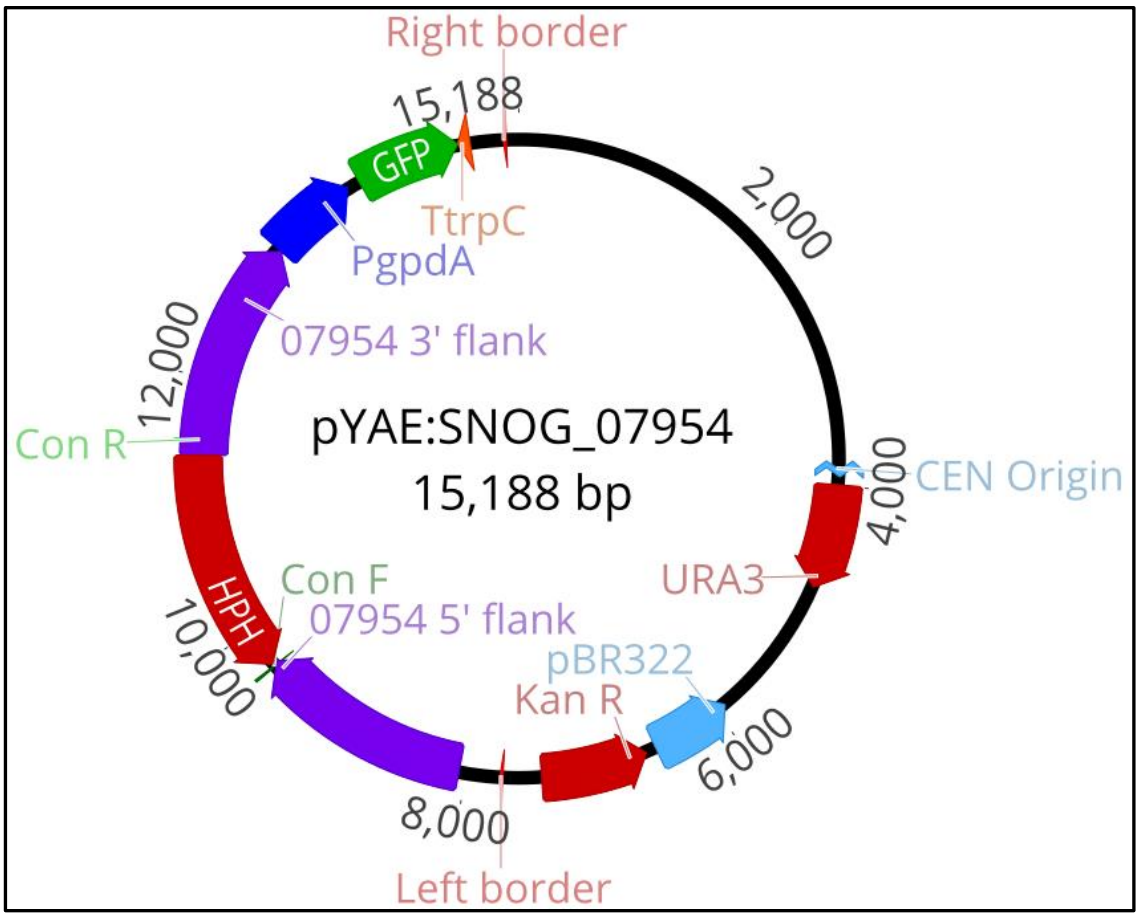


*(Figure 3.12: **A**: Knock-Out assembly vector pYAE_07954. The 5' and 3' 1.5kb flanking regions to SNOG_07954 encompass the* Hph *gene.* Hph *is driven by the PtrpC promoter and TtrpC terminator, and codes in the opposite direction to SNOG_07954 relative to the flanks)*

AMT of the SNOG_07954 disruption cassette and subsequent selection on Hygromycin B yielded ca. 180 *P. nodorum* colonies. Genomic DNA was extracted from these

mutants and PCR confirmed a size change in the SNOG_07954 locus (07954_ConII_F and 07954_ConII_R). These primers annealed to the inner sides of the flanking regions to SNOG_07954 used for homologous recombination. Genomes harbouring an intact SNOG_07954 locus were expected to produce a 1.3kb fragment, while those harbouring an *Hph* disruption at that locus were expected to produce a 1.7kb fragment. Genomes with an ectopic integration and an intact SNOG_07954 locus would produce two bands as the primers would bind the native locus, as well as the disruption cassette. The Δ*Pn.lig4* genome produced an ca. 1.4kb fragment and transformants #3, #4 and #21 produced single 1.6kb fragments, verifying the disruption to SNOG_07954 with two independent sets of primers Figure 3.13.

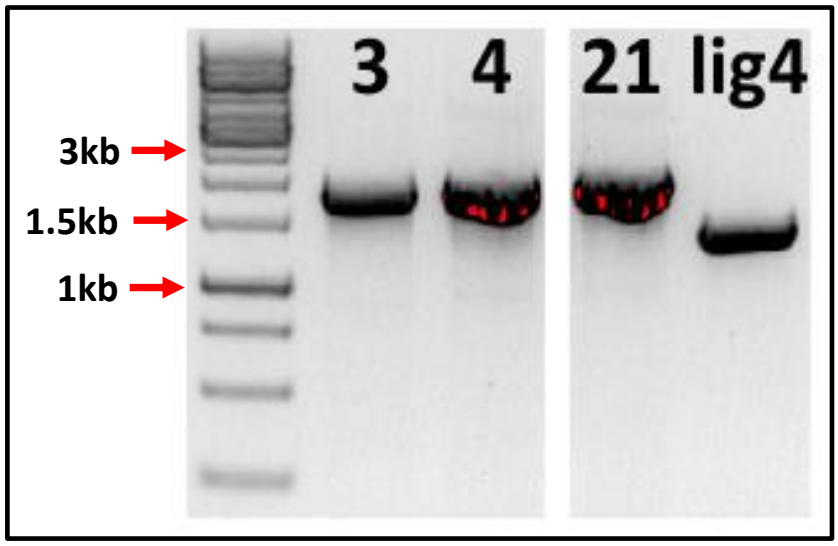


*(Figure 3.13: PCR confirmation of SNOG_07954 knock-out transformants* ΔPn.catd1-3, ΔPn.catd1-4, ΔPn.catd1-21, *and background strain* ΔPn.lig4. *A space was left between transformants 4 and 21 indicating where the gel image has been cropped. Samples in the removed lanes showed similar sized bands to the background strain, indicating ectopic integration)*

PCR confirmation verified three colonies with disruptions to the SNOG_07954 locus; these were subsequently named *Pn.catechol-1,2- dioxygenase1-3* (Δ*Pn.catd1-3*), *Pn.catechol-1,2- dioxygenase1-4* (Δ*Pn.catd1-4*), *Pn.catechol-1,2- dioxygenase1*-21

(Δ*Pn.catd-21*). The transformants were then screened for virulence on the susceptible wheat cultivars *Axe, Grandin* and *Summit*, shown in Figure 3.14.

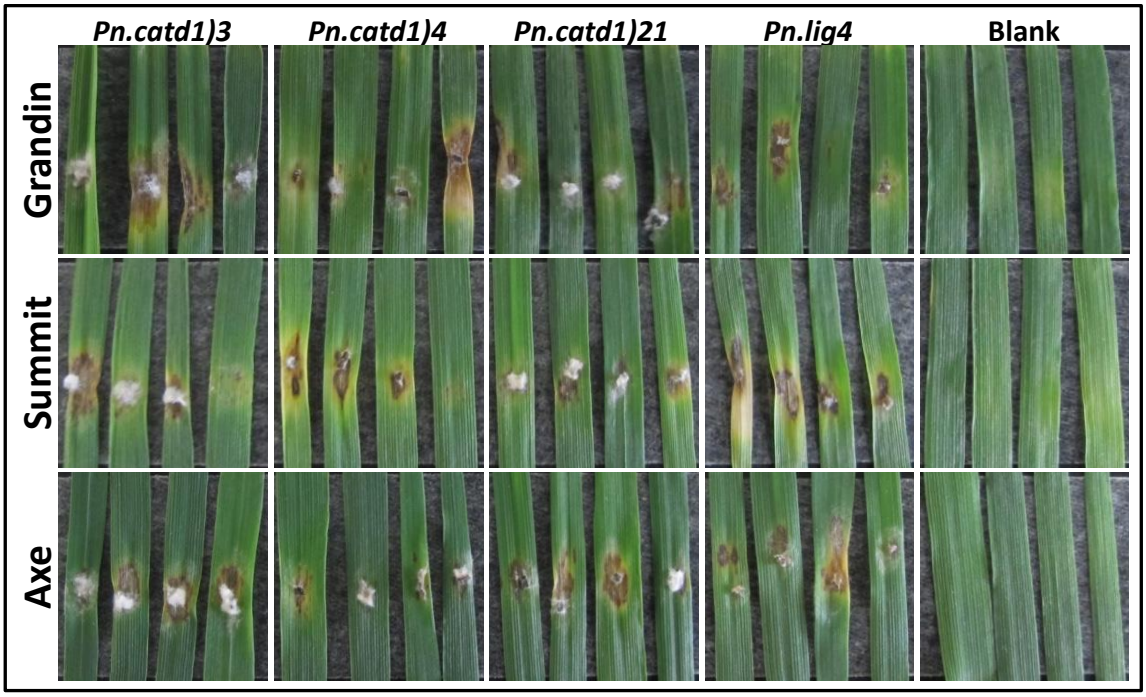


*(Figure 3.14: Virulence of* catechol-1,2-dioxygenase *knock-out transformants on the susceptible wheat cultivars* Grandin, Summit *and* Axe. *Agar plugs were used to inoculate leaves in a detached leaf assay. Leaves inoculated with the background strain,* ΔPn.lig4 *were the positive controls, and un-inoculated leaves labelled Blank were the negative controls. Image taken 7dpi.)*

The background strain Δ*Pn.lig4* produced small lesions on all wheat cultivars tested. All three knock-out mutants were able to induce similar or more necrosis compared to the positive control, across all wheat cultivars. The lesion length has been quantified and graphed in Figure 3.15.

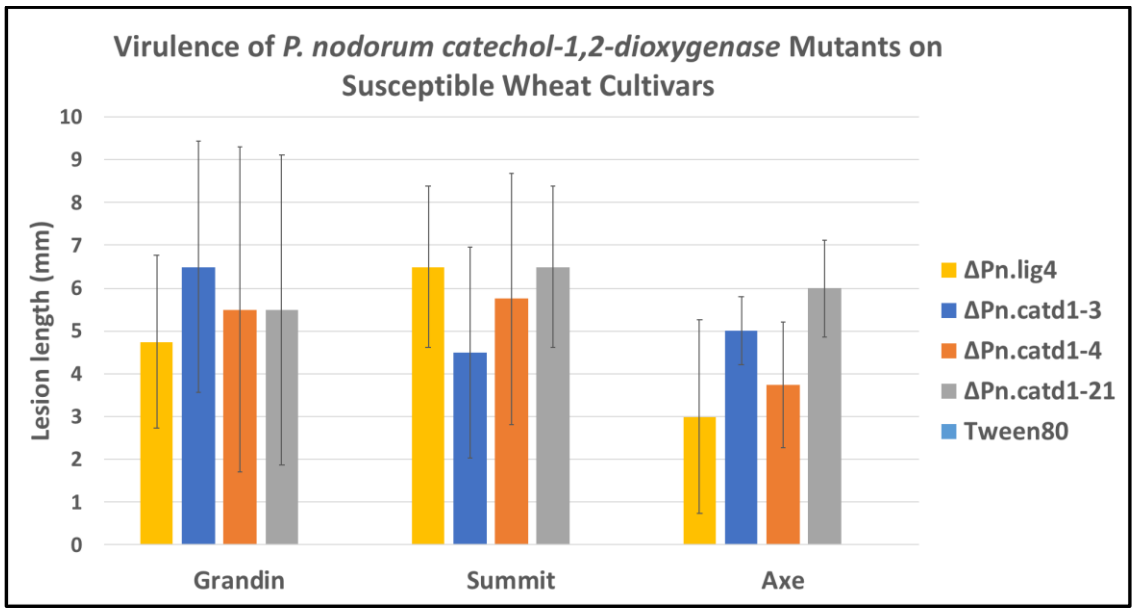


*(Figure 3.15: Virulence of* Pn.catechol-1,2-dioxygenase *knock-out transformants,* ΔPn.lig4 *positive control, and blank negative control on the wheat cultivars Grandin, Axe and Summit. Error bars represent 95%CI. The length of a resulting lesion was used as an indicator of virulence.)*

The lesions produced by this pathogenicity assay were highly variable across all wheat cultivars and *P. nodorum* strains. However, all strains displayed a similar trend and the lesion size produced by the knock-out mutants was not significantly different to that of the background strain on the same wheat cultivar. Repeating this pathogenicity assay produced comparable results where all three mutants were able to induce disease symptoms on the host cultivars (Supplementary Figure 3.07).

To test the effects of catechol on the growth of the *P. nodorum catechol-1,2-dioxygenase* mutants, each was grown on minimal media in Greiner™ 12 well plates, containing a dilution series of 0, 0.1, 0.3, 1, 3, 10, 30 and 100mM catechol. Differential growth between the Δ*catd1* mutants, compared to the *Pn.*Δ*lig4* background strain, was observed at 7 dpi shown in Figure 3.16. No significant growth differences were observed at 0mM catechol ($P>0.05$), except for Δ*catd1-3* which showed minor but significantly less growth compared to the *Pn.lig4* background strain ($P<0.05$).

Conversely, Δ*catd1-3 and* Δ*catd1-21* showed substantial and significantly reduced growth in 1mM catechol compared to the *Pn.lig4* background strain, ($P<0.05$) ($P<0.01$) respectively. Although Δ*catd1-4* growth was inhibited by catechol, this strain grew erratically. As such Δ*catd1-4* growth on 1mM catechol was not significantly different from either the other mutants nor the background strain ($P>0.05$). No strain grew in catechol concentrations above 1mM. Growth was allowed to continue for another seven days, at which point the growth of the Δ*catd1* mutants matched that of the Δ*lig4* background strain, covering the medium.

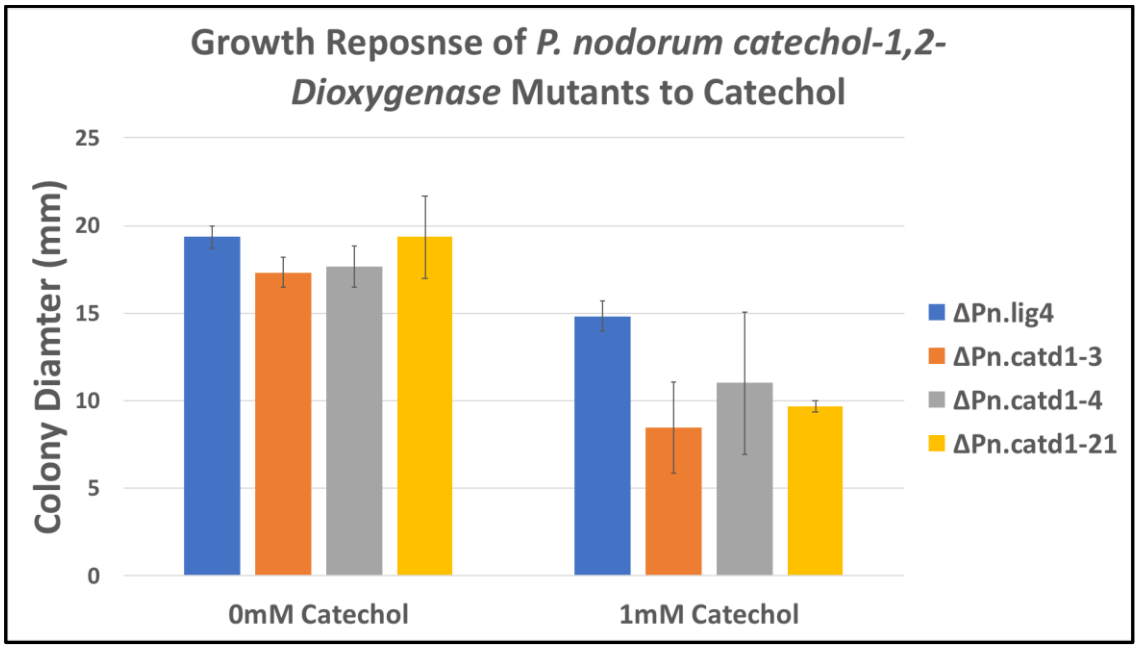


*(Figure 3.16: Growth of* Pn.catechol-1,2-dioxygenase *knock-out mutants* ΔPn.catd1-3, ΔPn.catd1-4, ΔPn.catd1-21, *and the background strain* ΔPn.lig4 *in the presence of 1mM catechol, when grown on minimal medium. Error bars represent 95% CI*)

### 3.3.5 Characterising the role of the predicted *Copper-dependent amine oxidase* (SNOG_02686) in the *P. nodorum*- wheat interaction

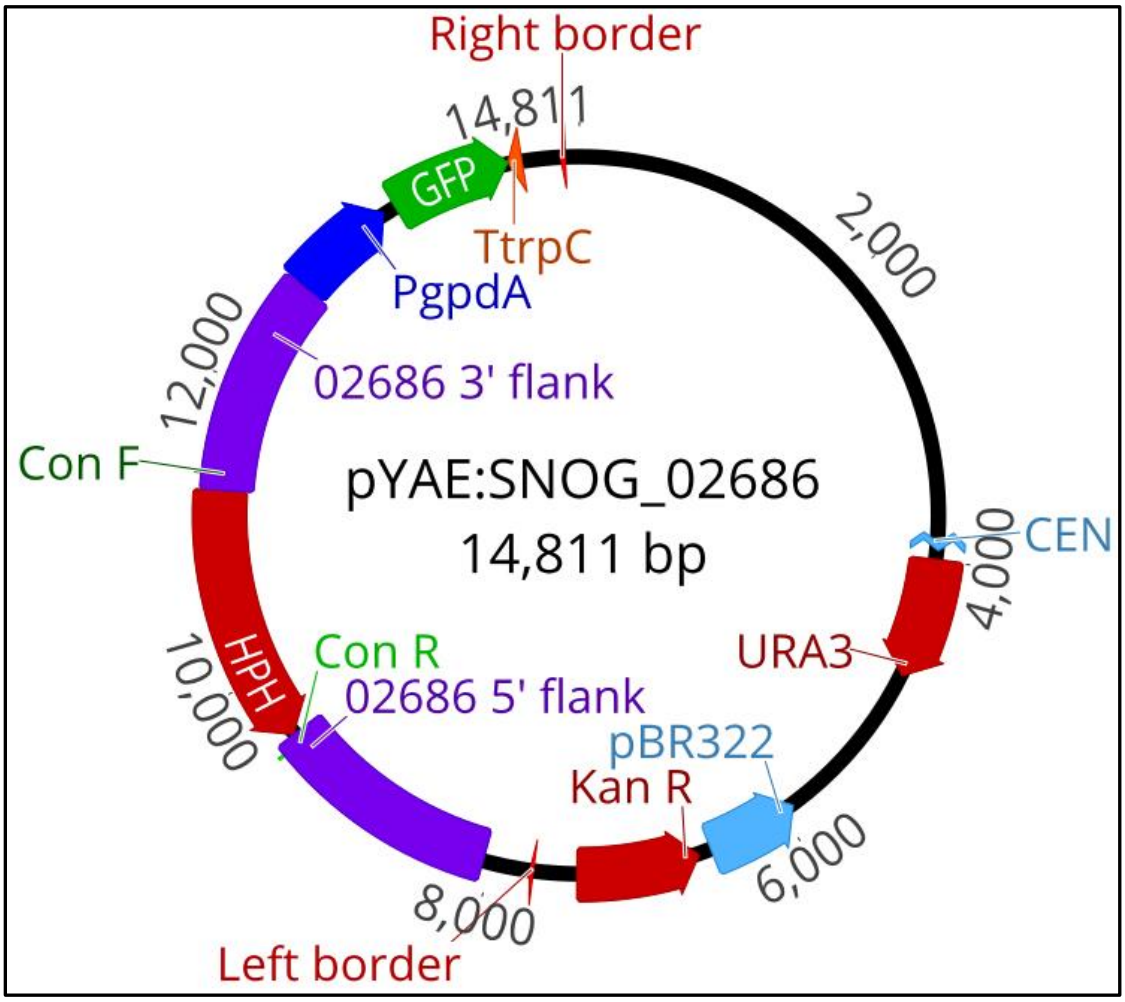


*(Figure 3.17: Knock-Out vector pYAE_02686. The 5' and 3' 1.5kb flanking regions to SNOG_02686 encompass the* Hph *gene.* Hph *is driven by the PtrpC promoter and TtrpC terminator, and codes in the opposite direction to SNOG_02686 relative to the flanks)*

AMT of the SNOG_02686 disruption cassette (Figure 3.17) and subsequent selection on Hygromycin B yielded ca. 145 *P. nodorum* colonies that were subsequently subcultured onto V8PDA plates containing 200µg/ml of Hygromycin B. These colonies provided the fungal tissue used directly as PCR template to verify integration of *Hph* at the SNOG_02686 locus. The initial screening PCR involved a primer binding outside of the 5' flanking region of the gene used for homologous recombination (02686_ConI_F), and a primer binding within the *Hph* gene (HYG_Con_R). Genomes harbouring

ectopically integrated disruption cassettes and the background Δ*Pn.lig4* genome were expected to elicit no band. While genomes harbouring an *Hph* disrupted SNOG_02686 locus were expected to produce a 2kb fragment. Primers ITS_1 and ITS_4 amplified the Internally Transcribed Spacer (ITS) region as an internal positive control, producing a 550bp fragment in all reactions. gDNA was extracted from candidate knock-out mutants and PCR screened with a second set of primers. The primers, 02686_ConII_F and 02686_ConII_R bound at the inner most edges homologous flanks used in the knock-out cassette. The background strain was expected to produce a 3.2kb fragment, while a correct insertion a 1.8kb fragment. Ectopic integrations of the knock-out cassette were expected to produce both 3.2kb and 1.8kb fragments. Despite considerable time and effort, no disruptions to the SNOG_02686 locus were identified from 145 transformants. Further mutants need to be generated and this investigation remains ongoing in the Solomon lab.

## 3.4 Discussion

In this *P. nodorum* forward genetics screen, whole genome sequencing identified two disrupted loci in the avirulent strain t112 - a putative *Catechol-1,2-dioxygenase* (*Pn.Catd1*) and a putative *Cu-dependent amine oxidase* (*Pn.Coa1*). Accordingly, independent *P. nodorum* mutants were generated harbouring disruptions to the *Catechol-1,2-dioxygenase* locus. These mutants, named Δ*Pn.catd1-3,* Δ*Pn.catd1-4* and Δ*Pn.catd1-21,* were screened for virulence using the same detached leaf assay developed for the forward genetics screen. However, the Δ*Pn.catd1* mutants retained virulence towards three susceptible wheat cultivars. Further tests revealed that disrupting *Pn.Catd1* significantly reduced the growth of *P. nodorum* in the presence of 1mM catechol, thereby beginning to define the role of this gene. The second candidate gene identified in mutant t112 was identified as a putative *Cu-dependent amine oxidase*

*(Pn.Coa1). Agrobacterium*-mediated transformations designed to disrupt this locus generated 145 Hygromycin B resistant *P. nodorum* colonies. While this method of gene disruption generally yields 5-10% correct gene knock-out mutants in the Solomon lab, PCR screening failed to identify any mutants harbouring a disruption to the *Pn.Coa1* locus. This indicates that this method of gene disruption is ineffectual for disrupting this locus and another method needs to be employed. Alternatively, this gene is required for viability, and the disruption in t112 was incomplete.

### 3.4.1 Whole genome sequencing efficiently identified two T-DNA insertions in the avirulent *P. nodorum* strain, t112

Historically, molecular methods have successfully identified mutations leading to interesting phenotypes in forward genetics screens (Michielse et al., 2009). However, in this study plasmid rescue, inverse PCR and TAIL-PCR all failed to identify the disrupted loci in any of the avirulent *P. nodorum* strains generated in chapter 2. Whole genome sequencing was then employed to identify mutations to these strains. The T-DNA insertion sequence, used to disrupt the *P. nodorum* genome, was identified only the genome assembly of strain t112. This strain contained two insertions at separate loci. One insertion disrupted the coding region of a predicted *Copper-dependent amine oxidase* (SNOG_02686), termed *Pn.Cao1*. The other insertion disrupted the promoter region of a predicted *Catechole-1,2-dioxygenase* (SNOG_07954) termed, *Pn.Catd1*. The assembled genomes of the other six avirulent strains, however, harboured no insertion cassettes.

It is interesting to note that reads map with mismatches to the 3' border region of the insertion sequence. The 3' border of the insertion sequence does not match the plasmid map we have for this plasmid. Later, re-sequencing of pPK2, as part of another students

project with Sanger sequencing, revealed clusters of mismatched nucleotides between the pPK2 plasmid map and the Sanger sequences. One cluster resided in the 3' region of the border sequence and another in the GFP encoding region. This may explain the poor mapping of reads to the insertion border as well as the poor efficacy of the TAIL-PCR approach. The Sanger sequenced insertion sequence could be inserted *in silica* into the genome and reads re-mapped to confirm the sequence. However, the aim of this exercise, to determine the integration site of the T-DNA, was achieved using this approach and plasmid map so the investigation was continued.

### 3.4.2 Hygromycin B resistance was lost in several mutants

How and when the *P.* nodorum transformants lost the T-DNA insertion remains unknown. The mutants were passaged on medium containing Hygromycin B [200µg/ml] for several generation prior to the genomic DNA extraction. However, they were not maintained on selection indefinitely. The gDNA was extracted and sequenced but the T-DNA sequence was not identified in any mutant genome, nor did any reads map to the insertion sequences, other than those from t112. The -80°C glycerol stock cultures used to inoculate cultures for sequencing were then inoculated onto medium containing [200µg/ml] Hygromycin B and failed to grow. However, they retained their avirulence. This indicates that between generations, the cells lost the selection marker but retained a phenotype inducing mutation. The excision of a T-DNA insert could leave a scar in the form of a SNP/InDel at the insertion site. A mutation like this could disrupt a gene required for virulence, but frustrate efforts to identify the causal mutation using the disruption cassette. The re-sequencing coverage was comparatively low for accurately call SNPs/InDels, compared to other SNP/InDel analyses, and resequencing at a high enough coverage is prohibitively expensive (Habig et al., 2017; McDonald et al., 2016). Despite the low coverage, a SNP/InDel analysis was performed to estimate

the number of masked mutations that might have arisen. These data provide possible avenues for future reverse genetics studies and suggests the likelihood of discovering novel virulence factors through high-coverage resequencing and SNP/InDel analysis. Further, this experiment indicates the level of off-target mutations accumulating during transformation.

The mechanism excising the T-DNA insertion from the fungal genome remains unknown. However, the insertion sequence is delineated by inverted repeats on the pPK2-*Hph:GFP* plasmid. These repeats are inserted by *A. tumefaciens* along with the disruption cassette (Jen and Chilton, 1986). Possibly, these repeat regions may act in a transposon-like manner and/or interact with endogenous DNA excision machinery and be removed. Type II transposons, common in filamentous fungi, are bound by inverted repeats and act in a classical "Cut and Paste" mechanism. This involves the sequence bound by the inverted repeats, as well as the repeats, being excised from the genome and reintroduced elsewhere. Conversely, the Type I transposons move via an RNA intermediate in a "Copy and Paste" mechanism (Daboussi and Capy, 2003; Wicker et al., 2007). Perhaps the inverted T-DNA repeats targeted the T-DNA insertion sequence for excision similarly to Type II transposons. Alternatively, repeats are known to cause genome instability in a variety of organisms. These instabilities are resolved by endogenous genome maintenance and repair mechanisms which may excise the T-DNA sequence (Feschenko et al., 2003; Gordenin et al., 1993). How this could occur in so few generations and in cultures that were not grown from single cells remains unresolved. Regardless of the mechanism involved, this ultimately confounded identification of causal mutations in these avirulent strains.

Absence of the T-DNA inserts explains why the molecular methods failed, however, these methods also failed to identify the confirmed T-DNA insert in t112. Whole genome sequencings' efficacy, reliability and ability to identify multiple or unintended mutations has made molecular methods of loci identification obsolete (Chambers et al., 2014). This is apparent in this current study by the speed (one month) and ease with which disruptions to *Cu-dependent amine oxidase1* and *Catechol-1,2-dioxygenase1* were accurately identified.

### 3.4.3 Catechols and polyphenols are dynamic plant defence compounds that many pathogens are required to degrade to invade host tissue

Catechols are the monomers of the extensive plant secondary metabolite family known as polyphenols (Bhattacharya et al., 2010; Yoruk and Marshall, 2003). These metabolites are involved in tissue structure, extra-cellular signalling, pigmentation, pollinator attractants, herbivory deterrents, wound healing and are produced in response to infection (Bhattacharya et al., 2010). During plant-pathogen interactions polyphenol oxidases (PPO) polymerize phenol-based molecules, such as catechol, increasing polyphenol abundance in surrounding tissues (Mikulič Petkovšek et al., 2009; Nagy et al., 2004; Yoruk and Marshall, 2003). Li and Steffens (2002) overexpressed a PPO in tomato plants, resulting in polyphenol accumulation and reduced severity of *Pseudomonas syringae* infections (Li and Steffens, 2002). Subsequently, *P. syringae* infections were exacerbated by transforming tomato plants with a PPO targeted RNAi construct that inhibited polyphenol production (Thipyapong et al., 2004). In response to polyphenols, plant-associated fungi have evolved enzymes to degrade polyphenolic compounds to exploit them as carbon sources (Tschaplinski et al., 2014; Wadke et al., 2016). The fungal tree pathogen, *Endoconidiophora polonica*, induced the Norwegian Spruce (*Picea abies*) to produce terpenoid resins and polyphenols (Wadke et al., 2016).

The abundance of these defence compounds declined during infection, while expression levels of their respective anabolic enzymes remained upregulated relative to uninfected plants. Wadke et al (2016) also showed that *E. polonica* metabolises these defence compounds into usable carbon sources *in vitro*. This substantiates the hypothesis that fungal metabolism of these defence compounds causes the decline in Norwegian Spruce polyphenols during *E. polonica* infection (Wadke et al., 2016).

Degradation and assimilation of polyphenolic compounds involve splitting the monomeric benzene-ring structures by a variety of enzymes, including catechol dioxygenases. Catechol-1,2-dioxygenases use oxygen to split catechol units into cis, cis-muconic acid, which is then further degraded into β-ketoadipate. β-ketoadipate can then be assimilated via the citric acid cycle (Wadke et al., 2016). This reaction has garnered a lot of interest in bioremediation, biofuel and chemical engineering research (Han et al., 2015; Mäkelä et al., 2015; Stoilova et al., 2006). Many environmental pollutants contain halogenated phenolics which can be detoxified through aromatic ring cleavage by catechol dioxygenases and subsequent microbial catabolism (Stoilova et al., 2006). Microbial production of biofuel is partially hindered by phenolic compounds found in plant biomass, such as lignin. These polyphenols degrade during fermentation releasing toxic monomeric phenolic compounds. Catechol dioxygenases provide an option for metabolizing these inhibitory compounds to improve yields (Mäkelä et al., 2015). Further, biogenic adipate is a feedstock for nylon production (Han et al., 2015). Aside from its industrial applications, catechol dioxygenases have also been shown to play a key role in plant-pathogen interactions.

Michielse et al (2009) distinguish catechol dioxygenase as a crucial virulence factor in a forward genetics screen of the tomato pathogen, *Fusarium oxysporum* f.sp. *lycopersici*

(Michielse et al., 2009). *F. oxysporum* f.sp. *lycopersici* is a root pathogen of tomato in the fungal class, Sordariomycete, which is distantly related to the class containing *P. nodorum*, Dothideomycete (Olivain and Alabouvette, 2009; Hane et al., 2007). These pathogens differ in their lifestyles, as well as taxonomically. *P. nodorum* is a host-specific foliar and glume pathogen of wheat, while *F. oxysporum* f.sp. *lycopersici* is a tomato-specific root pathogen (Solomon et al., 2006; Olivain and Alabouvette, 2009). To determine the role of the putative *Catechol-1,2-dioxygenase* during *P. nodorum* infection of wheat, I disrupted this gene and characterised virulence and growth of the resulting mutants.

### 3.4.4 The role of a putative *Catechol-1,2-dioxygenase* during the *P. nodorum*-wheat interaction

*Agrobacterium*-mediated transformation yielded 112 Hygromycin B resistant colonies, of which three harboured a disrupted SNOG_07954 locus. The growth of the *Pn.Δcatd1* strains on basal minimal medium was comparable to that of the background strain, *Pn.Δlig4.* There were no significant differences, with the exception of *Pn.Δcatd1-3* which showed a slight, but statistically significant growth reduction. However, in the presence of 1mM catechol, the colonies of all three mutants were on average approximately 66% the diameter of the *Pn.Δlig4* colonies, after seven days growth. This was statistically significant for two of the three mutants, *Pn.Δcatd1-3* and *Pn.Δcatd1-21*. The third mutant's (*Pn.Δcatd1-4)* growth on 1mM catechol, was highly variable between replications and therefore not statistically significant from the *Pn.Δlig4* background strain. This strain, however, grew normally on minimal medium, which indicates that the erratic growth may be an aspect of catechol induced stress not observed in the other strains. This suggests that the putative *Catechol-1,2-dioxygenase* indeed plays a role in degradation of catechol, and perhaps plant polyphenols.

Heterologous expression, protein purification and enzymatic assay would definitively determine the catalytic activity of this enzyme. For example, a photometric assay like that reported by Orston and Stainer (1966) could be used to measure the enzymatic cleavage of the benzene ring structure (Ornston and Stainer, 1966). After 14 days growth, all colonies had just covered the medium, indicating that catechol hindered but did not abolish growth in the *Catechol-1,2-dioxygenase* mutants. This could be explained by redundancy of catechol degrading enzymes in the *P. nodorum* genome, as there are two other genes predicted to cleave catechol-like compounds.

These mutants showed no significant difference in virulence in detached leaf assays when compared to the background *Pn.Δlig4* strain on any of three susceptible wheat cultivars. This signifies that the putative *Catechol-1,2-dioxygenase* plays no role during infection. The lack of a role during infection correlates with the *in planta* expression data from Ipcho et al (2012) showing consistently low expression during the infection time course. It is possible that this gene plays a role during infection under different conditions, such as on wheat cultivars producing abundant polyphenols, or during spore-based inoculation. Further, the natural life cycle of *P. nodorum* progresses for 365 days, and this assay only measures a small part of this. However, as the original forward genetics screen elucidated avirulent mutants using mycelial plugs on the wheat cultivar *Grandin,* the subsequent virulence assays were repeated accordingly. As the disease symptoms induced by the *Pn.Δcatd1* strains exceeded that of strain t112, the putative disrupted *Catechol-1,2-dioxygenase* is not the mutation leading to avirulence.

*Pn.catechol-1,2,-dioxygenase* knock-out mutants were generated in the *DNA ligase IV* background strain of *P. nodorum* (*Pn.Δlig4*). Previous studies have shown disruptions to the non-homologous end joining (NHEJ) pathway in other fungi reduced ectopic

integrations during transformation (Krappmann, 2007). Further, Feng et al (2012) showed that *P. nodorum Ku70* mutants, disrupted in the same DNA repair pathway as *lig4* mutants, produced far fewer mutants harbouring ectopic integrations than the wild-type strain (Feng et al., 2012). The *Pn.Δlig4* strain was previously shown in the Solomon Lab to display identical growth, sporulation and virulence to that of the wild-type.

The *Pn.Δlig4* background strain elicited three mutants harbouring correct integrations from 112 mutants screened (2.7%). This differs from the *Pn.Δku70* strain described by Feng et al (2012), where correct integration rates increased from 8% to between 60-80%. It may be that disrupting the non-homologous end joining pathway at Ku70, upstream of Lig4, is more efficient. Alternatively, *P. nodorum* maybe hold some redundancy in DNA repair proteins. The *Pn.Δlig4* strain used in this study harbours a disruption to the SNOG_20525 locus, which was selected on the basis of homology to characterised *Aspergillus* genes. However, SNOG_06940 holds some homology to the functional domains of these proteins, suggesting there may be redundancy of Ligase IV in *P. nodorum.* Alternatively, the chromosomal location of SNOG_07954 might be inhibitory to homologous recombination-based disruption, and poorer efficiency may have resulted from transforming the wildtype strain.

### 3.4.5 Copper-dependent amine oxidases mediate plant-pathogen interactions

There are two families of amine oxidase differentiated by their cofactors - Flavin and copper (Cona et al., 2006; Dawkes, 2001). Copper-dependent amine oxidases utilize oxygen, copper and topoquinone to remove primary amines from mono- and poly-amines. This reaction produces an aldehyde, ammonia and hydrogen peroxide (Dawkes,

2001), and has been observed in prokaryotes, plants, animals and fungi (Festa and Thiele, 2011).

Poly- and mono- amines appear to play an intriguing role during fungal-plant pathogenic interactions and has been heavily studied from the plant perspective. Walters (2003) reviewed the role of plant polyamines during disease in response to both biotrophic and necrotrophic fungal infection. Compatible biotrophic interactions between barley and *Blumaria graminis* f. sp. *hordei* consistently lead to increases in plant polyamines. While incompatible biotrophic interactions increased poly- and diamine oxidase activity. Walters (2003) hypothesized that these amine oxidases inhibited infection by producing reactive oxygen species (ROS). Juxtaposed with this, polyamine abundance diminished during the necrotrophic tobacco-*Alternaria tenuis* interaction (Walters, 2003). Cona et al (2006) further reviewed the role of plant amine oxidases in plant defence, wound healing and secondary metabolism (Cona et al., 2006). Rea et al (2002) reduced hydrogen peroxide levels in wounded chickpea leaves by inhibiting amine oxidases. This inhibition increased the disease symptoms of chickpea leaves inoculated with the *P. nodorum* relative, *Ascochyta rabiei* (Rea et al., 2002). However, amine oxidation and hydrogen peroxide production by *A. rabiei* were not measured in this study.

There is substantial information regarding plant poly- and monoamines, as well as amine oxidases during infection. However, our understanding of these process from the fungal point of view is severely limited. Du Fall and Solomon (2013) infiltrated wheat leaves with the *P. nodorum* effector protein, ToxA, resulting in significant upregulation of the monoamine, serotonin. Exogenous serotonin was consequently shown to inhibit pathogen pycnidia formation and sporulation, *in vitro*. However, wheat leaves infected

with *P. nodorum* expressing *ToxA* contained less serotonin than those infiltrated with ToxA protein. This suggests that the pathogen inhibits host serotonin production in order to reproduce (Du Fall and Solomon, 2013). Despite intriguing reports of the roles played by mono- and polyamines, and plant amine oxidases during infection there is little literature on the role of fungal amine oxidases during plant-microbe pathogenic interactions.

### 3.4.6 Determining the role of *Pn.Copper-dependent amine oxidase* during *P. nodorum* infection of wheat

Transformation of the *Pn.Δlig4* strain of *P. nodorum* produced 145 colonies with a disruption cassette targeting *Pn.Cao1* (SNOG_02686). However, two separate confirmation PCR reactions revealed no mutants harboured a disruption to the *Copper-dependent amine oxidase* identified in the avirulent isolate, t112. The previous transformation in this chapter yielded 2.7% efficiency of the *Pn.Δlig4* strain, while Feng et al (2012) report wild-type efficiency of 8% and *Pn.Δku70* efficiency between 60% and 80%. The absence of correctly integrated disruption cassettes could be explained if disruptions to this gene are lethal or severely detrimental to the cell. The original mutation in t112 cleaved the gene in half, leaving the 5' 1.2kb still driven by the native promoter. It is possible that the portion of the gene still expressed retained partial functionality. Supporting this hypothesis, t112 was able to induce a small necrotic circle encompassing the inoculation site. This could be indicative that the gene is semi-functional, allowing the cell to survive and produce limited disease symptoms without complete virulence. This project is ongoing in the Solomon lab, and may employ an RNAi knock-down approach, such as that reported by Kemppainen et al (2009), or by replacing the native promoter with a characterised inducible promoter (Kemppainen et al., 2009).

### 3.4.7 Conclusions

Whole genome sequencing easily identified the two T-DNA insertions in the avirulent *P. nodorum* strain, t112. These mutations disrupted the predicted promoter region of a putative *Catechol-1,2-dioxygenase* (*Pn.Catd1*) and the coding region of a *Copper-dependent amine oxidase* (*Pn.Cao1*). Disrupting *Pn.Catd1* inhibited growth in the presence of catechol, strongly suggesting the catalytic function encoded by this gene. However, growth was not abolished, which may be accounted for by the redundancy of aromatic dioxygenases in *P. nodorum*. Further, the ability to induce necrosis on detached was not affected by disrupting *Pn.Catd1*. This indicates that the avirulence of t112 is not due to harbouring a disrupted *Catechol-1,2-dioxygenase*. I was unable to generate mutants harbouring disruptions to the *Copper-dependent amine oxidase*, despite considerable effort. Disruptions to this gene may be lethal, and t112 was able to survive using a truncated and partially functional enzyme. This may further explain how t112 induced limited necrosis but failed to completely infect the host.

## 3.5 Supplementary Figures

(Supplementary table 3.01: The total number of raw and trimmed reads for each mutant strain of *P. nodorum* sequenced using the MiSeq short-read sequencing platform.)

| Strain | Read Pair | Raw Sequences | Retained Sequences | Removed Sequences | Proportion of sequences removed (%) |
|---|---|---|---|---|---|
| **t112** | R1 | 978,722 | 786,979 | 191,743 | 19.6 |
| **t112** | R2 | 978,722 | 786,979 | 191,743 | 19.6 |
| **t177** | R1 | 1,289,353 | 1,052,622 | 236,731 | 18.4 |
| **t177** | R2 | 1,289,353 | 1,052,622 | 236,731 | 18.4 |
| **t255** | R1 | 1,183,074 | 934,511 | 248,563 | 21.0 |
| **t255** | R2 | 1,183,074 | 934,511 | 248,563 | 21.0 |
| **t388** | R1 | 752,820 | 537,776 | 215,044 | 28.6 |
| **t388** | R2 | 752,820 | 537,776 | 215,044 | 28.6 |
| **t529** | R1 | 943,130 | 692,341 | 250,789 | 26.6 |
| **t529** | R2 | 943,130 | 692,341 | 250,789 | 26.6 |
| **t697** | R1 | 775,872 | 616,010 | 159,862 | 20.6 |
| **t697** | R2 | 775,872 | 616,010 | 159,862 | 20.6 |
| **t784** | R1 | 869,110 | 689,864 | 179,246 | 20.6 |
| **t784** | R2 | 869,110 | 689,864 | 179,246 | 20.6 |
| **t799** | R1 | 1,317,709 | 1,068,603 | 249,106 | 18.9 |
| **t799** | R2 | 1,317,709 | 1,068,603 | 249,106 | 18.9 |

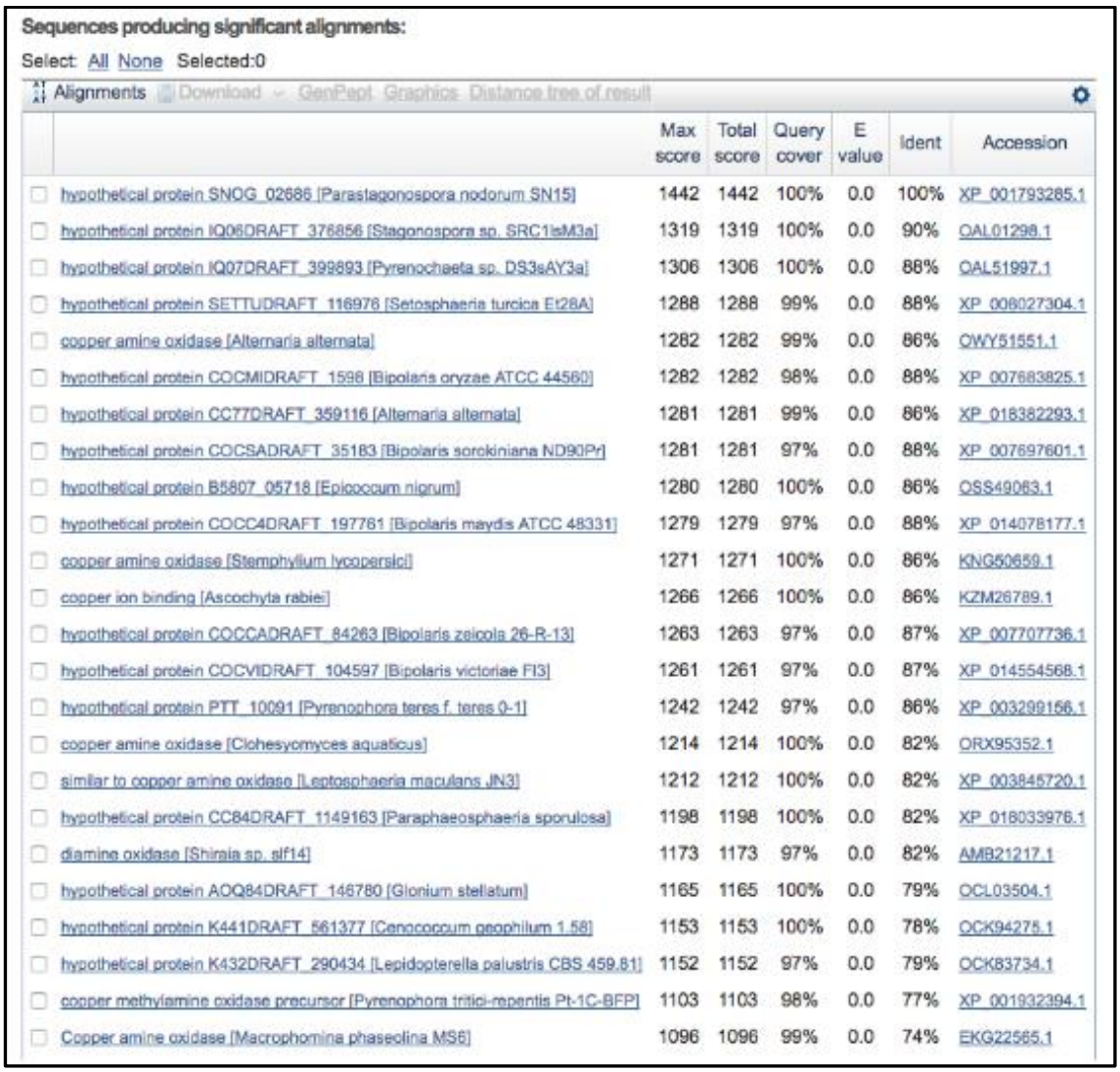

**Sequences producing significant alignments:**

Select: All None Selected:0

Alignments | Download | GenPept Graphics Distance tree of result

| | Max score | Total score | Query cover | E value | Ident | Accession |
|---|---|---|---|---|---|---|
| hypothetical protein SNOG_02686 [Parastagonospora nodorum SN15] | 1442 | 1442 | 100% | 0.0 | 100% | XP_001793285.1 |
| hypothetical protein IQ06DRAFT_376856 [Stagonospora sp. SRC1lsM3a] | 1319 | 1319 | 100% | 0.0 | 90% | OAL01298.1 |
| hypothetical protein IQ07DRAFT_399893 [Pyrenochaeta sp. DS3sAY3a] | 1306 | 1306 | 100% | 0.0 | 88% | OAL51997.1 |
| hypothetical protein SETTUDRAFT_116976 [Setosphaeria turcica Et28A] | 1288 | 1288 | 99% | 0.0 | 88% | XP_008027304.1 |
| copper amine oxidase [Alternaria alternata] | 1282 | 1282 | 99% | 0.0 | 86% | OWY51551.1 |
| hypothetical protein COCMIDRAFT_1598 [Bipolaris oryzae ATCC 44560] | 1282 | 1282 | 98% | 0.0 | 88% | XP_007683825.1 |
| hypothetical protein CC77DRAFT_359116 [Alternaria alternata] | 1281 | 1281 | 99% | 0.0 | 86% | XP_018382293.1 |
| hypothetical protein COCSADRAFT_35183 [Bipolaris sorokiniana ND90Pr] | 1281 | 1281 | 97% | 0.0 | 88% | XP_007697601.1 |
| hypothetical protein B5807_05718 [Epicoccum nigrum] | 1280 | 1280 | 100% | 0.0 | 86% | OSS49083.1 |
| hypothetical protein COCC4DRAFT_197761 [Bipolaris maydis ATCC 48331] | 1279 | 1279 | 97% | 0.0 | 88% | XP_014078177.1 |
| copper amine oxidase [Stemphylium lycopersici] | 1271 | 1271 | 100% | 0.0 | 86% | KNG50659.1 |
| copper ion binding [Ascochyta rabiei] | 1266 | 1266 | 100% | 0.0 | 86% | KZM26789.1 |
| hypothetical protein COCCADRAFT_84263 [Bipolaris zeicola 26-R-13] | 1263 | 1263 | 97% | 0.0 | 87% | XP_007707736.1 |
| hypothetical protein COCVIDRAFT_104597 [Bipolaris victoriae FI3] | 1261 | 1261 | 97% | 0.0 | 87% | XP_014554568.1 |
| hypothetical protein PTT_10091 [Pyrenophora teres f. teres 0-1] | 1242 | 1242 | 97% | 0.0 | 86% | XP_003299166.1 |
| copper amine oxidase [Clohesyomyces aquaticus] | 1214 | 1214 | 100% | 0.0 | 82% | ORX95352.1 |
| similar to copper amine oxidase [Leptosphaeria maculans JN3] | 1212 | 1212 | 100% | 0.0 | 82% | XP_003845720.1 |
| hypothetical protein CC84DRAFT_1149163 [Paraphaeosphaeria sporulosa] | 1198 | 1198 | 100% | 0.0 | 82% | XP_018033976.1 |
| diamine oxidase [Shiraia sp. slf14] | 1173 | 1173 | 97% | 0.0 | 82% | AMB21217.1 |
| hypothetical protein AOQ84DRAFT_146780 [Glonium stellatum] | 1165 | 1165 | 100% | 0.0 | 79% | OCL03504.1 |
| hypothetical protein K441DRAFT_561377 [Cenococcum geophilum 1.58] | 1153 | 1153 | 100% | 0.0 | 78% | OCK94275.1 |
| hypothetical protein K432DRAFT_290434 [Lepidopterella palustris CBS 459.81] | 1152 | 1152 | 97% | 0.0 | 79% | OCK83734.1 |
| copper methylamine oxidase precursor [Pyrenophora tritici-repentis Pt-1C-BFP] | 1103 | 1103 | 98% | 0.0 | 77% | XP_001932394.1 |
| Copper amine oxidase [Macrophomina phaseolina MS6] | 1096 | 1096 | 99% | 0.0 | 74% | EKG22565.1 |

(Supplementary Figure 3.01: NCBI BLASTp results for SNOG_02686. Blank space has been cropped out between the identifier and alignment scores)

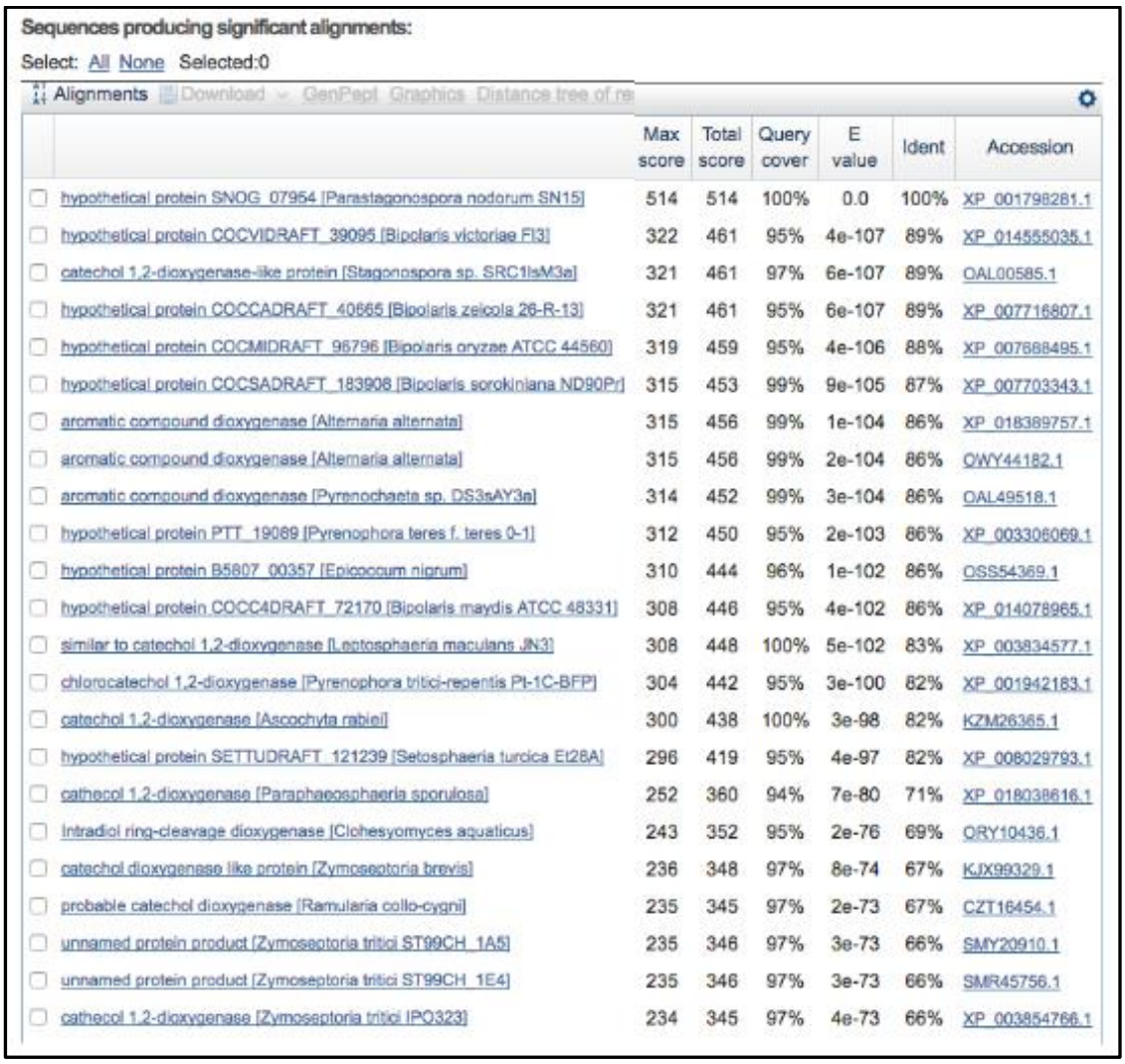

Sequences producing significant alignments:

Select: All None Selected:0

Alignments Download GenPept Graphics Distance tree of re

| | Max score | Total score | Query cover | E value | Ident | Accession |
|---|---|---|---|---|---|---|
| hypothetical protein SNOG_07954 [Parastagonospora nodorum SN15] | 514 | 514 | 100% | 0.0 | 100% | XP_001798281.1 |
| hypothetical protein COCVIDRAFT_39095 [Bipolaris victoriae FI3] | 322 | 461 | 95% | 4e-107 | 89% | XP_014555035.1 |
| catechol 1,2-dioxygenase-like protein [Stagonospora sp. SRC1lsM3a] | 321 | 461 | 97% | 6e-107 | 89% | OAL00585.1 |
| hypothetical protein COCCADRAFT_40665 [Bipolaris zeicola 26-R-13] | 321 | 461 | 95% | 6e-107 | 89% | XP_007716807.1 |
| hypothetical protein COCMIDRAFT_96796 [Bipolaris oryzae ATCC 44560] | 319 | 459 | 95% | 4e-106 | 88% | XP_007688495.1 |
| hypothetical protein COCSADRAFT_183908 [Bipolaris sorokiniana ND90Pr] | 315 | 453 | 99% | 9e-105 | 87% | XP_007703343.1 |
| aromatic compound dioxygenase [Alternaria alternata] | 315 | 456 | 99% | 1e-104 | 86% | XP_018389757.1 |
| aromatic compound dioxygenase [Alternaria alternata] | 315 | 456 | 99% | 2e-104 | 86% | OWY44182.1 |
| aromatic compound dioxygenase [Pyrenochaeta sp. DS3sAY3a] | 314 | 452 | 99% | 3e-104 | 86% | OAL49518.1 |
| hypothetical protein PTT_19069 [Pyrenophora teres f. teres 0-1] | 312 | 450 | 95% | 2e-103 | 86% | XP_003306069.1 |
| hypothetical protein B5807_00357 [Epicoccum nigrum] | 310 | 444 | 96% | 1e-102 | 86% | OSS54369.1 |
| hypothetical protein COCC4DRAFT_72170 [Bipolaris maydis ATCC 48331] | 308 | 446 | 95% | 4e-102 | 86% | XP_014078965.1 |
| similar to catechol 1,2-dioxygenase [Leptosphaeria maculans JN3] | 308 | 448 | 100% | 5e-102 | 83% | XP_003834577.1 |
| chlorocatechol 1,2-dioxygenase [Pyrenophora tritici-repentis Pt-1C-BFP] | 304 | 442 | 95% | 3e-100 | 82% | XP_001942183.1 |
| catechol 1,2-dioxygenase [Ascochyta rabiei] | 300 | 438 | 100% | 3e-98 | 82% | KZM26365.1 |
| hypothetical protein SETTUDRAFT_121239 [Setosphaeria turcica Et28A] | 296 | 419 | 95% | 4e-97 | 82% | XP_008029793.1 |
| cathecol 1,2-dioxygenase [Paraphaeosphaeria sporulosa] | 252 | 360 | 94% | 7e-80 | 71% | XP_018038616.1 |
| Intradiol ring-cleavage dioxygenase [Clohesyomyces aquaticus] | 243 | 352 | 95% | 2e-76 | 69% | ORY10436.1 |
| catechol dioxygenase like protein [Zymoseptoria brevis] | 236 | 348 | 97% | 8e-74 | 67% | KJX99329.1 |
| probable catechol dioxygenase [Ramularia collo-cygni] | 235 | 345 | 97% | 2e-73 | 67% | CZT16454.1 |
| unnamed protein product [Zymoseptoria tritici ST99CH_1A5] | 235 | 346 | 97% | 3e-73 | 66% | SMY20910.1 |
| unnamed protein product [Zymoseptoria tritici ST99CH_1E4] | 235 | 346 | 97% | 3e-73 | 66% | SMR45756.1 |
| cathecol 1,2-dioxygenase [Zymoseptoria tritici IPO323] | 234 | 345 | 97% | 4e-73 | 66% | XP_003854766.1 |

(Supplementary Figure 3.02: NCBI BLASTp results for SNOG_07954 Blank space has been cropped out between the identifier and alignment scores)

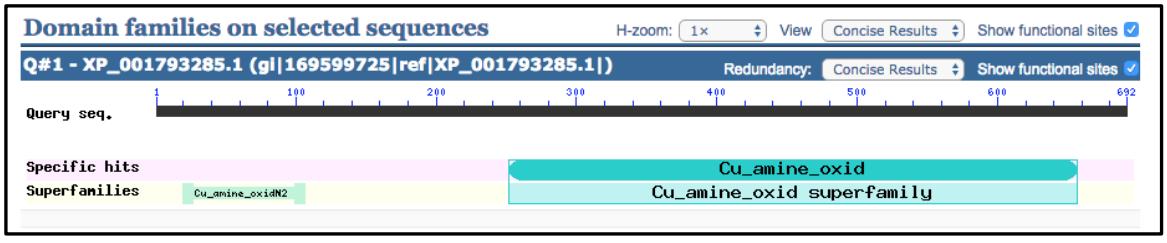


(Supplementary Figure 3.03: Conserved protein domains of SNOG_02686 predicted by the NCBI Conserved Domain Search function)

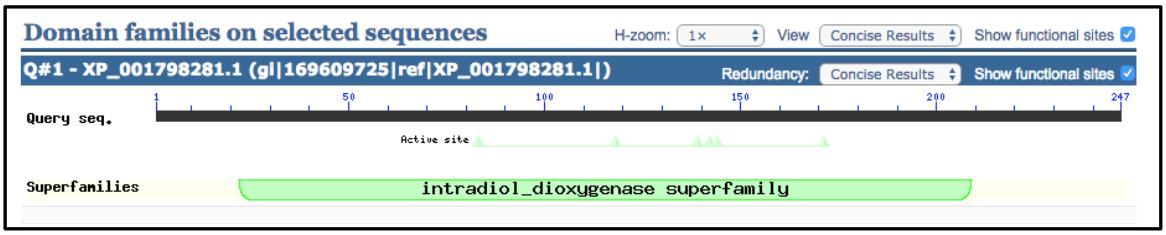


(Supplementary Figure 3.04: Conserved protein domains of SNOG_07954 predicted by the NCBI Conserved Domain Search function)

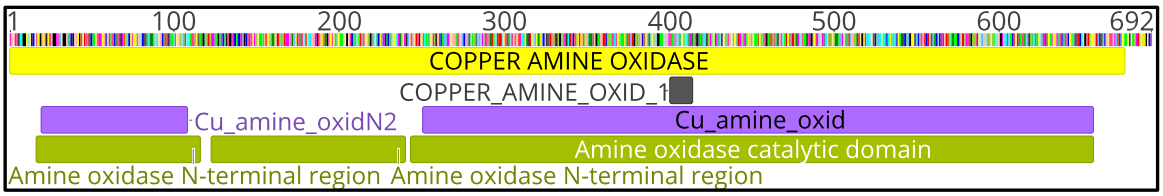


*(Supplementary Figure 3.05: InterProScan prediction of protein domains in the SNOG_02686 amino acid sequence. Yellow = Panther, Purple = Pfam, Grey = Prosite Patterns, Green = Superfamily.*

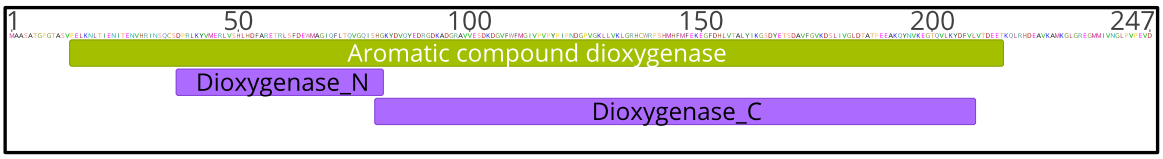


*(Supplementary Figure 3.06: InterProScan prediction of protein domains in the SNOG_07954 amino acid sequence. Purple = Pfam, Green = Superfamily)*

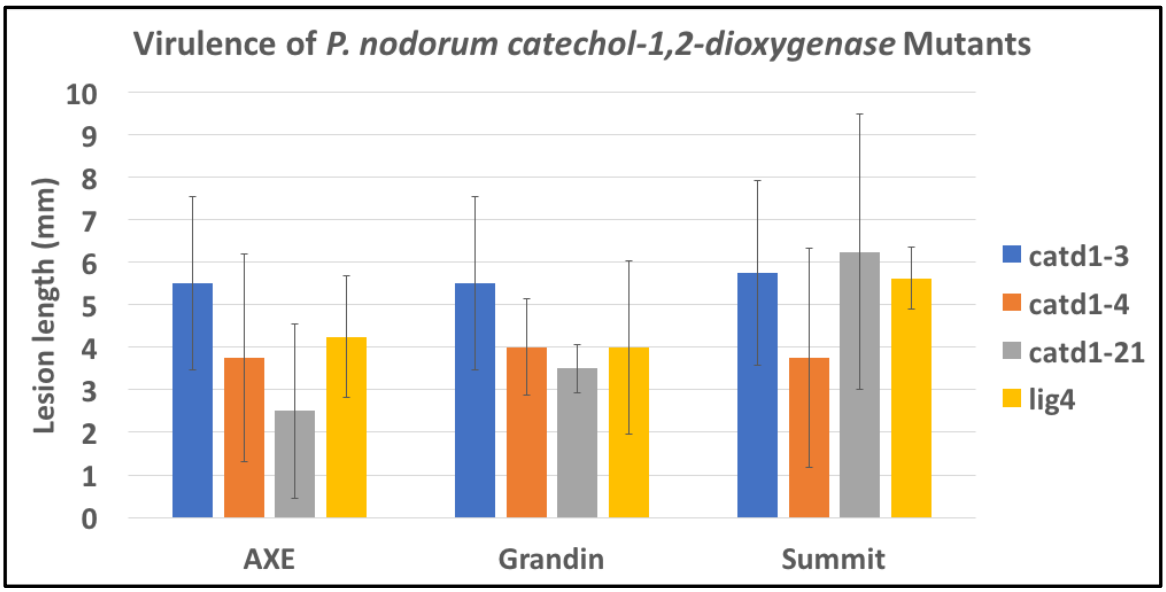


*(Supplementary Figure 3.07: Catechol-1,2-dioxygenase detached leaf pathogenicity assay, repetition. Error bars represent 95% CI.)*

## 3.6 References for Chapter 3


Andrews, S., n.d. FastQC A Quality Control tool for High Throughput Sequence Data. http://www.bioinformatics.babraham.ac.uk/projects/fastqc/.

Bankevich, A., Nurk, S., Antipov, D., Gurevich, A.A., Dvorkin, M., Kulikov, A.S., Lesin, V.M., Nikolenko, S.I., Pham, S., Prjibelski, A.D., Pyshkin, A. V., Sirotkin, A. V., Vyahhi, N., Tesler, G., Alekseyev, M. a., Pevzner, P. a., 2012. SPAdes: A New Genome Assembly Algorithm and Its Applications to Single-Cell Sequencing. Journal of Computational Biology 19, 455–477. https://doi.org/10.1089/cmb.2012.0021

Bhattacharya, A., Sood, P., Citovsky, V., 2010. The roles of plant phenolics in defence and communication during *Agrobacterium* and *Rhizobium* infection. Molecular Plant Pathology 11, 705–719. https://doi.org/10.1111/j.1364-3703.2010.00625.x

Bolger, A.M., Lohse, M., Usadel, B., 2014. Trimmomatic: A flexible trimmer for Illumina sequence data. Bioinformatics 30, 2114–2120. https://doi.org/10.1093/bioinformatics/btu170

Chambers, K., Lowe, R., Howlett, B., Zander, M., Batley, J., Van de Wouw, A., Elliott, C., 2014. Next-generation genome sequencing can be used to rapidly characterise sequences flanking T-DNA insertions in random insertional mutants of *Leptosphaeria maculans*. Fungal Biology and Biotechnology 1, 10. https://doi.org/10.1186/s40694-014-0010-y

Chang, C.M., Klema, V.J., Johnson, B.J., Mure, M., Klinman, J.P., Wilmot, C.M., 2010. Kinetic and Structural Analysis of Substrate Specificity in Two Copper Amine Oxidases from *Hansenula polymorpha*. Biochemistry 49, 2540–2550. https://doi.org/10.1016/j.chemphyslip.2013.12.003.Characterization

Cona, A., Rea, G., Angelini, R., Federico, R., Tavladoraki, P., 2006. Functions of amine oxidases in plant development and defence. Trends in Plant Science 11, 80–88. https://doi.org/10.1016/j.tplants.2005.12.009

Daboussi, M.-J., Capy, P., 2003. Transposable elements in filamentous fungi. Annual Reviews in Microbiology 57, 275–299. https://doi.org/10.1146/annurev.micro.57.030502.091029

Dawkes, H., 2001. Copper amine oxidase: cunning cofactor and controversial copper. Current Opinions in Structural Biology 11, 666–673. https://doi.org/10.1016/S0959-440X(01)00270-6

Du Fall, L.A., Solomon, P.S., 2013. The necrotrophic effector SnToxA induces the synthesis of a novel phytoalexin in wheat. New Phytologist 200, 185–200.

https://doi.org/10.1111/nph.12356

Feng, J., Li, W., Hwang, S.F., Gossen, B.D., Strelkov, S.E., 2012. Enhanced gene replacement frequency in KU70 disruption strain of *Stagonospora nodorum*. Microbiology Research 167, 173–178. https://doi.org/10.1016/j.micres.2011.05.004

Ferraroni, M., Seifert, J., Travkin, V.M., Thiel, M., Kaschabek, S., Scozzafava, A., Golovleva, L., Schlömann, M., Briganti, F., 2005. Crystal structure of the hydroxyquinol 1,2-dioxygenase from *Nocardioides simplex 3E*, a key enzyme involved in polychlorinated aromatics biodegradation. Journal of Biological Chemistry 280, 21144–21154. https://doi.org/10.1074/jbc.M500666200

Feschenko, V. V, Rajman, L. a, Lovett, S.T., 2003. Stabilization of perfect and imperfect tandem repeats by single-strand DNA exonucleases. Proceedings of the National Acadamy for Science U. S. A. 100, 1134–9. https://doi.org/10.1073/pnas.0233122100

Festa, R.A., Thiele, D.J., 2011. Copper: An essential metal in biology. Current Biology 21, R877–R883. https://doi.org/10.1016/j.cub.2011.09.040

Gordenin, D.A., Lobachev, K.S., Degtyareva, N.P., Malkova, A.L., Perkins, E., Resnick, M.A., 1993. Inverted DNA Repeats: a Source of Eukaryotic Genomic Instability. Molecular and Cellular Biology 13, 5315–5322. https://doi.org/10.1128/MCB.13.9.5315.Updated

Habig, M., Quade, J., Stukenbrock, E.H., 2017. Forward genetics approach reveals host genotype-dependent importance of accessory chromosomes in the fungal wheat pathogen *Zymoseptoria tritici*. MBio 8, 1–16. https://doi.org/10.1128/mBio.01919-17

Han, L., Liu, P., Sun, J., Wu, Y., Zhang, Y., Chen, W., Lin, J., Wang, Q., Ma, Y., 2015. Engineering *catechol 1, 2-dioxygenase* by design for improving the performance of the cis, cis-muconic acid synthetic pathway in *Escherichia coli*. Scientific Reports 5, 13435. https://doi.org/10.1038/srep13435

Hane, J.K., Lowe, R.G.T., Solomon, P.S., Tan, K.-C., Schoch, C.L., Spatafora, J.W., Crous, P.W., Kodira, C., Birren, B.W., Galagan, J.E., Torriani, S.F.F., McDonald, B.A., Oliver, R.P., 2007. Dothideomycete Plant Interactions Illuminated by Genome Sequencing and EST Analysis of the Wheat Pathogen *Stagonospora nodorum*. Plant Cell Online 19, 3347–3368. https://doi.org/10.1105/tpc.107.052829

Idnurm, A., Reedy, J.L., Nussbaum, J.C., Heitman, J., 2004. *Cryptococcus neoformans*

Virulence Gene Discovery through Insertional Mutagenesis. Eukaryotic Cell 3, 420–429. https://doi.org/10.1128/EC.3.2.420-429.2004

Ipcho, S., Hanes, J,. Antoni, E., Ahren, D., Henrissat, B., Friesen, T., Solomon, P., Oliver, R., 2012. Transcriptome analysis of Stagonospora nodorum: gene models, effectors, metabolism and pantotenate dispensability. Molecular Plant Pathology 13, 531-545.

Jen, G.C., Chilton, M.D., 1986. Activity of T-DNA borders in plant cell transformation by mini-T plasmids. Journal of Bacteriology 166, 491–499. https://doi.org/10.1128/jb.166.2.491-499.1986

Jones, P., Binns, D., Chang, H.Y., Fraser, M., Li, W., McAnulla, C., McWilliam, H., Maslen, J., Mitchell, A., Nuka, G., Pesseat, S., Quinn, A.F., Sangrador-Vegas, A., Scheremetjew, M., Yong, S.Y., Lopez, R., Hunter, S., 2014. InterProScan 5: Genome-scale protein function classification. Bioinformatics 30, 1236–1240. https://doi.org/10.1093/bioinformatics/btu031

Kearse, M., Moir, R., Wilson, A., Stones-Havas, S., Cheung, M., Sturrock, S., Buxton, S., Cooper, A., Markowitz, S., Duran, C., Thierer, T., Ashton, B., Meintjes, P., Drummond, A., 2012. Geneious Basic: An integrated and extendable desktop software platform for the organization and analysis of sequence data. Bioinformatics 28, 1647–1649. https://doi.org/10.1093/bioinformatics/bts199

Kemppainen, M., Duplessis, S., Martin, F., Pardo, A.G., 2009. RNA silencing in the model mycorrhizal fungus *Laccaria bicolor*: Gene knock-down of nitrate reductase results in inhibition of symbiosis with *Populus*. Environmental Microbiology 11, 1878–1896. https://doi.org/10.1111/j.1462-2920.2009.01912.x

Krappmann, S., 2007. Gene targeting in filamentous fungi: the benefits of impaired repair. Fungal Biology Reviews 21, 25–29. https://doi.org/10.1016/j.fbr.2007.02.004

Li, G., Zhou, Z., Liu, G., Zheng, F., He, C., 2007. Characterization of T-DNA insertion patterns in the genome of rice blast fungus *Magnaporthe oryzae*. Current Genetics 51, 233–243. https://doi.org/10.1007/s00294-007-0122-5

Li, L., Steffens, J.C., 2002. Overexpression of polyphenol oxidase in transgenic tomato plants results in enhanced bacterial disease resistance. Planta 215, 239–247. https://doi.org/10.1007/s00425-002-0750-4

Liu, Y., Mitsukawa, N., Oosumi, T., Whittier, R.F., 1995. Efficient isolation and mapping of Arabidopsis thaliana T-DNA insert junctions by thermal asymmetric interlaced PCR. Plant Journal 8, 457–463.

Mäkelä, M.R., Marinović, M., Nousiainen, P., Liwanag, A.J.M., Benoit, I., Sipilä, J., Hatakka, A., de Vries, R.P., Hildén, K.S., 2015. Aromatic metabolism of filamentous fungi in relation to the presence of aromatic compounds in plant biomass. Advances in Applied Microbiology 91, 63–137. https://doi.org/10.1016/bs.aambs.2014.12.001

Mandal, A., Lång, V., Orczyk, W., Palva, E.T., 1993. Improved efficiency for T-DNA-mediated transformation and plasmid rescue in *Arabidopsis thaliana*. Theoretical and Applied Genetics 86, 621–628. https://doi.org/10.1007/BF00838718

Marchler-Bauer, A., Bo, Y., Han, L., He, J., Lanczycki, C.J., Lu, S., Chitsaz, F., Derbyshire, M.K., Geer, R.C., Gonzales, N.R., Gwadz, M., Hurwitz, D.I., Lu, F., Marchler, G.H., Song, J.S., Thanki, N., Wang, Z., Yamashita, R.A., Zhang, D., Zheng, C., Geer, L.Y., Bryant, S.H., 2017. CDD/SPARCLE: Functional classification of proteins via subfamily domain architectures. Nucleic Acids Research 45, D200–D203. https://doi.org/10.1093/nar/gkw1129

Maruthachalam, K., Klosterman, S.J., Kang, S., Hayes, R.J., Subbarao, K. V., 2011. Identification of pathogenicity-related genes in the vascular wilt fungus *Verticillium dahliae* by *Agrobacterium tumefaciens*-mediated T-DNA insertional mutagenesis. Molecular Biotechnology 49, 209–221. https://doi.org/10.1007/s12033-011-9392-8

McDonald, M.C., McGinness, L., Hane, J.K., Williams, A.H., Milgate, A., Solomon, P.S., 2016. Utilizing Gene Tree Variation to Identify Candidate Effector Genes in *Zymoseptoria tritici*. G3 Genes|Genomes|Genetics 6, 779–791. https://doi.org/10.1534/g3.115.025197

Michielse, C.B., van Wijk, R., Reijnen, L., Cornelissen, B.J., Rep, M., 2009. Insight into the molecular requirements for pathogenicity of *Fusarium oxysporum* f. sp. *lycopersici* through large-scale insertional mutagenesis. Genome Biology 10, R4. https://doi.org/10.1186/gb-2009-10-1-r4

Mikulič Petkovšek, M., Štampar, F., Veberič, R., 2009. Accumulation of phenolic compounds in apple in response to infection by the scab pathogen, *Venturia inaequalis*. Physiology and Molecular Plant Pathology 74, 60–67. https://doi.org/10.1016/j.pmpp.2009.09.003

Nagy, N.E., Fossdal, C.G., Krokene, P., Krekling, T., Lönneborg, A., Solheim, H., 2004. Induced responses to pathogen infection in Norway spruce phloem: changes in polyphenolic parenchyma cells, chalcone synthase transcript levels and peroxidase activity. Tree Physiology 24, 505–515.

https://doi.org/10.1093/treephys/24.5.505

Ochman, H., Gerber, A.S., Hartl, D.L., 1988. Genetic applications of an inverse polymerase chain reaction. Genetics 120, 621–623.

Olivain, C., Alabouvette, C., 2009. Process of Tomato Root Colonization by a Pathogenic Strain of *Fusarium oxysporum* f . sp . *Lycopersici* in Comparison with a Non-Pathogenic Strain. New Phytologist 141, 497–510.

Ornston, L.N., Stainer, R.Y., 1966. The conversion of catechol and protocatechuate to beta -oxadipate by *Pseudomonas putida*. Journal of Biological Chemistry 241, 3800–3810.

Parra, G., Bradnam, K., Korf, I., 2007. CEGMA: A pipeline to accurately annotate core genes in eukaryotic genomes. Bioinformatics 23, 1061–1067. https://doi.org/10.1093/bioinformatics/btm071

Pfannenstiel, B.T., Zhao, X., Wortman, J., Wiemann, P., Throckmorton, K., Spraker, J.E., Soukup, A.A., Luo, X., Lindner, D.L., Lim, Y., Knox, B.P., Haas, B., Fischer, G.J., Choera, T., Butchko, R.A.E., Bok, J., Affeldt, K.J., Keller, N.P., Palmer, J.M., 2017. Revitalization of a Forward Genetic Screen Identifies Three New Regulators of Fungal Secondary Metabolism in Genus *Aspergillus*. American Society for Microbiology 8, 1–15. https://doi.org/https://doi.org/10.1128/mBio.01246-17

Rea, G., Metoui, O., Infantino, A., Federico, R., Angelini, R., 2002. Copper amine oxidase expression in defense responses to wounding and *Ascochyta rabiei* invasion. Plant Physiology 128, 865–75. https://doi.org/10.1104/pp.010646

Robert, X., Gouet, P., 2014. Deciphering key features in protein structures with the new ENDscript server. Nucleic Acids Research 42, 320–324. https://doi.org/10.1093/nar/gku316

Solomon, P.S., Lowe, R.G.T., Tan, K.-C., Waters, O.D.C., Oliver, R.P., 2006. *Stagonospora nodorum*: cause of stagonospora nodorum blotch of wheat. Molecular Plant Pathology 7, 147–156. https://doi.org/10.1111/j.1364-3703.2006.00326.x

Stoilova, I., Krastanov, A., Stanchev, V., Daniel, D., Gerginova, M., Alexieva, Z., 2006. Biodegradation of high amounts of phenol, catechol, 2,4-dichlorophenol and 2,6-dimethoxyphenol by *Aspergillus awamori* cells. Enzyme Microbiology and Technology 39, 1036–1041. https://doi.org/10.1016/j.enzmictec.2006.02.006

Thipyapong, P., Hunt, M.D., Steffens, J.C., 2004. Antisense downregulation of polyphenol oxidase results in enhanced disease susceptibility. Planta 220, 105–

117. https://doi.org/10.1007/s00425-004-1330-6

Tschaplinski, T.J., Plett, J.M., Engle, N.L., Deveau, A., Cushman, K.C., Martin, M.Z., Doktycz, M.J., Tuskan, G.A., Brun, A., Kohler, A., Martin, F., 2014. *Populus trichocarpa* and *Populus deltoides* Exhibit Different Metabolomic Responses to Colonization by the Symbiotic Fungus *Laccaria bicolor*. Molecular Plant-Microbe Interactions 27, 546–556. https://doi.org/10.1094/MPMI-09-13-0286-R

Tsuji, G., Fujii, S., Fujihara, N., Hirose, C., Tsuge, S., Shiraishi, T., Kubo, Y., 2003. *Agrobacterium tumefaciens* -mediated transformation for random insertional mutagenesis in *Colletotrichum lagenarium*. Journal of General Plant Pathology. 69, 230–239. https://doi.org/10.1007/s10327-003-0040-4

Urban, M., King, R., Hassani-Pak, K., Hammond-Kosack, K.E., 2015. Whole-genome analysis of *Fusarium graminearum* insertional mutants identifies virulence associated genes and unmasks untagged chromosomal deletions. BMC Genomics 16, 261. https://doi.org/10.1186/s12864-015-1412-9

Wadke, N., Kandasamy, D., Vogel, H., Lah, L., Wingfield, B.D., Paetz, C., Wright, L.P., Gershenzon, J., Hammerbacher, A., 2016. Catechol dioxygenases catalyzing the first step in Norway spruce phenolic degradation are key virulence factors in the bark beetle-vectored fungus *Endoconidiophora polonica*. Plant Physiology 171, pp.01916.2015. https://doi.org/10.1104/pp.15.01916

Walters, D.R., 2003. Polyamines and plant disease. Phytochemistry 64, 97–107. https://doi.org/10.1016/S0031-9422(03)00329-7

Wicker, T., Sabot, F., Hua-Van, A., Bennetzen, J.L., Capy, P., Chalhoub, B., Flavell, A., Leroy, P., Morgante, M., Panaud, O., Paux, E., SanMiguel, P., Schulman, A.H., 2007. A unified classification system for eukaryotic transposable elements. Nature Reviews Genetics. 8, 973–982. https://doi.org/10.1038/nrg2165

Yoruk, R., Marshall, M.R., 2003. Physicochemical Properties and Function of Plant Polyphenol Oxidase: a Review. Journal of Food Biochemistry. 27, 361–422. https://doi.org/10.1111/j.1745-4514.2003.tb00289.x

Zerbino, D.R., 2011. Using the Velvet de novo assembler for short-read sequencing technologies. Current Protocols in Bioinformatics 11, 1–13. https://doi.org/10.1002/0471250953.bi1105s31.Using

Zerbino, D.R., Birney, E., 2008. Velvet: Algorithms for de novo short read assembly using de Bruijn graphs. Genome Research. 18, 821–829. https://doi.org/10.1101/gr.074492.107

# Chapter 4: Developing a new model of asexual development in the Dothideomycete, *Parastagonospora nodorum*

## 4.1 Introduction

Like many other Dothideomycetes, *P. nodorum* exhibits a polycyclic lifestyle whereby the pathogen infects the host, asexually reproduces, and reinfects the host multiple times throughout a growing season (Solomon et al., 2006; Rudd et al., 2015). Asexual reproduction in *P. nodorum* begins with the melanisation of mycelia, which differentiate and fuse into the asexual fruiting body known as a pycnidium (*pl.* pycnidia). Asexual spores develop within these fruiting bodies, eventually releasing in a pink fluid known as cirrus before dispersing by rain-splash across infected leaf tissue or onto nearby plants, repeating the infection cycle (Douaiher et al., 2004; Solomon et al., 2006).

Disrupting sporulation in *P. nodorum* breaks this cycle, effectively disarming the pathogen. Although able to infect the host plant, the fungus is unable to cause the field epidemics that reduce yields to growers. Several core genetic elements and primary metabolic pathways, essential for *P. nodorum* sporulation, have been elucidated over the last few decades (Oliver, Friesen, Faris, & Solomon, 2012). However despite these advances, our core understanding of asexual sporualtion in *P. nodorum,* and more broadly the Dothideomycetes, is lacking. To dissect *P. nodorum* asexual reproduction *in vitro,* I previously identified conditions to induce a state of hyper-sporulation under laboratory conditions by growing the fungus on the amino acid, γ-aminobutyric acid (GABA). Low concentrations (1mM) of GABA induced sporulation in the Dothideomycetes, *P. nodorum* and *Eutiarosporella darliae*, under conditions normally prohibitive of sporulation (Mead et al. 2013). GABA is a small, non-proteinaceous amino acid found ubiquitously through-out all kingdoms of life. It is generated and catabolised though a primary metabolic pathway, stemming from the citric acid cycle, known as the GABA shunt. This shunt diverts carbon, as α- ketoglutarate, from the citric acid cycle and returns it as succinate, negating a key energy producing step (Ogata

et al., 1999). Figure 4.01 illustrates the GABA shunt, highlighting the bypassed energy producing reactions.

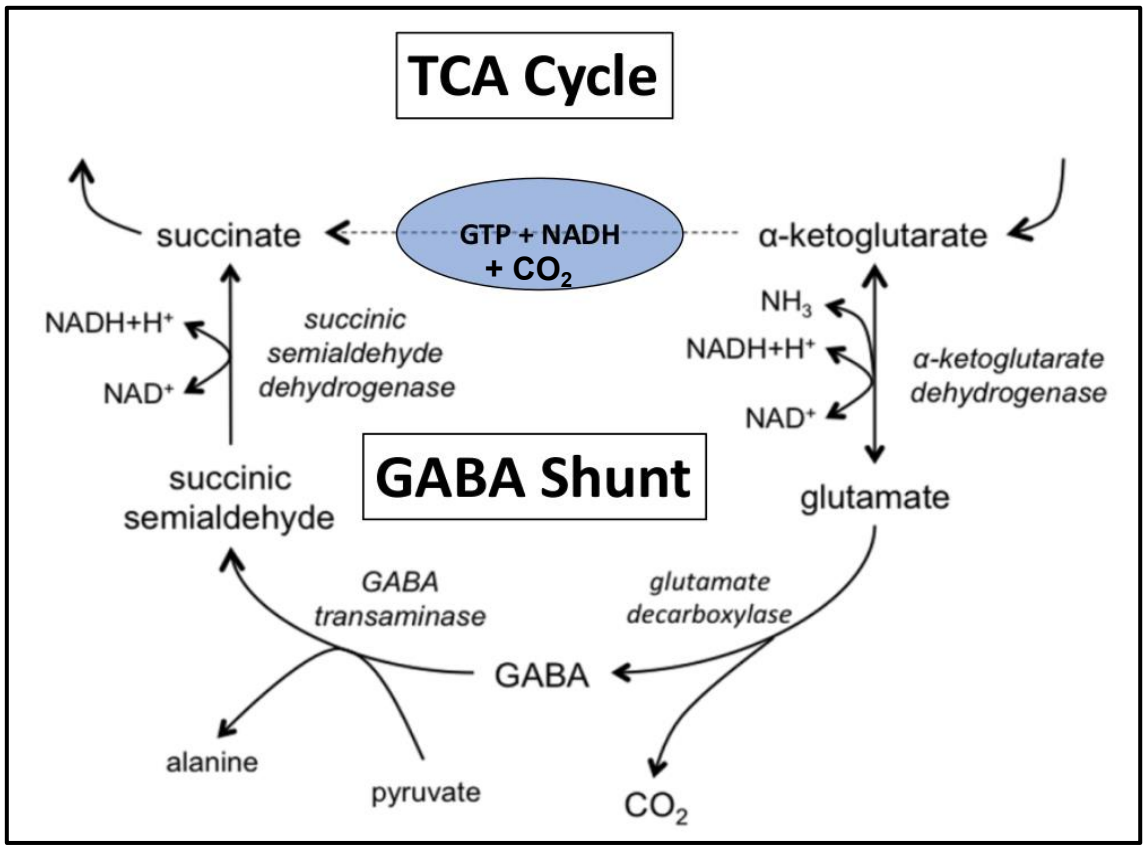


*(Figure 4.01: Schematic representation of the GABA shunt. This images shows the enzymatic pathways producing, degrading and bypassing GABA, known in eukaryotes. Image adapted from Mead et al (2013))*

The conservation of this pathway across species, despite its metabolic cost to the cell, indicates the importance of GABA and its metabolism. In vertebrates, GABA acts as a neurotransmitter, and has been extensively studied with regards to neurology (Galarreta & Hestrin, 2001; Ge et al., 2006), mental health, and pharmaceuticals (Wassef et al., 1999). The role of GABA in plants is currently less thoroughly understood but has been reported to play roles in abiotic and biotic stress responses. Kinnersley and Turano (2000), comprehensively reviewed the role of GABA during plant stress by explaining the metabolic role of GABA and the GABA shunt during different forms of stress. Further, they explore GABA/Calcium mediated signalling in plants and suggest that an

animal-like signalling cascade may be present in plants (Kinnersley & Turano, 2000). Ramesh et al. (2015) reported GABA binding the plant Aluminium activated Malate Transporter (ALMT), inhibiting anion flux through that transporter. They show that site directed mutations to selected ALMT amino acids disrupted GABA binding without interfering with anion transport, and suggest this forms the first plant GABA receptor to be discovered (Ramesh et al., 2015). Despite the attention this molecule has received for its role in plants and animals, its role in fungi is still relatively unknown. Disruptions to the GABA shunt were shown to perturb pathogenicity in *P. nodorum*, *Fusarium graminearum* and *Magnaporthe oryzae* (Bönnighausen et al., 2015; Guo et al., 2011; Mead et al., 2013). However, the cause for reduced virulence is speculative and the mechanism of GABA induced sporulation remains elusive.

In this study, I employed a combined transcriptomics and metabolomics approach to begin defining sporulation pathways in the Dothideomycete, *Parastagonospora nodorum*. To identify differentially expressed genes and abundant metabolites during *P. nodorum* asexual development I used GABA to induce sporulation under normally prohibitive conditions. RNA and metabolite samples from these two conditions were then compared at key developmental time-points. Further, the mechanism of GABA perception was investigated using known GABA receptor agonists and antagonists to elicit an effect on *P. nodorum* sporulation.

### Hypotheses:

1. *GABA is recognised by the fungus and induces expression of a gene cascade ultimately leading to sporulation.*

2. *GABA perception by* P. nodorum *is mediated by a GABA receptor-like mechanism.*

## 4.2 Materials and Methods

4.2.1 *(Table 4.01: Media use in this chapter for the growth of* P. nodorum *and induction of sporulation. Minimal medium was used, with or without the addition of a chemical modifier to test that chemicals ability to induce sporulation. The concentrations of each reagent and their origins are also listed)*

| Name | Constituent | /L |
|---|---|---|
| Minimal Medium (pH 6.0) | Sigma Aldrich™ Sucrose | 8g |
| | Sigma Aldrich™ NaNO3 | 850mg |
| | Sigma Aldrich™ K2HPO4 | 500mg |
| | 100x Trace Stock | 10ml |
| | Agar | 15g |
| | | |
| *Modifier (2mM) | Sigma Aldrich™ Gamma Aminobutyric Acid | 212mg |
| *Modifier (10mM) | Sigma Aldrich™ Gamma Aminobutyric Acid | 1.06g |
| *Modifier (5mM) | Sigma Aldrich™ Gamma Aminobutyric Acid | 530mg |
| *Modifier (5mM) | Sigma Aldrich™ Sodium Glutamate | 852mg |
| *Modifier (5mM) | Sigma Aldrich™ Glutamine (free base) | 1.46g |
| *Modifier (5mM) | Astral Scientific™ Ornithine Monohydrochloride | 1.68g |
| *Modifier (5mM) | Sigma Aldrich™ Putrescine Dichloride | 1.6g |
| *Modifier (5mM) | Sigma Aldrich™ Proline (free base) | 1.15g |
| *Modifier (5mM) | Astral Scientific™ Arginine (free base) | 1.74g |
| *Modifier (5mM) | Sigma Aldrich™ Spermidine Trihydrochloride | 1.22g |
| *Modifier (5mM) | Astral Scientific™ Sodium Nitrate | 1.28g |
| *Modifier (68µM) | Sigma Aldrich™ Bicuculline | 25mg |
| *Modifier (6.8mM) | Sigma Aldrich™ Gamma Amino Beta Hydroxybutyrate | 1g |
| | | |

| | | |
|---|---|---|
| 100x trace elements stock solution | Astral Scientific™ Potassium Chloride | 50g |
| | Astral Scientific™ Magnesium Sulphate Heptahydrate | 50g |
| | Sigma Aldrich™ Zinc Sulphate Heptahydrate | 1g |
| | Sigma Aldrich™ Iron Sulphate Heptahydrate | 1g |
| | Sigma Aldrich™ Copper Sulphate Pentahydrate | 0.25g |

### 4.2.2 Protocols

#### 4.2.2.1 RNA and metabolite sample preparation

312 minimal medium plates (100mm diam.) were inoculated with 100µl of a *P. nodorum* spore suspension at $1x10^5$ spores/ml. Half (156) of these plates contained 0mM GABA and the other, 2mM GABA. These plates were left to grow at 22ºC with a 12hour day night cycle, under near U.V. light. At 8, 10 and 14dpi 52 plates of each treatment (+/- GABA, total 104) were chosen at random for metabolite and RNA collection, as well as pycnidia and spore count assays. Four plates from each treatment (total 8) were selected to measure pycnidiation (non-destructive) and sporulation (destructive). 48 plates of each treatment were scraped with a sterile razor blade to collect the fungal material, which was deposited into 2ml micro-centrifuge tubes and flash-frozen in liquid nitrogen. The plates were scraped in under 5 seconds each and in lots of four plates, to gather enough material for a single sample without degradation. A new blade was used for each sample. In this way 48 plates of each treatment produced 12 samples of each treatment, at each time point. Six samples of each treatment and time point were freeze dried for GC-MS analysis by Dr. Joel Gummer, and the RNA of the remaining six was immediately extracted using the Qiagen™ RNA extraction kit. RNA samples quality checked by nanodrop spectrophotometer and Bioanalyzer before being sent to the Biomolecular Resource Facility (BRF) at the John Curtin School of

Medical Research for library preparation and sequencing on the Illumina HiSeq platform. In total 6 replicates of each treatment at each time point (36) were prepared for gas chromatography-mass spectrometry analysis, and equal measures were prepared for RNA sequencing. Four of each set of 6 were chosen for each analysis.

#### 4.2.2.2 Read trimming with Trimm-o-matic

The bioinformatics program Trimm-o-matic was used to remove poor quality bases and adapters from the short read sequencing data generated by the Illumina platform. A moderate stringency was used to trim poor quality bases from the heads and tails of reads, as well as using a "sliding window" to detect and remove sections of poor overall quality. Usage and an example script are shown below:

**Usage:** java -jar <path to trimmomatic.jar> PE [-threads <threads] [-phred33 | -phred64] [-trimlog <logFile>] <input 1> <input 2> <paired output 1> <unpaired output 1> <paired output 2> <unpaired output 2> <step 1>

**Example Script:**

```
#! /bin/bash
echo _____Starting_sample_1/24_____
java -jar /usr/local/bin/trimmomatic-0.32.jar PE -threads 10 -phred33 /home/oliver/Desktop/RNAseq/stagoRNAseq_GABA/01_RAW_DATA/-1-1_S1_R1_001.fastq.gz /home/oliver/Desktop/RNAseq/stagoRNAseq_GABA/01_RAW_DATA/-1-1_S1_R2_001.fastq.gz -1-1_S1_R1_001_paired.fastq.gz -1-1_S1_R1_001_unpaired.fastq.gz -1-1_S1_R2_001_paired.fastq.gz -1-1_S1_R2_001_unpaired.fastq.gz ILLUMINACLIP:/usr/local/bin/Trimmomatic-0.32/adapters/NexteraPE-PE.fa:2:30:10 LEADING:20 TRAILING:20 SLIDINGWINDOW:4:24 MINLEN:50
echo _____Finished_sample_1/24_____
```

#### 4.2.2.3 Splicing exons and build index with HiSat2

The bioinformatics program HiSat2 extracted predicted exons and RNA splice sites from the Gene Transfer Format files (.gtf) that locate features on the *P. nodorum* reference genome. Using these extracted features, HiSat2 then created an index file of the trimmed short reads generated by the Illumina platform. Example scripts are shown below:

**Example Scripts:**

python /usr/local/bin/extract_splice_sites.py
/Users/olivermead/Desktop/RNAseq/GABArna/04_Mapping/index_building/Parastagonospora_nodorum_SN15.gff3 > stago_gtf_splice_sites_extract

python /usr/local/bin/extract_exons.py
/Users/olivermead/Desktop/RNAseq/GABArna/04_Mapping/index_building/Parastagonospora_nodorum_SN15.gff3 > stago_gtf_exon_extract

hisat2-build --ss /Users/olivermead/Desktop/RNAseq/GABArna/04_Mapping/index_building/stago_gtf_splice_sites_extract --exon
/Users/olivermead/Desktop/RNAseq/GABArna/04_Mapping/index_building/stago_gtf_exon_extract
/Users/olivermead/Desktop/RNAseq/GABArna/04_Mapping/index_building/Parastagonospora_nodorum_SN15_scaffolds.fasta
/Users/olivermead/Desktop/RNAseq/GABArna/04_Mapping/index_building/stago_bt_index

#### 4.2.2.4 Mapping reads to reference genome with HiSat2.

Using the indexing file generated in section 4.2.2.3 HiSat2 mapped the trimmed Illumina short-reads to the *P. nodorum* SN15 reference genome. This generated Sequence Alignment Map (.SAM) files

**Usage:** hisat2 [options]* -x <hisat2-idx> {-1 <m1> -2 <m2> | -U <r> | --sra-acc <SRA accession number>} [-S <hit>]

**Explain usage:** hisat2-idx = index file, m1 and m2 are paired reads, r is the unpaired reads file, S is the Sequence Alignment Map

**Example Script:**

#! /bin/bash

```
echo ********************************************___STARTING_SAMPLE_1/24___*****************************************
hisat2 -q -p 10 -x ~/Desktop/RNAseq/stagoRNAseq_GABA/04_Mapping/index_building/stago_bt_index -1
~/Desktop/RNAseq/stagoRNAseq_GABA/03_Trimmomatic/-1-1_S1_R1_001_paired.fastq.gz -2
~/Desktop/RNAseq/stagoRNAseq_GABA/03_Trimmomatic/-1-1_S1_R2_001_paired.fastq.gz -S
/LargeDataSet_PS/Solomon_Lab/Oliver/GABArna/04_Mapping/-1-1_S1.sam
echo ********************************************___FINISHED_SAMPLE_1/24___*****************************************
```

#### 4.2.2.5 Convert SAM to BAM.

The .SAM files generated in section 4.2.2.4 were converted to a binary format (.BAM) for faster processing, using the program SAM tools. An example script is shown below.

**Example Script:**

```
#! /bin/bash
echo _____Running_Sample_1/24_____
samtools view -bS -@ 10 /LargeDataSet_PS/Solomon_Lab/Oliver/GABArna/04_Mapping/-1-1_S1.sam >
/LargeDataSet_PS/Solomon_Lab/Oliver/GABArna/04_Mapping/-1-1_S1.bam
echo _____Finished_Sample_1/24_____
```

#### 4.2.2.6 Sort BAM files

The binary mapping files generated in section 4.2.2.5 were then sorted for more efficient processing using SAM tools. An example script is shown:

**Example Script:**

```
#! /bin/bash
echo _____Running_Sample_1/24_____
samtools sort -@ 10 /LargeDataSet_PS/Solomon_Lab/Oliver/GABArna/04_Mapping/-1-1_S1.bam
/LargeDataSet_PS/Solomon_Lab/Oliver/GABArna/04_Mapping/
echo _____Finished_Sample_1/24_____
```

#### 4.2.2.7 Transcriptome assembled with StringTie

The mapped reads were then assembled into transcriptomes. Each sample yielded its own transcriptome. These transcriptomes were then merged to create a global transcriptome of the experiment. This created a pool of all transcripts observed in the experiment to compare different treatments against. Example scripts are shown below:

**Usage:** stringtie <sorted binary alignment map(sorted.BAM)>< general feature format of reference genome (.GFF or .GTF)><Options><Output>

**Transcriptome Assembly Example Script:**

```
#! /bin/bash
echo _____Running_Sample_1/24_____
```

stringtie /LargeDataSet_PS/Solomon_Lab/Oliver/GABArna/04_Mapping/-1-1_S1_sorted.bam -G

/LargeDataSet_PS/Solomon_Lab/Oliver/GABArna/04_Mapping/index_building/Parastagonospora_nodorum_SN15.gff3 -p 10 -B -l -1-1 -o

/LargeDataSet_PS/Solomon_Lab/Oliver/GABArna/05_Assembly_and_Count/-1-1_S1

echo _____Finished_Sample_1/24_____

### Transcriptome Merge Script:

**Usage:** stringtie –G <reference genome.gff><output><list of transcriptomes>

### Script:

#! /bin/bash

echo ----------merging all assemblies in a reference list----------

stringtie --merge -G /LargeDataSet_PS/Solomon_Lab/Oliver/GABArna/04_Mapping/index_building/Parastagonospora_nodorum_SN15.gff3 -o

/LargeDataSet_PS/Solomon_Lab/Oliver/GABArna/05_Assembly_and_Count/stringtie_merged_ref

/LargeDataSet_PS/Solomon_Lab/Oliver/GABArna/05_Assembly_and_Count/sample_1/S1

/LargeDataSet_PS/Solomon_Lab/Oliver/GABArna/05_Assembly_and_Count/sample_2/S2

/LargeDataSet_PS/Solomon_Lab/Oliver/GABArna/05_Assembly_and_Count/sample_**N**/ **[$S_n$]**

echo ----------Finished generating reference list----------

#### 4.2.2.8 Read count by HTSeq

HTSeq counted the reads mapping to each transcript from each sample. Generating a table of read counts for each transcript in a text file for each sample. These text file was manually converted into Comma Seperated Values (.CSV) files for entry into an R statistics package. An example script is shown:

**Usage:** htseq-count <options><Sorted Binary Alignment Map><output>

**Example Script:**

```
#! /bin/bash
echo _____Running_Sample_1/24_____
htseq-count -f bam -s no -r pos -t exon -i transcript_id -m intersection-nonempty /LargeDataSet/Oliver/GABArna/04_Mapping/-1-1_S1_sorted.bam /LargeDataSet/Oliver/GABArna/05_Assembly_and_Count/stringtie_merged_ref > NG_1-1_S1.txt
echo _____Finished_Sample_1/24_____
```

#### 4.2.2.9 Statistical Analysis in R

The packages edgeR and Limma were used for the following analysis. The read count files were then grouped by treatment and time point in R using the readDGE command. The read library size was calculated and low abundance filter then filtered out reads below five counts per million. The library size was then recalculated and normalised using the calcNormFactors command. Data quality check was performed using a multivariate plot and common dispersal plots. Pairwise comparisons were then calculated between each treatment and time point. From each comparison the 50 differentially expressed genes, by significance and fold-change, were tabulated and exported. These top 50 lists were collated into a single .CSV file.

#### 4.2.2.10 Gas Chromatography-Mass Spectrometry sample preparation

Samples were homogenised using mortar and pestle and 30mg of each was weighed into cryo-mill tubes and homogenized in a cryo-mill. 500 µl of ice-cold 100% Methanol was added, containing the internal standards: 0.004mg/mL (C13-Sorbitol and C13-Valine) and 0.0008mg/mL (2-aminoanthracene and pentafluorobenzoic acid). The samples were then re-homogenised in the cryo-mill followed by incubation at 4°C, with shaking at 850rpm for 15 minutes. Samples were then centrifuged at 13,000 rpm at 4°C for 10 minutes. 350µl of supernatant was transferred carefully to a 2ml micro-centrifuge tube. The extraction process was repeated on the sample pellet using methanol containing no internal standards. 400µl of supernatant was combined with the previous supernatant containing internal standards. The extraction was then repeated a third time on the sample pellet, using 500µl of 50/50 methanol/water. 450µl of supernatant was combined with the previous supernatant containing internal standards. Combined extracts were vortexed for 3-5 seconds and

dispensed into 1.5ml micro-centrifuge tubes for freeze drying and subsequent GC-MS analysis.

#### 4.2.2.11 Gas Chromatography-Mass Spectrometry analysis

Extracts were dried and TMS-derivatised for analysis. The Agilent 7200 series Gas Chromatography quantitative Time of Flight-Mass Spectrometer (GCqTOF-MS) equipped with an Agilent 7693 auto injector and Agilent Factor Four VF-5ms capillary column was used (Agilent Technologies, Santa Clara, USA). One microliter of sample was injected into the GC inlet (270°C), and anolytes separated using a 60-minute temperature gradient and helium as the carrier gas. The initial oven temperature was 70°C. A temperature ramp of 1°C/min for 5 min followed by 5.63°C/min until the final temperature of 330°C, with a hold time of 10 min, was reached. The transfer line was set to 300°C and the ion source was set to 280°C. Ionisation was achieved by electron ionisation using a 70eV electron beam and the time of flight mass analyser operated over the range *m/z* 45-600, acquiring at 10 Hz.

#### 4.2.2.12 Colony growth assay

Spot inoculated 100mm plates were grown under a 12hour day/night at 22°C for 14 days, with four replicate plates for each treatment. At 14 days post inoculation (dpi) colony diameters were measured, taking two transecting measurements on the bottom of the plate. Measurements were taken from hyphal tips on opposite sides of the colony to the nearest millimetre.

## 4.3 Results

### 4.3.1 Experimental design to find key developmental time points of *P. nodorum*

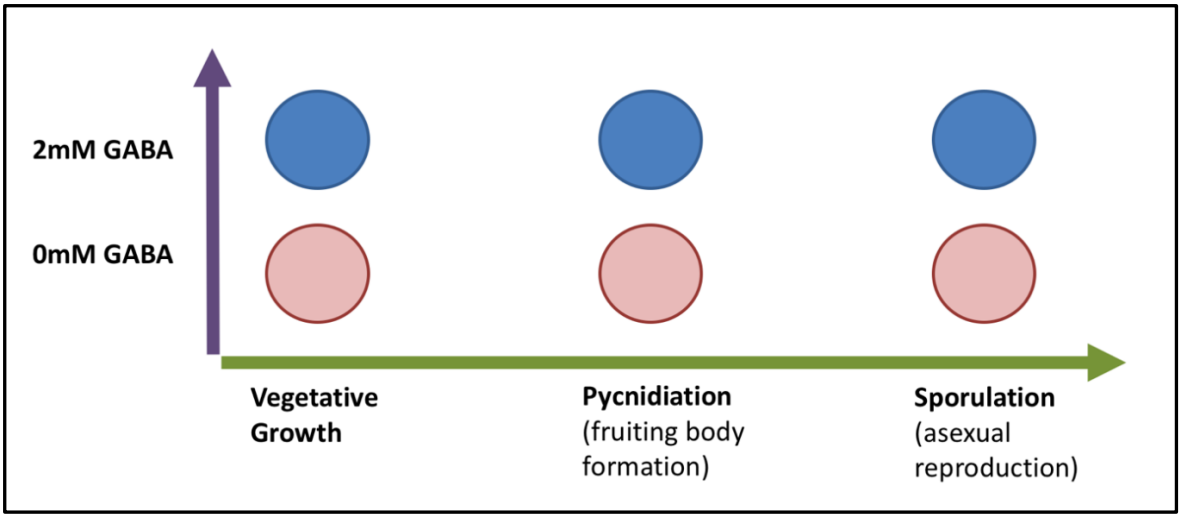


*(Figure 4.02: Diagram of experimental design, indicating the key developmental time points and treatments of* P. nodorum *from which RNA and metabolite samples were taken. RNA and metabolites were extracted from mycelia at the vegetative, pycnidiation and sporulation time points, in the presence and absence of GABA.)*

To elucidate crucial genetic and chemical changes leading to pycnidiation and sporulation in *P. nodorum* I determined the exact time points corresponding to these developmental stages (Figure 4.02). These developmental time points were determined by spread inoculating minimal medium, containing 0mM or 2mM GABA, with a spore suspension. Spread inoculation ensured that all fungal development was synchronous, preventing transcript and metabolite contamination from other developmental stages. The initiation of pycnidiation and sporulation was determined by counting the number of pycnidia and spores each day after inoculation.

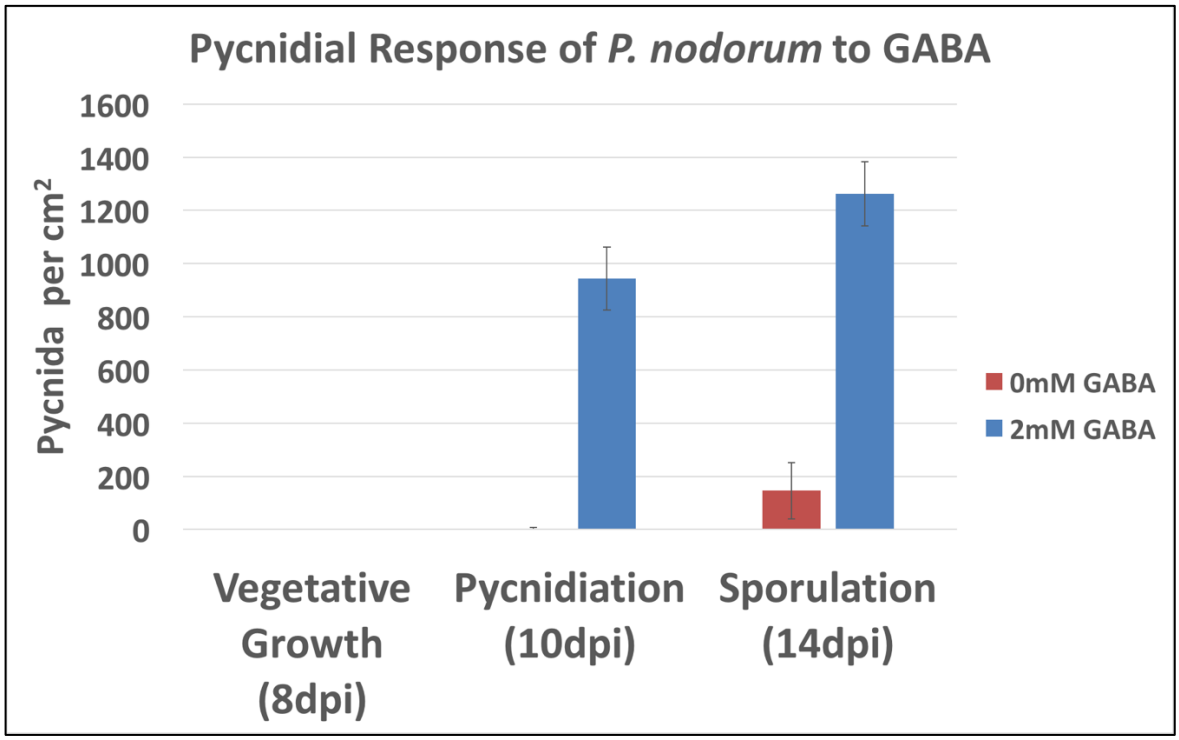


*(Figure 4.03a: Pycnidiation at key developmental time points of* P. nodorum *during* in vitro *growth. Maroon bars represent samples untreated with GABA, while blue bars represent samples treated with 2mM GABA. Error bars represent 95% CI)*

Figure 4.03a shows the time course for *P. nodorum* asexual fruiting body formation in the presence and absence of GABA. Vegetative growth was apparent for eight days identically in the presence and absence of GABA. However, at the beginning of the 9$^{th}$ day mycelia on plates containing 2mM GABA began to melanise and form pycnidia. Large, defined, pycnidia had developed by 10dpi in the presence of GABA, but not in its absence. Spores were not observed until 12 dpi, however these were only apparent in the presence of GABA and there were too few to count accurately (Figure 4.03b). The 14dpi time point showed maximum spore numbers, but again only in the presence of GABA. The critical time points in *P. nodorum* asexual reproduction during *in vitro* growth were determined to be 8, 10 and 14dpi. These time points were chosen to contrast transcriptomic and metabolic changes initiating cell differentiation, and asexual development in *P. nodorum*.

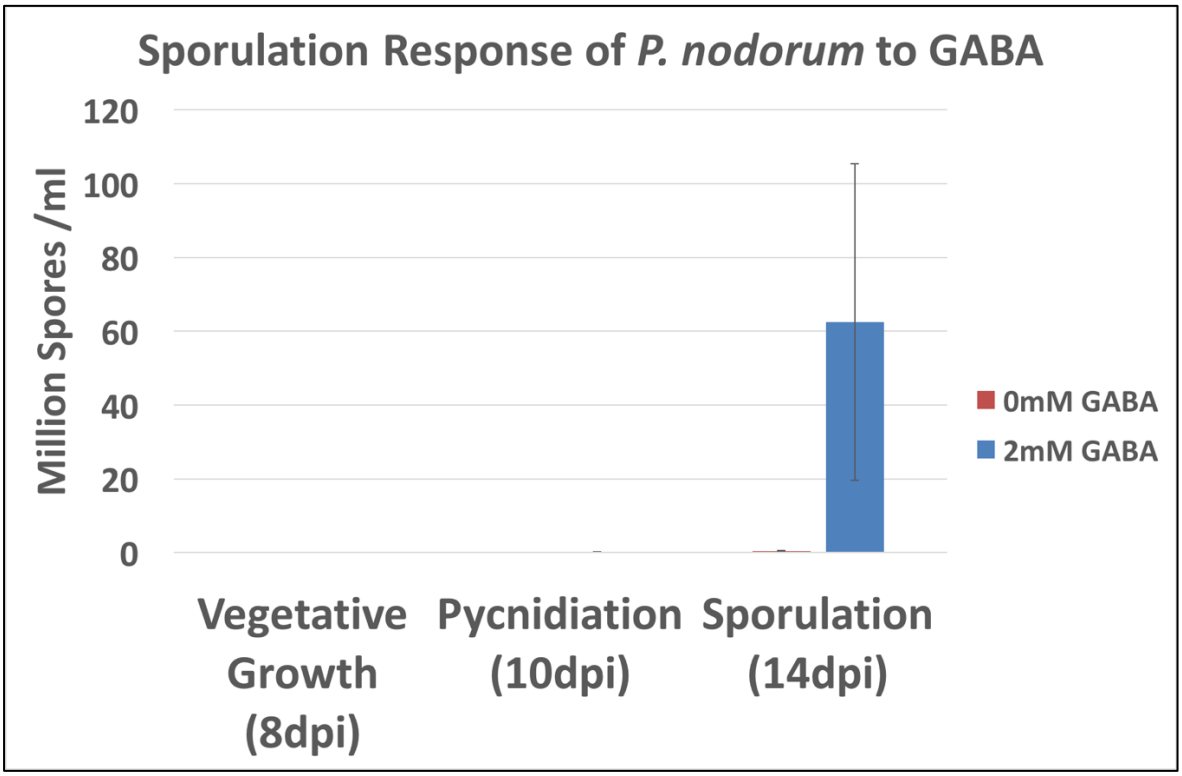


*(Figure 4.03b: Sporulation at key developmental time points of* P. nodorum *during* in vitro *growth. Maroon bars represent samples untreated with GABA, while blue bars represent samples treated with 2mM GABA. Error bars represent 95% CI)*

Subsequently, fungal material grown in both the absence and presence of GABA was collected, at these time-points, with 12 replicates. These 72 samples were then split between two analyses. Six replicates from each time point and GABA treatment, [0mM] or [2mM], were flash frozen in liquid nitrogen and the RNA extracted. The quantity and quality, including degradation, as well as DNA and protein contamination, of extracted RNA was measured via gel electrophoresis and Nanodrop™ spectrophotometry. Four samples from each time point and treatment showing the highest quality were sequenced. The remaining 36 samples were freeze-dried and posted to Dr Joel Gummer at Murdoch University, Perth, WA, for Gas Chromatography-Mass Spectrometry (GC-MS) analysis. The Gas Chromatography quantitative Time of Flight-Mass Spectrometry (GCqTOF-MS)

determined the metabolite composition of *P. nodorum* at different stages of development, in the presence and absence of GABA.

### 4.3.2 Assembly of the *P. nodorum* "developmental-stage" transcriptome

The Illumina HiSeq platform generated 75 bp paired-end (PE) reads, from a minimum of 150ng of RNA in each sample, averaging 40million PE reads per sample. Read quality was assessed by FastQC on the basis of per base quality, per sequence quality, as well as sequence length and adapter contamination (Andrews, n.d.). In general, no adapter contamination was found, nor were any sequences flagged as poor quality. Poor quality bases were then removed by Trimm-o-matic using a high stringency screen, leaving only high quality reads (Section 4.2.2.2) (Bolger, Lohse, & Usadel, 2014). HiSat2 mapped high-quality reads from all samples to the *P. nodorum* reference genome (D. Kim, Langmead, & Salzberg, 2015). Reads were mapped under moderate stringency to balance including all potential gene models with correctly defining those models (Section 4.2.2.4). The Sequence Alignment Maps (.SAM) generated by HiSat2 were converted to sorted Binary Alignment Maps (.Sorted.BAM) by SAMTools (H. Li et al., 2009) for transcriptome assembly (Sections 4.2.2.5 and 4.2.2.6).

StringTie assembled mapped reads from all samples into a transcriptome for each sample and included novel transcripts (D. Kim et al., 2016; Pertea et al., 2015). The transcriptomes were then merged to generate a non-redundant transcriptome for read counting and differential gene expression (DGE) analysis (Section 4.2.2.7). Raw counts for each transcript were then generated by HTSeq (Anders, Pyl, & Huber, 2015), which were

normalized and statistically analysed using the R package EdgeR in R-studio (Ritchie et al., 2015; Robinson et al., 2009; R-Team, 2015, 2011) (Sections 4.2.2.8 and 4.2.2.9).

### 4.3.3 Differential gene analysis identified structural, metabolic and signalling related genes during *P. nodorum* developmental stages

A multivariate analysis of the RNAseq data confirmed the sequencing quality and the biological relevance of the data (Figure 4.04). The different biological samples separated clearly, while replicates of the same treatment grouped tightly. Further, the treatments were separated by the first and second dimensions. This indicated that the GABA treatment and developmental stages were the leading factors for differences between samples. The first-dimension, on the horizontal axis, paired the treatments groups chronologically from the vegetative growth stages through pycnidiation to sporulation. The second-dimension separated samples vertically by treatment groups.

Statistical analyses in R ranked differentially expressed genes between treatments at each time point by significance, false discovery rate and expression. The top 50 differentially expressed genes at the three time points were analysed with corresponding predicted functions. These predicted functions were based on amino acid sequence homology to other amino acid sequences in the NCBI nr BLASTp database. Genes with no known homologues, homology only within *P. nodorum*, uncharacterised proteins, or alignments with less than 40% alignment identity or coverage, were not ascribed a functional annotation. These genes remained in the table as they indicated the frequency of differentially expressed genes lacking a predicted function.

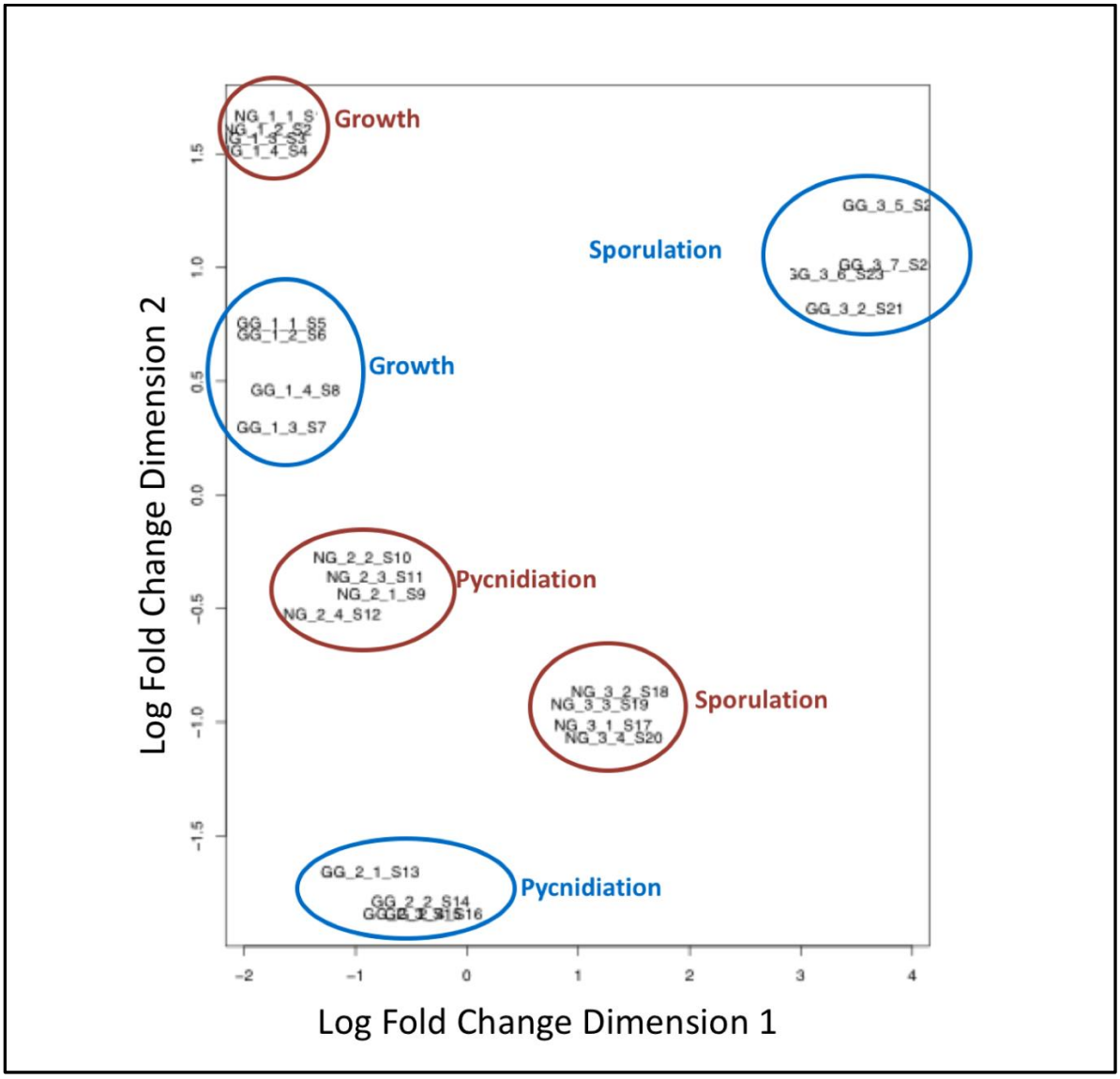


*(Figure 4.04: Multivariate analysis of RNAseq samples taken from key developmental time points of* P. nodorum *growth in the presence and absence of GABA [2mM]. Maroon circles indicate untreated samples, while blue circles indicate samples treated with GABA [2mM])*

The table of differentially expressed genes, three timepoints filtered by significance and three filtered by expression change, were condensed to a short list proposed for future investigation, shown in Table 4.02. This study aimed to identify a genetic cascade orchestrating sporulation, as such, genes predicted to play roles in primary and secondary

metabolism, GABA transport, and downstream cell growth and maintenance, such as chitin synthase, were not included in the short list.

There were four noteworthy features of Table 4.02. **1)** Several aquaporin-like proteins were differentially expressed at multiple time points. Although these proteins may not play a role in a genetic cascade, they have been included due to their abundance and under-studied biological role in fungi. **2)** A PR1-like protein was included in this short-list as this family of proteins are well known plant defence markers (Breen et al 2017). **3)** Several homologues of yeast developmental genes were significantly differentially expressed but were omitted from Table 4.02. These genes were omitted as they were reported to play mechanistic or chemical roles during cell differentiation, such as spore wall formation, rather than regulatory, signalling or environmental sensing functions. For example, a homologue of the *Dityrosine synthase 1* (*Dit1*) gene was identified that was reported to be required for chitosan synthesis, ultimately generating the fungal cell wall (Briza, Eckerstorfer, & Breitenbach, 1994). However, identifying the differential expression of these genes confirms that this line of investigation can elucidate developmental genes leading to cell differentiation. **4)** Many elements of secondary metabolism, such as polyketide synthases and O-methyl transferases, were significantly differentially expressed. However, these elements were precluded from Table 4.02 and discussed in more detail in Figures 4.06-4.09 and Section 4.4.5.

*(Table 4.02: Short-list of gene candidates differentially expressed in* P. nodorum *undifferentiated fungal cells and cells undergoing various stages of asexual development. Genes were ordered by respective developmental stage and expression. Fold-change compared cells treated with GABA with untreated. Asterisks denote a gene identified in two developmental stages. Gene products were estimated by most homologous amino acid sequence in the NCBI nr BLAST database. Fold-change by counts per million)*

| Gene ID | Product Estimate | Fold Change | (P-value) | Devlopmental Stages |
|---|---|---|---|---|
| SNOG_01727 | Helicase-like transcription factor [Fusarium fujikuroi] | 9.88 | 1.0E-06 | Vegetative growth |
| SNOG_00518 | *Aquaporin [Colletotrichum higginsianum IMI 349063] | 15.18 | 6.3E-02 | Vegetative growth |
| SNOG_13481 | Histidine kinase HHK8p [Alternaria alternata] | 25.56 | 1.5E-02 | Vegetative growth |
| SNOG_03097 | Blue light-inducible protein Bli-3 [Aspergillus fumigatus Af293] | 12.49 | 2.5E-05 | Pycnidiation |
| SNOG_00518 | *Aquaporin [Colletotrichum higginsianum IMI 349063] | 19.91 | 1.0E-03 | Pycnidiation |
| SNOG_16432 | Integral membrane protein [Neofusicoccum parvum UCRNP2] | 27.29 | 3.6E-05 | Pycnidiation |
| SNOG_01519 | PR-1-like protein [Alternaria alternata] | 33.59 | 1.5E-05 | Pycnidiation |
| SNOG_06491 | Subtilisin-like serine protease PR1A [Metarhizium anisopliae var. anisopliae] | 34.83 | 1.3E-05 | Pycnidiation |
| SNOG_04900 | Aquaporin-5 [Pyrenochaeta sp. DS3sAY3a] | 48.69 | 3.2E-06 | Pycnidiation |
| SNOG_04810 | Aquaporin-like [Leptosphaeria maculans JN3] | 0.02 | 1.1E-05 | Sporulation |
| SNOG_12399 | Hard-surface inducible protein [Colletotrichum gloeosporioides Nara gc5] | 0.02 | 1.5E-06 | Sporulation |

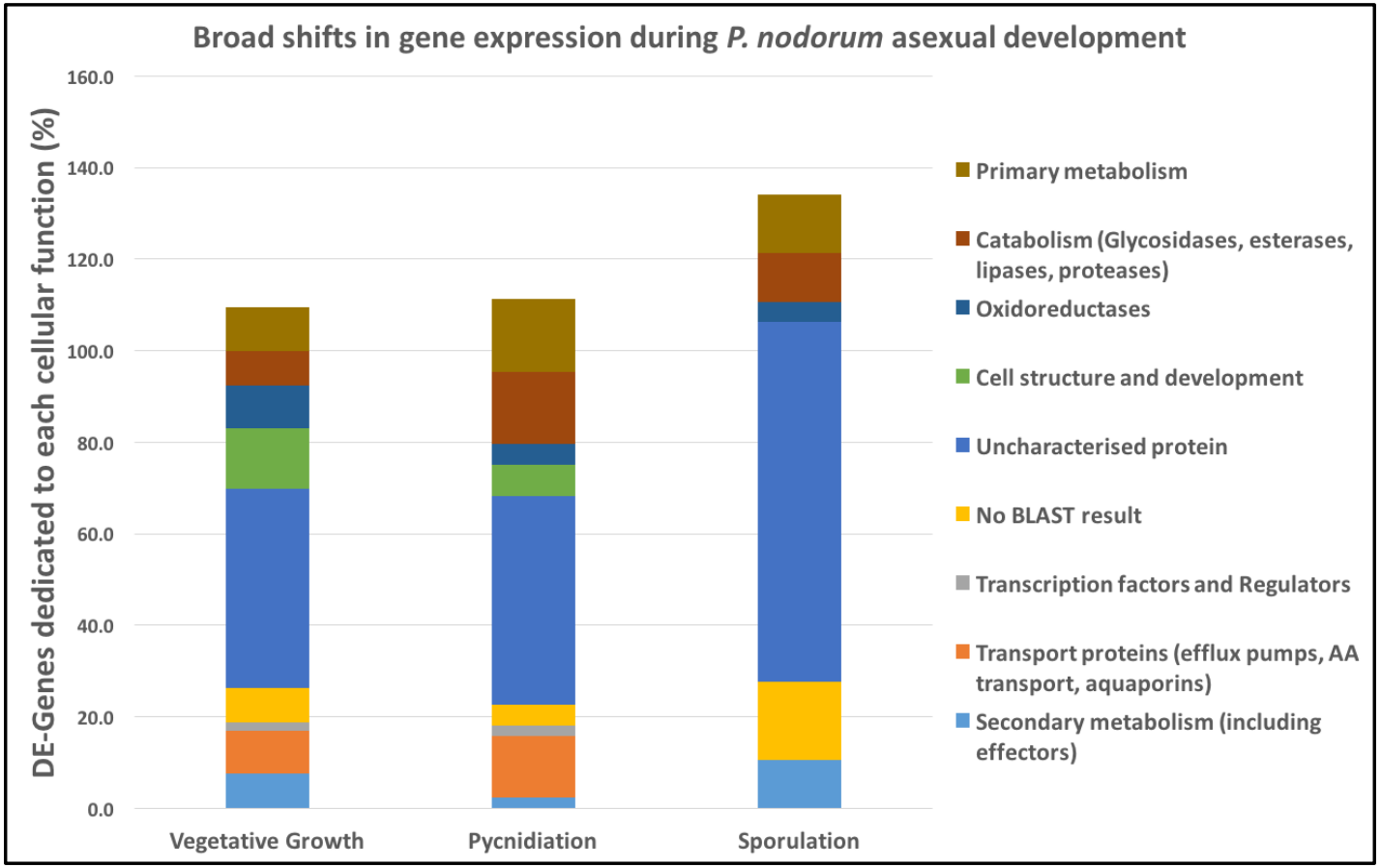


*(Figure 4.05: Cellular function of the top 50 differentially expressed genes in* P. nodorum *between undifferentiated cells and cells undergoing various stages of asexual reproduction. Genes distinguished by significance (P<0.05) and fold-change were included. Genes with multiple functions were included once for each possible function, leading to totals exceeding 100%)*

The predicted functions of the top 50 differentially expressed genes at each developmental stage were categorically grouped and shown graphically, in Figure 4.05. The proportions of each category were suggestive of changes in cell chemistry, mechanics and structure leading to the following developmental stage. For example, green represents the proportion of DE genes dedicated to cell structure and development, and was largest during vegetative growth preceding pycnidia formation. However, this gene class was not represented post-spore formation during sporulation. Transport related genes, as well as transcription factors and signal transducers were also absent from the final time point.

A BLAST search for the canonical *Aspergillus* and *Neurospora* genetic sporulation cascades revealed few homologues in the *P. nodorum* genome. Of those genes that showed homology to genes in the canonical sporulation cascades only the homologue of the *Aspergillus WetA* gene showed a strong and significant ($P<0.001$) response to GABA. This indicted that the *Aspergillus* and *Neurospora* sporulation genetic pathways were not active in *P. nodorum*. Subsequently, I investigated the expression of secondary metabolite clusters in *P. nodorum* responding to GABA to determine if the fungus was using a chemical mechanism to instigate sporulation.

### 4.3.4 Expression of secondary metabolite biosynthetic genes in the presence of 2mM GABA

To investigate the interaction between asexual development and secondary metabolism in *P. nodorum* I analysed the expression differences of the ca. 40 biosynthetic gene clusters reported in this fungus (Chooi, Muria-Gonzalez, & Solomon, 2014). Initially the core backbone gene of each cluster was surveyed for expression differences in the presence and

absence of GABA, at all developmental stages. An example is shown in Supplementary Figure 4.01. 22 core genes showed differential expression, which allowed identification of their parent biosynthetic gene clusters for further analysis. The expression of whole clusters was graphed at each time point to illustrate the co-ordinated expression of co-localised genes as an expression 'bubble'. Of the 22 core genes differentially expressed between GABA treated and untreated samples, four were co-expressed within a cluster of biosynthetic genes. Coordinated expression of these biosynthetic gene clusters is shown in Figures 4.06-4.09. The clusters are named after the identification number of the core backbone gene, indicated by brackets.

Cluster Pn.03620, in Figure 4.06, was differentially expressed during pycnidiation. This cluster consisted of a non-ribosomal peptide synthase (NRPS) as a core back bone gene, surrounded by four tailoring genes up-regulated in the presence of GABA during pycnidiation. During sporulation, the core backbone gene markedly decreased expression in samples treated with GABA, below that of samples untreated with GABA, while the surrounding tailoring genes remained constant between treated and untreated samples.

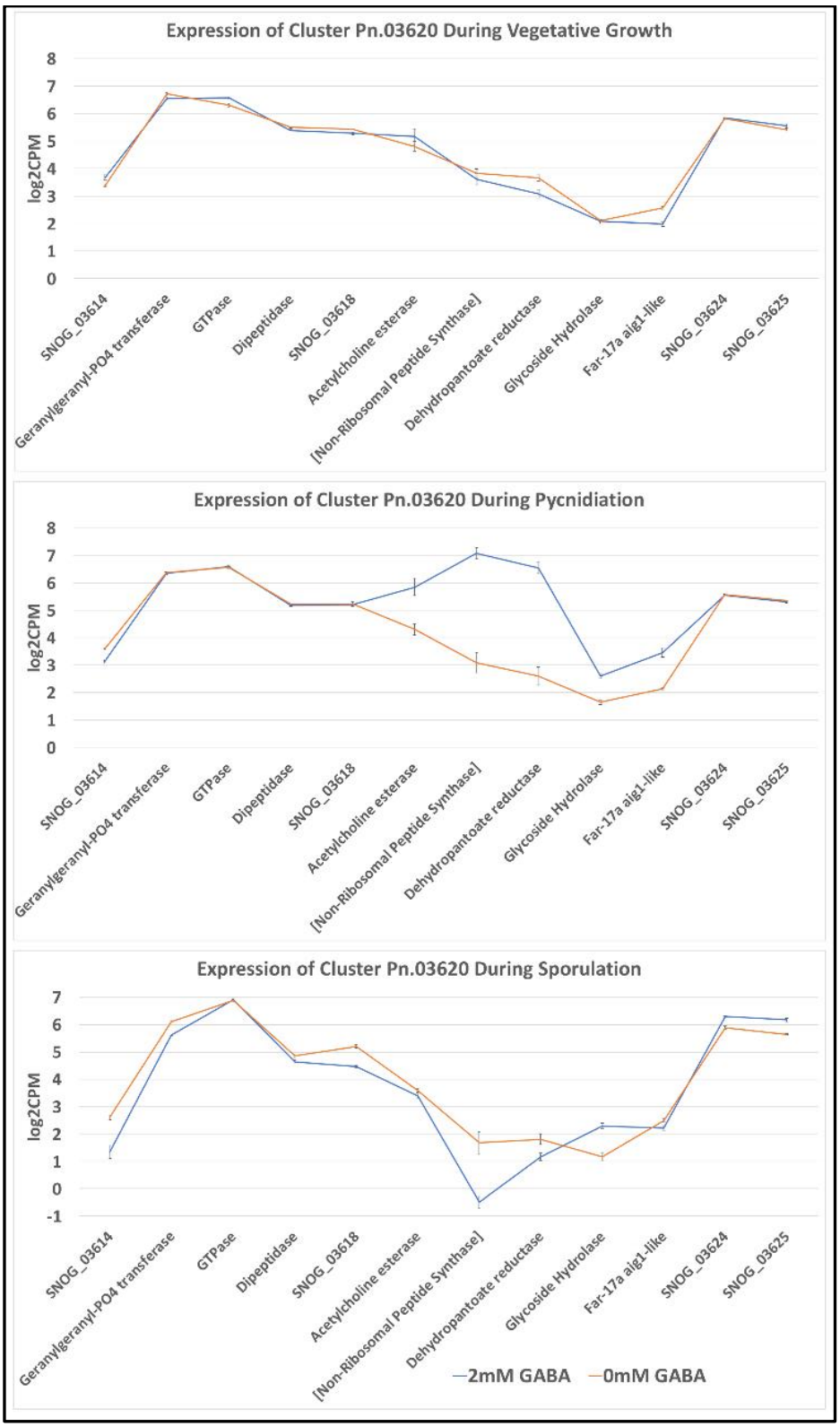


*(Figure 4.06: Expression of the non-ribosomal peptide synthase biosynthetic gene cluster, Pn.03620, during* P. nodorum *asexual development. Blue indicates gene expression in the presence of 2mM GABA, while orange indicates 0mM GABA. Error bars represent 95% CI.)*

The large biosynthetic gene cluster in Figure 4.07, Pn.08274, contained 19 co-localised genes that were co-expressed during vegetative growth. This cluster centred on a polyketide synthase (PKS) backbone gene and was downregulated in the presence of GABA. The PKS in this cluster was homologous to several annotated pigment-producing PKS genes. The closest homology to one of the annotated PKS was to Conidial yellow pigment biosynthesis polyketide synthase in *Neonectria ditissima* (75% coverage, 52% identity, Accession: KPM40039.1).

The cluster Pn.11076, shown in Figure 4.08, centres around a polyketide synthase backbone gene. This core gene is co-regulated with five other surrounding genes during vegetative growth and pycnidiation, forming an expression bubble. In the presence of GABA this bubble is suppressed. However, expression in GABA untreated samples dropped to similar levels as GABA treated samples during sporulation. Interestingly, there is a predicted C6 transcription factor within the cluster that is not differentially expressed between GABA treated and untreated samples at any time point.

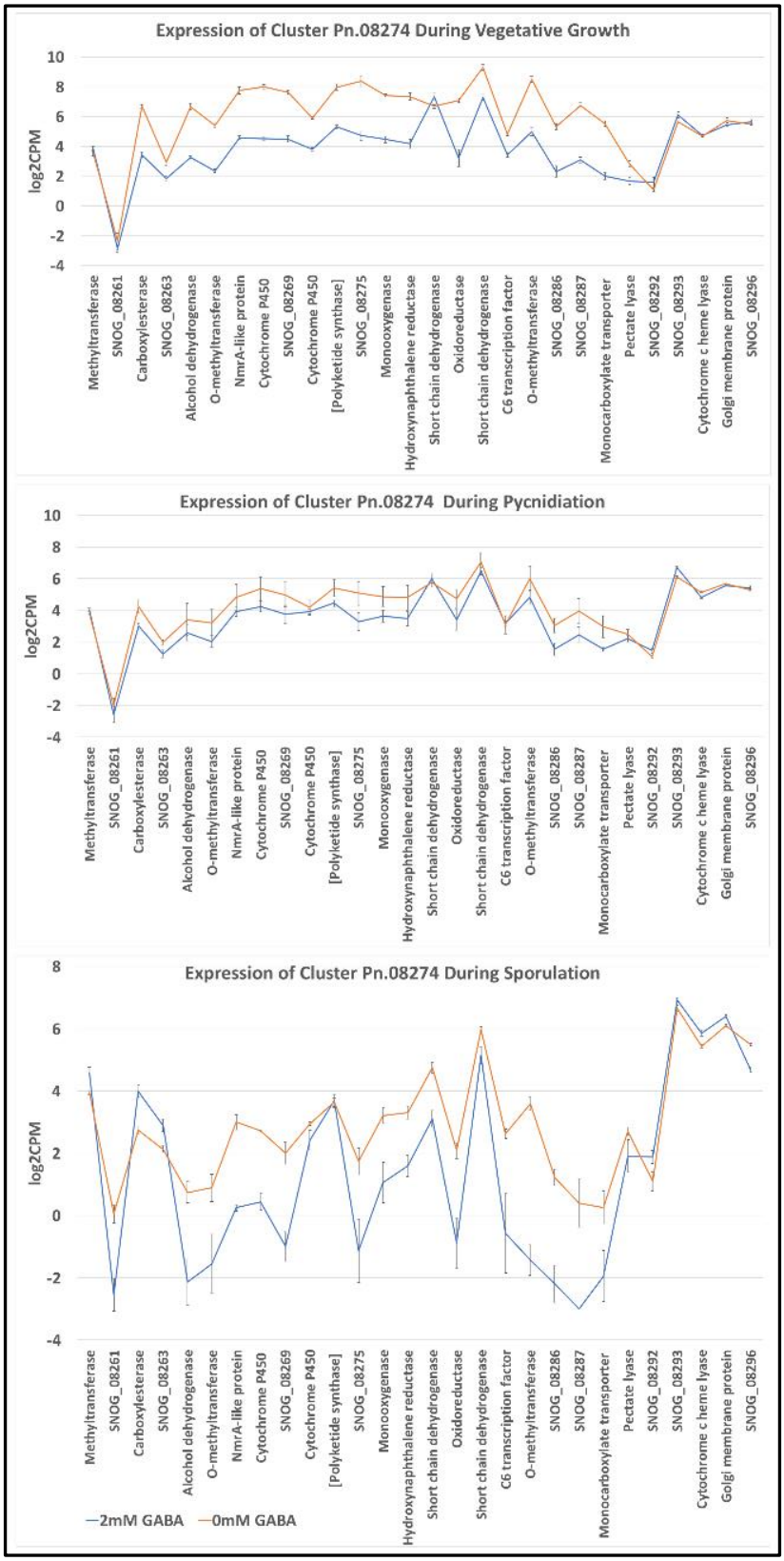


*(Figure 4.07: Expression of the polyketide synthase biosynthetic gene cluster, Pn.08274, during* P. nodorum *development. Blue indicates expression in the presence of 2mM GABA, orange 0mM GABA. Error bars represent 95% CI)*

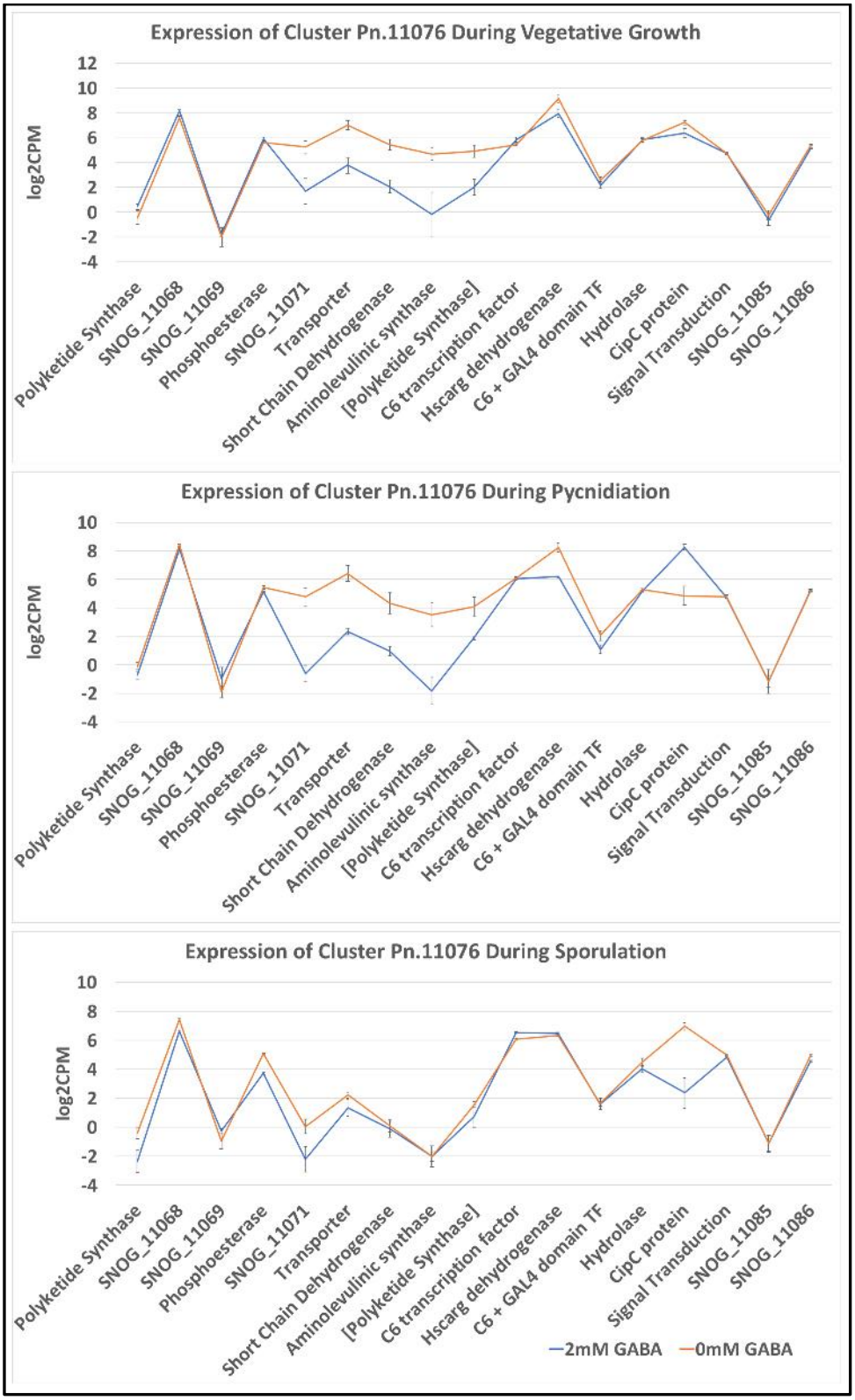


*(Figure 4.08: Expression of the polyketide synthase biosynthetic gene cluster, Pn.11076, during* P. nodorum *asexual development. Blue indicates gene expression in the presence of 2mM GABA, while orange indicates 0mM GABA. Error bars represent 95% CI.)*

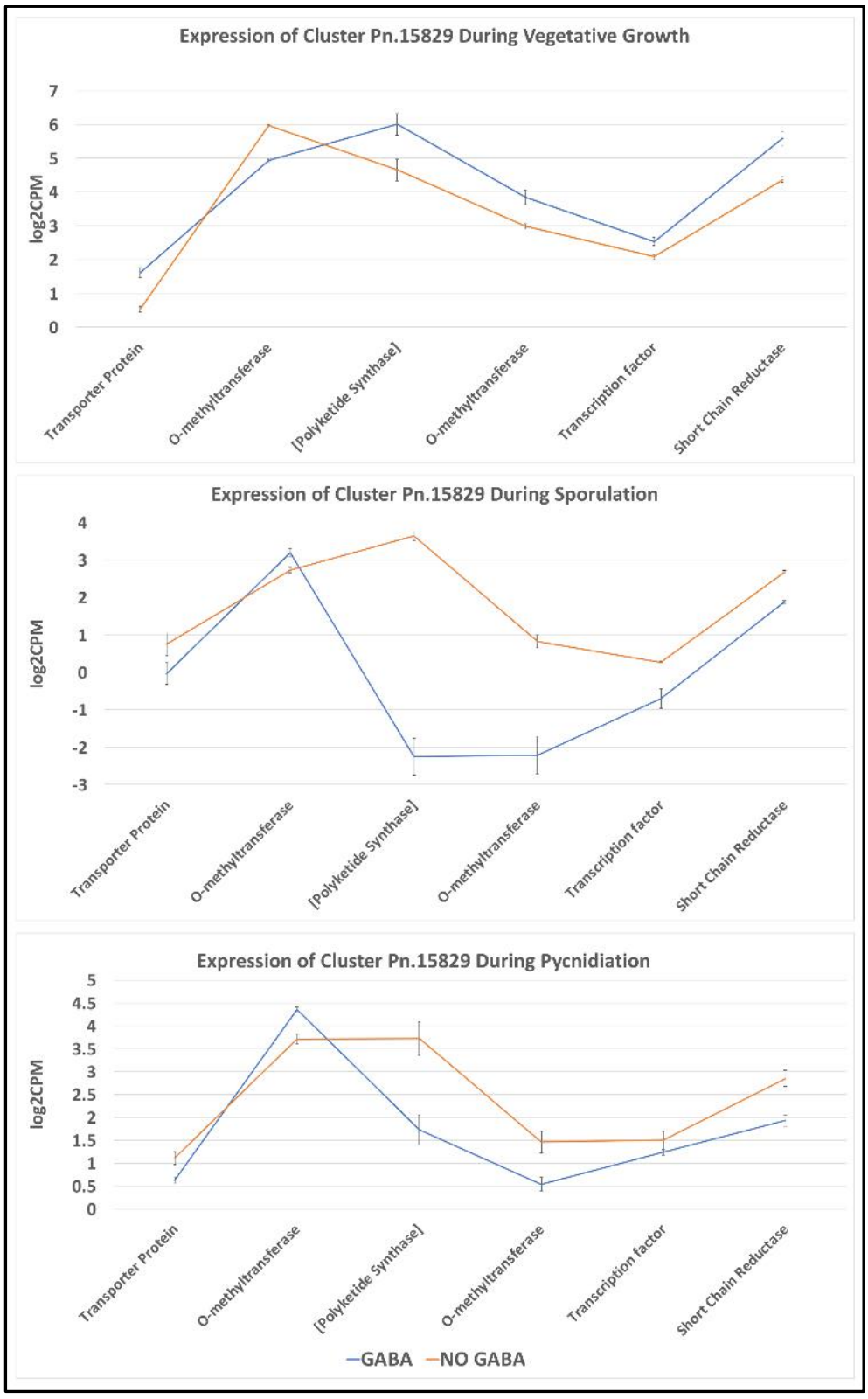


*(Figure 4.09: Expression of the polyketide synthase biosynthetic gene cluster, Pn.15829, in the during* P. nodorum *asexual development. Blue indicates gene expression in the presence of 2mM GABA, while orange indicates 0mM GABA. Error bars represent 95% CI.)*

The polyketide synthase based cluster, Pn.15829, has been previously shown to produce the mycotoxin, alternariol (Chooi, Muria-Gonzalez, Mead, & Solomon, 2015). The expression of this five-gene cluster was upregulated by GABA during vegetative growth, shown in Figure 4.09. Albeit, in the absence of GABA this cluster was also highly expressed. During pycnidiation and sporulation this clusters' expression declined under both treatments. However, in the presence of GABA the expression of these genes was far lower than in the absence of GABA.

### 4.3.5 Ornithine metabolism is affected during P. nodorum sporulation

Complementing the gene expression analysis, gas chromatography-mass spectrometry elucidated differentially abundant metabolites during *P. nodorum* asexual development. The fungal material for GCqTOF-MS analysis was processed and analysed as described in sections 4.2.2.10 and 4.2.2.11 by Dr. Joel Gummer. The raw data was subsequently deconvoluted by Dr Gummers lab technician Hayley Abbiss as a project investigating novel methods of deconvolution. A principal component analysis of the samples submitted for chemical analysis, shown in Figure 4.10, grouped replicates together. The samples separated both by treatment and time-point, with one exception. A single replicate from the samples untreated with GABA and collected from the pycnidiation time-point grouped more closely with samples collected from the earlier time point of the same treatment and was excluded from further analyses. The sample groupings of the principal component analysis indicated that the chemical analysis was biologically relevant, separating developmental stage horizontally on dimension 1, and GABA treated and untreated samples vertically on dimension 2. Further the quality control samples, dark blue, grouped very tightly.

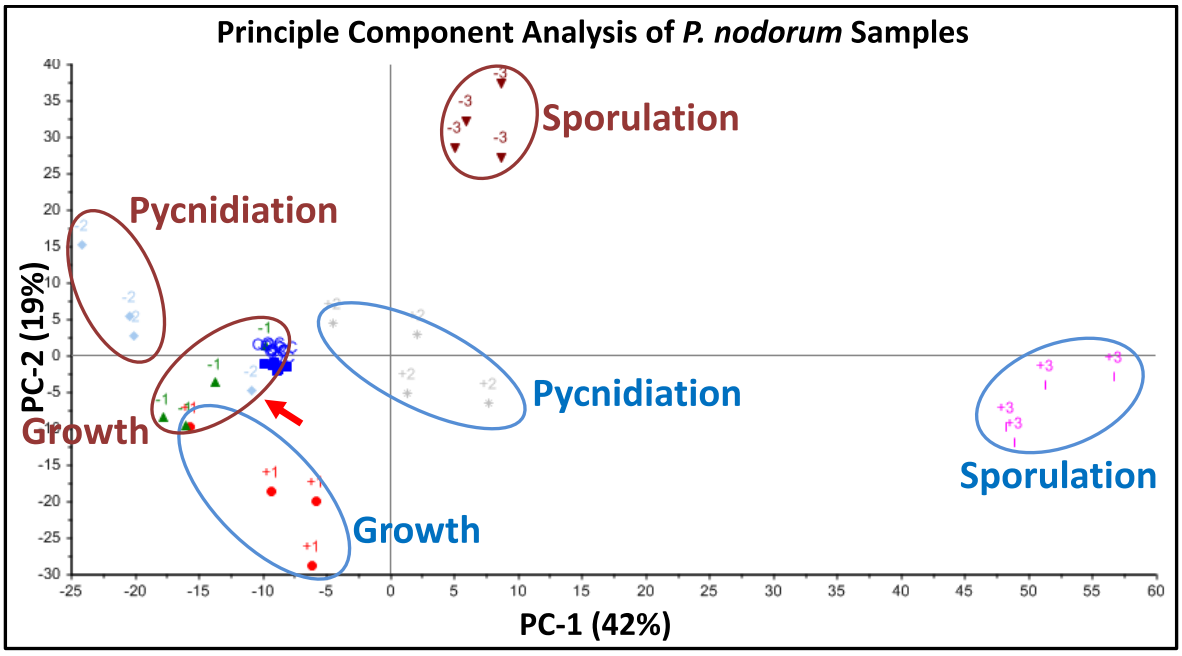


*(Figure 4.10: Principal component analysis, depicting dimensions 1 and 2, of* P nodorum *samples chemically analysed by gas chromatography-mass spectrometry. Samples encircled in blue were grown in the presence of 2mM GABA, while those encircled in maroon were grown in the absence of GABA. Samples were taken with four replicates at 8, 10 and 14 dpi, indicated by the developmental stages-* growth, pycnidiation *and* sporulation *respectively. A single replicate of untreated* P. nodorum *at the pycnidiation stage grouped with the untreated samples at the prior time point, indicated by a red arrow. Dark blue data points at ca. position, -10,0, indicate quality control samples.)*

GC-MS analysis generated a library of ca. 2500 spectral peaks combined from all samples. However, many peaks corresponded to each metabolite and in total only four metabolites were able to be identified (Personal communication with Dr Joel Gummer and Hayley Abbiss). These four metabolites were the disaccharide, trehalose; ornithine; the citric acid cycle intermediate, succinic acid; and the fatty acid, oleic acid.

Trehalose and ornithine were highly and significantly differentially abundant and are discussed in detail below. Succinic acid was also significantly differentially abundant however the difference in abundance can be attributed to the catabolism of GABA through the TCA cycle. This is further supported by succinate's initially higher abundance in GABA treated samples, followed by a decline to levels comparable of untreated samples. Oleic acid is not discussed further as it was not differentially abundant until sporulation. This could be attributed to a shift towards lipid metabolism within the cell as the fungus depletes the medium of sucrose.

The abundance of trehalose, shown in Figure 4.11, increased significantly during sporulation, as was reported earlier (Lowe et al., 2009). This was congruent with the expression data for the gene responsible for trehalose anabolism, Trehalose-6-Phosphate Synthase (*Sn.Tps1*), shown in Figure 4.12. The consistency between transcriptomic and metabolic data, as well as the previous investigation, further validated these data.

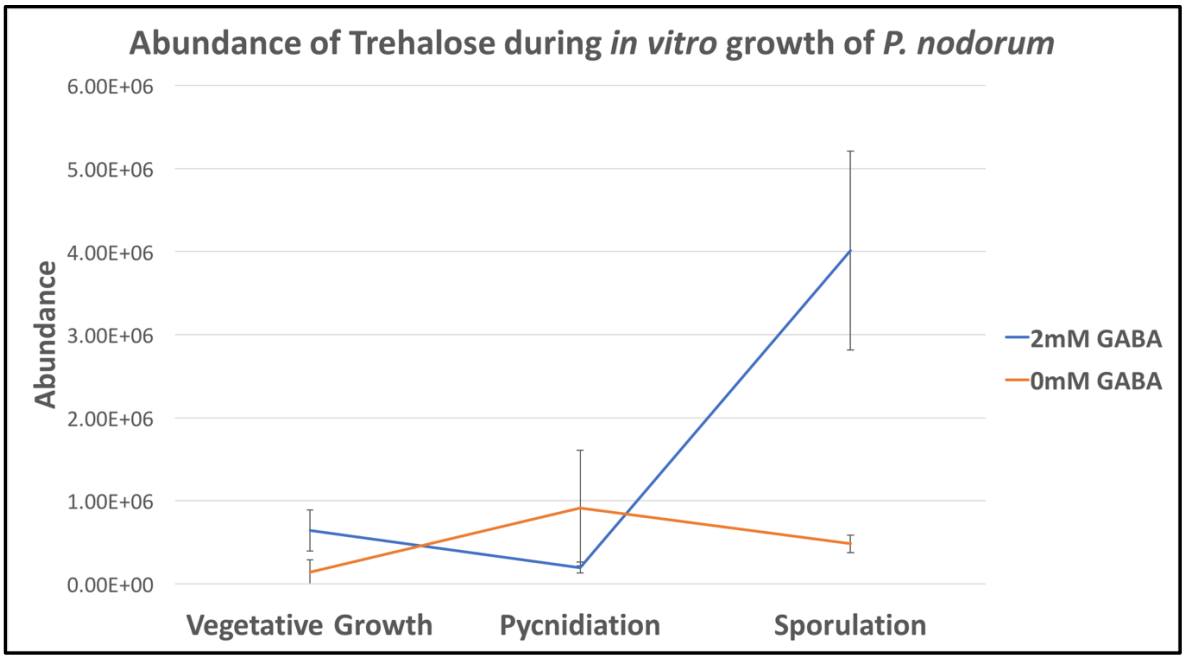

*(Figure 4.11: Abundance of trehalose in* P. nodorum *at key developmental time points. Error bars represent 95% CI. Abundance is unit-less.)*

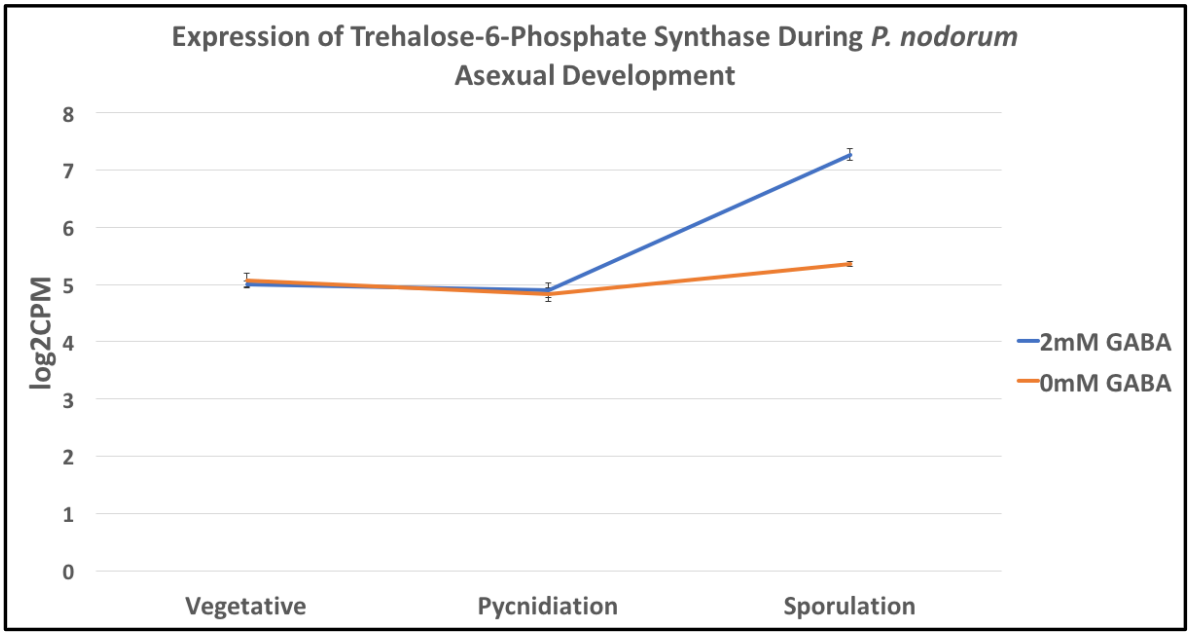


*(Figure 4.12: Gene expression of known Trehalose-6-phosphate synthase at developmental stages of* P. nodorum *asexual development in the presence and absence of GABA. Error bars represent 95% CI)*

Ornithine was significantly less abundant in *P. nodorum* at all developmental stages when grown in the presence of 2mM GABA. Most significantly ornithine abundance dropped 154-fold, in the presence of GABA during sporulation, relative to samples untreated with GABA, Figure 4.13. As the ornithine metabolic pathway is linked to GABA metabolism, I investigated the developmental role of ornithine in *P. nodorum* grown on minimal medium supplemented with compounds closely linked to ornithine metabolism.

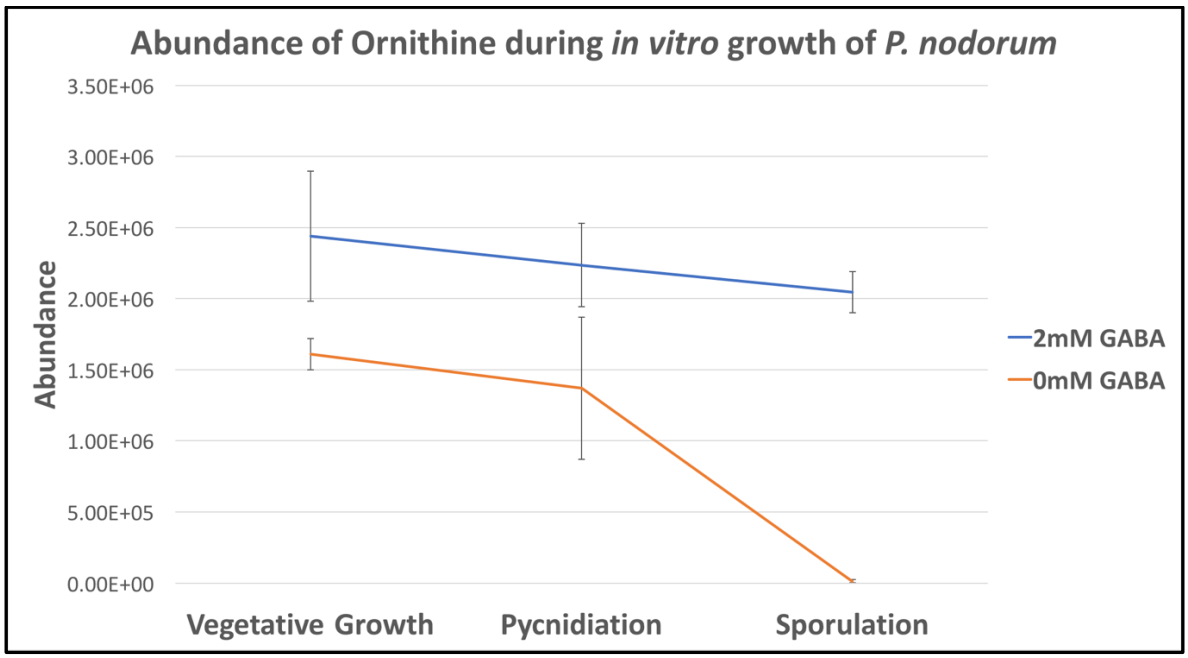


*(Figure 4.13: Abundance of ornithine in* P. nodorum *at key developmental time points. Error bars represent 95% CI. Abundance is unit-less)*

The growth rate and sporulation of wild-type *P. nodorum* on the different compounds are shown in Figures 4.14 and 4.15 respectively. The basal minimal medium contained 10mM sodium nitrate as the sole nitrogen source. The supplement media contained 10mM sodium nitrate and 5mM of respective supplement. Minimal media containing 10mM nitrate and 15mM nitrate were the negative controls, while minimal medium containing 10mM nitrate and 5mM GABA constituted the positive control. 15mM nitrate was used in subsequent significance testing as the extra 5mM nitrate accounts for the additional nitrogen in supplemented media. No significant differences in growth rate were observed, except for growth on media containing arginine or spermidine. Arginine slightly, but significantly decreased the colony diameter on spot inoculated plates, while spermidine completely inhibited growth (Figure 4.14). Despite relatively uniform growth rates, these metabolites variably induced sporulation (Figure 4.15).

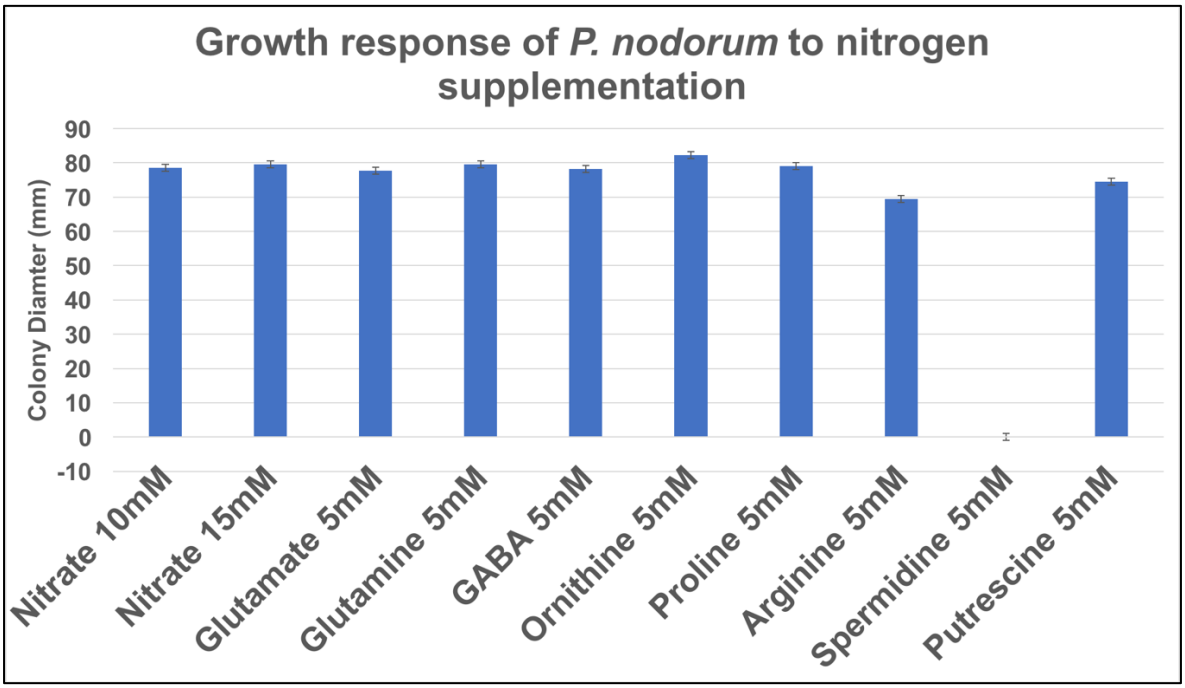


*(Figure 4.14: Radial growth of* P. nodorum *colonies grown on solid minimal medium supplemented with 5mM of intermediates of the ornithine biosynthetic pathway. Error bars represent 95% CI)*

Neither concentration of nitrate initiated substantial spore production in *P. nodorum* ($P>0.5$). Correspondingly, medium supplemented with 5mM GABA dramatically induced spore production ($P<0.05$). Glutamate, the upstream precursor to ornithine and GABA likewise did not induce significant sporulation ($P>0.1$). However, Glutamine induced moderate and significant levels of sporulation ($P<0.01$). Ornithine induced sporulation but not significantly ($P=0.08$). Similarly, the products of ornithine metabolism, arginine and spermidine, did not induce any sporulation, with spermidine completely inhibiting growth. Proline and putrescine, also products of ornithine metabolism, significantly induced sporulation.

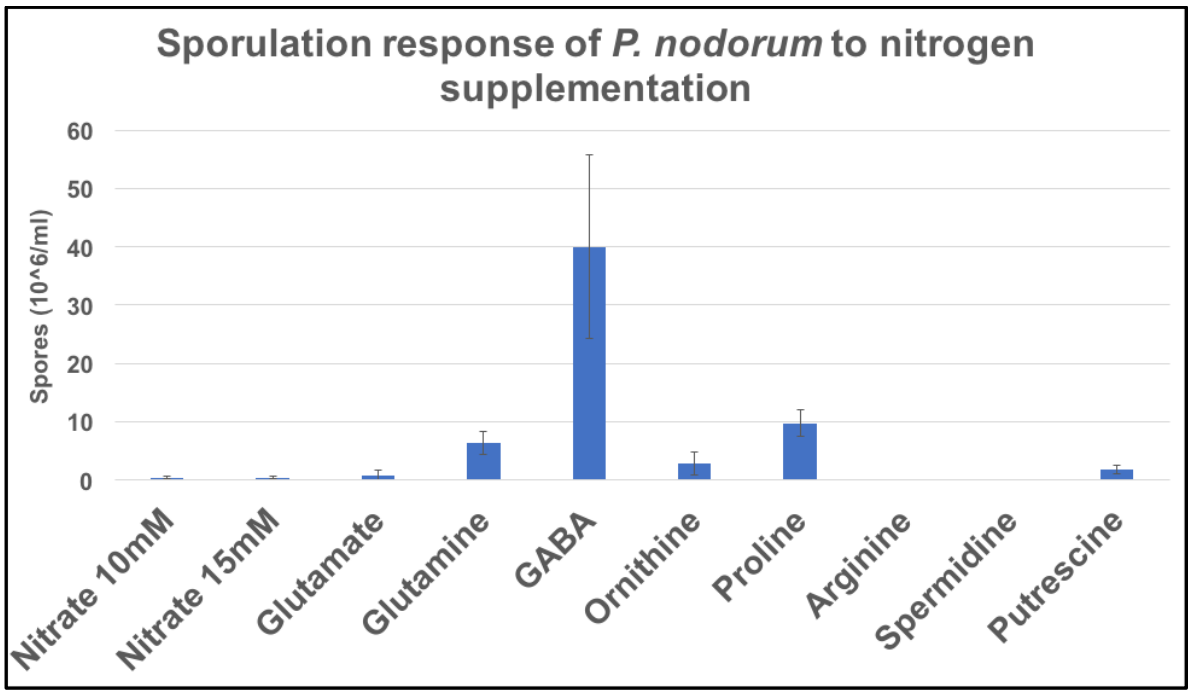


*(Figure 4.15: Sporulation of* P. nodorum *in response to 5mM supplementation of minimal medium with intermediates of the ornithine biosynthetic pathway. Error bars represent 95% CI)*

Proline induced sporulation in *P. nodorum* at 25% the rate that GABA induced sporulation and was the strongest inducer other than GABA. Glutamine appeared the third strongest inducer of sporulation, however large variability in spore numbers accounted for an insignificant difference when compared to the 15mM nitrate control.

Although the ornithine metabolites did not induce sporulation to the same extent as GABA, several compounds were still able to induce sporulation to varying degrees. Further, they strongly influenced mycelia and pycnidia morphology. Several of the metabolites were able to induce the production of pycnidia, however these pycnidia were misshapen, fused together or abnormally sized and variably produced spores. Spores that were produced had regular physiology and viability.

To clarify and summarise the effects of these metabolites on *P. nodorum* development, these broad observations were overlaid onto a simplified schematic of ornithine metabolism, shown in Figure 4.16. The effects included the rate of sporulation normalised to 15mM nitrate, a qualitative measure of pycnidia and presence/absence of cirrus. The schematic was simplified from the Kyoto Encyclopaedia of Gene and Genomes (KEGG) biochemical pathways database (Ogata et al., 1999).

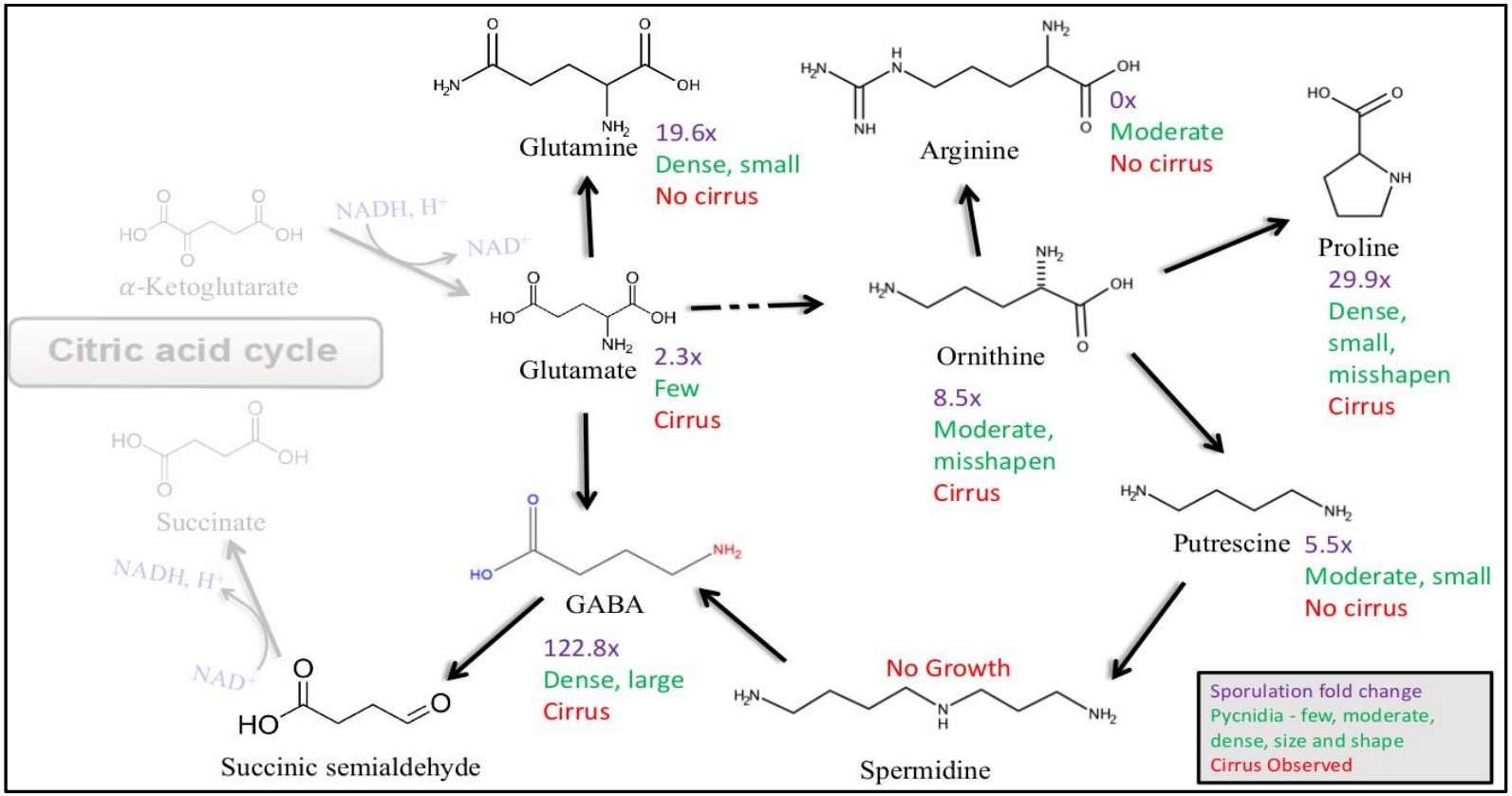


*(Figure 4.16: Schematic representation of the ornithine biosynthetic pathway and the response of* P. nodorum *to selected intermediates in terms of sporulation, pycnidial production and observable cirrus. Solid arrows represent a single enzymatic step, while broken arrows indicate multiple enzymatic steps. Sporulation is measure in fold change relative to the un-supplemented medium and designated in purple. Pycnidial production was designated into three levels of abundance: few, moderate and dense and is shown in green, observable cirrus is shown in red)*

### 4.3.6 Perception of environmental GABA may be mediated, in *P. nodorum*, by a mammalian-like GABAA receptor

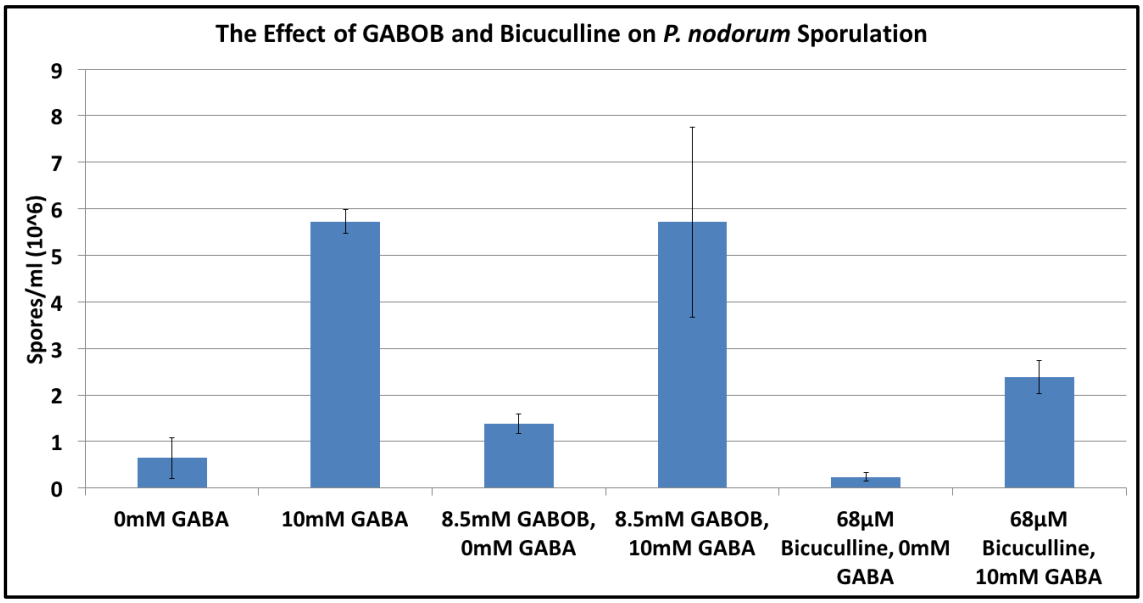


*(Figure 4.17: The sporulation response of* P. nodorum *to the $GABA_A$ agonist, GABOB, and the antagonist, Bicuculline, in the presence and absence of 10mM GABA. Error bars represent 95% CI)*

The mechanism by which GABA induces sporulation in fungi is currently unknown. A range of mammalian GABA receptor agonists and antagonists were screened for their ability to block or initiate GABA induced sporulation. 25µg/ml (68µM) of the mammalian $GABA_A$ receptor antagonist, bicuculline, significantly ($p<0.001$) inhibited sporulation of *P. nodorum* in the presence of 10mM GABA (Figure 4.17). Bicuculline had no effect on growth, nor did it significantly affect sporulation in the absence of GABA. Further, 1mg/ml (8.5mM) of the $GABA_A$ agonist, γ-amino-ß-hydroxybutyric acid (GABOB), induced sporulation to a small but significant degree ($P<0.05$). GABOB caused large variation in sporulation when combined with 10mM GABA, as indicated by the error bars in Figure 4.17. Despite the evidence for a $GABA_A$ receptor, no homologues of characterised mammalian $GABA_A$ receptor sub-unit proteins were found in *P. nodorum*.

## 4.4 Discussion

### 4.4.1 Combined metabolomics and transcriptomics provided a unique insight into *P. nodorum* asexual development

Previous investigations into the asexual development of *P. nodorum* involved identifying genes and metabolites crucial to sporulation. These studies were directed by gene homology and expression, as well as chemical analysis of metabolites (IpCho et al., 2010; P S Solomon, Waters, & Oliver, 2007; Tan et al., 2008). In this study, a combined transcriptomic and metabolomic approach quantified changes in gene expression and metabolite abundance during three distinct stages of asexual development. This study provides evidence that the mechanism triggering sporulation in *P. nodorum* did not resemble any of the canonical gene cascades described in the literature. Subsequently, a metabolomics approach revealed the developmental role of ornithine and related nitrogenous metabolites during asexual reproduction. Following this I provide provisional evidence that GABA perception and sporulation induction, in *P. nodorum*, was mediated by a mammalian-like $GABA_A$ receptor. This chapter establishes the basis for future investigations into the unknown Dothideomycete asexual developmental pathways.

### 4.4.2 Gene expression profiling during *P. nodorum* asexual development describes the metabolic, structural and mechanical changes of cell differentiation

The broad changes in gene expression at each developmental stage reflected the changes in cellular processes. Several expected traits provided further confidence that these data described genetic and metabolic shifts during asexual reproduction. Genes predicted to play roles in primary metabolism (brown) and catabolism (maroon) were upregulated during pycnidiation when spores were developing. This may reflect the

metabolic cost of producing spores and the subsequent decline in expression of these genes, after spore production, may reflect a more senescent state. The occurrence of a senescent developmental stage is further supported by the lack of expression of genes predicted to play roles in cell structure and development (green) as well as signal transduction (grey) and transport (orange). This can be attributed to the completion of cell differentiation and spore production.

There were two key features of the gene classes differentially expressed in the presence of GABA. First, the decline in secondary metabolism during pycnidiation, while there was comparatively high expression of these genes during vegetative growth and sporulation. Second, the high proportion of differentially expressed genes without homologues in other organisms or predicted protein function. Genes with no predicted function were particularly prevalent during sporulation. This shows how much more there is to learn about fungal biology.

### 4.4.3 Genes showing highly differential expression

The top 50 differentially expressed *P. nodorum* genes at each stage of asexual development were filtered into a shortlist. This list contained genes that may be involved in the genetic triggering of each stage of development, as well as several unexpected and interesting genes. Excluded from this table were genes with predicated roles in amino acid metabolism and transport, primary metabolism and production of cellular structural components. Although genes falling in these classes were abundant in the top 50 candidate lists, they were expected to play downstream roles in development or were expressed in a non-specific response to amino acid abundance. It is unlikely these genes played a role in triggering cell differentiation. Further, genes with unknown function were also excluded from the short list. These genes predicted to produce

uncharacterised proteins may play a crucial role in the Dothideomycete sporulation pathway. However, significant effort would be required to begin elucidating the functions of uncharacterised proteins and their potential role in sporulation. Instead, this study focused only on proteins with predicted functions, specifically those putatively involved in signal transduction. This was to begin outlining genetic mechanisms of sporulation in a class of fungi for which little is known about development.

Several genes predicted to play roles in signal transduction were present in the top 50 lists. These included a *Helicase-like transcription factor*, *Histidine kinase*, *Blue light inducible protein* and a *Hard surface inducible protein*. An *Integral membrane protein* was also included. Although this protein had numerous potential functions, it was highly differentially expressed during pycnidiation and could be involved in environmental sensing. These genes provide excellent targets for reverse genetics approaches to elucidate novel genetic sporulation networks.

Unsurprisingly, several of the identified genes had predicted environmental sensing functions. The *Blue light inducible* gene from *Neurospora crassa*, and *Hard surface inducible* genes from *Colletotrichum spp.* are regulated by environmental stimuli (Linden et al., 1997; Kahmann and Basse, 2001). The conidiation inducing effect of blue light and the *White collar* signal transduction system has been extensively studied in the fungal model, *Neurospora crassa* (Linden et al., 1997). The *Colletotrichum Hard surface* inducible genes encode a diverse range of proteins including a transcription factor, cell membrane integrated protein and a ubiquitin-conjugated enzyme (Kahmann & Basse, 2001). However, the role of these proteins during differentiation of vegetative cells into penetration structures remains relatively unknown. While several *Hard surface inducible* genes have been disrupted with no effect on cell differentiation or

pathogenicity (Y. K. Kim, Liu, Li, & Kolattukudy, 2000; Liu & Kolattukudy, 1998), a forward genetics screen identified *Colletotrichum hard surface inducible protein 5* (*Chip5*) as a key virulence factor (Cai et al., 2013). These environmental stimuli response genes appear to play diverse and often unknown roles in fungal development and virulence. Consequently, they were included in the short list of genes nominated for further investigation.

Continuing a theme of potential virulence proteins, the list of the top 50 differentially expressed genes included two PR1-like proteins. The broad PR1 (Pathogenesis related 1) family of proteins are highly up regulated in plants upon infection, and contain the sterol binding domain, CAP (Cysteine-rich secreted protein, Antigen 5 and Pr1 related), and the stress signalling peptide, CAPE1 (CAP-derived peptide) (Breen et al. 2017; Choudhary & Schneiter, 2012). It is interesting that a plant pathogen would harbour *PR1-like* genes, and further that they would be upregulated during the production of spores, the transmissible unit of infection. Deploying pycnidospores with these proteins could potentially aid initial stages of the necrotrophic infection by hijacking the plant immune system and helping to trigger cell death. Supporting this idea, Lu et al (2014), showed that co-infiltrating wheat plants with the effector protein, ToxA, and Pr1-5 increased the resulting necrosis, compared to ToxA alone (Lu, Faris, Sherwood, Friesen, & Edwards, 2014).

Genes encoding aquaporins were also highly abundant in the top 50 list. This included the most differentially expressed gene with a predicted function, *SNOG_04900.* The expansive aquaporin protein family has been extensively studied in plants and was initially thought to exclusively facilitate water transport. However, these transmembrane pore proteins have now been shown to also facilitate movement of many solutes

(Maurel, Verdoucq, Luu, & Santoni, 2008). Previously fungal aquaporins had received little attention, but new interest in their functionality is reflected in recent studies. For example, gene expression and reverse genetics studies have shown that mycorrhizal interactions between a variety of fungi and plant-hosts require the orchestrated expression of multiple aquaporins. These interactions promote nutrient acquisition and drought tolerance in the host, and the aquaporins are hypothesised to play roles in osmotic regulation, nutrient transfer and signal transduction (Aroca et al., 2009; Aroca, Porcel, & Ruiz-Lozano, 2007; Dietz, von Bülow, Beitz, & Nehls, 2011; T. Li et al., 2013; Navarro-ródenas, Xu, Kemppainen, Pardo, & Zwiazek, 2015). Pathogenic fungi have also been shown to require aquaporins for different purposes. Deletion of the aquaporin, *Aqp1*, in the human pathogen *Cryptococcus neoformans* lead to an increase in secondary metabolites and survival fitness, but did not affect virulence (Meyers et al., 2017). Conversely, disruption of *Aquaporin-8* in *Botrytis cinerea* abolished both virulence and the fungus' ability to develop penetration structures (An et al., 2015). Aquaporins may play a mechanical or structural role during *P. nodorum* cell differentiation rather than a signalling role. However, the role of aquaporins in other fungal pathogens, their high expression and abundance during *P. nodorum* asexual development and their potential for transporting signalling molecules makes them an intriguing target for future investigation.

### 4.4.4 *P. nodorum* engages an unknown mechanism to initiate and co-ordinate sporulation

The model fungi, *Aspergillus nidulans* and *Neurospora crassa*, have revealed genetic bases for many aspects of fungal growth and development, including the complex genetic regulatory networks orchestrating sporulation (Etxebeste et al., 2010; Park & Yu, 2012). Work spanning the last four to five decades has established these sporulation

cascades as the canonical models for fungal asexual reproduction (Clutterbuck, 1969; Matsuyama, Nelson, & Siegel, 1974). However, the asexual fruiting bodies of *Neurospora*, *Aspergillus* and *Parastagonospora nodorum* are structurally unrelated, and there are no parallels in morphological development. Despite its importance, the genetic regulation of *P. nodorum* asexual development remains unknown.

Sporulation and secondary metabolism were shown to be co-regulated in the *P. nodorum* relative, *Dothistroma septosporum,* by the master regulatory gene, *Velvet-like* (*VeA*) (Chettri et al., 2012). The *P. nodorum VeA* homologue was not found to be significantly differentially expressed in response to GABA. However, the role of secondary metabolism during sporulation is an attractive prospect for investigation as it has been tightly associated with sporulation in other species of fungi (Sekiguchi & Gaucher, 1977; Calvo, Wilson, Bok, & Keller, 2002). For example, the *Aspergillus* regulatory network involving the *Flb* series of genes and *LaeA* have been shown to coordinate secondary metabolism with fungal development (Bayram, 2008). In some cases, disrupting biosynthetic gene clusters co-regulated with sporulation had no impact on fungal development (Sekiguchi & Gaucher, 1977). Conversely, the secondary metabolite, zearalenone, induces fruiting body formation in *Fusarium graminearum* (Sekiguchi & Gaucher, 1977), and disrupting sterigmatocystin production in *A. nidulans* decreased spore production (Calvo et al., 2002).

### 4.4.5 Four biosynthetic gene clusters were differentially expressed in response to 2mM GABA

Accordingly, I looked for GABA induced differential expression of core genes in the ca. 40 known *P. nodorum* biosynthetic gene clusters (Chooi et al., 2014). Four clusters,

Pn.03630, Pn.08274, Pn.11076, Pn.15829, were differentially expressed in the presence of 2mM GABA. Intriguingly, Pn.15829 is known to produce the mycotoxin, alternariol (Chooi et al., 2015). However, the role of the compounds produced by these clusters remains unknown. Cluster expression may result directly from GABA perception, or the clusters and sporulation could be regulated by redundant regulatory elements. Further, the compounds produced may play a pivotal role in regulating cell differentiation or may simply be structural elements to spore production. As such, these clusters provide intriguing avenues for investigating the largely unknown secondary metabolism of *P. nodorum* as well as its role in fungal asexual development.

### 4.4.6 Ornithine metabolism plays a crucial role in cell differentiation during *P. nodorum* pycnidogenesis

A metabolomic analysis of *P. nodorum* at different stages of asexual reproduction yielded unexpectedly few positive metabolite identifications, however, provided a fruitful avenue for investigation.

Ionisation and fragmentation during GCqTOF-MS analysis leads to the production of many spectral peaks for each compound. Therefore, although 2500 peaks were produced in this study, this does not indicated that 2500 compounds were present. The spectral peaks generated by this analysis require deconvolution for compound identification. The chemical analysis and compound identification was performed by Dr Joel Gummer and Hayley Abbiss. Hayley Abbiss, Dr Gummers lab technician, was investigating a novel deconvolution method, and in return for analyzing my samples, Dr Gummers team used the raw data in their novel deconvolution pipeline. Generating 2500 spectral peaks from these fungal samples was encouraging and not unexpected. However, the deconvolution of peaks into compound identification unfortunately, and

unexpectedly, only yielded four positive IDs. Further, Ms Abbiss and Dr Gummer no longer have the time to re-analyse our data, and I do not have the technical resources. Ideally I would repeat this experiment, however, that would also require repeating the gene expression analysis to maintain the validity in comparing gene expression with metabolite abundance. Further, the resources required for this type of investigation are highly limiting.

At the final stage of maturation, during GABA-induced sporulation, there was a dramatic and significant decrease in ornithine abundance. Ornithine metabolism is closely related to the GABA shunt, and has previously been shown to be crucial for *P. nodorum* virulence and sporulation (Bailey et al., 2000). The fungal cell relies upon ornithine to produce polyamines. Rajam et al (1985) and Rajam and Galston (1985) showed in a series of experiments that the fungicidal activity of DL-α-difluoromethylornithine, was due to ornithine decarboxylase inhibition in several biotrophic and necrotrophic fungi. This inhibition disrupted polyamine production, but fungal growth could be recovered by supplementing the fungi with 0.1mM to 1.0mM of the downstream polyamines, spermine and spermidine (M. V. Rajam, Weinstein, & Galston, 1985; M. V Rajam & Galston, 1985). Polyamines are required for cell viability, however, the reason for this and the complex feedback and storage mechanisms of polyamine synthesis have been contentious (Davis, Morris, & Coffino, 1992). Alongside polyamines, the role of the polyamine progenitor, ornithine, and related metabolites during fungal asexual development remains a mystery. Accordingly, metabolites from the GABA shunt and ornithine biosynthetic pathway were screened for their ability to induce *P. nodorum* sporulation in a similar way to GABA.

The variation of *P. nodorum* morphology in response to these metabolites suggested a key role in coordinating cell differentiation during asexual reproduction. This was not due to additional nitrogen as spore numbers, on minimal media containing these metabolites, exceeded that of minimal medium containing additional nitrate. Interestingly, spermidine inhibited growth completely and may be toxic at 5mM. The response of *P. nodorum* to these metabolites revealed a previously unknown aspect of asexual reproduction. The regulation and mechanisms of these effects remains unknown. Nevertheless, this metabolomics investigation has provided new insight into fungal asexual development and provides new opportunities for enquiry.

There remains a fundamental question as to how these metabolites exerted their effect on *P. nodorum*. Possibly, they worked through either a metabolic or a receptor-based mechanism. The strength of GABA-induced sporulation compared to the related metabolites may indicate that different effects are being observed. It is possible that GABA triggered sporulation via a receptor, and that metabolites in the ornithine pathway were simply downstream structural or metabolic requirements for sporulation. Supplementing the medium with these metabolites may have interfered with sporulation regulatory feedback loops, leading to miss-regulated asexual development. This hypothesis is supported by the inability of the immediate metabolic precursor to GABA, glutamate, to induce sporulation.

### 4.4.7 *P. nodorum* may utilise a GABAA-like receptor to sense environmental GABA and co-ordinate asexual development

This study predominantly focused on deciphering the genetic processes driving asexual development, and the mechanism of GABA induced sporulation in *P. nodorum*.

However there remains the question of how the fungal cell perceives GABA, and for what benefit.

The concept of plant-generated GABA as a reliable nutrient source for pathogens is not a new idea, Solomon, Tan and Oliver (2003) extensively reviewed nutrient acquisition by plant fungal-pathogens during infection. Accordingly, Solomon et al (2002) determined that during compatible interactions between the fungal biotroph, *Cladosporium fulvum*, and tomato plants, the abundance of GABA increased. Conversely, during incompatible interactions the abundance of GABA remained constant. Further, their study found that *C. fulvum* was capable of using GABA as a sole nitrogen source, and the enzymes required to metabolize this molecule were upregulated during infection (Solomon & Oliver, 2002). However, in context of the fungal necrotrophic lifestyle, perhaps this enigmatic molecule plays a different role.

The necrotrophic and polycyclic life strategy of *P. nodorum* (Solomon et al., 2006) may require the pathogen to sense the health of its surrounding plant tissue and coordinate reproduction accordingly. Stages of reproduction could be synchronized to plant stress hormones such as GABA. To investigate receptor-mediated GABA perception in *P. nodorum*, commercial agonists and antagonists of mammalian GABA receptors were screened for their ability to modulate sporulation. GABA-induced sporulation was inhibited by the $GABA_A$ antagonist Bicuculline (Johnston, 1996). Correspondingly, the $GABA_A$ agonist, GABOB mildly induced sporulation in the absence of GABA (Johnston, 1996). GABOB is a hydroxylated form of GABA and may have exerted a sporulation effect due to similarities in metabolism of these molecules. However, Bicuculline did not structurally resemble GABA. This preliminary evidence supports the hypothesis that GABA-induced sporulation was mediated by a GABA receptor that

may have resembled the mammalian $GABA_A$ receptor. There is evidence for a fungal GABA receptor in the literature. Calcott and Fatig (1984) showed that the $GABA_A$ receptor antagonist, Avamectin, inhibited GABA binding to the cellular membrane of the fungus, *Mucor miehei*. Interestingly, their study found no effect of Bicuculline on GABA binding to the fungal cell membrane. However, to my knowledge no GABA receptor has been identified in fungi.

Identifying a GABA receptor in *P. nodorum* would contribute to the current models of plant-microbe interactions and provide avenues for industrial research. Inhibiting sporulation of *P. nodorum,* and similar pathogens, effectively disarms the pathogen (Solomon et al., 2006). A fungal specific, GABA receptor antagonist may represent a novel form of fungicide to break the *P. nodorum* disease cycle. GABA receptor binding molecules, specific to insects, have successfully been exploited as insecticides (Hosie et al., 1995; Rattan, 2010), and a similar developmental pipeline may generate novel fungicides.

### 4.4.8 Conclusions

Sporulation is crucial for *P. nodorum* to instigate disease on the host plant, as well as to cause the devastating field epidemics that lead to losses to the wheat industry. However, the genetic and metabolic basis for the asexual development of this fungus remains largely unknown. A transcriptomics approach to deciphering the development of *P. nodorum* revealed that the canonical sporulation pathways defined in model fungi are not present in this fungus. However, this approach has elucidated several key genes predicted to play roles in signal transduction and secondary metabolism that are differentially expressed during asexual development. These genes represent the initial

avenues for further investigation, leading to development of a Dothideomycete model for asexual development.

Complementing the transcriptomics approach, metabolomics identified an amino acid biosynthesis pathway playing a regulatory role in cell differentiation. This pathway centred on ornithine, however the metabolites in this pathway originated from the GABA shunt and linked to polyamine metabolism. The coordination of fungal growth, pycnidia formation and sporulation were found to be regulated by amino acids in this pathway. This pathway was previously known to play a role in virulence and sporulation (Bailey et al., 2000). However, the extent to which this biochemical pathway influenced fruiting body formation was previously unknown. This study laid the ground work to investigate the chemical features of asexual development in *P. nodorum*.

The sporulation effect of GABA described by Mead et al (2013) was used to model sporulation. This effect allowed the fungus to be grown under near identical conditions to compare the transcriptome of sporulating and vegetative fungal biomass. However, the mechanism by which *P. nodorum* perceived exogenous GABA was unknown. I hypothesised that the sporulation effect of GABA was either intrinsically metabolic or due to perception of environmental GABA via a receptor mechanism. The effect of mammalian GABA receptor agonists and antagonists on *P. nodorum* sporulation suggested that a GABA receptor mechanism, resembling those found in mammals, was present in *P. nodorum*. Excitingly, the $GABA_A$ receptor agonist, GABOB, induced sporulation and the $GABA_A$ receptor antagonist, Bicuculline, inhibited GABA induced sporulation. While GABOB is structurally similar to GABA and may have initiated sporulation due to a shared metabolic pathway, Bicuculline does not structurally or

metabolically resemble GABA. This provides evidence of a receptor-based mechanism for the perception of environmental GABA, and induction of *P. nodorum* sporulation.

Together, these experiments begin to define a new model of asexual development for the economically important fungus, *P. nodorum*, and perhaps more broadly for the pathogen enriched class, the Dothideomycetes.

## 4.5 Supplementary Figures

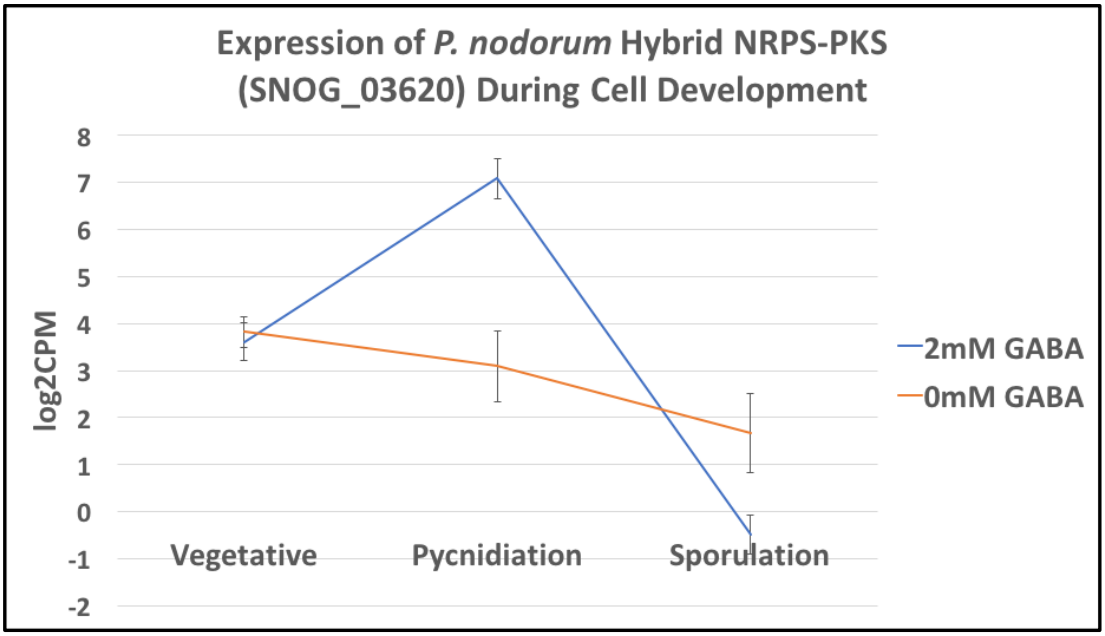


*(Supplementary Figure 4.01: Expression of hybrid NRPS-PKS, SNOG_03620, during* P. nodorum *asexual development.)*

## 4.6 References for chapter 4


An, B., Li, B., Li, H., Zhang, Z., Qin, G., & Tian, S. (2015). Aquaporin8 regulates cellular development and reactive oxygen species production, a critical component of virulence in *Botrytis cinerea*. *New Phytologist*. https://doi.org/10.1111/nph.13721

Anders, S., Pyl, P. T., & Huber, W. (2015). HTSeq-A Python framework to work with high-throughput sequencing data. *Bioinformatics*, *31*(2), 166–169. https://doi.org/10.1093/bioinformatics/btu638

Andrews, S. (n.d.). FastQC A Quality Control tool for High Throughput Sequence Data. *Http://www.bioinformatics.babraham.ac.uk/projects/fastqc/*. Retrieved from citeulike-article-id:11583827

Aroca, R., Bago, A., Sutka, M., Paz, J. A., Cano, C., Amodeo, G., & Ruiz-Lozano, J. M. (2009). Expression analysis of the first arbuscular mycorrhizal fungi aquaporin described reveals concerted gene expression between salt-stressed and nonstressed mycelium. *Molecular Plant-Microbe Interactions : MPMI*, *22*(9), 1169–1178. https://doi.org/10.1094/MPMI-22-9-1169

Aroca, R., Porcel, R., & Ruiz-Lozano, J. M. (2007). How does arbuscular mycorrhizal symbiosis regulate root hydraulic properties and plasma membrane aquaporins in *Phaseolus vulgaris* under drought, cold or salinity stresses? *New Phytologist*, *173*(4), 808–816. https://doi.org/10.1111/j.1469-8137.2006.01961.x

Bailey, A., Mueller, E., & Bowyer, P. (2000). Ornithine decarboxylase of *Stagonospora (Septoria) nodorum* is required for virulence toward wheat. *Journal of Biological Chemistry*, *275*(19), 14242–14247.

Bayram, Ö. et al. (2008). VelB / VeA / LaeA Complex Coordinates Light Signal with Fungal Development and Secondary Metabolism. *Science*, *320*, 1504–1506. https://doi.org/10.1126/science.1155888

Bolger, A. M., Lohse, M., & Usadel, B. (2014). Trimmomatic: A flexible trimmer for Illumina sequence data. *Bioinformatics*, *30*(15), 2114–2120. https://doi.org/10.1093/bioinformatics/btu170

Bönnighausen, J., Gebhard, D., Kröger, C., Hadeler, B., Tumforde, T., Lieberei, R., Bormann, J. (2015). Disruption of the GABA shunt affects mitochondrial respiration and virulence in the cereal pathogen *Fusarium graminearum*. *Molecular Microbiology*, *98*(6), 1115–1132. https://doi.org/10.1111/mmi.13203

Breen, S., Williams, S. J., Outram, M., Kobe, B., & Solomon, P. S. (2017). Emerging

Insights into the Functions of Pathogenesis-Related Protein 1. *Trends in Plant Science*, *22*(10), 871–879. https://doi.org/10.1016/j.tplants.2017.06.013

Briza, P., Eckerstorfer, M., & Breitenbach, M. (1994). The sporulation-specific enzymes encoded by the DIT1 and DIT2 genes catalyze a two-step reaction leading to a soluble LL-dityrosine-containing precursor of the yeast spore wall. *Proceedings of the National Academy of Sciences of the United States of America*, *91*(10), 4524–4528. https://doi.org/10.1073/pnas.91.10.4524

Cai, Z., Li, G., Lin, C., Shi, T., Zhai, L., Chen, Y., & Huang, G. (2013). Identifying pathogenicity genes in the rubber tree anthracnose fungus *Colletotrichum gloeosporioides* through random insertional mutagenesis. *Microbiological Research*, *168*(6), 340–350. https://doi.org/10.1016/j.micres.2013.01.005

Calcott, P. H., & Fatig, R. O. (1984). Avermectin Modulation of GABA Binding To Membranes of Rat Brain, Brine Shrimp and a Fungus, *Mucor Miehei*. *The Journal of Antibiotics*, *37*(7), 797–801.

Calvo, A. M., Wilson, R. A., Bok, J. W., & Keller, N. P. (2002). Relationship between Secondary Metabolism and Fungal Development. *Microbiology and Molecular Biology Reviews*, *66*(3), 447–459. https://doi.org/10.1128/MMBR.66.3.447–459.2002

Chettri, P., Calvo, A. M., Cary, J. W., Dhingra, S., Guo, Y., McDougal, R. L., & Bradshaw, R. E. (2012). The *veA* gene of the pine needle pathogen *Dothistroma septosporum* regulates sporulation and secondary metabolism. *Fungal Genetics and Biology*, *49*(2), 141–151.

Chooi, Y.-H., Muria-Gonzalez, J. M., Mead, O. L., & Solomon, P. S. (2015). SnPKS19 encodes the polyketide synthase for alternariol mycotoxin biosynthesis in the wheat pathogen *Parastagonospora nodorum*. *Applied and Environmental Microbiology*, *81*(16), 5309–5317. https://doi.org/10.1128/AEM.00278-15

Chooi, Y.-H., Muria-Gonzalez, M. J., & Solomon, P. S. (2014). A genome-wide survey of the secondary metabolite biosynthesis genes in the wheat pathogen *Parastagonospora nodorum*. *Mycology*, *5*(3), 192–206. https://doi.org/10.1080/21501203.2014.928386

Choudhary, V., & Schneiter, R. (2012). Pathogen-Related Yeast (PRY) proteins and members of the CAP superfamily are secreted sterol-binding proteins. *Proceedings of the National Academy of Sciences*, *109*(42), 16882–16887. https://doi.org/10.1073/pnas.1209086109

Clutterbuck, A. J. (1969). A mutational analysis of conidial development in *Aspergillus*

*nidulans*. *Genetics*, *63*(2), 317–327.

Davis, R. H., Morris, D. R., & Coffino, P. (1992). Sequestered End Products and Enzyme Regulation: The Case of Ornithine Decarboxylase. *Microbiological Reviews*, *56*(2), 280–290.

Dietz, S., von Bülow, J., Beitz, E., & Nehls, U. (2011). The aquaporin gene family of the ectomycorrhizal fungus *Laccaria bicolor*: Lessons for symbiotic functions. *New Phytologist*, *190*(4), 927–940. https://doi.org/10.1111/j.1469-8137.2011.03651.x

Douaiher, M. N., Halama, P., & Janex-Favre, M. C. (2004). The ontogeny of *Stagonospora nodorum* pycnidia in culture. *SYDOWIA-HORN-*, *56*, 39–50.

Dutar, P., & Nicoll, R. A. (1988). A physiological role for GABAB receptors in the central nervous system. *Nature*, *332*(6160), 156–158. https://doi.org/10.1038/332156a0

Etxebeste, O., Garzia, A., Espeso, E. A., & Ugalde, U. (2010). *Aspergillus nidulans* asexual development: Making the most of cellular modules. *Trends in Microbiology*, *18*(12), 569–576. https://doi.org/10.1016/j.tim.2010.09.007

Galarreta, M., & Hestrin, S. (2001). Electrical synapses between GABA-releasing interneurons. *Nature Reviews Neuroscience*, *2*(6), 425–433. https://doi.org/10.1038/35077566

Ge, S., Goh, E. L. K., Sailor, K. A., Kitabatake, Y., Ming, G. L., & Song, H. (2006). GABA regulates synaptic integration of newly generated neurons in the adult brain. *Nature*, *439*(7076), 589–593. https://doi.org/10.1038/nature04404

Guo, M., Chen, Y., Du, Y., Dong, Y., Guo, W., Zhai, S., … Zheng, X. (2011). The bZIP transcription factor MoAP1 mediates the oxidative stress response and is critical for pathogenicity of the rice blast fungus *Magnaporthe oryzae*. *PLoS Pathogens*, *7*(2). https://doi.org/10.1371/journal.ppat.1001302

Hanba, Y. T., Shibasaka, M., Hayashi, Y., Hayakawa, T., Kasamo, K., Terashima, I., & Katsuhara, M. (2004). Overexpression of the barley aquaporin HvPIP2; 1 increases internal CO2 conductance and CO2 assimilation in the leaves of transgenic rice plants. *Plant and Cell Physiology*, *45*(5), 521–529.

Hane, J. K., Lowe, R. G. T., Solomon, P. S., Tan, K.-C., Schoch, C. L., Spatafora, J. W., … Oliver, R. P. (2007). Dothideomycete Plant Interactions Illuminated by Genome Sequencing and EST Analysis of the Wheat Pathogen *Stagonospora nodorum*. *The Plant Cell Online*, *19*(11), 3347–3368. https://doi.org/10.1105/tpc.107.052829

Hosie, A. M., Baylis, H. A., Buckingham, S. D., & Sattelle, D. B. (1995). Actions of the

insecticide fipronil, on dieldrin-sensitive and -resistant GABA receptors of *Drosophila melanogaster*. *British Journal of Pharmacology*, *115*(6), 909–912. https://doi.org/10.1111/j.1476-5381.1995.tb15896.x

IpCho, S. V. S., Tan, K.-C., Koh, G., Gummer, J., Oliver, R. P., Trengove, R. D., & Solomon, P. S. (2010). The transcription factor StuA regulates central carbon metabolism, mycotoxin production, and effector gene expression in the wheat pathogen *Stagonospora nodorum*. *Eukaryotic Cell*, *9*(7), 1100–1108.

Johnston, G. A. R. (1996). GABAA receptor pharmacology. *Pharmacology and Therapeutics*, *69*(3), 173–198. https://doi.org/10.1016/0163-7258(95)02043-8

Kahmann, R., & Basse, C. (2001). Fungal gene expression during pathogenesis-related development and host plant colonization. *Current Opinion in Microbiology*, *4*(4), 374–380. https://doi.org/10.1016/S1369-5274(00)00220-4

Keller, N. P., Turner, G., & Bennett, J. W. (2005). Fungal secondary metabolism—from biochemistry to genomics. *Nature Reviews Microbiology*, *3*(12), 937–947.

Kim, D., Langmead, B., & Salzberg, S. L. (2015). HISAT: A fast spliced aligner with low memory requirements. *Nature Methods*, *12*(4), 357–360. https://doi.org/10.1038/nmeth.3317

Kim, D., Pertea, M., Kim, D., Pertea, G. M., Leek, J. T., & Salzberg, S. L. (2016). Transcript-level expression analysis of RNA- seq experiments with HISAT , StringTie and Transcript-level expression analysis of RNA-seq experiments with HISAT , StringTie and Ballgown. *Nature Protocols*, *11*(9), 1650–1667. https://doi.org/10.1038/nprot.2016-095

Kim, Y. K., Liu, Z. M., Li, D. X., & Kolattukudy, P. E. (2000). Two novel genes induced by hard-surface contact of *Colletotrichum gloeosporioides* conidia. *Journal of Bacteriology*, *182*(17), 4688–4695. https://doi.org/10.1128/JB.182.17.4688-4695.2000.Updated

Kinnersley, A. M., & Turano, F. J. (2000). Gamma Aminobutyric Acid (GABA) and Plant Responses to Stress. *Critical Reviews in Plant Sciences*, *19*(6), 479–509. https://doi.org/10.1080/07352680091139277

Li, H., Handsaker, B., Wysoker, A., Fennell, T., Ruan, J., Homer, N., … Durbin, R. (2009). The Sequence Alignment/Map format and SAMtools. *Bioinformatics*, *25*(16), 2078–2079. https://doi.org/10.1093/bioinformatics/btp352

Li, T., Hu, Y.-J., Hao, Z.-P., Li, H., Wang, Y.-S., & Chen, B.-D. (2013). First cloning and characterization of two functional aquaporin genes from an arbuscular mycorrhizal fungus *Glomus intraradices*. *New Phytologist*, *197*(2), 617–630.

https://doi.org/10.1111/nph.12011

Linden, H., Ballario, P., & Macino, G. (1997). Blue light regulation in Neurospora crassa. *Fungal Genetics and Biology*, *22*(3), 141–150. https://doi.org/S1087-1845(97)91013-6 [pii] 10.1006/fgbi.1997.1013

Liu, Z. M., & Kolattukudy, P. E. (1998). Identification of a gene product induced by hard-surface contact of *Colletotrichum gloeosporioides* conidia as a ubiquitin-conjugating enzyme by yeast complementation. *Journal of Bacteriology*, *180*(14), 3592–3597.

Lowe, R. G. T., Lord, M., Rybak, K., Trengove, R. D., Oliver, R. P., & Solomon, P. S. (2009). Trehalose biosynthesis is involved in sporulation of *Stagonospora nodorum*. *Fungal Genetics and Biology*, *46*(5), 381–389. https://doi.org/10.1016/j.fgb.2009.02.002

Lu, S., Faris, J. D., Sherwood, R., Friesen, T. L., & Edwards, M. C. (2014). A dimeric PR-1-type pathogenesis-related protein interacts with ToxA and potentially mediates ToxA-induced necrosis in sensitive wheat. *Molecular Plant Pathology*, *15*(7), 650–663. https://doi.org/10.1111/mpp.12122

Matsuyama, S. S., Nelson, R. E., & Siegel, R. W. (1974). Mutations specifically blocking differentiation of macroconidia in *Neurospora crassa*. *Developmental Biology*, *41*(2), 278–287. https://doi.org/10.1016/0012-1606(74)90306-6

Maurel, C., Verdoucq, L., Luu, D.-T., & Santoni, V. (2008). Plant aquaporins: membrane channels with multiple integrated functions. *Annual Review of Plant Biology*, *59*, 595–624. https://doi.org/10.1146/annurev.arplant.59.032607.092734

Mead, O., Thynne, E., Winterberg, B., & Solomon, P. S. (2013). Characterising the Role of GABA and Its Metabolism in the Wheat Pathogen *Stagonospora nodorum*. *PLoS ONE*, *8*(11), e78368. https://doi.org/10.1371/journal.pone.0078368

Meyers, G. L., Jung, K. W., Bang, S., Kim, J., Kim, S., Hong, J., … Bahn, Y. S. (2017). The water channel protein aquaporin 1 regulates cellular metabolism and competitive fitness in a global fungal pathogen *Cryptococcus neoformans*. *Environmental Microbiology Reports*, *9*(3), 268–278. https://doi.org/10.1111/1758-2229.12527

Möbius, N., & Hertweck, C. (2009). Fungal phytotoxins as mediators of virulence. *Current Opinion in Plant Biology*, *12*(4), 390–398. https://doi.org/10.1016/j.pbi.2009.06.004

Navarro-ródenas, A., Xu, H., Kemppainen, M., Pardo, A. G., & Zwiazek, J. J. (2015). *Laccaria bicolor* aquaporin LbAQP1 is required for Hartig net development in

trembling aspen (*Populus tremuloides*). *Plant, Cell and Environemnt,* (38), 2475-2486 https://doi.org/10.1111/pce.12552

Ogata, H., Goto, S., Sato, K., Fujibuchi, W., Bono, H., & Kanehisa, M. (1999). KEGG: Kyoto encyclopedia of genes and genomes. *Nucleic Acids Research*, *27*(1), 29–34. https://doi.org/10.1093/nar/27.1.29

Oliver, R. P., Friesen, T. L., Faris, J. D., & Solomon, P. S. (2012). *Stagonospora nodorum* : From Pathology to Genomics and Host Resistance. *Annual Review of Phytopathology*, *50*(1), 23–43. https://doi.org/10.1146/annurev-phyto-081211-173019

Park, H.-S., & Yu, J.-H. (2012). Genetic control of asexual sporulation in filamentous fungi. *Current Opinion in Microbiology*, *15*(6), 669–677. https://doi.org/10.1016/j.mib.2012.09.006

Pertea, M., Pertea, G. M., Antonescu, C. M., Tsung-Cheng, C., Mendell, J. T., & Salzberg, S. L. (2015). StringTie enables improved reconstruction of a transcriptome from RNA-seq reads. *Nature Biotechnology*, *33*(3), 290–295. https://doi.org/10.1038/nbt.3122.StringTie

Rae, B. D., Long, B. M., Förster, B., Nguyen, N. D., Velanis, C. N., Atkinson, N., … McCormick, A. J. (2017). Progress and challenges of engineering a biophysical carbon dioxide-concentrating mechanism into higher plants. *Journal of Experimental Botany*, *68*(14), 3717–3737. https://doi.org/10.1093/jxb/erx133

Rajam, M. V., Weinstein, L. H., & Galston, A. W. (1985). Prevention of a plant disease by specific inhibition of fungal polyamine biosynthesis. *Proceedings of the National Academy of Sciences of the United States of America*, *82*(20), 6874–6878.

Rajam, M. V, & Galston, A. W. (1985). The effects of some polyamine biosynthetic inhibitors on growth and morphology of phytopathogenic fungi. *Plant & Cell Physiology*, *26*(4), 683–692. https://doi.org/10.1093/oxfordjournals.pcp.a076958

Ramesh, S. A., Tyerman, S. D., Xu, B., Bose, J., Kaur, S., Conn, V., … Gillham, M. (2015). GABA signalling modulates plant growth by directly regulating the activity of plant-specific anion transporters. *Nature Communications*, *6*, 7879. https://doi.org/10.1038/ncomms8879

Rattan, R. S. (2010). Mechanism of action of insecticidal secondary metabolites of plant origin. *Crop Protection*, *29*(9), 913–920. https://doi.org/10.1016/j.cropro.2010.05.008

Ritchie, M. E., Phipson, B., Wu, D., Hu, Y., Law, C. W., Shi, W., & Smyth, G. K. (2015). limma powers differential expression analyses for RNA-sequencing and

microarray studies. *Nucleic Acids Research*, *43*(7), e47. https://doi.org/10.1093/nar/gkv007

Robinson, M. D., McCarthy, D. J., & Smyth, G. K. (2009). edgeR: A Bioconductor package for differential expression analysis of digital gene expression data. *Bioinformatics*, *26*(1), 139–140. https://doi.org/10.1093/bioinformatics/btp616

Rudd, J. J., Kanyuka, K., Hassani-Pak, K., Derbyshire, M., Andongabo, A., Devonshire, J., … Courbot, M. (2015). Transcriptome and Metabolite Profiling of the Infection Cycle of *Zymoseptoria tritici* on Wheat Reveals a Biphasic Interaction with Plant Immunity Involving Differential Pathogen Chromosomal Contributions and a Variation on the Hemibiotrophic Lifest. *Plant Physiology*, *167*(3), 1158–1185. https://doi.org/10.1104/pp.114.255927

Sekiguchi, J., & Gaucher, G. M. (1977). Conidiogenesis and secondary metabolism in *Penicillium urticae*. *Applied and Environmental Microbiology*, *33*(1), 147–158.

Smith, D. J., Earl, a J., & Turner, G. (1990). The multifunctional peptide synthetase performing the first step of penicillin biosynthesis in *Penicillium chrysogenum* is a 421,073 dalton protein similar to *Bacillus brevis* peptide antibiotic synthetases. *The EMBO Journal*, *9*(9), 2743–2750.

Solomon, P. S., Lowe, R. G. T., Tan, K.-C., Waters, O. D. C., & Oliver, R. P. (2006). *Stagonospora nodorum*: cause of stagonospora nodorum blotch of wheat. *Molecular Plant Pathology*, *7*(3), 147–156. https://doi.org/10.1111/j.1364-3703.2006.00326.x

Solomon, P. S., & Oliver, R. P. (2002). Evidence that gamma-aminobutyric acid is a major nitrogen source during *Cladosporium fulvum* infection of tomato. *Planta*, *214*(3), 414–420. https://doi.org/10.1007/s004250100632

Solomon, P. S., Tan, K. C., & Oliver, R. P. (2003). The nutrient supply of pathogenic fungi; a fertile field for study. *Molecular Plant Pathology*, *4*(3), 203–210. https://doi.org/10.1046/j.1364-3703.2003.00161.x

Solomon, P. S., Waters, O. D. C., & Oliver, R. P. (2007). Decoding the mannitol enigma in filamentous fungi. *Trends in Microbiology*, *15*(6), 257–262.

Solomon, P. S., Wilson, T. J. G., Rybak, K., Parker, K., Lowe, R. G. T., & Oliver, R. P. (2006). Structural characterisation of the interaction between *Triticum aestivum* and the dothideomycete pathogen *Stagonospora nodorum*. *European Journal of Plant Pathology*, *114*(3), 275–282.

Tan, K. C., Heazlewood, J. L., Millar, A. H., Thomson, G., Oliver, R. P., & Solomon, P. S. (2008). A signaling-regulated, short-chain dehydrogenase of *Stagonospora*

*nodorum* regulates asexual development. *Eukaryotic Cell*, *7*(11), 1916–1929. https://doi.org/10.1128/EC.00237-08

Team, R. (2015). RStudio: Integrated Development for R. Boston, USA: RStudio Inc.

Team, R. D. C. (2011). R: A Language and Environment for Statistical Computing. Vienna, Austria: The R Foundation for Statistical Computing.

Wassef, A. A., Dott, S. G., Harris, A. R., Brown, A. R., O'Boyle, M., Meyer, W. J., & Rose, R. M. (1999). Critical Review of GABA-ergic Drugs in the Treatment of Schizophrenia. *Journal of Clinical Psychopharmacology*, *19*(3), 222–232.

Yu, J., Chang, P., Ehrlich, K. C., Cary, J. W., Bhatnagar, D., Cleveland, T. E., … Bennett, J. W. (2004). MINIREVIEW Clustered Pathway Genes in Aflatoxin Biosynthesis. *Applied and Environmental Microbiology*, *70*(3), 1253–1262. https://doi.org/10.1128/AEM.70.3.1253

# Chapter 5: General discussion and concluding remarks

## 5.1 General discussion

The devastating wheat disease Stagonospora nodorum blotch (SNB) is caused by the Dothideomycete, *Parastagonospora nodorum*. This necrotrophic fungus creates lesions of decaying plant tissue on the flag and flag-1 through a polycyclic life strategy. This strategy involves multiple cycles of infection, reproduction and re-infection of the host, leading to the spread of necrosis across and between plants. Necrotic lesions lower the photosynthetic capacity of the host and ultimately reduce grain yields. Disrupting the ability of *P. nodorum* to reproduce or infect and kill the host effectively disarms the pathogen (Oliver et al., 2012). This project successfully gained novel insight into these two crucial aspects of disease by elucidating potential virulence factors and describing the genetic and chemical orchestration of asexual development in *P. nodorum.*

### 5.1.1 Discovery of novel virulence factors through a *P.* nodorum forward genetic screen

In Chapter 2, I used a forward genetic screen to discover novel mechanisms of virulence in *P. nodorum*. *P. nodorum* mutants were identified that were unable to initiate disease symptoms on a susceptible wheat cultivar, as well as those that gained virulence on a non-susceptible cultivar. This was the first reported use of forward genetics with this pathogen and yielded seven avirulent strains. A mutant database was generated describing mutants by phenotype. This database allows the mutant library to be screened in the future at lower cost, as well as revealing possible phenotypes for future investigation. The seven avirulent mutants displayed differing phenotypes at the microscopic level during infection and disease was halted at different stages of infection. This indicated that the mutants were harbouring different mutations and that there were at least seven different virulence factors present. The aims for this chapter were successfully met, and this part of the project laid the foundations for the following

chapter. Further the results of this study highlight the value of unbiased methods of gene discovery, such as forward genetics, and provide resources for future investigations.

In Chapter 3 I used whole genome sequencing to retrieve the disrupted loci in the seven avirulent strains of *P. nodorum*. Sequencing these genomes revealed the loss of the disruption cassette used to generate the mutant library in six of the mutants. This may explain why the molecular methods of loci retrieval failed. However, these methods failed to identified disruptions in the seventh strain, t112, which harboured two disruption cassettes. A BLASTp alignment identified the two disrupted loci in strain t112 to be a *Catechol-1,2-dioxygenase* and a *Copper-dependant amine oxidase*. The proteins encoded by these genes have been implicated in virulence in other plant-pathogen models (Michielse et al., 2009; Rea et al., 2002). Further, a forward genetics screen for avirulence in the tomato pathogen, *Fusarium oxysporum* f.sp. *lycopersici*, identified a *Catechol-1,2-dioxygenase* as a key virulence factor (Michielse et al., 2009).

It was disheartening to discover that six of seven avirulent strains had lost their disruption cassettes through some unknown mechanism. The phenotype of these strains was retained indicating that the mutation leading to the phenotype still exists. These mutations could be the result of genome scarring by the original disruption cassette and may be found using deeper resequencing. Further, identifying these mutation sites may reveal aspects of genome maintenance and transposon defence in fungi. The loss of the disruption cassettes severely limited this part of the project. Fortuitously, two disruptions cassettes were identified in t112 allowing the aims of this project to be partially met. Two disrupted loci in strain t112 were identified. To meet the aims of this

project, the identified mutations needed to be independently verified in the wild-type background.

I was able to independently disrupt *Pn.Catechol-1,2-dioxygenase1*. Disrupting this gene inhibited the *in vitro* growth of *P. nodorum* in the presence of catechol. However, the gene was not required for virulence under the conditions used to assay pathogenicity. I was unable to disrupt the *Pn.Copper-dependent amine oxidase1* using the same method used for *Pn.Catechol-1,2-dioxygenase1*. The *Pn.Copper-dependent amine oxidase1* in strain t112 harboured a disruption to the promoter region. This may indicate that *Pn.Copper-dependent amine oxidase1* is required for viability and t112 harbours a partially functional copy of this gene. This correlated with the partial virulence of strain t112, but confounded efforts to link the phenotype of t112 to a genotype and novel virulence factor. Considering the loss of disruption cassettes from the other six avirulent strains it is possible the mutation leading to t112 avirulence was caused by lost disruption cassette. In this scenario, neither *Pn.Copper-dependent amine oxidase1* nor *Pn.Catechol-1,2-dioxygenase1* are required for virulence. This part of the project partially met its aims by identifying two disruption cassettes in a single avirulent strain and determining that one of those mutations was not causal to the avirulent phenotype.

### 5.1.2 Genetic and metabolic coordination of asexual development in *P. nodorum*

Complementing the search for novel virulence factors I then sought to gain insight into the other key element to SNB, asexual reproduction. I combined transcriptomics and metabolomics to decipher the genetic and chemical regulation of GABA-induced sporulation in *P. nodorum*. Gene expression analysis revealed that the canonical genetic cascades orchestrating sporulation in *Aspergillus* and *Neurospora* were not active

during *P. nodorum* cell differentiation and sporulation (Etxebeste et al., 2010; Park and Yu, 2012). This analysis invites further investigation by indicating there is a mechanism orchestrating sporulation in *P. nodorum* that remains to be discovered.

Gene expression analysis showed four secondary metabolite clusters were differentially expressed between sporulating and non-sporulating samples. Expression of these clusters may play a direct role in sporulation or are simply activated downstream of a sporulation cascade. Further they may be artefacts of using GABA to induce sporulation. Regardless, they provide targets for future reverse genetics studies, as well as heterologous expression and molecule identification studies. Followingly, the chemical analysis of revealed the differential abundance of ornithine during asexual development. This amino acid and its metabolism have been implicated in *P. nodorum* sporulation and virulence previously (Bailey et al., 2000). Expanding upon this I showed the induction of sporulation to varying degrees by the metabolites in the ornithine metabolic pathway. Unfortunately, the gas chromatography-mass spectrometry method used in this study failed to identify any other metabolites of interest. These results highlight the integral role of primary metabolism during cell differentiation and asexual development.

The non-proteinaceous amino acid, GABA, was used to induce sporulation in *P. nodorum*. This molecule has been used to induce sporulation in other related fungi, however, the mechanism behind this phenomenon is unknown (Mead et al., 2013). Agonists and antagonists to vertebrate GABA receptors were shown to modulate the effect of GABA. This indicates that the fungus may perceive GABA via a similar mechanism as neurons in vertebrates. These results provide scope to further understand the *P. nodorum*-wheat interaction, as well as potential for industrial application. GABA

based insecticides have been successfully deployed and may be appropriate for managing fungi that rely on sporulation to cause disease

The molecular mechanisms triggering sporulation, orchestrating cell differentiation and ultimately leading to release of viable spores are poorly defined in the Dothideomycetes. This study begins to define the genetic and chemical pathways involved in asexual reproduction in the pathogen model, *P. nodorum*.

## 5.2 Concluding remarks

This body of work aimed to elucidate novel mechanisms required by *P. nodorum* to cause disease by dissecting the two critical aspects of SNB. A forward genetics approach identified two gene targets as possible virulence factors. This was complemented by a combined gene expression and chemical analysis of *P. nodorum* asexual development. Asexual development in this fungus was found to be coordinated by unknown mechanism that does not resemble the canonical gene cascades in *Neurospora* or *Aspergillus*. Further, the primary metabolic pathway producing ornithine was implicated in coordinating cell differentiation and sporulation. This body of work provides foundations and resources for future investigations as well as highlighting the magnitude of fungal biology still to be understood.

## 5.3 References for Chapter 5

Bailey, A., Mueller, E., Bowyer, P., 2000. Ornithine decarboxylase of Stagonospora (Septoria) nodorum is required for virulence toward wheat. J. Biol. Chem. 275, 14242–14247.

Etxebeste, O., Garzia, A., Espeso, E.A., Ugalde, U., 2010. Aspergillus nidulans asexual development: Making the most of cellular modules. Trends Microbiol. 18, 569–576. https://doi.org/10.1016/j.tim.2010.09.007

Mead, O., Thynne, E., Winterberg, B., Solomon, P.S., 2013. Characterising the Role of GABA and Its Metabolism in the Wheat Pathogen <italic>Stagonospora nodorum</italic>. PLoS One 8, e78368. https://doi.org/10.1371/journal.pone.0078368

Michielse, C.B., van Wijk, R., Reijnen, L., Cornelissen, B.J., Rep, M., 2009. Insight into the molecular requirements for pathogenicity of Fusarium oxysporum f. sp. lycopersici through large-scale insertional mutagenesis. Genome Biol. 10, R4. https://doi.org/10.1186/gb-2009-10-1-r4

Oliver, R.P., Friesen, T.L., Faris, J.D., Solomon, P.S., 2012. *Stagonospora nodorum* : From Pathology to Genomics and Host Resistance. Annu. Rev. Phytopathol. 50, 23–43. https://doi.org/10.1146/annurev-phyto-081211-173019

Park, H.-S., Yu, J.-H., 2012. Genetic control of asexual sporulation in filamentous fungi. Curr. Opin. Microbiol. 15, 669–77. https://doi.org/10.1016/j.mib.2012.09.006

Rea, G., Metoui, O., Infantino, A., Federico, R., Angelini, R., 2002. Copper amine oxidase expression in defense responses to wounding and Ascochyta rabiei invasion. Plant Physiol. 128, 865–75. https://doi.org/10.1104/pp.010646